Sheffield Hallam University
Learning and IT Services
Adsetts Centre City Campus
Sheffield S1 1WB

Mechanical and Metallurgical Properties of Dissimilar Metal Joints Using Novel Joining Techniques

Emma Jane Ashcroft

A thesis submitted in partial fulfilment of the requirements of Sheffield Hallam University for the degree of Doctor of Philosophy

October 2008

Collaborating Organisations:
The Engineering and Physical Sciences Research Council
Outokumpu Stainless Research Foundation

Abstract

In recent years there have been significant new developments in welding processes for joining stainless steel and dissimilar metals. This is associated with the rise in interest of using stainless steel in the automotive industry from both car manufacturers and stainless steel producers. The main reason for using stainless steel within the automotive industry is the combination of formability and high strength but also the improved corrosion resistance when compared to zinc coated mild steel.

This research explores the mechanical and metallurgical properties of dissimilar metal joining and determines a relationship between the fatigue properties and weld geometry. The research focuses on the relatively unexplored joining techniques of Laser Hybrid Welding and Cold Metal Transfer applied to joining stainless steel grades Hy-Tens 1000 and LDX 2101 to Dogal 260RP-X mild steel. The joints are assessed in terms of tensile, fatigue and metallurgical properties.

Experimental results and analysis show that the fatigue properties of both laser hybrid welding and cold metal transfer joints are a linear relationship with a negative gradient to value of the root angle on the mild steel side of the joints, as the angle at the root decreases the fatigue life increases.

It was found that when joining the material combinations outlined in this research with Laser Hybrid Welding the resulting solidified weld pool was chemically inhomogeneous. However, welds produced using Cold Metal Transfer resulted in a chemically homogenous weld pool and consistent microhardness.

Comparisons with laser welding show that laser hybrid welding and cold metal transfer can produce joints with mechanical properties comparable to welding methods currently being used in the automotive industry, for example, laser welding.

Acknowledgements

The author would like to express thanks to the following people who without their help and guidance this work would never have been completed. To my supervisor Professor Alan Smith for continually providing support and encouragement and to Professor Staffan Hertzman, Hans Nordberg and David Dulieu for their expertise.

A special thanks to all the technical support I have received throughout my research with particular thanks going to, Johan Tolling and Pal Dyberg of ESAB Process and Development Centre, Ingemar Aslieng, Marcus Andersson and all staff at the Avesta Research Centre for all the help and support I received and welcoming me to Avesta. To all the technical support staff at Sheffield Hallam University with a special thanks going John Bradshaw, Steve Magowen, Tim O'Hara and John Vickers.

I would like to express gratitude to the fellow members of the Outokumpu research group at SHU for entertainment and thought provoking conversation throughout: Andy Clifton, Jamie Moschini and Frank Burgin.

I would also like to thank the Outukumpu Research Foundation and EPSRC for financial support throughout the research.

Finally a huge thank you to my family and friends for their support and a special thanks to Shaun who has put up with me throughout the research and encouraged me to get it done!

List of Contents

List of Figures

List of Tables

List of Equations

1 Introduction

By definition welding is the joining of materials together using a heat source. Welding has been used for many thousands of years, with the first recorded welding being carried out by the Egyptians. The first patent for electric welding was filed in the early nineteenth century and the process has been developed continuously ever since. Today there are a large number of joining and welding techniques available and design engineers are often faced with the task of choosing the optimum technique in terms of efficiency, costs and weldability for the materials to be joined[1].

In recent years there have been significant new developments in welding processes for joining stainless steel and dissimilar metals. This is associated with the recent rise in interest of using stainless steel in the automotive industry from both car manufacturers and stainless steel producers.

The main reason for using stainless steel within the automotive industry is the combination of formability and high strength, and improved corrosion resistance when compared to zinc coated mild steel.

In current car manufacture one of the main materials used is mild steel (often with a zinc coating to provide corrosion protection). Incorporation of stainless steel into automotive manufacture would be facilitated through the use of existing design and production techniques. Therefore in order to achieve this, appropriate joining processes for joining stainless steel to zinc coated mild steel need to be investigated.

The joining of dissimilar metals provides many challenges, with the major problem being the formation of intermetallic phases. Generally these phases are characterised by their high hardness and therefore brittleness, which can limit the applications of a welded joint with these phases present. In order to overcome this problem the diffusion process needs to be controlled in order to avoid these detrimental intermetallic phases[2].

However, intermetallic phases are rarely observed in 304 and 316 grade stainless steels if welded using recommended practice. The problem is more evident in high Mo, high Cr and high W grades used in sea water and other aggressive environments.

Any welding techniques highlighted for use within the automotive industry must have the ability to produce mechanically sound dissimilar metal joints. This allows areas that are safety critical to be produced with a material for example, stainless steel that exhibits superior properties in terms of strength and impact energy absorption when compared to mild steel. New techniques must also have the potential to be easily incorporated into production lines and must combine welding speed with reproducibility, reliability and cost effectiveness[3]. The major factor when considering the application of new technologies is cost, especially if a material substitution is taking place. For a typical structure in a transport system, such as a car fabricated from steel, aluminium, titanium or magnesium the estimated cost of manufacturing is 25% as shown in figure 1 below[2].

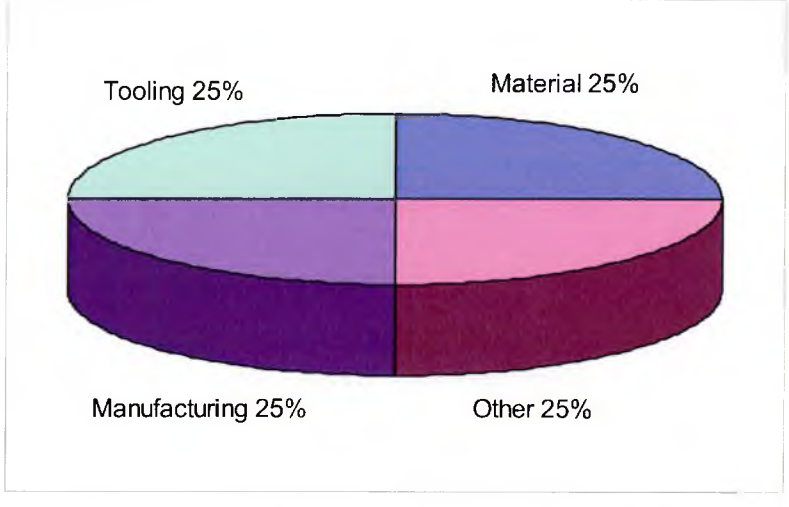

Figure 1. Distribution of cost for typical structures within the transport industry[2]

Two notable and significant innovations in welding processes for use in the automotive industry in recent years are Laser Hybrid Welding (LHW) and Cold Metal Transfer (CMT). This report outlines an investigation into these novel joining processes for joining high strength stainless steel grades to zinc coated mild steel which can be easily transferred and integrated cost effectively into current automotive manufacture.

The overall aim of this research is to investigate novel joining techniques identified for successful joining of stainless steel grades LDX 2101 and HyTens 1000 to automotive grade zinc coated mild steel (Dogol 260RP-X).

1.1 *Objectives*

The objectives for achieving the overall aim of this research are:

- To find an acceptable process window for each of the material combination and joining techniques, the initial assessment will be visual in terms of bead quality and penetration.
- To optimise the mechanical properties of the joints produced by each technique in terms of tensile and fatigue properties. The criteria for the tensile test are for the joint to be as good as the weakest parent material, e.g. the mild steel.
- To identify and characterise potential failure modes associated with the novel joining techniques.
- Finally propose a model for predicting fatigue properties of dissimilar metal joints.

2 Literature Review

An extensive study of the literature has been carried out on topics of interest to this research. This includes the more established joining techniques of laser welding and Gas Metal Arc Welding (GMAW) and the less widely reported techniques of Laser Hybrid Welding (LHW) and Cold Metal Transfer (CMT). Also discussed in the sections below are the materials that have been used in this research and the mechanical testing carried out.

2.1 *Laser Welding*

Laser welding is a well established welding technique that can join a variety of materials and thicknesses. The coherent nature of the laser beam allows it to be focussed to a small spot, leading to high energy densities and spot sizes that can range from as small as 0.2mm up to 13mm[11]. Until the 1970's laser welding was restricted to pulsed power and for joining relatively thin materials at low speeds due to a limited availability of continuous power. Development has been carried out on the use of lasers to produce continuous power or continuous waveform (CW) lasers in order to enable higher welding speed and deeper penetration[4].

Lasers most commonly used, particularly within the automotive industry, are Carbon Dioxide (CO_2) gas laser and a solid state Neodymium-doped Yttrium Aluminium Garnet (Nd:YAG) or more commonly known as YAG lasers.

2.1.1 Mechanism of Laser Welding

The principle of Laser (Light Amplification by Stimulated Emission of Radiation) is the use of this stimulated energy to produce a beam of coherent monochromatic light. Lasers operate at a wavelength in the visible and infra-red region. Focussing the laser beam into a small spot creates sufficient energy for welding, cutting and piercing operations on metals as well as other materials[5].

During welding, the high power density in the focal point evaporates the materials and causes a narrow deep entry hole which moves through the work piece as the laser beam is manipulated[6]. This mechanism produces a keyhole and can be used to weld a variety of materials of various thicknesses.

CO_2 lasers are most commonly used for high power welding emitting light with a wavelength of 10.6μm. The gas mixture used in this type of laser is mainly helium, carbon dioxide and nitrogen. The helium is present to ensure the removal of generated heat, the CO_2 is the laser active medium, in order to create the necessary energy for excitation to take place a gas discharge needs to occur and this is why the nitrogen is present. Nd:YAG lasers have a wavelength ten times shorter than CO_2 lasers, neodymium is the laser-active medium and is located in a rod shaped yttrium-aluminium-garnet solid crystal. Optical excitation in pulsed lasers usually occurs by means of krypton flash-lamps, whereas krypton arc lamps are used in high powered continuous waveform lasers[6].

CO_2 lasers are cost effective for high speed welding and are used in thin walled structures such as car bodies. The drawbacks of CO_2 gas lasers are the complex delivery systems of the laser beam to the work piece and sometimes beam quality is lost due to the transfer of the laser beam via mirrors. Alternatively, the light from Nd:YAG lasers can be transmitted via optical fibres and can be more easily integrated into a variety of automated systems[6].

The primary factor in establishing the potential for laser welding is that the power density generated is $10^6 W/cm^2$ (6×10^6 W/in^2), compared to 5×10^2-$10^4 W/cm^2$ (3×10^3-6×10^4 W/in^2) for arc welding. Lasers also permits precision welded joints rivalled only by those produced using an electron beam. Table 1 below shows comparisons of the energy consumption and efficiency of different welding processes[4].

Welding Process	Intensity of energy source		Joining efficiency mm^2/kJ	Fusion zone profile
	W/cm^2	$W/in.^3$		
Oxyacetylene (OAW)	10^2-10^3	$6x10^2$-$6x10^3$	0.2 – 0.5	Shallow for single pass
Arc Welding	5 x 10^2-10^4	$3x10^3$-$6x10^4$	0.8 – 2 (a) 2 – 3 (b) 4 – 10 (c)	Shallow for single pass
Plasma Arc (PAW)	10^3-10^6	$6x10^3$-$6x10^6$	5 – 10	Shallow at low-energy end, deep penetration at high energy end
Laser Beam	10^5-10^7	$6x10^5$-$6x10^7$	15 – 25	Deep penetration at high-energy density range
Electron Beam	10^5-10^8	$6x10^5$-$6x10^8$	20 - 30	Deep penetration
(a)Gas-Tungsten Arc Welding (GTAW). (b) Gas-Metal Arc Welding (GMAW). (c) Submerged Arc Welding (SAW)				

Table 1. Energy consumption and efficiency of various welding techniques

As can been seen in Table 1 laser beam welding has the highest efficiency with the exception of electron beam welding making it a highly desirable process for industry to utilise.

2.1.2 Advantages and Limitations of Laser Welding

Laser welding has many advantages and can be favourably compared to other well established welding and joining techniques such as brazing, soldering, arc welding, electron beam and the technique most commonly used in the automotive industry resistance spot welding. Advantages of laser welding include:

- The focused laser light provides high energy density.
- High processing speeds can be achieved.
- Narrow weld seams and narrow Heat Affected Zone (HAZ) are produced.
- Laser welding can take place without the need for a vacuum.
- No electrode or filler materials are required.
- Variety of depths of penetration can be achieved including deep penetration.
- Precision welding can be carried out using robots.

However, as with all processes there are some limitations to laser welding which include:

- Edge preparation and accurate joint fit up is critical in laser welding due to the autogenous nature of the process.
- The narrow profile and low overall heat input in laser welds results in rapid cooling, which can subsequently lead to the formation of hard martensitic/bainitic microstructures corresponding with low toughness, in steels[7].
- Initial equipment setup costs are expensive almost 10 times that of an arc process.
- The cost of accurate joint fit up during production is more expensive that other processes such as Resistance Spot Welding and Arc Welding.

2.1.3 Applications of Laser Welding

Laser welding can be applied to many different industries and applications, including the automotive industry, shipbuilding industry, land pipeline applications, thermoplastic welding and the micro plastic industry.

In the late 1990's the automotive industry began to re-evaluate manufacturing systems in the body shop after new laser technology became available for commercial use and the push towards economically fabricating vehicle structures whilst not losing quality led to laser welding being used in spot welding form[8]. Keywords often relating to automotive manufacture include quality, flexibility, high productivity and cost effectiveness. Laser welding appears to meet these high requirements and testament to this is the vast numbers of laser welders already in operation in a variety of companies[6]. On average a speed of 5m/min is used as this was the prerequisite speed needed in order to ensure the cost effectiveness of the introduction of laser welding into the industry. Laser welding can be used for seam welding as well as laser spot welding.

One common use of laser welding within the automotive industry is for the welding of tailored blanks. The production of tailored blanks requires high processing speeds and consistent weld quality. Many of the large automotive manufacturers introduced laser welding during the 1990's and these included, Volvo, Ford, BMW, Audi, Volkswagen and Renault[9]. A popular use for laser welding, within the manufacture of a car, is roof welding. Volvo began using laser welding for the construction of the roof of the 850 model in 1991, due to the nature of the design and the strength requirements of the part laser welding or adhesive bonding were the only options. After careful consideration of the product requirement, reliability and the environmental impact in terms of production, laser welding emerged as the most favourable methods of joining[6].

BMW launched the use of laser welding to join the 5 series model with 11 metres of laser weld on each car body. This extended further than the roof section and included the rear cross member, boot and the front closure panel. Ford also utilise laser welding for the roof section, the use of a continuous joint enhances the stiffness and seal tightness of the car and reduces the noise generation and the use of sealant operations. Audi and Volkswagen also use laser welding for the roof and other areas inside the cars demonstrating the versatility of the process. Audi also began to use Laser Welding on

the C-pillar of the car and began to use stitch welding with the laser in order to avoid distortion in the car body. Volkswagen moved away from a lap joint on the roof, as welding galvanised mild steel in the lap position led to spatter and unstable welding conditions. Instead the weld is positioned at the edge of the panels reducing the occurrence of the process issues and increasing the welding speed. The process was also extensively introduced in the production of the Renault Laguna, this included stitch welding of the windscreen opening and the A-pillar[6].

Laser welding is not only limited to the automotive industry it is widely used in other industries including the micro-processing and plastics industries. Laser spot welding is an accepted technology within the electronics industry, every Cathode Ray Tube (CRT) Televisions (TV) and CRT computer screen manufacturers use laser welding for the assembly of the electron gun. Additionally, laser welding can be utilised in the plastics industry for a variety of thermoplastic components[6].

2.2 *Gas Metal Arc Welding (GMAW)*

Gas Metal Arc Welding (GMAW) is classed as an arc welding process. The principle of gas metal arc welding is to join two metals together by heating them with an electric arc that is established between a consumable electrode and the workpiece[10]. A suitable gas shroud or shielding gas is fed through the welding torch to protect the arc and the molten weld pool from the surrounding environment.

The basic concept of Gas Metal Arc Welding (GMAW) was first invented in the 1920's it was not until 1948 that it became commercially available. Originally GMAW was a high current-density, bare metal electrode process, however, over the years it has been extensively developed and now has many operational parameters including low current densities, pulsed and continuous current, a variety of shielding gasses, weld consumable wires and welding parameters such as voltage, welding speed, wire feed speed, current, and modes of metal transfer[10].

The primary application of Gas Metal Arc Welding (GMAW) was for welding of carbon steels, the process has been extensively developed to successfully join different metals such as high strength low alloyed steels, stainless steels, copper and nickel alloys. Initially an inert gas was used for shielding which led to the common nomenclature of Metal Inert Gas (MIG) welding, as developments were made both inert and reactive gases have been used and the process is now referred to as Gas Metal Arc Welding.

2.2.1 Mechanism of Gas Metal Arc Welding

GMAW is an arc welding process that uses an arc struck between a continuously fed filler wire, which acts as the electrode, and the weld pool. This process is invariably carried out with a shielding gas and without the application of pressure[12]. The process of GMAW is illustrated in figure 2 below.

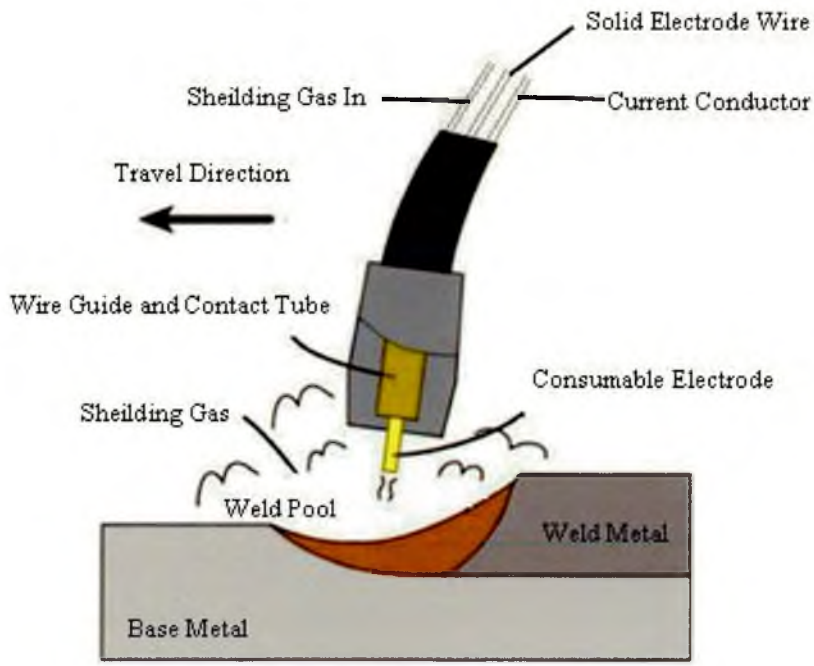

Figure 2. Schematic Diagram of Gas Metal Arc Welding Process

The heat of the arc melts the surface of the base metal/metals and the tip of the electrode, the melted metal from the electrode, is transferred across the arc to the weld pool[11]. The weld process parameters need to be controlled in order for a high quality weld to be produced.

After initial setup by the operator the electrical characteristics of the arc are automatically self regulated, providing a semi-automatic process. The only controls required to be set by the operator are the welding speed, direction and gun position. The arc length and current are automatically maintained[12].

There are three basic modes for metal transfer between the electrode and the workpiece during GMAW, short circuiting transfer, globular transfer or spray arc transfer. The most common types are short circuit transfer and spray transfer.

Short circuit transfer is more commonly used for thin section welding due to this type of transfer producing a small, fast freezing weld pool[10].The metal is only transferred when the electrode comes into contact with the workpiece. The molten metal droplet begins to form on the tip of the electrode, as the electrode is fed towards the workpiece and touches the weld pool the current increases causing the droplet to be pinched off, this initiates the arc causing short circuit. While the arc is initiated the tip of the wire melts and is fed forward for the next short circuit. Short circuit can occur from 20 to over 200 times a second.

Spray transfer uses an increased current in the GMAW process when compared with other metal transfer modes. As the current increases the rate at which the molten droplet is projected across the arc increases, the size of the droplet decreases and the transfer that is occurring appears like a fine spray[5]. Spray transfer has a rate of several hundred droplets per second and argon or an argon rich shielding gas is required to protect the arc and promote arc stability. Due to the increase in current and high energy output of spray transfer, this mode is better suited to thick sheet section and welding in the down hand position. Using spray transfer in thin sheets tends to cut through the base materials and due to the high deposition rates spray transfer can produce large weld pools that lack surface tension in the vertical or overhead position.

Globular transfer is the final mode of transfer and takes place when the current is relatively low and generally using a CO_2 rich shielding gas particularly for mild steel. The molten droplets at the tip of the filler wire are transferred across the arc in globules propelled by the arc forces. The droplet size of globular transfer is always larger than that of the electrode diameter.

2.2.2 Shielding Gases used in Gas Metal Arc Welding

The role of the shielding gas in most welding processes is to provide the molten metal protection from the surrounding environment. In GMAW the shielding gas also plays an additional role in having an effect on the arc characteristics, the mode of metal transfer, the depth of penetration, the profile of the weld bead, the welding speed and the cleaning action.

The inert gases of argon and helium are commonly used along with active gases such as carbon dioxide and oxygen. Mixtures of inert and active gases may be employed for specific applications. Further information on the use and efficiency of shielding gases used in GMAW is given by Holliday[10].

2.2.3 Advantages and Limitations of Gas Metal Arc Welding (GMAW)

Gas Metal Arc Welding (GMAW) has numerous advantages over other welding process and often the advantages are application dependant. Advantages of GMAW include:

- It is the only consumable electrode process that can be used to weld all commercial metals and alloys[12].
- The continuous wire feed enables long welds to be produced continuously without breaks.
- The welding speeds are often greater than other processes such as Shielded Metal Arc Welding (SMAW).
- Material deposition rates are significantly greater than Shielded Metal Arc Welding (SMAW).
- Lack of post weld slag minimises the post weld cleaning required.
- GMAW is a versatile process and can be executed in all positions.

The advantages of GMAW lean towards high production and automated welding operations and the process is often the first choice for applications which require continuous automated welding. The process does have certain limitations, which include:

- Welding equipment can be more costly than SMAW.
- Any air drafts that may be present in the work area need to be blocked as this could disperse the shielding gas away from the weld pool causing contamination.
- Operators have to withstand the high levels of radiated heat and arc intensity.
- GMAW requires compressed gas to operate, when welding manually the welder needs to be in close proximity to the source of compressed gas.

2.3 *Novel Joining Techniques*

The term 'Novel Joining Techniques' relates to methods of welding/joining processes that have been developed in recent years but have yet to become fully integrated and used to their full potential within an industrial setting. The 'novel' techniques highlighted in this research are those of primary interest to the automotive industry, Laser Hybrid Welding and Cold Metal transfer. A literature survey of both these processes has been carried out in order to assess and develop these processes for use in joining high strength stainless steel to zinc coated mild steel.

2.3.1 Laser Hybrid Welding

Laser hybrid welding is defined as *'the coupling of laser beam welding with a conventional welding process'*, with the arc and the laser operating in a single elongated process zone. Conventional welding processes which can be used in this hybrid system are Gas Metal Arc Welding (GMAW), Gas Tungsten Arc Welding (GTAW) or plasma arc welding. Currently the most common welding processes to be combined with Laser is GMAW and GTAW and is often referred to in different ways such as hybrid laser-MIG welding, Laser MIG/MAG welding, Laser-arc welding and various combinations of the above. For the purpose of this research GMAW welding was used and the process will be referred to as Laser Hybrid Welding (LHW). Figure 3 below shows the schematic diagram of the laser hybrid system using GMAW.

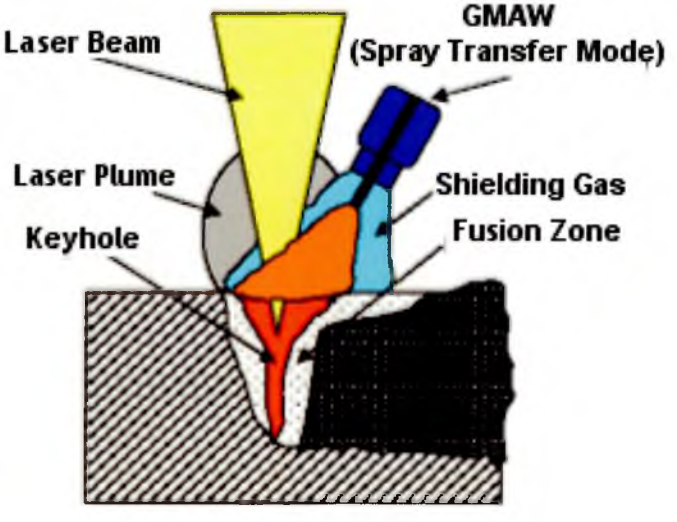

Figure 3. Schematic diagram of the laser hybrid welding modified from source[13]

The concept of laser hybrid welding was first introduced in the 1970's by *Eboo and Steen*[14], who used a 2kW continuous wave CO_2 laser together with a GTAW welding set to weld samples of 0.2mm tin sheet. It was established that the electric arc will preferentially root into the hot spot generated by the laser welding, this allowed greater welding speeds to be achieved as the additional energy of the electric arc was allowing full penetration to occur at speeds when a laser welding process would only penetrate a fraction of the required thickness. This research established that laser hybrid systems could produce higher processing speeds than any other fusion process at this time.

Work by *Alexander and Steen*[15], looked into the effect that the speed and the arc characteristics were having on the weld bead and penetration, they welded mild steel in two different thicknesses, 12mm and 2mm, the outcome was that 100 amps of arc current could be added to the laser process with no significant detrimental effects on the weld bead. The processing speed was double that of laser welding or a 20% increase in penetration could be observed at a given welding speed.

Since the early innovation of laser hybrid welding improvements have been made to the process and a variety of research projects have been undertaken, mainly using GTAW welding with materials such as steel and aluminium being investigated. However, as *Walduck and Biffin*[16] explained in 1994 there had been no commercial application or adoption of the technique to that date, due to the instability of the process during welding. Research throughout the 1990's mainly in Germany and Japan allowed the process to become more established and thus it began to be utilised within industry[17].

Laser Hybrid Welding was originally developed using a CO_2 type laser, developments over the years have enabled Nd:YAG lasers to be used with studies being carried out on both setups. It has been found that LHW using a Nd:YAG has been studied widely for thin sheet applications mainly for use in the automotive industry. Where higher power is required, for example in the welding of thick sheets LHW with a CO_2 laser is one of the most promising solutions in terms of optimum power to cost ratio, having a significant advantage over using a Nd:YAG laser for the same application[18].

Work by *Tani et al*[19]investigated the effect of shielding gas in the laser hybrid process. They carried out experiments on 304 stainless steel billets (15 x 10 x 120mm) in a butt joint configuration with poor quality edge preparation and the investigation looked at

three different shielding gases, 30% He + 67% Ar + 3% O_2, 40% He + 57% Ar + 3% O_2 and 50% He + 47% Ar + 3% O_2. The work concluded that the shielding gas with the minimum helium content of 30% is required in order to limit the plasma formation and consequent low laser power absorption. Between 30% and 40% helium content will allow the GMAW synergic line to be followed with good process feasibility. The synergic line is a relationship between the current and voltage for a particular wire and gas combination as defined by the manufacturer of the equipment. A helium content above 40% leads to unstable arc conditions and it was found that for a cost effective welding environment the shielding gas flow rate could be between 10 and 30L/min[19].

Modelling of the prediction of the weld pool shape in plasma augmented laser welding was carried out by *Vitek et al*[20] from 1997, until that point there was no commercial use for laser hybrid processes. The worked looked at combining laser welding with that of plasma arc welding, joining 1.5mm thick cold rolled carbon steel sheet. Autogenous welds were produced, the weld geometry was then assessed and neural network analysis carried out, this enabled Vitek et al to form a viable model to predict the weld pool shape. The model indicated that the weld pool penetration is a sensitive function of the laser power (this was confirmed with experimental data). The critical laser power increases with increasing welding speed and that the depth of penetration is insensitive to the current of the arc process[20].

Work carried out by *Wouters*[21] confirmed that the joint penetration was dependent on the laser power during laser hybrid welding and that the hybrid process is insensitive to gaps below 3mm as long as the MIG parameters are set to bridge the gap. The research also assessed the influence of joint gap on the strength of the welds, the welds were partial penetration butt joints it was concluded that gaps less than 0.5mm or greater than 2mm should be avoided in partial penetration welds because they introduce stress concentration into the weld geometry consequently affecting the overall strength of the joints. The work by *Wouters*[21] was carried out on carbon steel sheets.

2.3.1.1 Advantages of Laser Hybrid Welding

Coupling laser welding and gas metal arc welding combines the advantages from the two processes, the laser welding contributes deep penetration, high processing speeds and low heat input leading to lower distortion, while the GMAW part of the process enables low cost and good tolerance to joint fit up overall producing high quality welds.

The higher welding speed of the process means that the productivity increases and with sheet material a 40% increases in production is possible compared to conventional laser welding. The lower distortion also means a decrease in post-weld work and the improved edge preparation tolerance means that in a heavy industrial setting for example shipbuilding, there could be 20-30% reduction in labour costs[21].

A common problem with laser welding is undercut, with laser hybrid welding this is overcome by the addition of a filler wire as demonstrated in figure 4.

Figure 4. Effect of filler wire in the laser hybrid welding process when compared to that of laser welding[222]

Figure 4 demonstrates the difference between laser welding and laser hybrid welding in terms of the addition of a filler wire. Undercut is seen on the photo on the right in figure 4 and potential stress concentrations are caused by the difference in height between the parent material and the weld material. With the laser hybrid process a greater bead width and deeper penetration is observed when compared to the laser hybrid process and this in turn will improve the mechanical properties.

Laser Hybrid Welding has an increased heat input when compared to laser welding, this slows down the cooling rate and along with the filler wire, alters the weld metal composition and the resulting microstructure allowing hard areas of martensite or bainite to be avoided and allow the formation of acicular ferrite in pipeline steels which offer good strength and toughness[7].

2.3.1.2 Applications of Laser Hybrid Welding Process

Laser Hybrid Welding has a growing number of industrial applications due to both the technological and economic advantages LHW has over other welding processes. The majority of the applications currently in use concentrate on laser hybrid welding of 2mm to 10mm thick sheets[21].

Laser Hybrid welding has already been introduced into the automotive industry, both Audi and Volkswagen have been using this process. Volkswagen[22,23] has been using the laser hybrid process for the aluminium doors of the VW Phaeton. They have also introduced it in the manufacture of the tailgate of the VW Bora and this includes laser hybrid welding galvanised steel.

Audi are also using this process in the production of the aluminium lateral roof area of the Audi A8 and have used it for welding the galvanised steel C-Pillar of the Audi TT.

Uses of this process in the shipbuilding, land pipeline and aerospace industries are also on the increase, with a recent introduction of a portable laser hybrid kit for the shipbuilding industry[24].

Laser Hybrid Welding is fully automated and requires a robot to operate successfully.

2.3.2 Cold Metal Transfer

Cold Metal transfer is a relatively recent innovation. It became commercially available in the autumn of 2004, and was developed by TPS- Fronius[25]. Originally marketed to the automotive industry to join aluminium to steel in order to benefit from the strength of steel and the weight saving of aluminium[26], it is also looking promising for welding stainless steel and zinc coated mild steel.

Cold Metal Transfer (CMT) is essentially a gas metal arc welding process with a significantly lower heat input when compared with conventional dip arc processes. "Cold" is a relative term in this process and its based on controlling the dip transfer of the arc.

CMT differentiates from the more common dip transfer processes because the wire motion is incorporated into the process control, thermal input is diminished and finally the transfer of the metal takes place without causing any spatter[27].

In the CMT process the wire is not only fed towards, but also withdrawn, from the work piece giving an oscillating wire, at an average frequency of 70Hz. The wire is fed towards the work piece until short circuit occurs; as this happens the wire direction is reversed and the wire retracted. When the short circuit opens again the wire speed is reversed again and the wire fed towards the work piece[28]. Figure 5 below shows the principle of the CMT process with the oscillating wire feed[28].

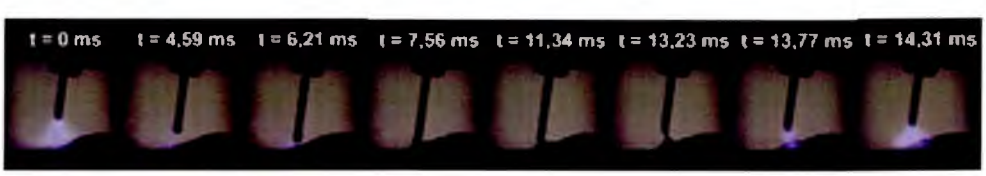

Figure 5. The CMT Process - demonstration of the oscillating wire[28]

The thermal input during the CMT process is low; this is due to the almost current free metal transfer. In standard dip arc process a high short circuit current is observed, whereas in the CMT process the current is not responsible for the opening of the short circuit. The movement created from the withdrawing of the wire supports the metal transfer because of the surface tension of the molten material. This leads to the current

being kept very low and consequently the heat input is kept at a minimum. Figure 6 shows a schematic picture of the current and voltage during the CMT process[28].

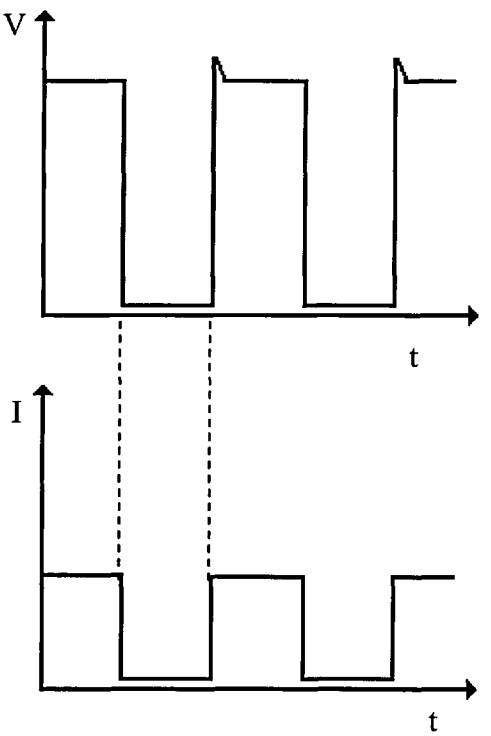

Figure 6. Schematic picture of the current and voltage in relation to time during the CMT process[28]

Due to the controlled motion of the wire and the controlled short circuit, virtually spatter free welding is possible when the CMT process is used.

Limited work has been carried out on CMT as a process, and even less has been carried out on the materials highlighted within this research. The majority of research carried out to date for the CMT process has been with aluminium. CMT is showing promising results for aluminium when compared to laser welding and laser hybrid welding. *Pinto et al*[29] investigated the effects of microstructure and residual stress in aluminium welds using the CMT process, MIG and Laser Hybrid Welding (LHW), It was found that the microstructure of all three welds was very similar, the shape of the weld bead were quite different dependent on the process, notably CMT had a more prominent and larger weld bead than the other two process with quite a circular shape with the Laser Hybrid Weld

having an asymmetrical weld bead. It was found that the CMT and LHW welds had a smaller Heat Affected Zone (HAZ) than the GMAW welds and finally the residual stresses were lower in the CMT welds than the GMAW welds which can be attributed to a lower heat input[29].

2.3.2.1 Applications of Cold Metal Transfer

CMT welding is reportedly being used at Volkswagen Sachsen, Germany[30], for the C-Pillar in the Bentley Continental and the VW Phaëton as of January 2006, this is an important part of construction and requires the welding of three different thicknesses of material. The process is being used because of the spatter free advantage thus minimising any post weld work. The CMT process is still being researched for extensive use within the automotive industry but has been used to successfully join thin sheets of aluminium to mild steel.

Other applications of the CMT process could include the aerospace industry along with structural and shipbuilding applications although these industries have yet to report successful use of CMT. Currently successful joining of zinc coated mild steel to stainless steel within an industrial or commercial setting has not been reported. Although some preliminary research has been carried out with promising results[31].

2.3.2.2 Advantages and Limitations of Cold Metal Transfer

Advantages of the CMT process include spatter free welding thus eliminating localised hard spots, when welding carbon manganese steels, due to the occurrence of phase transformation when molten spatter comes into contact with the cold parent material. An elimination or reduction in spatter minimises the need for post weld work. Cold Metal Transfer has a reduced heat input when compared to other arc welding processes due to the controlling of the dip transfer and good gap bridgeability when compared to autogenous processes due to the addition of a filler wire. These advantages make the process ideal for use within the automotive industry.

Whilst initial equipment setup costs are on a par with most arc welding processes and favourably cheaper than that of hybrid welding, laser welding and electron beam welding, limitations of cold metal transfer are that the process cannot be carried out manually due to the controlling of the dip transfer, and there is a need for a robot to operate, this then increases the setup costs depending on the cost of the robot.

2.4 *Materials*

Three materials were chosen for this research project; two grades of high strength stainless steel and one grade of zinc coated mild steel.

2.4.1 Stainless Steel

Stainless steel is a generic term for many grades of steel with a range of compositions and material properties. Stainless steels are classified in six categories according to their microstructure at room temperature which in turn corresponds to their alloy composition. The six classes are ferritic, martensitic, austenitic, martensitic-austenitic, ferritic-austenitic (duplex) and precipitation hardening. The first five are named after the dominant components of the microstructure and the sixth category, precipitation hardening is named because these steels are hardened by a mechanism involving the formation of precipitates within the microstructure[32,33].

2.4.1.1 Austenitic Stainless Steels

Austenitic stainless steels are the most commonly used type of stainless steel and are characterised by excellent corrosion resistance, very good toughness, good weldability and good ductility. Austenitic stainless steels have lower melting points, higher electrical resistance, lower coefficients of thermal conductivity and higher coefficients of thermal expansion than carbon steels[34]

This group of stainless steel have a face centred cubic microstructure and this is retained at room temperature by suitable alloying, the most common being nickel. Austenitic stainless steels are also highly alloyed with chromium to offer good corrosion resistance. They can be used in many applications including, piping systems, heat exchangers, tanks, in high temperature applications and in any application where a non magnetic material is required[32].

2.4.1.2 Duplex Stainless Steels

Duplex stainless steels contain both ferritic and austenitic microstructures in approximately equal proportions. Duplex stainless steel is produced by balancing austenite forming elements such as Ni, Mn, C and N with ferrite forming elements such as Cr, Mo, Ti, Nb, Si and Al[35]. Duplex steels are characterised by high strength, good toughness, and good corrosion resistance with excellent stress corrosion cracking and corrosion fatigue resistance[32]. Duplex structures are also resistant to solidification cracking which can occur in stainless steels during welding[35].

Applications for duplex stainless steels is on the increase, particularly with the development of LDX 2101, because not only does it have higher strength than commonly used grades of austenitic stainless steel, it has a significantly lower nickel content, making the material less sensitive to price variation[36]. Applications for duplex stainless steels include hot water tanks in breweries, various applications of chemical tanks, heat exchangers and vessels. They are also used in the offshore industry, super duplex steels with higher contents of Cr and Mo are used in environments where there are high chloride concentrations, for example, sea water[32].

2.4.2 Zinc Coated Mild Steel

The term mild steel usually means a carbon content up to about 0.3%. Many grades of mild steel are used within the automotive industry. The grade identified for use in this work is rephosphorised steel with increased ultimate tensile strength between 380 and 420 MPa and a yield strength of 190 to 270 MPa, commercially it is known as Dogal 260RP-X[37].

The steels gain their strength from the addition of phosphorous usually about 0.1%, to an aluminium killed based steel. The phosphorous additions give the increased strength by means of solid solution strengthening and exhibit yields strengths of up to 30% more than normal carbon steels.

The mild steel is received in the hot-dip galvanised condition in order to achieve adequate corrosion protection. The hot-dip galvanising process places a layer of zinc on the surface of the steel providing protection against corrosion on any exposed surfaces.

The hot-dip galvanising process involves 4 stages:

- Surface Preparation
- Galvanizing
- Quenching
- Inspection

Before the steel is galvanised surface preparation needs to take place. This occurs in 3 sub-stages, caustic cleaning first removes any dirt, paint, oil or grease. The second stage is acid pickling to remove any scale and dust then finally fluxing is carried out to prevent any oxides from forming prior to galvanising.

The next stage of the process is galvanising. The steel is completely immersed in a bath of molten zinc at a temperature of 440°C, the zinc is then metallurgically bonded to the steel by the formation of an iron-zinc layer. The excess zinc is then drained or vibrated off on removal from the bath.

The steel is then quenched in dilute chromate solution allowing immediate handling and inspection to take place. Finally the coating is inspected in order to assess the coating thickness, adherence and appearance[38].

Various coating thickness are available and in accordance with BS EN 10142:2000[39], with thickness from 7μm on both sides of the steel sheets.

2.5 *Effect of the Zinc Coating During Welding of Dissimilar Metals*

Liquid Metal Embrittlement (LME) is the brittle failure of a normally ductile material when it comes into contact with a liquid metal when subjected to an internal or external tensile stress.

Zinc has a melting point of 419°C and will begin to diffuse into and penetrate primarily along the grain boundaries of unstressed austenitic stainless steel above 450°C, this is known as type I embrittlement. Above temperatures of 750°C stressed austenitic stainless steel exposed to molten zinc will exhibit rapid crack propagation perpendicular to the applied stress, and this is type II embrittlement which is widely known as LME. During the welding of stainless steel if zinc is present close to the weld then cracking can occur and have a detrimental effect on the mechanical properties. In order to completely eliminate such cracking zinc coatings should be completely removed for the areas of material undergoing welding[40], this is not always practical particularly in an industrial environment.

During welding the zinc is vaporised (900°C) and this can have an adverse effect on the resulting weld bead, when zinc vapour is present during welding blowholes and zinc induced cracking to the surface can be present. The risk of LME is present during both Laser Hybrid Welding and CMT, however, there are ways of reducing the effect of the zinc by controlling the process parameters[31,41,42].

Zinc coated steel sheets are widely used in the automotive industry and are more often than not joined using arc welded processes or laser welding, the welding speed is restricted to 1.2m/min because of problems with spatter and pits. Experimental work carried out by *Pan and Richardson*[43] assessed laser welding for lap joining of zinc coated steel sheets, it looked at the problems and common solutions for issues associated with zinc vapour during welding. The most popular technique to reduce the damage of the zinc vapour is to employ an air gap between the sheets to be welded, usually about 0.1mm to provide a venting channel for the zinc, allowing a better quality weld to be produced. However, this is not a practical and cost effective solution for manufacturers. Therefore *Pan and Richardson* developed a clamping system which

allowed an air gap to be present below the two sheets in the hope of allowing enough air circulation around the joint to minimise the effect of the zinc. It was concluded that the air gap did have a significant influence on the process, however, some surface defects were still evident.

Research has been carried out for welding of zinc coated mild steel using the Laser Hybrid process[41]. The advantages of Laser Hybrid Welding when compared with GMAW were found to be, a wider range of applicable welding current, arc voltage and higher welding speeds (1.2m/min when compared with 2m/min), a reduction in spatter and a reduction in the number of pits.

Problems associated with zinc vapour could not be completely eliminated using the Laser Hybrid process. The research showed that there is potential to improve LHW in order for defect free welds to be consistently produced.

Other work carried out concludes that laser hybrid welding suppresses the formation of blowholes when compared to laser welding[42]. It is thought that due to the GMAW torch following the laser welding in the hybrid process the molten metal solidifies at a slower rate than that during laser welding, this gives sufficient time for the zinc vapour to escape from the molten weld pool leaving the weld bead relatively free from porosity.

Work carried out on zinc coated ultra high strength steel 1.5mm thick in an lap joint configuration using Laser Hybrid Welding concluded that the process is less stable for zinc coated sheets than uncoated sheets of the same material. Therefore the window for welding coated steel sheets is much narrower than the process window for uncoated sheets[44].

2.6 *Dissimilar Metal Joining of Stainless Steel to Zinc Coated Mild Steel*

Research has been carried out for many years into welding and joining processes for the successful joining of dissimilar metals. Dissimilar metals means that the two materials to be joined vary in chemical composition, microstructure and material properties for example different grades. The aim of this research is to investigate the joining of stainless steel to zinc coated mild steel using recently developed welding processes with particular focus on the automotive industry. Dissimilar metal joining is notoriously difficult and is more challenging than similar metal joining because of the differences in physical, mechanical and metallurgical properties of the two parent materials to be joined[45].

When welding metals it is important that the correct filler wire and shielding gases are used. The manufacturers of the materials usually have recommendations for particular material combinations, and these have been tested so that welds with desirable mechanical and corrosion properties can be obtained. Welding stainless steel to zinc coated mild steel is more difficult and therefore the filler wire selection requires a compromise between the two dissimilar metals[45]. In this situation the Schaeffler-Delong diagram is used in order to predict the microstructure of the weld, so enabling the correct filler wire to be chosen.

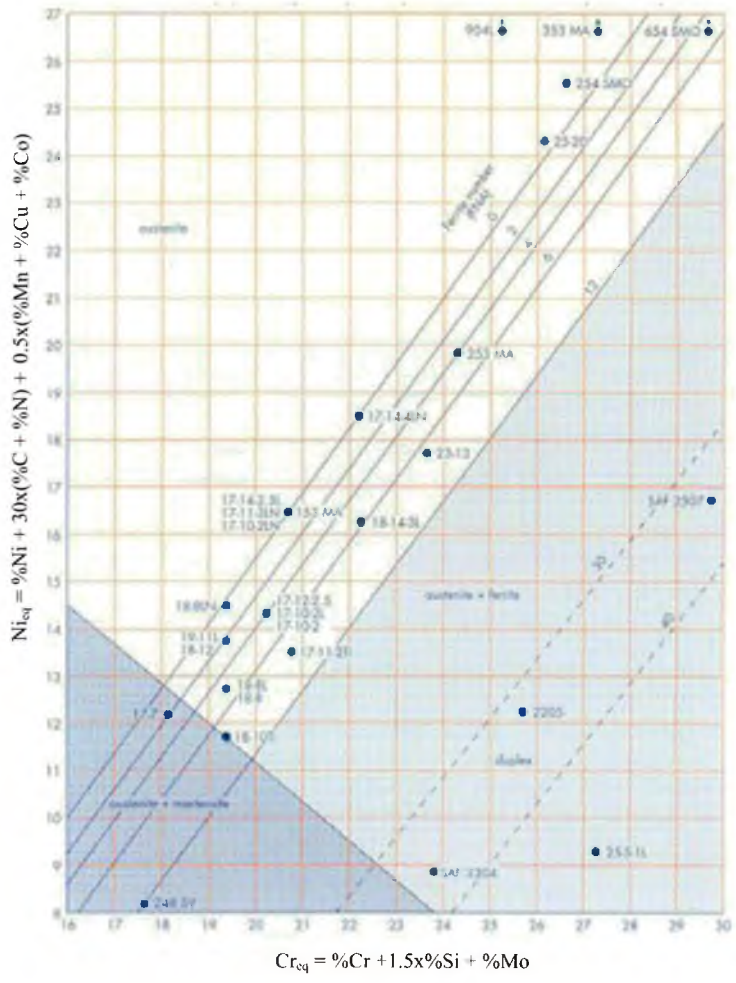

Figure 7. The Schaeffler-Delong Diagram[32]

Figure 7 shows the Schaeffler-Delong Diagram it summarises the effect of alloying additions on the structure of stainless steel, in order to predict the microstructure of a stainless steel the Chromium and Nickel equivalents need to be calculated as outlined below.

Chromium equivalent = %Cr +1.5x%Si + %Mo

Nickel equivalent = %Ni + 30x(%C + %N) + 0.5x(%Mn + %Cu + %Co)

The diagram can be used to predict the microstructure of a weld, by calculating the chromium and nickel equivalents for both parent materials and the filler wire and taking into consideration the dilution during the welding process. This was carried out for the material combinations in this research and the results are shown in section 4.

As outlined in Chapter 1, challenges are faced when trying to weld dissimilar metals with the major challenge being the formation of brittle intermetallic phases that can have detrimental effects on the mechanical properties of a joint[2].

Limited work has been carried out using Laser Hybrid Welding and Cold Metal Transfer, but the results to date indicate that dissimilar metal joining using these processes will be successful.

Dissimilar metal joining has been investigated using Laser beam welding. Work carried out by *Matsunawa et al*[46] looked at the effect of weld profile, porosity in the weld zone and LME in lap joints of austenitic stainless steels joined to zinc coated carbon steel. The work investigated different shielding gasses and process parameters to try and optimise the process for this application of dissimilar joining. It was concluded that in order to produce high quality lap welds (austenitic stainless steel to zinc coated mild steel) that were free from porosity and LME, the zinc coating needed to be completely removed before welding.

A small amount of work has been carried out using the laser hybrid process for joining Hy-Tens stainless steel to Dogal 220 RP (zinc coated mild steel), in a lap joint configuration[47]. It was suggested that the welding spot should be focussed on the Hy-Tens material in order to minimise the zinc vaporisation, this enabled smooth weld bead transition and deep penetration to be achieved, and no internal or surface breaking defects were observed.

Recent work carried out by *Westin et al*[36] investigated laser hybrid welding for the joining of LDX 2101 to Dogal 220 RP Z 100 (mild steel with a 7μm zinc coating) in a lap joint configuration, with the mild steel on the top. It was concluded that the joint showed sufficient strength and that the LDX was resistant to Liquid Metal Embrittlement (LME) or zinc attributed cracking, unlike austenitic stainless steels, making LDX 2101 highly suitable for automotive applications where, the joining of stainless steel and zinc coated mild steel is required.

Research has been carried out for dissimilar metal joining in a lap joint configuration for using the CMT process[31]. The work joined Hy-Tens stainless to zinc coated Dogal DP 600. The aim of the research was to find a window within the CMT process where Liquid Metal Embrittlement (LME) does not occur. It was concluded that CMT is capable of producing spatter free and aesthetically pleasing weld seams. However, a lot more work is needed in order to understand and evaluate the process for this application.

2.7 *Fatigue*

Engineering components very rarely fail due to a single application of load and often the design engineers work well within the boundaries of the 'safe' static load it can withstand. Engineering materials will experience a wide variety of operating conditions. The majority of components in motor vehicles and other applications will undergo variable loading conditions throughout service life. The loading conditions can be a result of changes in vibration, power, load and temperature to name a few.[48]

Many failures occur due to repeated cyclic loading lower than that of the components static strength, this mechanism is referred to as fatigue. *General Principles for Fatigue Testing of Metals (1964)*[49] states that the term fatigue 'applies to changes in properties which can occur in a metallic material due to the repeated application of stresses or strains, although usually this term applies specially to those changes which lead to cracking or failure.'

In industry, there is a need to understand the mechanisms of fatigue for different materials and components because it is estimated that over 75% of structural and mechanical failures are caused by some form of fatigue[50]. Fatigue failure in service can often be catastrophic, in order to prevent this, laboratory fatigue testing is carried out and is often an important part of a material or component validation procedure for in service applications.

August Wöhler was the first person to propose a relationship between fatigue limit and applied stress. Wöhler was a German railway engineer whose studies involved fatigue tests on full scale railway axles for the Prussian Railway Service between 1852 and 1870[51]. From the results of his tests Wöhler plotted the nominal stress (S),against the number of cycles to failure (N), to produce what is now commonly known as the S-N curve.

S-N curves are produced within a laboratory environment by testing a series of identical specimens to establish the relationship between the nominal stress and the number of cycles to failure for any type of loading regime. S-N curves are the most readily available form of fatigue data and can be used to predict the expected fatigue endurance for components subject to a particular cyclic stress[48].

S-N curves are usually plotted with the nominal stress, S on the y-axis and the number of cycles to failure, N on the x-axis. N is almost always plotted using a log scale with S on a linear scale. Figure 8 below shows a typical S-N curve[51, 52, 53].

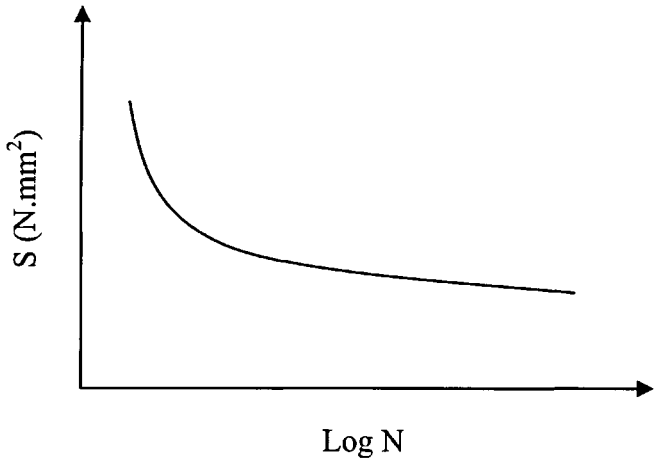

Figure 8. Typical S-N Curve

There are different approaches for fatigue testing of materials or joints, and often planning of fatigue tests is specific and dependant on the material, the specimen shape and the information that is required from the testing.

To carry out a fatigue test the loading conditions need to be decided and this will vary depending on the situation to be tested. The two main parameters to be considered when planning a fatigue test are the stress ratio and the stress cycle.

2.7.1 Stress Ratio

The stress ratio, R, is the ratio between the minimum stress component and the maximum stress component in one cycle of a fatigue test[52]. Equation 1 below outlines the calculation for the stress ratio value.

$$R = \frac{Stress_{\min}}{Stress_{\max}}$$

Equation 1. Stress Ratio, R, equation

2.7.2 Stress Cycle

The stress cycle of a fatigue test is defined as the smallest segment of the stress-time function which is repeated periodically and identically, it is defined by the stress component, shape and the frequency[52].

Usually the fluctuating stress is represented as a series of peaks and troughs connected by a sine wave, as shown in figure 9 below.

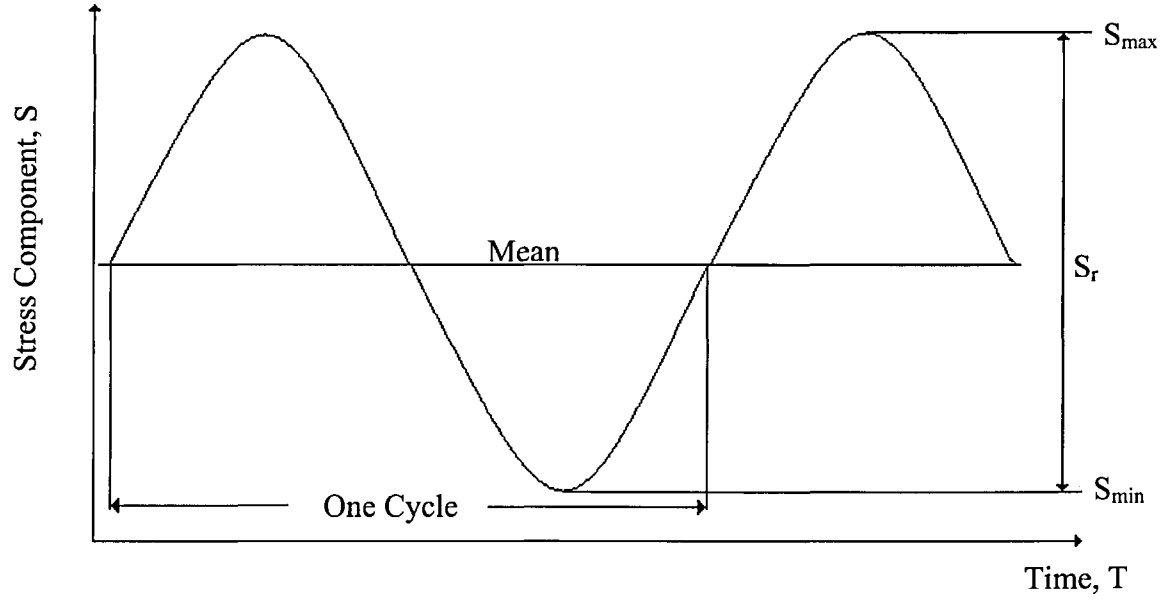

Figure 9. Diagram outlining terminology and form of a fatigue stress cycle

The test is carried out at this constant amplitude with each cycle having the same maximum and minimum stress values[53]. This cyclic testing can be described with the following parameters:

Maximum stress limit, S_{max}
Minimum stress limit, S_{min}
Mean stress, $S_m = 0.5(S_{max} + S_{min})$
Stress range, $S_r = S_{max} - S_{min}$

It is often necessary for positive and negative values of minimum and maximum stress and mean stress to be considered for design purposes.

During a fatigue test each stress cycle contributes to the initiation and growth of the fatigue crack, with the number of cycles needed to cause a failure depending on the type of loading. As a general rule, it is tensile stresses which produce fatigue damage, any stress cycle which involves a compressive period will have a less damaging effect than a stress cycle which is wholly tensile. A fully tensile stress cycle will increase in damage as the mean stress component increases. Fatigue behaviour of 'as-welded' joints can sometimes differ from this rule, due to the residual stresses sometime imposed during welding[53].

2.7.3 Staircase Fatigue Testing

Staircase fatigue testing also known as the 'up and down' method is a statistical method of determining mean fatigue strength of a sample at a pre determined cycle life. The method was first introduced in 1943 at the Explosives Research Laboratory, Bruceton, Pennsylvania[54].

Staircase fatigue testing is a well established method and is increasingly being used within the automotive industry to predict the fatigue behaviour of components. In a move to shorten the cycle of design to production the automotive industry relies heavily on finite element analysis in order to analyse the stresses in components. Characterising fatigue strength is difficult due to the length of the tests and the variation in results. Staircase fatigue tests are the solution because they allow the fatigue tests to concentrate at the fatigue life or level of stress the designer is interested in. Another advantage is that the method is simple in its execution and the calculated outputs (mean strength and standard deviation), giving a statistically determined minimum (the mean minus 3 standard deviations) for the specification of components[55].

This method is often also used on welded joints because a length of joint can vary in quality and by using the staircase method anomalous samples can be identified and thus not give a false indication of fatigue strength, whether positive or negative.

The test specimens are tested sequentially with only one specimen tested at a time. The first specimen is tested at a stress level equal to the estimated mean fatigue strength of the sample at the pre-determined number of cycles. The first level is often a guess but can also be based on experience of previous testing. If the specimen fails before reaching the pre-determine number of cycles, then the next specimen is tested at a lower level, if the specimen reaches the pre-determined number of cycles then the next specimen is tested at a higher load level.

The stress level increments are set by the experimenter and it is important that the increment is chosen correctly. Ideally the majority of the test should be made at 3 stress levels, with about 50% surviving at the middle level, 70% surviving at the lower level and approximately 30% surviving at the higher load level. In order to chose the correct load increment efficiently previous test data for similar materials or specimens should be used. However, if none is available preliminary tests will need to be carried out in

order to best determine the increment for the main staircase test. The stress level increment is usually comparable to the standard deviation of the results[52,54,56].

The primary advantage of this method of testing is that the tests are automatically concentrated on the mean fatigue strength of the samples and the statistical analysis is quite simple when compared to other statistical methods of fatigue testing. One disadvantage of this method is that each test has to be carried out separately as the stress level of the next test depends on the preceding test, this means that testing can take a long time depending on the pre-determined cycle and the frequency of test[54,56].

To ensure the accuracy of the results and to reduce the number of unnecessary test then usually between 20 and 50 specimens are required for a single staircase test for a given material combination[57].

2.7.4 Fatigue Failure Mechanism

There are three stages of fatigue failure, crack initiation, crack propagation and total fatigue failure. Fatigue failure occurs at the atomic level of the material and the effect of the cyclic loading will begin from the first stress cycle.

Repeated cyclic loading on a material results in slip of the atoms within the grains as they moved against each other, resulting in the irreversible shear dislocations which are then moved towards the surface of the material as loading continues. As the fatigue cycling continues, dislocations begin to pile up and form a structure known as Persistent Slip Bands (PSB). The constant movement of the PSB's at the surface causes the material to be pushed out, this is known as 'roughening'. Roughening results in the production of microscopic waves at the material surface often referred to as 'extrusion' (the peaks of the waves) and 'intrusion' (the trough of the waves), the intrusions then act as micro notches (figure 10). Acting as stress concentrations these micro notches cause additional slip eventually leading to fatigue crack nucleation[48,51].

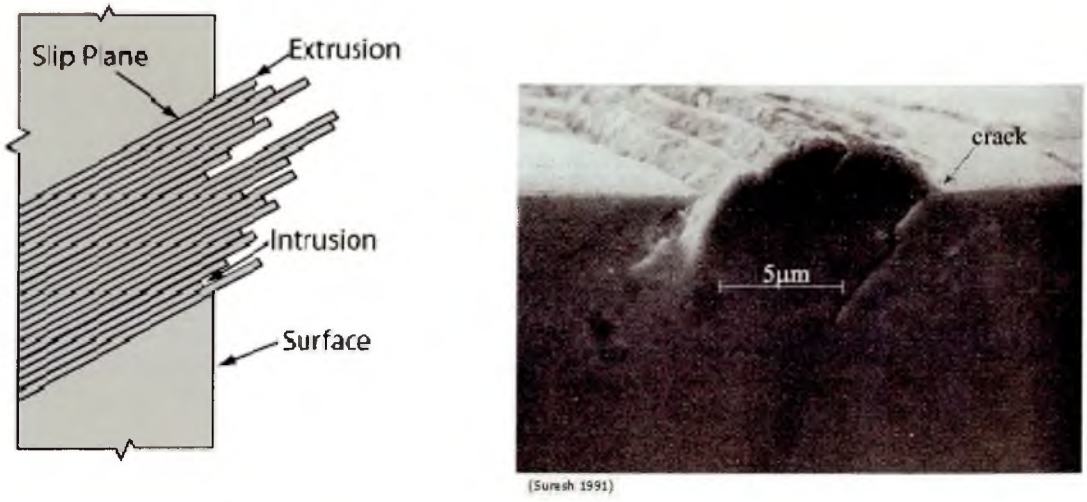

Figure 10. Crack Initiation Mechanism[58]

Once a crack has nucleated there is a substantial discontinuity through the material leading to an increase of local stress at the crack tip. As the material continues to undergo cyclic loading, the material along the crack is stretched and on the repeated opening and closing of the crack propagation occurs.

As the crack propagates through the material the fractured surfaces rub together creating a smooth area of the fracture face which also shows 'beach' marks or concentric rings to indicate the point of origin of the crack. Finally, the remaining section of the intact material becomes too small to support the cyclic loading causing the rate of propagation to increase leading to complete fracture[59,60,61]. Figure 11 below shows a schematic image of a typical fatigue fracture surface.

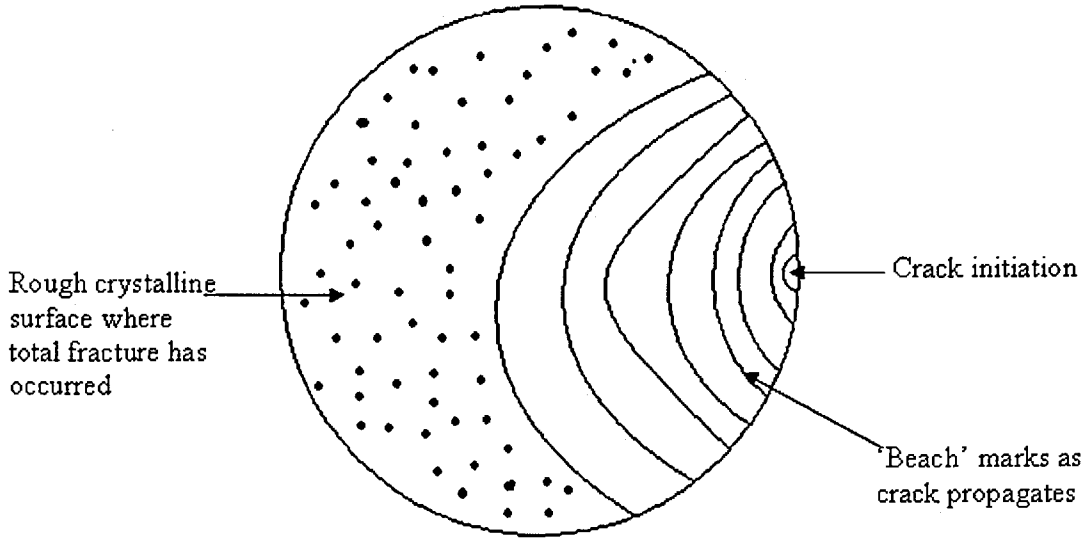

Figure 11. Schematic diagram of a typical fatigue fracture surface

The rate of fatigue crack initiation and propagation through the material depends on a number of factors. Surface defects including machine markings or welds will act as immediate stress concentrations and the materials may have internal defects such as inclusions both will affect the rate of initiation and propagation of a fatigue crack.

2.7.5 Factors Affecting Fatigue Properties

There are many potential factors that can affect the fatigue properties of engineering components. Fatigue failures generally occurs due to effects of the surface or sub surface of the material, or through the occurrence of stress concentrations in the material causing the local stress to be raised higher than the average stress of the component during test. Factors that can affect the fatigue properties of welded joints are geometrical, environmental and rotational.

2.7.5.1 Geometrical Factors

A change in the geometry of a component is one of the most common effects of fatigue and can be caused by cracks, notches or severe changes in cross section. Often the discontinuities are as a result of a design requirement or specification, the change in geometry will then cause uneven loading at the discontinuity of an otherwise evenly loaded component. The increase in stress concentration at the change in geometry will then allow a crack to nucleate and propagate through the component at the point of increased stress concentration[51].

Many engineering components are welded; an immediate change in geometry through the section of a component is evident if a weld is present. This change in geometry can have an effect on the performance of a component due to the added stress concentration at particular points particularly if the welded part is subjected to fatigue loading during the components life cycle.

For welds if the transition between the weld toe and the parent material is smooth then the stress concentration is likely to be low, however, in most cases of welding there is an abrupt change between the two components and therefore the stress concentration is likely to be high[53].

2.7.5.2 Environmental Factors

The conditions in which a fatigue test is carried out can often have an effect on the outcome. Work carried out by *Gough and Sopwith*[62] demonstrated that oxygen containing media and moist and aqueous environments will generally have a negative effect on fatigue life. Many fatigue tests are carried out in air to provide reference data for particular materials and components. During service many components can be exposed to other mediums, such as corrosive, elevated or low temperature environments.

Components may be subject to a corrosive environment whilst undergoing fatigue loading, the environment may produce negligible general corrosion of the structure, if there are cracks or crevices present then intensive localised attack can occur. Both fatigue loading and a corrosive environment can often cause more damage than if the two effects were imposed separately[53,51].

If a component or welded structure is subject to elevated temperatures then as a general rule the fatigue strength tends to decrease with an increase in temperature. If a component or welded structure is subjected to low temperature then the fatigue strength can increase. This is because at temperatures below ambient the rate of propagation of a fatigue crack is reduced thus increasing the fatigue strength. Alternatively, if the materials fracture toughness is reduced, to a point where the component can fail by brittle fracture from a fatigue crack early on in the test then the fatigue will be negatively effected[53].

2.7.5.3 Rotation

Previously, work using laser hybrid welding has been carried out on butt, lap and fillet joint configurations[14,15,22, 63 , 64] . Butt joints are more commonly used within the automotive industry especially for the manufacture of laser welded tailored blanks and both lap and butt joints were considered in previous work carried out at SHU. Therefore, lap and butt joints will be the main joint configurations considered in this study.

The lap joint configuration will cause the joint to be eccentrically loaded during mechanical testing, causing rotation of the joint. The mechanism of the rotation of the joint is outlined in Figure 12.

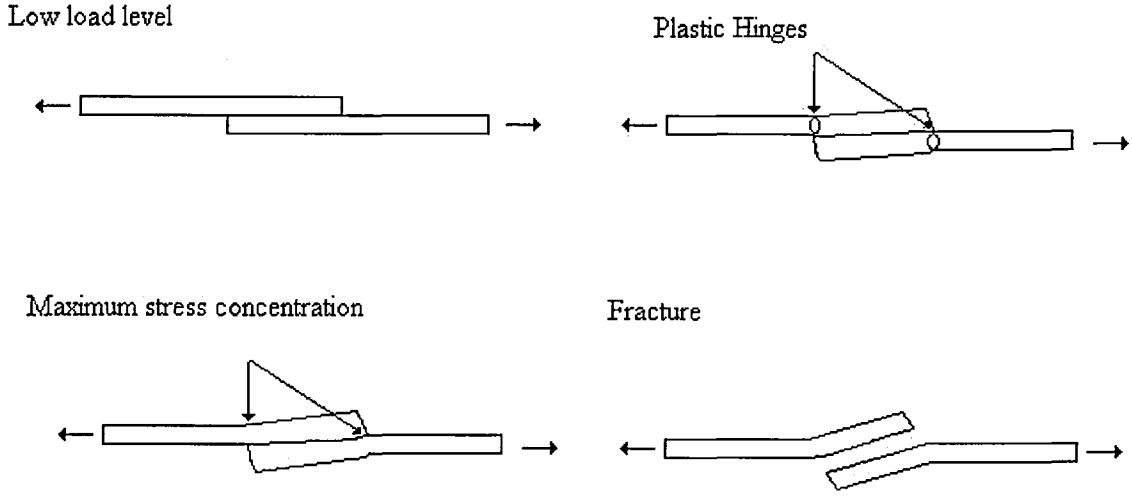

Figure 12. Deformation of lap joint during loading[65]

Figure 12 shows that from the moment of loading the lap joint will align itself so that the load will run through the centre of both plates.

Nordberg and McCann developed an analytical model to predict joint rotation using beam-bending theory[65]. The equation is shown below.

$$\theta = \frac{2 \cdot a}{E \cdot t^2} \cdot P$$

Equation 2. Rotation Angle Calculation

Where,

P =	Line Load	(N/mm)
a =	"free" half length of the specimens or sheets	(mm)
t =	sheet thickness	(mm)
θ =	rotation in radians	
E =	Elastic Modulus	(MPa)

However, in welds where dissimilar thickness base materials are used the average thickness needs to be calculated so:

$$t = \frac{t_1 + t_2}{2}$$

Equation 3. To calculate t for joints with dissimilar thickness base materials

Dinsley[66] considered this model during work regarding the fatigue life properties of dissimilar metal laser welded lap joints and concluded that the fatigue properties of the dissimilar lap joints were controlled by the severity of the stress concentration at the internal lap face and the early crack growth rate. It was also concluded that the severity of the stress concentration is directly linked to the applied load and rotation angle.

2.7.6 Fatigue Testing of Dissimilar Laser Hybrid Welded Joints

There is no current literature of fatigue properties of dissimilar laser hybrid welded joints, particularly stainless steel sheets joined to zinc coated mild steel. However, there has been research to determine the statistically valid mean fatigue properties of laser welds conducted by Dinsley[66] and resistance spots welds conducted by Marples[67] and Wray[68]. The results from these studies have also been reported in work by Nordberg[69] where adhesive bonding and clinched joints were also reviewed.

The results of the fatigue properties of the different joining techniques are presented in terms of line load. This is the applied load per unit length allowing comparisons of joints with different thicknesses on a line load bearing basis.

2.7.7 Fatigue Testing of Dissimilar Cold Metal Transfer Joints

Currently there is very little literature involving the Cold Metal Transfer process and even less, if at all, for the fatigue properties of the welds produced using the materials in this research.

2.8 *Effect of Weld Geometry on Fatigue Properties*

Geometry is one of the main factors for causing fatigue failure as discussed previously in section 2.7.5.1. When welded samples are fatigue tested any stress concentrations present will affect the outcome and more often than not the stress concentrations present in a welded samples are as a result of weld geometry[53]. Within the literature there have been many studies carried out predicting the relationship between weld geometry and fatigue life, often using Finite Element Analysis to assist in the modelling[70, 71].

Teng et al[72] proposed a mathematical model to predict the effect of butt weld geometrical parameters and residual stresses on the Fatigue Crack Initiation (FCI) life of butt welded joints. The weld geometry parameters considered were; weld toe radius, weld bead flank angle, preparation angle and plate thickness. Figure 13 below shows a schematic diagram of the critical weld parameters.

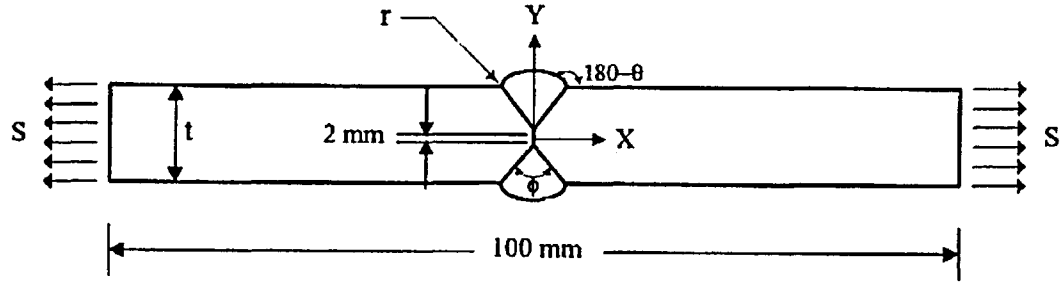

Where,

r = weld toe radius of a butt welded joint

t = plate thickness

θ = weld bead flank angle with surface

ø = weld preparation angle

Figure 13. Schematic diagram of weld geometry parameters[72]

The critical location for the weld and the initiation of fatigue failure is the weld toe, variations in this geometry will vary the stress concentrations accordingly. *Teng et al*[72] used Finite Element Analysis (FEA) to obtain local stress and residual stress distribution. Figure 14 below shows the effect of flank angle (θ) on the Fatigue Crack Initiation (FCI) life of the tested samples. The graph shows that the FCI increases as the value of flank angle decreases. This occurs because the stress concentration becomes more obvious with increasing flank angle therefore decreasing the fatigue strength of the specimen.

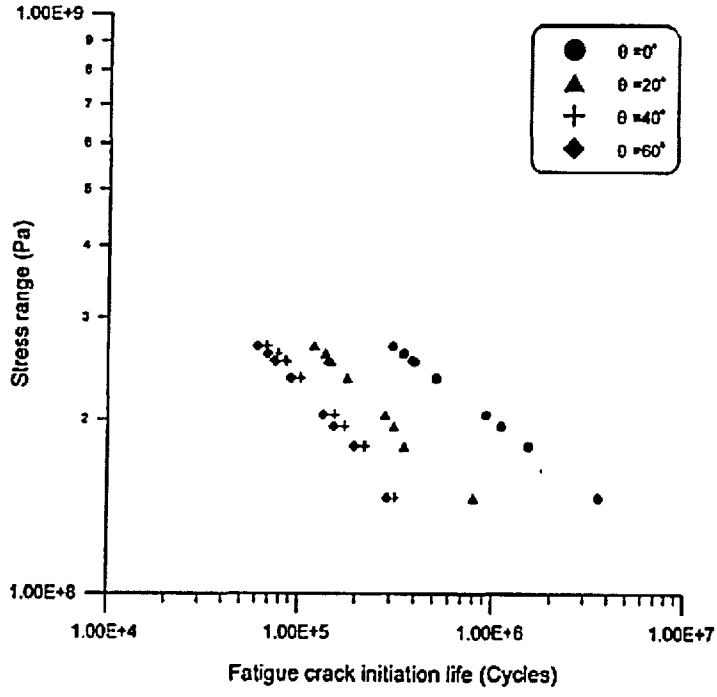

Figure 14. The effect of flank angle (θ) on the FCI life of tested specimens[722]

The fatigue life of a specimen can be controlled if the geometry and, in this case, the flank angle can be controlled. The main conclusions from this study were, that localised heating and rapid cooling during welding can cause tensile residual stresses at the weld toe of the butt joint. By controlling the weld geometry parameters the FCI can be improved and this can be done by increasing the weld toe radius, decreasing the flank angle or by carrying post-weld work for example grinding. Finally the more effective geometric change for increasing the FCI is to reduce the flank angle (θ)[722]

Nguuyen and Wahab[73]carried out a theoretical study of the effect of different parameters (the same as used in *Teng et al*[72]*)* of weld geometry on the fatigue life, the work used FEA and Linear Elastic Fracture Mechanics (LEFM) and the main conclusions drawn from this work were, the fatigue life and strength of butt joints can be improved by adapting one of the weld geometry parameters as follows; increase the radius of the weld toe (r), decrease the value of flank angle (θ), (it was also found that the best results were when the angle was below 20°), decrease the plate thickness (t), decrease the edge preparation angle (ø) or by eliminating weld toe undercut. The weld geometry of butt welds only affects the early stages of crack growth including crack initiation, it has little or no effect on the fatigue crack propagation.

2.9 *Summary of Literature Review*

As outlined in previous sections limited research has been carried out on LHW and CMT as joining processes and work has been carried out on dissimilar metal joining using other welding and joining techniques. Very little research has been carried out on LHW and CMT processes for dissimilar metal joining particularly high strength stainless steel to zinc coated mild steel.

Extensive research on the fatigue properties of welded joints has been taking place for many years, often resulting in the conclusion that the fatigue properties of a welded structure are directly related to the geometry of the resultant joint.

This research will assess the mechanical and metallurgical properties of dissimilar metal joining and determine a relationship between the fatigue properties and weld geometry. The research focuses on the relatively unexplored joining techniques of Laser Hybrid Welding and Cold Metal Transfer applied to joining high strength stainless steel to zinc coated mild steel. The joints are assessed in terms of tensile, fatigue and metallurgical properties.

3 Experimental Procedure

3.1 *Introduction*

Two experimental welding setups were used to produce the samples; one for the Laser Hybrid Welding and one for the Cold Metal Transfer process. The majority of the LHW work carried out in this research used the Laser Hybrid Welding equipment located at ESAB's Research and Development Laboratory, Gothenburg, Sweden. This was used for dissimilar joining for both butt and lap joint configurations.

The Cold Metal Transfer equipment was used for dissimilar joining in a butt joint configuration only. The specifics of the equipment can be found in sections 3.1.1 and 3.1.2 respectively.

Once weld optimisation had taken place for each technique samples were produced and mechanical and metallurgical tests were performed. The specifics of the testing and methodology used are outlined in the following sections.

3.2 *Weld Sample Geometry*

Figure 15 details the geometry of the welds produced using both LHW and CMT equipment.

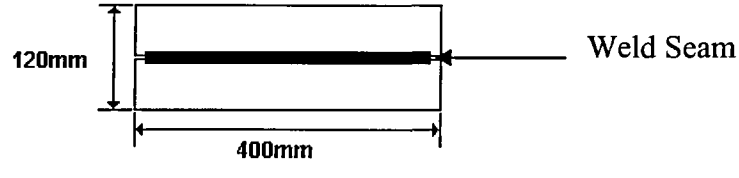

Figure 15. Butt Joint Configuration for Welds produced

3.3 *Laser Hybrid Welding*

ESAB Research and Development Laboratory, Gothenburg, Sweden provided the equipment used for the Laser Hybrid Welding. The hybrid system uses a laser welder and a GMAW welder simultaneously. The laser welder used was a Trumpf HLY006D 4kW industrial lamped pumped Nd: YAG laser. The GMAW used in the set up was an AristoMIG 500W. The system was fully automated and controlled using a KUKA IR 761 robot, figure 16 below shows the equipment setup.

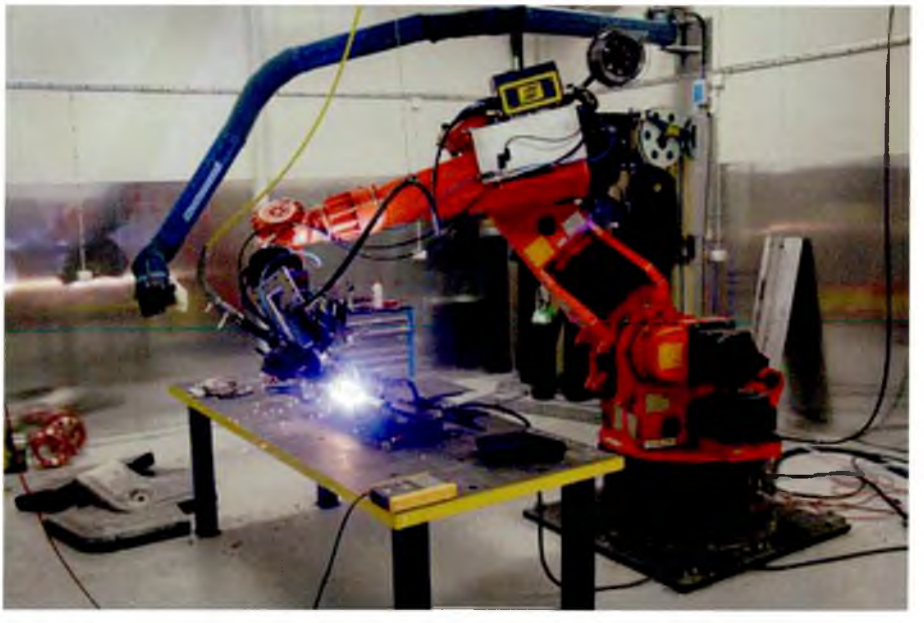

Figure 16. Laser Hybrid Welding Equipment at ESAB Process and Development Centre, Gothenburg, Sweden, April 2006.

3.3.1 Joint Geometry

Both butt and lap joint configurations were produced with the Laser Hybrid joining technique. Figures 17 and 18 show the joint setup.

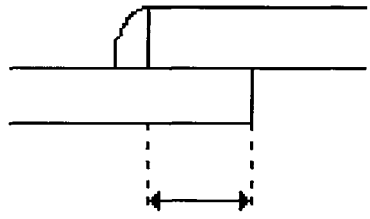

Figure 17. Lap Joint Configuration

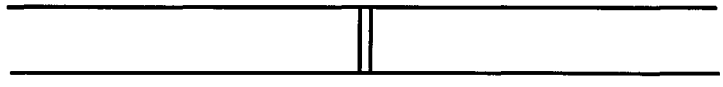

Figure 18. Butt Joint Configuration

Varying overlap lengths of 10mm, 20mm and 30mm were considered for lap joints for both LHW and CMT and for each material combination. After initial trials and previous work[66], it was decided that a 20mm overlap length would be the main focus for lap joints because this would allow comparisons to be made with previous work at SHU[66].

3.3.2 Weld Optimisation for Laser Hybrid Welded Butt Joints

Initial welding trials were carried out in order to find the optimum process window with regard to the production of dissimilar metal butt joints. The materials used in the initial weld optimisation were:

- HyTens 1000 (austenitic stainless steel) 1.5mm
- LDX 2101 (duplex stainless steels) 1.5mm
- Dogal 260RP-X (zinc coated mild steel) 1.5mm

The weld consumables used in the initial welding trials were:

- 308L-Si filler wire 1mm diameter
- 309L-Si filler wire 1mm diameter

The process parameters controlled during the weld optimisation stage were:

- Welding speed
- Wire feed speed
- Voltage

The focal length of the laser, which is distance from the focussing mirror to the work piece, was kept constant at 200mm, with a laser spot diameter of 0.6mm. The focus point for the laser was the middle of the joining line of the two materials.

For all samples the Laser led the GMAW torch in the position as outlined in the schematic diagram in figure 19 below, The inter distance, that's the distance between the laser point to the electrode tip was 2mm, with an electrode stick out of 16mm.

The shielding gas used was 98% Ar with 2% CO_2, which was fed through the GMAW torch at a flow rate of 24l/min.

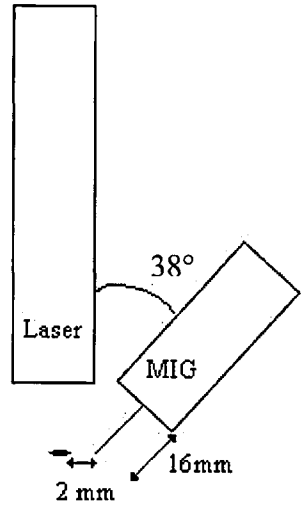

Figure 19. Schematic Diagram of Laser and GMAW setup for the Laser Hybrid Welding process

For the materials listed above the laser power was kept constant at 1.6kW. Initial optimisation for LHW produced good atheistically pleasing joints for the above combinations. These parameters were then transferred to the material below to optimise:

- HyTens 1000 (austenitic stainless steel) 0.75mm
- LDX 2101 (duplex stainless steels) 0.75mm
- Dogal 260RP-X (zinc coated mild steel) 1.5mm

The weld consumables used in the initial welding trials were:

- 308L-Si filler wire 1mm diameter
- 309L-Si Filler wire 1mm diameter

All the parameters were kept the same as above except for the laser power which was reduced to 1.5kW due to the thinner stainless material.

3.3.3 Weld Optimisation of Laser Hybrid Welded Lap Joints

Welding trials were carried out in order to find the optimum process window with regard to the production of dissimilar metal lap joints. The materials used in the initial weld optimisation were:

- HyTens 1000 (austenitic stainless steel) 1.5mm
- LDX 2101 (duplex stainless steel) 1.5mm
- Dogal 260RP-X (zinc coated mild steel) 1.5mm

The weld consumable used in the initial welding trials was:

- 308L-Si filler wire 1mm diameter

The material combinations initially tried included the zinc coated mild steel being used as the top sheet of the lap joint and as the bottom sheet, more success was found with the zinc coated mild steel being on the top of the lap joint with the relevant stainless grade as the bottom sheet. It remained this way throughout the remainder of the optimisation process.

The process parameters controlled during the weld optimisation stage were:

- Welding speed
- Wire feed speed
- Voltage
- Laser tilt angle
- Joint gap

The focal length, focal spot, laser diameter, equipment setup, electrode stick out, inter distance and shielding gas remained identical to the butt joint optimisation as described in section 3.3.2.

The major difference in the optimisation process for lap joints was the laser tilt angle, this is shown in figure 20 below, the angle was varied from the vertical position through 10° to 60° in 10° increments to try and improve the stability of the process.

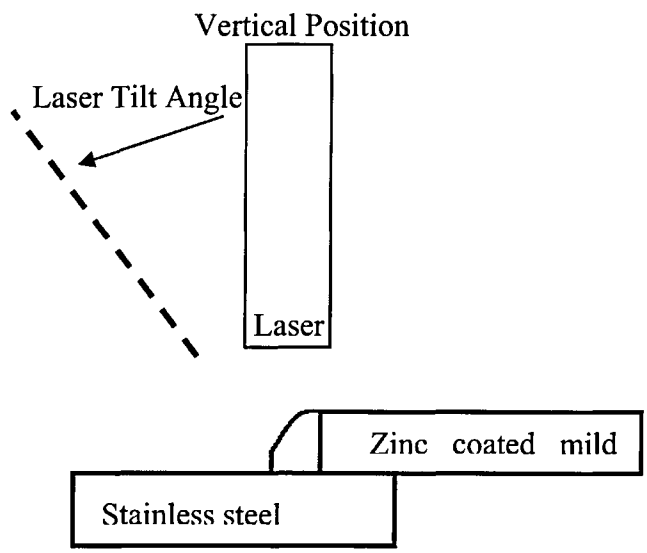

Figure 20. Schematic diagram for laser tilt angle for Laser Hybrid Welded lap joints

The zinc coating present during welding caused some initial problems with spatter and zinc related cracking, therefore during the optimisation stage a gap (see figure 21) of varying distance was introduced between the plates to try and eliminate this problem. The gap sizes attempted were 0.1mm, 0.2mm, 0.3mm, 0.4mm, 0.5mm and 1mm.

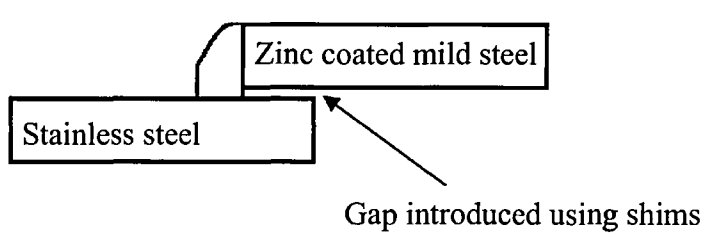

Figure 21. Schematic diagram to show where the gap was introduced between the plates during the Laser Hybrid Welding optimisation of lap joints

3.4 *Cold Metal Transfer*

Cold Metal Transfer equipment used in this research was located at Sheffield Hallam University. The CMT equipment consisted of a Fronius TransPulsSynergic 4000 CMT unit which was controlled using a Fronius RCU 500i control unit. The CMT equipment was then mounted onto a trolley and track robot system to allow the process to be semi - automated (figure 22).

Figure 22. CMT Welding Equipment at Sheffield Hallam University.

3.4.1 Weld Optimisation for Cold Metal Transfer Butt Joints

Initial welding trials were carried out in order to find the optimum process window with regard to the production of dissimilar metal butt joints using the CMT process. The criterion for the process was to produce joints with minimum spatter without surface breaking porosity and cracks. The materials used in the initial weld optimisation were:

- LDX 2101 (duplex stainless steels) 1.5mm
- Dogal 260RP-X (zinc coated mild steel) 1.5mm

The weld consumables used in the initial welding trials were:

- 308L filler wire 0.8mm diameter
- 308L-Si filler wire 1.0mm diameter

The process parameters controlled during the weld optimisation stage were:

- Welding speed
- Wire feed speed
- Arc Length Correction (ALC)
- Joint gap
- Shielding gas

Each parameter was varied accordingly in order to optimise the process for the joint configuration. The welding speed was varied from 0.508m/min to 1.524m/min, at increments of 0.250m/min. The wire feed speed was changed from 6.5m/min to 12.0m/min, at increments of 0.5m/min. The Arc Length Correction (ALC) value was varied between -30% and +30% at 5% increments and the plate gap was varied from 0.0mm to 0.7mm, at increments of 0.1mm.

Three different shielding gases were also tested, 100% Argon, 2.5% Carbon Dioxide with 97.5% Argon and 3% Oxygen with 97% Argon.

The effect of filler wire, shielding gas and ALC were considered in a separate study[74].

3.5 *Sample Identification*

For both the Laser Hybrid Welding (LHW) and Cold Metal Transfer (CMT), weld runs were produced and given relevant identification the following section outlines the nomenclature given to each type of series. All joints produced were marked with the relevant identification and the process parameters.

3.5.1 Laser Hybrid Welded Butt Joint Samples

Table 2 below outlines the joint combination and series identification for butt joints produced with the laser hybrid process.

Series ID	Material 1	Material 1 thickness (mm)	Material 2	Material 2 thickness (mm)	Filler Wire
1	LDX 2101	0.75	Zinc Coated Mild Steel	1.50	308L-Si
2	LDX 2101	1.50	Zinc Coated Mild Steel	1.50	308L-Si
3	Hy-Tens 1000	0.75	Zinc Coated Mild Steel	1.50	308L-Si
4	Hy-Tens 1000	1.50	Zinc Coated Mild Steel	1.50	308L-Si
5	LDX 2101	0.75	Zinc Coated Mild Steel	1.50	309L-Si
6	LDX 2101	1.50	Zinc Coated Mild Steel	1.50	309L-Si
7	Hy-Tens 1000	0.75	Zinc Coated Mild Steel	1.50	309L-Si
8	Hy-Tens 1000	1.50	Zinc Coated Mild Steel	1.50	309L-Si

Table 1. Series ID for Laser Hybrid Welded dissimilar butt joints

Each series had 8 weld runs, each weld run was number 1.1 - 1.8 etc, then 6 fatigue samples were taken from each run and number 1.1.1-1.1.8. Therefore the position of each sample was known by the number given to it.

All results for Laser Hybrid butt joints are denoted in relation to the series ID, e.g., T1 are the tensile properties for series 1, F2 are the Fatigue results for series 2 and H5 are the Hardness results for series 5 etc.

3.5.2 Laser Hybrid Welded Lap Joint Samples

A full matrix of test pieces were not produced for lap joints, due to the instability of the process, however, the samples produced during optimisation were all given a number denoted as TL1 - TL64, where TL is Test Lap.

3.5.3 Cold Metal Transfer Butt Joints

During the process optimisation stage samples were numbered 1-95. Only 1 combination of joints was tested for the CMT method using the optimised parameters of sample 94, twelve joints was produced for mechanical testing, and identified as C1.1 to C1.12.

Three tensile samples from each run were denoted as CT1.1.1 to CT1.1.3 and four fatigue samples were produced from each weld run were denoted are CF1.1.1 to CF1.1.4. Therefore the position of each sample was known by the identification given to it.

3.6 *Mechanical Testing*

The welded joints were assessed in terms of Tensile and Fatigue properties in order to determine the suitability of the joints for applications within the automotive industry.

Both tensile and fatigue specimens were water jet cut from welds produced as shown in figure 15, 50mm from each end of the welds was discarded therefore no start and finish point of the weld was included in a sample. The water jet diameter was 1mm with tolerances of ±0.2mm. Water jet cutting was chosen because of the zinc coating on the mild steel, any cutting process involving heat for example laser cutting, could have resulted in the zinc layer being removed. Methods for testing are outlined in the section below

3.6.1 Tensile Testing

Tensile testing was carried out on the parent materials to determine the ultimate tensile strength (UTS), 0.2% yield strength and percentage elongation to BS EN 10002-1:2001[75] for tensile testing of metallic materials at ambient temperature.

3.6.1.1 Tensile specimens

Parent material tensile specimens were machined to figure 23 below.

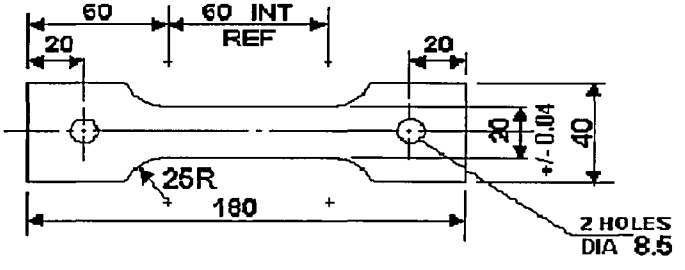

Figure 23. Tensile testing specimen for parent materials

Tensile testing was also carried out on welded specimens to determine the 0.2% yield strength, UTS and percentage elongation to BS EN 895:1995[76] for destructive tests on welds in metallic materials - transverse tensile test. The welded tensile specimens were water jet cut to figure 24.

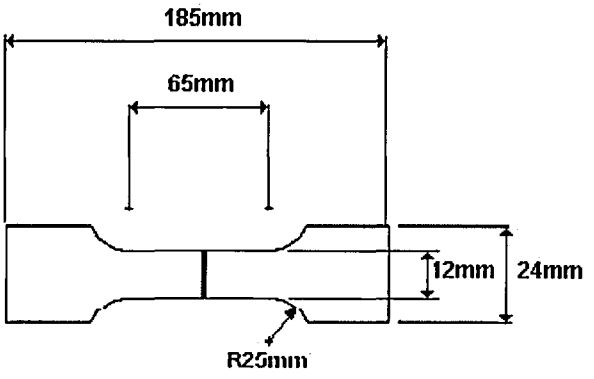

Figure 24. Tensile testing specimen for welded joints

3.6.1.2 Tensile Testing Equipment

Tensile testing for this project was carried out using an Instron 4206 uniaxial tensile machine fitted with a 150kN load cell. The Instron is connected to a dedicated PC, which records the test data, and all specimens were tested with a strain rate of $10mm.min^{-1}$.

For each test, load against extension was recorded until failure occurred. The data was then plotted and the UTS, yield strength and percentage elongation determined for each test.

For the welded sample failure could occur in three possible locations on the specimen, in either of the parent materials, through the welded joint or in the HAZ.

The results of the tensile tests will be used to calculate the joint efficiency of the welded joints produced by the novel techniques. The criteria set out for the tensile test is for the joint to be as strong as the weakest parent material.

3.6.2 Fatigue Testing

Fatigue testing was carried out on eight dissimilar metal laser hybrid welded (LHW) butt joint combinations. As explained in section 3.1.2 these joints were produced during welding trials at ESAB Process and Development Centre. Further fatigue testing was carried out on one series of Cold Metal Transfer butt joints.

The fatigue tests were carried out in air at room temperature. The tests were a pull-pull repeating sinusoidal stress cycle. The load ratio also known as the R-ratio (minimum load/maximum load) was 0.1. The fatigue test frequency was 25Hz. Which was selected in order to compare results with previous work[66]. The joints were tested for $2x10^6$ cycles and if a joint survived to this number then the test was deemed a "run out" and was terminated. Failure was determined as total sheet separation and as in previous work, the fatigue machines were set up to trip when >2mm actuator travel occurred.

Figures 25 and 26 below shows the specimen set up for the fatigue tests.

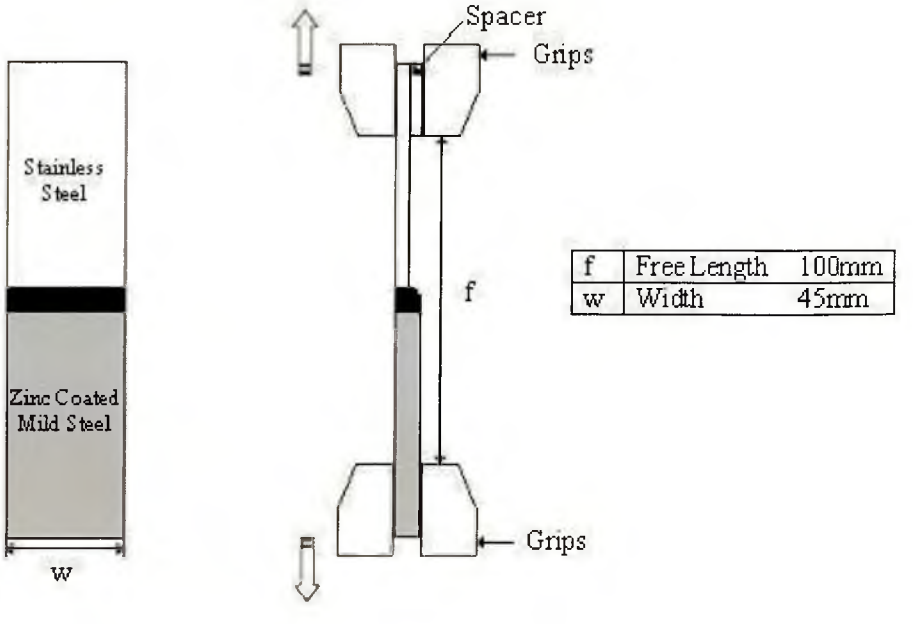

Figure 25. Schematic diagram showing dimensions and setup for dissimilar thickness fatigue tests

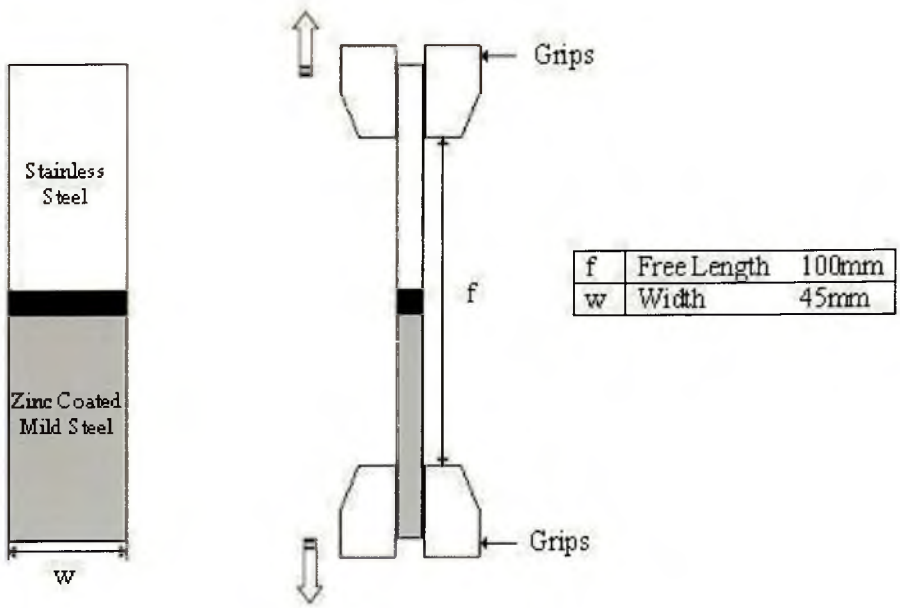

Figure 26. Schematic diagram showing dimensions and setup for similar thickness fatigue test

3.6.2.1 Staircase Fatigue method

The staircase fatigue method of testing was used to determine the statistically valid mean fatigue strength at $2x10^6$ cycles. Staircase fatigue testing is a method of testing by which the next test level for the next trial or group of trials depends on the results of the preceding trial or group of trials. Only one test is carried out at once and a starting level is usually around where 50% of the results are expected, therefore the test load is moved up an increment if a specimen survives the testing or moved down an increment if the specimen fails[77].

In order to carry out the staircase test, preliminary setup tests were conducted to give an indication of the first load level, the range of load and the step divide. For the initial tests load increments of 1.0kN was used. A load predicted by the operator (usually around the estimated fatigue load) was used for the first test, if the test failed then the load was reduced by 1.0kN, if the test survived then the load was increased by 1.0kN. This continued until upper and lower load limits were determined.

Once the upper and lower limits of the fatigue tests were determined, the load increments was reduced to 0.5kN and in later series the standard deviation calculated from the earlier tests of similar material combination were used. The tests were then carried out until each series had 25 tested samples.

Figure 27 below outlines an example of the table that the fatigue tests follow in order to carry out the relevant calculations. From the results the mean fatigue load, standard deviation, convergence factor and standard error for the mean fatigue strength were calculated as outlined below. The convergence factor determines whether the fatigue results are statistically valid.

Load Range (kN)	Step No. (i)	Test Specimen Number								Number of		Using LFE as N	
		1	2	3	4	5	6	7	8	Failures (f)	Runouts (r)	iN	i^2N
P_3	3			X						1	0	0	0
P_2	2		O		X		X			2	1	2	4
P_1	1	X				O		X		2	1	1	1
P_o	0								O	0	1	0	0
										Σf	Σr	ΣiN	Σi^2N
										5	3	3	5

X denotes a failure, O denotes a runout

Figure 27. Example of Staircase fatigue test table for data collection and the outlines the values needed for the relevant calculations

Calculated Mean Fatigue Strength:

$$x = P_0 + d\left(\frac{A}{N} \pm \frac{1}{2}\right)$$

When N = failure $+\frac{1}{2}$, when N = runout $-\frac{1}{2}$

Equation 4. Equation for Mean Fatigue Strength

Convergence Factor:

$$\left(\frac{(N*B)-A^2}{N^2}\right) => 0.3 or < 1.2 \text{ for statistical validity}$$

Equation 5. Equation for Convergence Factor

Standard Deviation:

$$s = 1.620 * d\left(\frac{(N*B) - A^2}{N^2} + 0.029\right)$$

Equation 6. Equation for Standard Deviation

Where,

x = Mean Fatigue Strength

s = standard deviation

P_o = Total Stress (kN) for step 0

N = Total number of Least Frequent Event (LFE) - failure or runout

d = step divide/load interval

A = $\sum i * N_i$

B = $\sum i^2 * N_i$

i = Step number

N_i = Number of failures in a step

Standard Error for the Mean Fatigue Strength

$$S_x = \frac{S}{\sqrt{n}} \cdot g$$

Equation 7. Equation for Standard Error of the Mean Fatigue Strength

Where,

s = Standard deviation

n = Total number of Least Frequent Event (LFE) - failure or runout

g = 1.15[57]

3.7 *Metallographic Examination*

Various metallographic techniques were carried out in order to characterise both the parent materials and dissimilar metal butt and lap joints. The metallographic techniques allowed the following to be determined:

- Microstructure
- Grain size analysis

For all the techniques the samples were prepared in conducting Bakelite, this allowed optical analysis, including microhardness, as well as Scanning Electron Microscope (SEM) examination to be carried out in characterising the samples.

3.7.1 Etching

A number of different etchants were used to aid visual examination of the parent materials and the welded samples. The etchants used for the stainless steels were more aggressive than those used for the zinc-coated mild steels, this was due to the requirement to remove the passive layer which naturally occurs on stainless steel and dissolves the corrosion resistant bulk material. Therefore, the etchants used for the stainless often over etched the mild steel. For the dissimilar metal welded samples two etchants were used, one to etch the zinc-coated mild steel then a second one to etch the stainless steel and the weld material.

Etchants used on the stainless steel varied depending on the grade. Electrolytic etches using 10% oxalic acid and 20% sodium hydroxide (NaOH) was used for the duplex grade 2101 to highlight the different phases of the material.

The austenitic grades of Hy-Tens 1000 and 301LN samples were electrolytically etched in 60% nitric acid (HNO_3) to reveal the grain boundaries.

2% Nital (a solution of nitric acid and alcohol) is the most common etchant for mild steel and was used to etch the grain boundaries and general microstructure of the material.

For the welded samples several different etchants were used, limited success was had due to the mild steel preferentially etching over the stainless steel similar to a sacrificial anode. Masking the less noble metal with petroleum jelly did help to facilitate some etching of the weld pool and stainless steel. One etchant of this kind was 15ml HCL, 10ml acetic acid, 5ml HNO_3, 15ml H_2O and 2 drops of glycerol. A successful etchant for the Cold Metal Transfer joints was metasulphate, which contains HCL.

3.7.2 Hardness Testing

Hardness values are a useful tool in determining material properties. Vickers hardness testing was carried out on the parent materials and microhardness examination was carried out on welded samples.

The Vickers hardness values were determined using a Vickers Armstrong Diamond Indent Machine with an applied load of 20kg.

Microhardness readings were taken across the welded joint on a sectioned sample. This was done using the Buehler Micromet® 2100 series microhardness machine. A load of 500g was used. Indentations were taken with increments of 0.50mm through the welded samples. Microhardness profiles through the centre of the sectioned welds in the vertical and traverse directions were carried out as shown in figures 28 and 29.

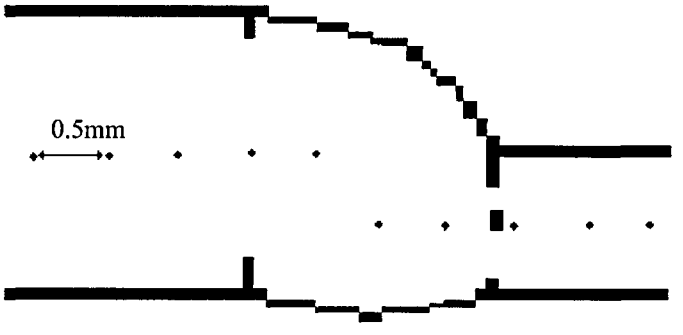

Figure 28. Microhardness Profiles (traverse and vertical) across a dissimilar thickness Laser Hybrid Butt Weld

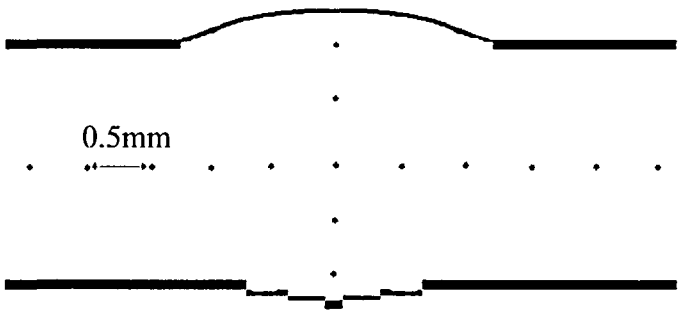

Figure 29. Microhardness Profiles (traverse and vertical) across a similar thickness Laser Hybrid Butt Weld

Microhardness maps were plotted in order to show any changes in microhardness across the weld pool and HAZ's, a grid of indentations were taken across the welded samples spaced 0.5mm apart. An example of the grid can be found in figures 30 and 31.

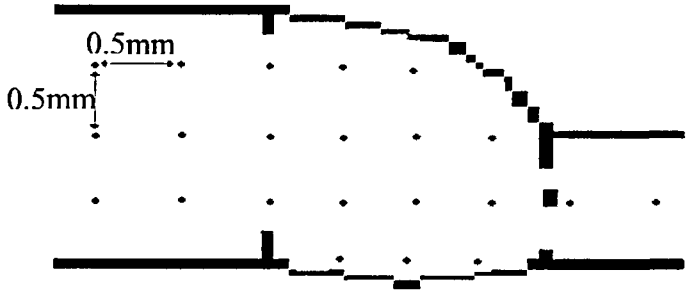

Figure 30. Microhardness Map (0.5mm) across a dissimilar thickness Laser Hybrid Butt Weld

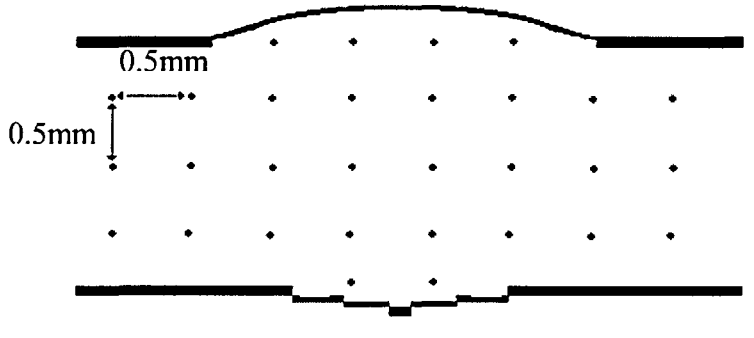

Figure 31. Microhardness Map (0.5mm) across a similar thickness Laser Hybrid Butt Weld

3.7.3 Grain Size Analysis

Grain size is represented by a number referred to as a ASTM Grain Size Number and originates from ASTM E112 - Standard test methods for determining Average grain Size.

There are different methods of determining the average grain size of steels, the Mean Linear Intercept Method (m.l.i) is also widely used.

The m.l.i is measured by counting the number of grain boundaries or grains that intercept a traverse line on a metallographic sample. The m.l.i is given by:

$$\bar{d} = \frac{L}{N}$$

Equation 8. Mean Linear Intercept

Where,

L =the length of line (mm)

N= the number of grain boundaries or grains

$\bar{d}$ in mm then relates to an ASTM grain size number from 00 – 12 as per table in BS EN ISO 643:2003.

Grain size analysis was carried out on the parent materials and within the heat affected zone (HAZ) of the welded specimens to assess the effect, if any, that the welding processes were having on the microstructure.

3.7.4 Optical Light Microscopy

Optical Light Microscopy was carried out to examine and characterise the microstructure of both the parent materials and welded joints, in addition to examination of the fracture surfaces of fatigue samples, root penetration angle measurements and heat affected zone grain measurements.

Equipment used includes a Carl Zeiss Photomicroscope and an Olympus Stereoscope with a Highlight 2000 Olympus light source. Both could be used with a Spot Insight Colour, Diagnostic Instrument digital camera to allow images to be taken by image analysis software through an attached PC.

3.7.4.1 Fatigue Failure Analysis

The fracture surfaces were examined and fatigue initiation sites identified using optical light microscopy, SEM analysis and video recording of fatigue tests for dissimilar thickness Laser Hybrid Welded joints using a webcam and laptop.

3.7.4.2 Heat Affected Zone (HAZ) Measurements

The width of the Heat Affected Zone was measured and the different joint combinations and processes were compared to each other. The samples were sectioned, polished and etched then viewed on an optical microscope with camera and PC attached and using image analysis software the width of the HAZ and grain size were measured.

3.7.4.3 Penetration Angle Measurements

As discussed in section 2.7.5.1 geometry is a critical factor in the fatigue performance of welded samples. Any change in geometry can influence early crack initiation on the weaker side of the weld. Therefore the angle (θ') between the bead root penetration and the mild steel were measured as shown in figure 32, this value was then subtracted from 180° as shown in equation 9 to give the true angle (θ) as demonstrated in figure 33. Angle θ was then compared to the fatigue result of each sample.

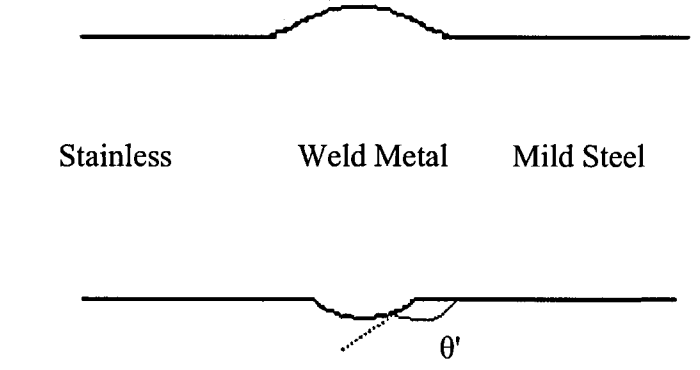

Figure 32. Diagram showing measured angle θ' for root angle penetration

Figure 33. Enlarged area of figure 21 showing desired angle θ

$$\theta = 180 - \theta'$$

Equation 9. Equation to calculate angle θ from measured angle θ'

3.7.5 Infinite Focus Microscopy

An Alicona Imaging Infinite Focus Microscope (IFM) at Sheffield Hallam University was employed to look more closely at the root penetration angle. An IFM microscope is an optical 3D measuring device which operates on varying focus combining the small depth of focus with an optical system with vertical scanning. A light source illuminates the samples on a motorised stage, the distance between the lens and the sample is varied and as this happens images are continuously captured to build up a 3D image of the specimen[78].

The IFM was used to produce 3D images of the weld profile both the front side (reinforcement) and the back side (root) of the weld, then surface profiles were carried out across the surface of the welds, looking at the shape of the weld bead and the angle at the root reinforcement. A selection of samples were chosen from each series of fatigue tests with varying number of cycles to failure and analysed in order to determine whether a relationship exists between the weld geometry and fatigue life. From each sample 3 surface profiles were taken, the root angle measured and then the average calculated per sample.

3.7.6 SEM Examination

SEM examination was carried out on a Philips XL40 Scanning Electron Microscope, which incorporates Energy Dispersive X-ray (EDX) Analysis for quantitative and qualitative chemical analysis. Both secondary and backscattered electron-imaging modes were use to record images of the samples and fracture surfaces.

3.7.6.1 Weld Bead Chemical Compositions

For each series of joints tested the weld bead chemical compositions were semi-quantitatively analysed in order to plot the Schaeffler diagrams for each material combination. The weld bead was imaged in its entirety using secondary electron-imaging an area in the upper region of the weld pool was highlighted and magnified and 3 spot analysis were carried out using EDX analysis to identify the elements present in weld bead, the area was then scanned to give the percentage of each element present. The elements scanned for were Fe, Cr, Ni, Mn and Si and an average of the 3 readings was taken. The process was repeated for an area in the middle part of the weld bead and the lower region.

This method of chemical analysis does not give values for C and N for each sample. Therefore values for C and N were calculated using the dilution equation outlined below.

$$D = \frac{(Cw - Cp)}{Cf - Cp}$$

Therefore,

$$Cw = Cp + D(Cf - Cp)$$

Where;

D = Dilution

Cw = Composition of weld

Cf = Composition of filler material

Cp = Composition of parent material

Equation 10. Dilution equation for calculating carbon values for each joint combination

The results were used to calculate the Nickel and Chromium (equations 11 and 12 below) equivalents to enable weld bead constitution to be assessed from the Schaeffler diagram.

$$\text{Chromium equivalent} = \%Cr + 1.5x\%Si + \%Mo$$

Equation 11. Chromium equivalent equation

$$\text{Nickel equivalent} = \%Ni + 30x(\%C + \%N) + 0.5x(\%Mn + \%Cu + \%Co)$$

Equation 12. Nickel equivalent equation

3.7.6.2 Elemental Mapping

Elemental mapping was carried out using the EDAX analysis on the Philips XL 40 SEM in order to assess the chemical composition of the weld and the distribution of elements throughout weld pool. This was to assess the chemical homogeneity of the weld pool during welding for the two different techniques.

4 Results

The following section outlines the results and analysis of experimental work for the research.

4.1 *Material Characterisation*

Two grades of high strength stainless steel, an austenitic grade and a duplex grade were joined to zinc coated mild steel. Grades and thickness of the materials used were:

Austenitic Stainless Steels

- HyTens 1000 (EN 1.4310, BS 301S21), with a thickness of 0.75mm and 1.5mm

Duplex Stainless Steel

- LDX 2101 (EN 1.4162), with a thickness of 0.75mm and 1.5mm, with a 2D finish

Zinc Coated Mild Steel

- SSAB Z100 Hot Dip Galvanised Mild Steel (Dogal 260RP-X), with a thickness of 1.5mm

Two 1mm diameter welding wires were used for joining the parent materials

- 309L-Si
- 308L-Si

4.1.1 Parent Materials

The chemical and mechanical properties of the parent materials used are outline in tables 3 to 10 below.

4.1.1.1 Chemical Composition

This section outlines the specified chemical compositions for the grades as well as the measured chemical composition for all the parent materials tested. Chemical analysis was carried out using the Spark Emission process.

Austenitic HyTens 1000 Stainless Steel									
Element	**C**	**Si**	**Mn**	**P**	**S**	**Cr**	**Ni**	**Mo**	**N**
Specification (%)	0.10	-	-	-	-	17	7	-	-
Measured (%) Thickness 0.75mm	0.093	0.87	1.24	0.023	0.008	17.20	7.22	0.24	-
Measured (%) Thickness 1.50mm	0.095	0.99	1.22	0.027	0.008	17.18	7.28	0.26	-

Table 2. Hy-Tens 1000 Chemical Composition (Mass %)

Duplex LDX 2101 Stainless Steel									
Element	**C**	**Si**	**Mn**	**P**	**S**	**Cr**	**Ni**	**Mo**	**N**
Specification (%)	0.03	-	5	-	-	21.5	1.5	0.3	0.22
Measured (%) Thickness 0.80mm	0.045	0.68	5.41	0.024	0.008	21.2	1.52	0.23	2100 ppm
Measured (%) Thickness 1.50mm	0.046	0.70	5.38	0.024	0.008	20.9	1.51	0.24	2210 ppm

Table 3. LDX 2101 Chemical Composition (Mass)

Zinc Coated Mild Steel								
Element	**C**	**Si**	**Mn**	**P**	**S**	**Cr**	**Ni**	**Mo**
Specification (%)	0.04	0.01	0.30	0.06	0.01	-	-	-
Measured (%) Thickness1.50mm	0.02	<0.2	0.21	0.068	0.009	0.07	0.06	0.02

Table 4. Hot-Dip Galvanised Mild Steel Chemical Composition (Mass %)

4.1.1.2 Mechanical Properties

This section outlines the mechanical properties of the parent materials in terms of tensile properties and hardness.

Austenitic Hy-Tens 1000 Stainless Steel				
	UTS (MPa)	**0.2%Proof Stress (MPa)**	**% Elongation**	**Hardness (Hv) Load 1kg**
Specification	1000	750	30	-
Measured Thickness 0.75mm	1111	735	32	345
Measured Thickness 1.5mm	1149	850	32	381

Table 5. Mechanical properties of HyTens 100 stainless steel, 0.75mm and 1.5mm

Duplex LDX 2101 Stainless Steel				
	UTS (MPa)	**0.2% Proof Stress (MPa)**	**% Elongation**	**Hardness (Hv) Load 1kg**
Specification	700	480	38	-
Measured Thickness 0.75mm	810.9	565.8	31.4	242
Measured Thickness 1.5mm	785.7	548.4	32.8	261

Table 6. Mechanical properties of LDX 2101, 0.75mm and 1.5mm

Zinc Coated Mild Steel				
	UTS (MPa)	**0.2% Proof Stress (MPa)**	**% Elongation**	**Hardness (Hv) Load 1kg**
Specification	380-460	260-320	28	-
Measured Thickness 1.5mm	402	280	30	144

Table 7. Mechanical properties of hot dip galvanised mild steel

4.1.1.3 Zinc Coating

The mild steel sheets had been hot-dip galvanised to the SSAB Z100 specification. Table 9 below outlines this specification in terms of coating thicknesses and zinc mass per unit area. The mass per unit area is based on a density of 7.14g/m^2. Measurements were taken to confirm the specification; it was done using an elcometer thickness gauge, which estimates the thickness of the zinc coating. Two samples were tested both back and front and 5 readings were taken across the samples on the front and back sides, the results can be found below in table 10.

Zinc Coated Mild Steel			
	Weight determination on two sides, (g/m^2)		Coating thickness per side (µm)
Specification	Triple-Spot test (min)	Single-Spot test (min)	Nominal
Z100	100	85	7

Table 8. Zinc coating specification thickness and mass for the mild steel

Sample/Side	Mean Thickness (µm)	Standard Deviation (µm)
A1 (top side)	5.2	0.53
A2 (underside)	6.6	1.73
B1 (top side)	5.9	0.87
B2 (underside)	7.1	1.14

Table 9. Zinc coating measurements using a thickness gauge.

4.1.1.4 Metallurgy

The parent materials were etched in order to reveal the as received microstructures which can be seen in figures 34 to 37.

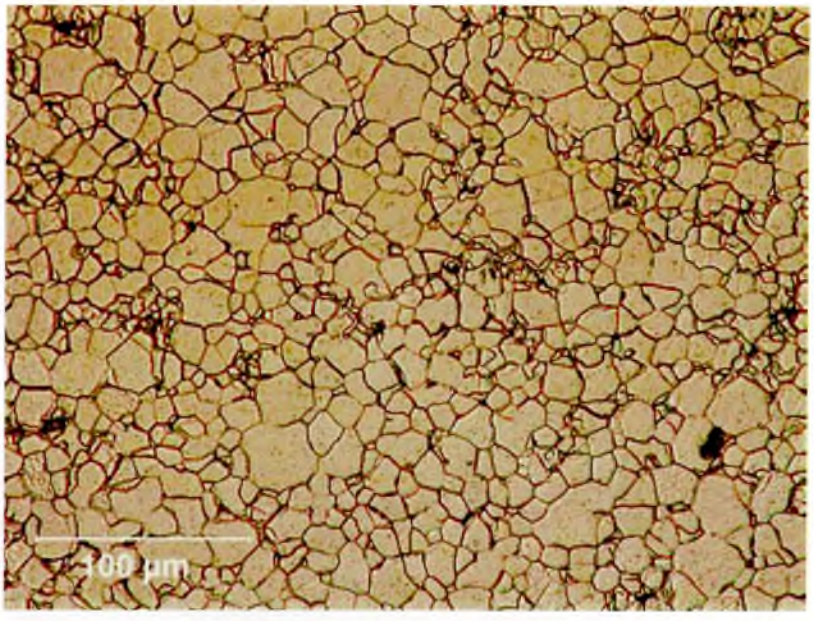

Figure 34. Mild steel as received microstructure etched 2% nital

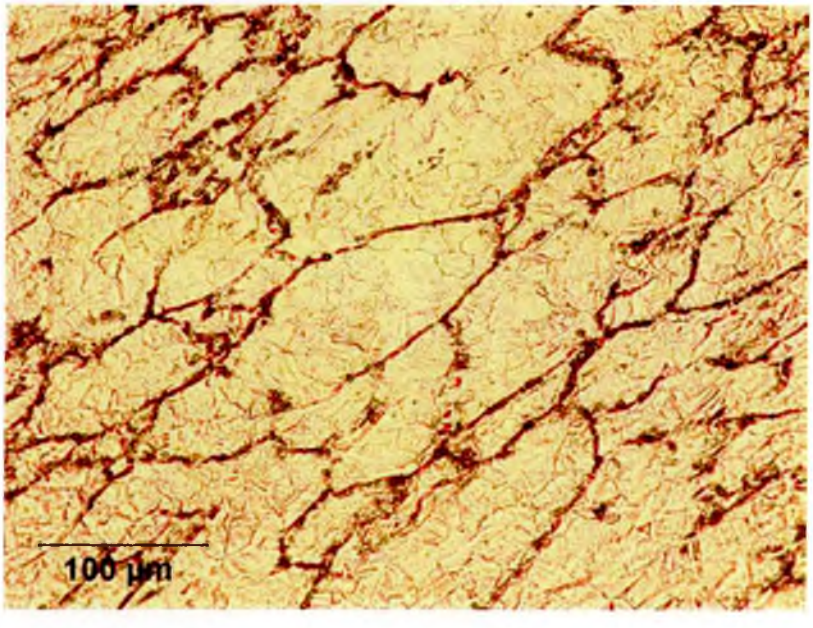

Figure 35. Hy-Tens 1000 stainless steel as received microstructure etched 60% nitric acid

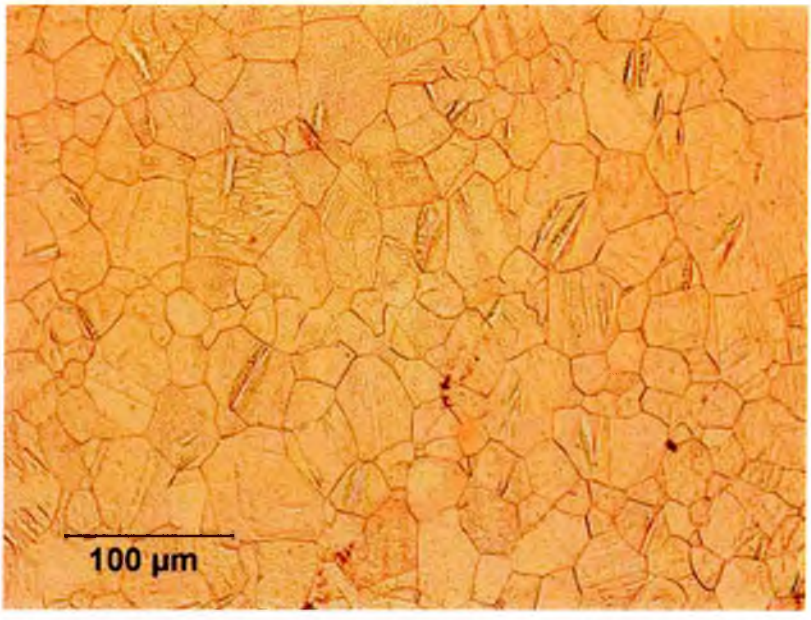

Figure 36. 301LN Stainless steel as received microstructure etched 60% nitric acid

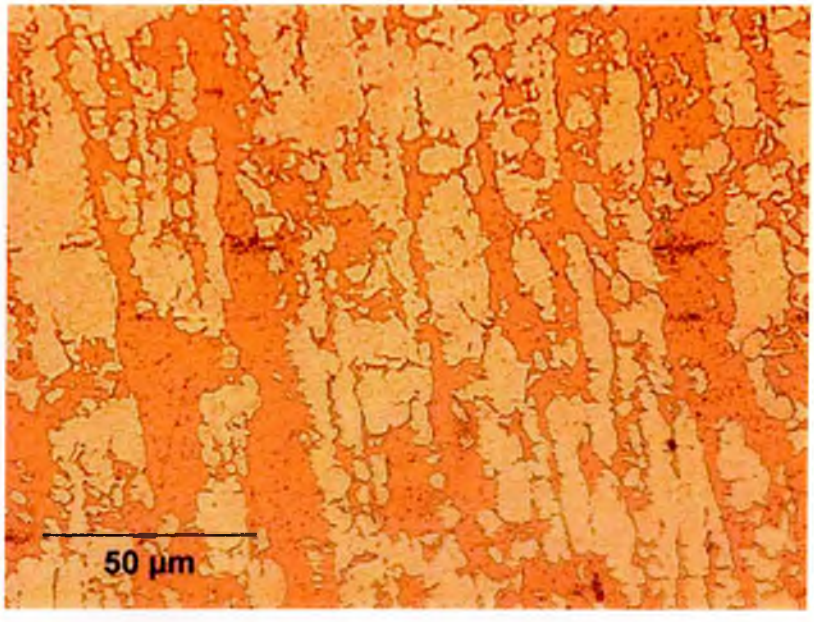

Figure 37. LDX 2101 stainless steel as received microstructure using electrolytic etch 20% sodium hydroxide

4.1.2 Filler Wires

The welding filler wires used for this project were 308L-Si and 309L-Si the chemical composition and mechanical properties of each wire are outlined in tables 11 and 12.

Wire	C (%)	Si (%)	Mn (%)	Cr (%)	Ni (%)
308L-Si	0.02	0.85	1.8	20.0	10.5
309L-Si	0.02	0.80	1.8	23.5	13.5

Table 10. Chemical compositions of filler wires

Wire	0.2% Proof Stress (MPa)	UTS (MPa)	Elongation (%)	Hardness (Hv) Load 1kg
308L-Si	420	600	36	208
309L-Si	400	600	32	208

Table 11. Typical mechanical properties of filler wires

4.1.3 Schaeffler-Delong Diagrams for Material Combinations

Outlined below are Schaeffler-Delong diagrams for the material combinations used in this research. From previous research and general literature values of dilution, (where dilution is the percentage of parent metal melted,) is approximately 30%-40% for a standard butt joint with filler wire[66].

For the purposes of the Schaeffler diagrams (figures 38-41) 35% dilution has been assumed which is made up of the two base materials which will represent 50% each (denoted as filled in circle on diagram) of the 35%. The red diamond on the Schaeffler diagram is where the predicated weld microstructure should be for all material combinations in this work. The Schaeffler diagrams apply to both Laser Hybrid Welding and Cold Metal Transfer.

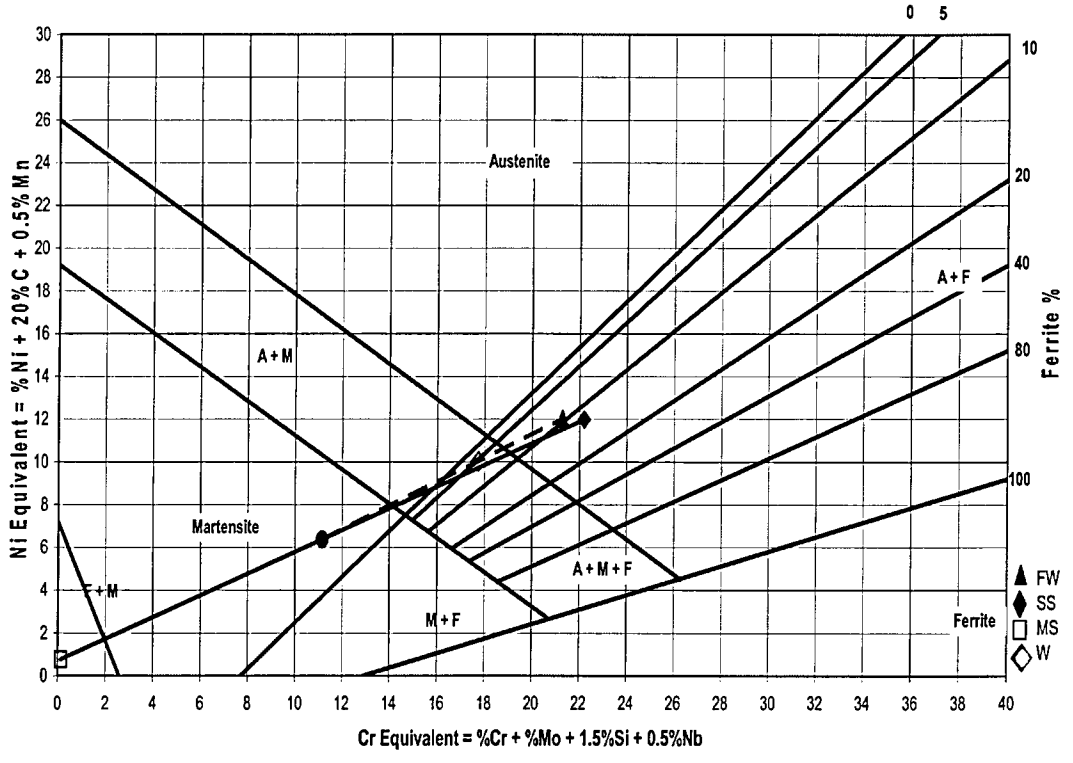

Figure 38. Schaeffler-Delong Diagram for Stainless LDX 2101 and Zinc Coated Mild Steel using 308L-Si filler wire

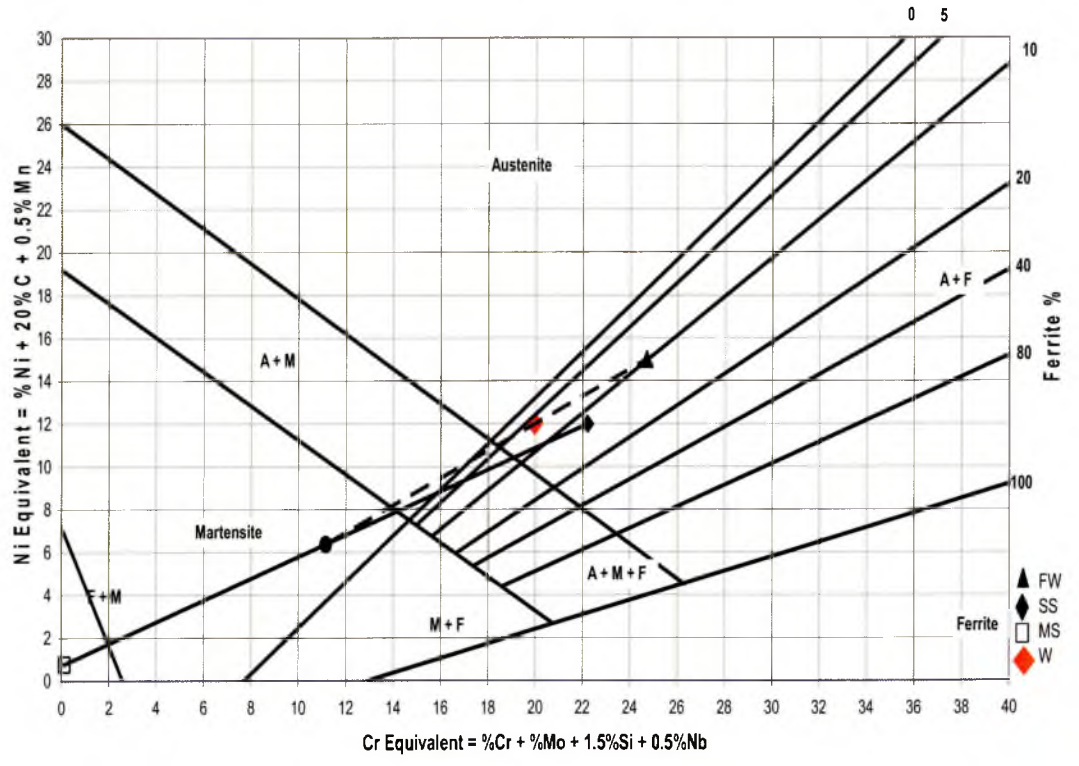

Figure 39. Schaeffler-Delong Diagram for Stainless LDX 2101 and Zinc Coated Mild Steel using 309L-Si filler wire

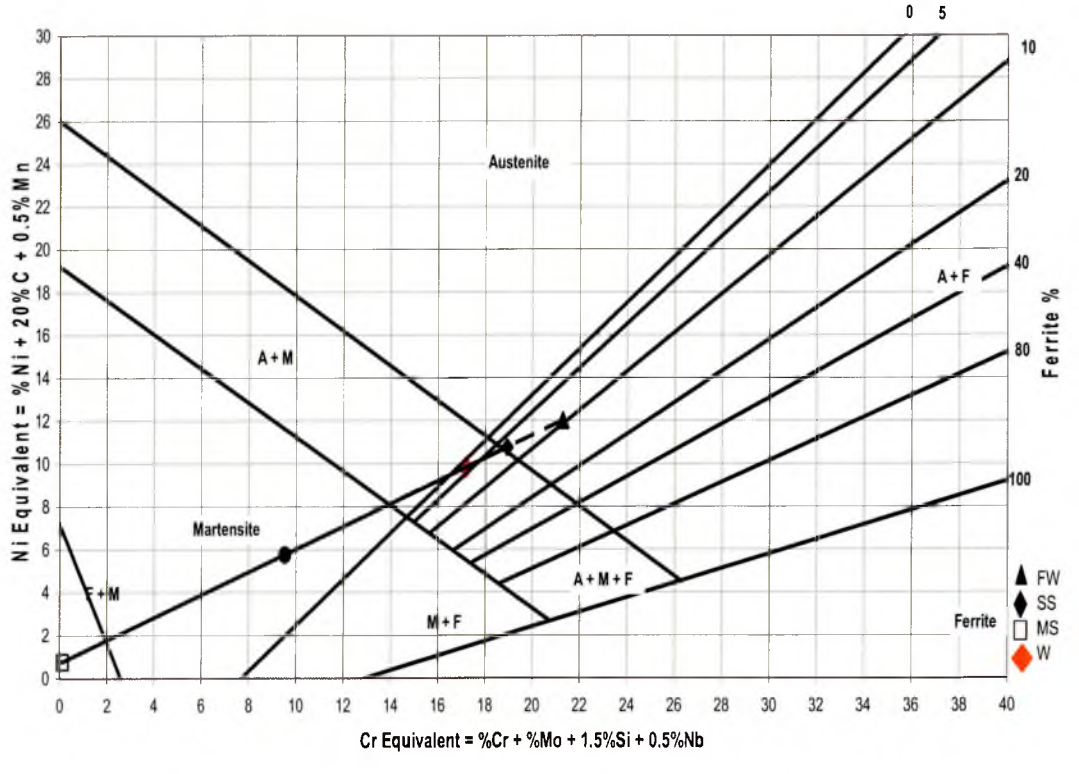

Figure 40. Schaeffler-Delong Diagram for Stainless Hy-Tens 1000 and Zinc Coated Mild Steel using 308L-Si filler wire

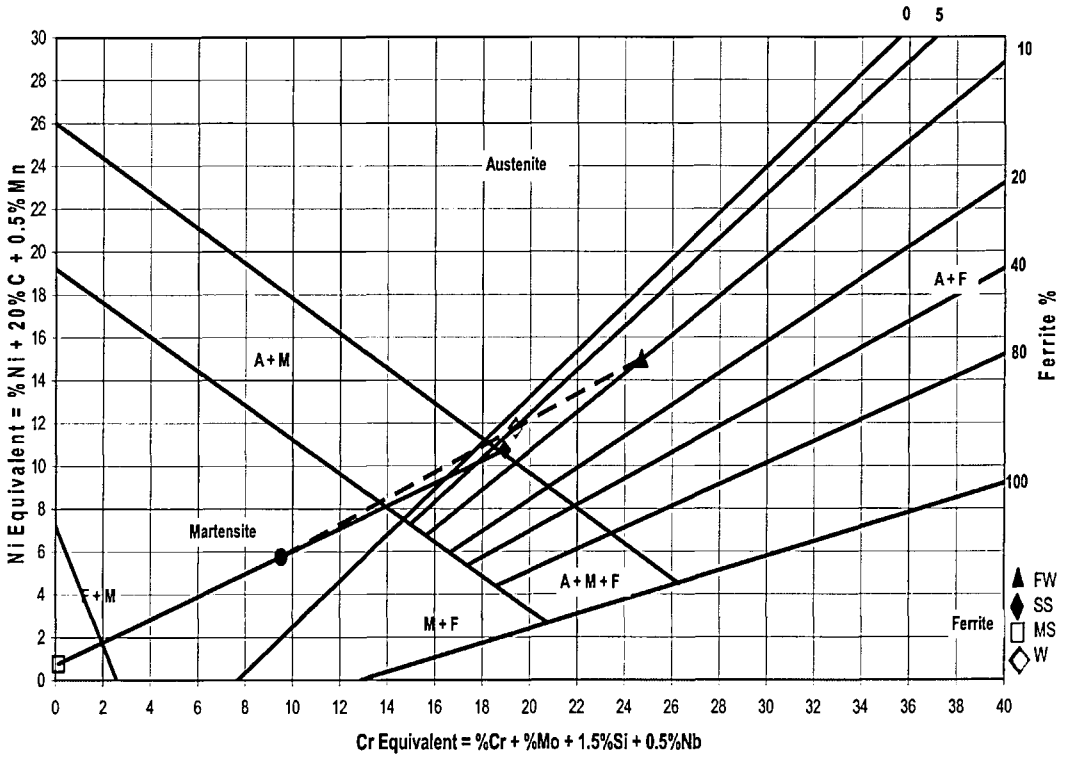

Figure 41. Schaeffler-Delong Diagram for Stainless Hy-Tens 1000 and Zinc Coated Mild Steel using 309L-Si filler wire

4.2 *Laser Hybrid Welded Butt Joints*

In order to optimise the process parameters initial butt joint trials took place at ESAB Process and Development Centre in Gothenburg, 16 welds were produced using the Hytens 1000 material and LDX 2101 to zinc coated mild steel joined with filler wires 308L-si and 309L-si.

Tables 13 and 14 below show the parameters for each combination of material and filler wires.

The welds were then tested in terms of tensile, fatigue, microhardness and the weld metallurgy and the results are outlined in the following sections.

Sample Number	Material	Thickness (mm)	Laser Power (kW)	Wire Feed Speed (m/min)	Voltage (V)	Welding Speed (m/min)	Measured Values					
							Laser Power (kw)	Current (A)	Voltage (V)	Weld Distance (mm)	Time (s)	MIG Heat Input (KJ/mm)
T1	LDX 2101	0.80	1.5	4.6	15.8	3.0	1.47	94.92	15.44	350	6.9	0.02
T1	LDX 2101	0.80	1.5	4.6	15.8	3.0	1.47	94.92	15.44	350	6.9	0.02
T2	LDX 2101	1.50	1.6	4.6	15.8	3.0	1.49	95.77	15.40	350	6.9	0.02
T2	LDX 2101	1.50	1.6	4.6	15.8	3.0	1.49	95.77	15.40	350	6.9	0.02
T3	Hy-Tens 1000	0.75	1.5	4.6	15.8	3.0	1.47	95.15	15.44	350	6.8	0.02
T3	Hy-Tens 1000	0.75	1.5	4.6	15.8	3.0	1.47	95.15	15.44	350	6.8	0.02
T4	Hy-Tens 1000	1.50	1.6	4.6	15.8	3.0	1.5	96.21	15.41	360	7.2	0.02
T4	Hy-Tens 1000	1.50	1.6	4.6	15.8	3.0	1.5	96.21	15.41	360	7.2	0.02

Table 12. Butt Joint Configurations of LDX 2101 Joined to 1.5mm Galvanised Mild Steel (SSAB) using 1mm 308 Filler and 98%Ar + 2%Co_2 Shielding Gas

Series ID	Material	Thickness (mm)	Laser Power (kW)	Wire Feed Speed (m/min)	Voltage (V)	Welding Speed (m/min)	Measured Values					
							Laser Power (kw)	Current (A)	Voltage (V)	Weld Distance (mm)	Time (s)	MIG Heat Input (KJ/mm)
T5	LDX 2101	0.80	1.5	4.6	15.8	3.0	1.48	95.64	15.38	360	7.2	0.02
T5	LDX 2101	0.80	1.5	4.6	15.8	3.0	1.50	96.43	15.27	370	7.3	0.02
T6	LDX 2101	1.50	1.6	4.6	15.8	3.0	1.51	97.57	15.32	370	7.3	0.02
T6	LDX 2101	1.50	1.6	4.6	15.8	3.0	1.46	94.67	15.20	380	7.7	0.02
T7	Hy-Tens 1000	0.75	1.5	4.6	15.8	3.0	1.46	94.33	15.22	380	7.7	0.02
T7	Hy-Tens 1000	0.75	1.5	4.6	15.8	3.0	1.51	96.57	15.34	370	7.3	0.02
T8	Hy-Tens 1000	1.50	1.6	4.6	15.8	3.0	1.52	97.73	15.17	380	7.7	0.03
T8	Hy-Tens 1000	1.50	1.6	4.6	15.8	3.0	1.53	97.53	15.38	380	7.7	0.02

Table 13. Butt Joint Configurations of HyTens 1000 Joined to 1.5mm Galvanised Mild Steel (SSAB) using 1mm 309L Filler and 98%Ar + 2%Co_2 Shielding Gas

4.2.1 Tensile Testing Results for Laser Hybrid Butt Joints

All laser hybrid butt joints samples were tensile tested using an Instron tensile testing machine, figures 42 and 43 along with table 15 outline the results below.

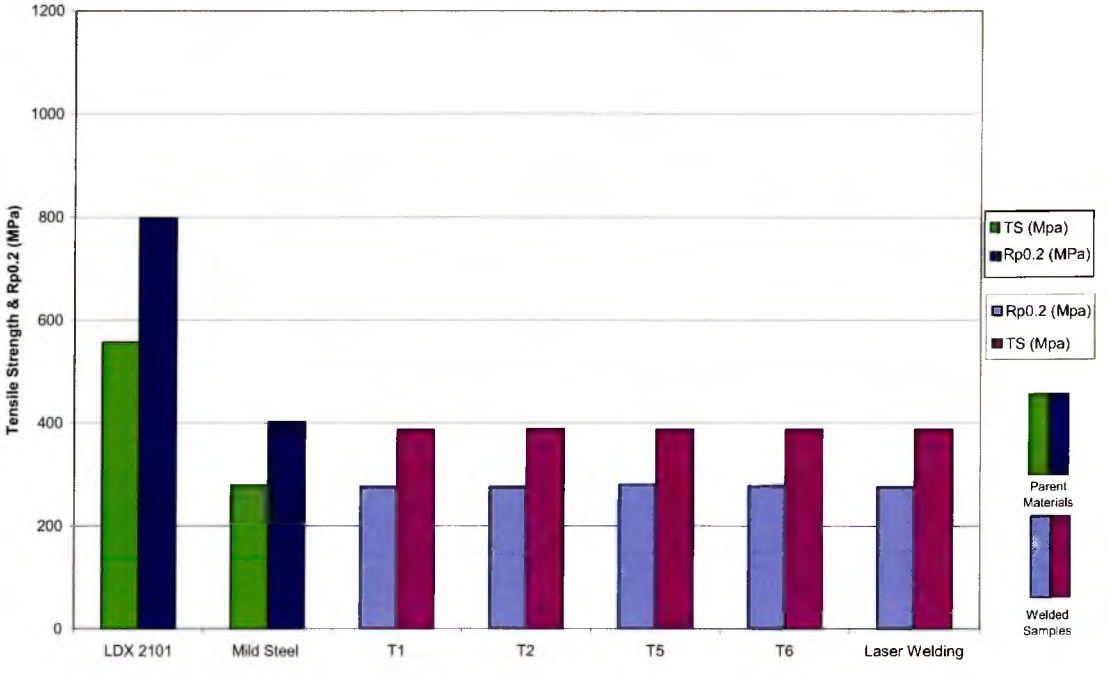

Figure 42. The results of tensile testing (UTS and $R_{p0.2}$) of LHW dissimilar metal butt joints using LDX 2101 and zinc coated mild steel

See table 15 for details of weld joint configuration and filler wire used in figure 42. The UTS and $R_{p0.2}$ for both parent materials are also shown along with equivalent laser welds for reference.

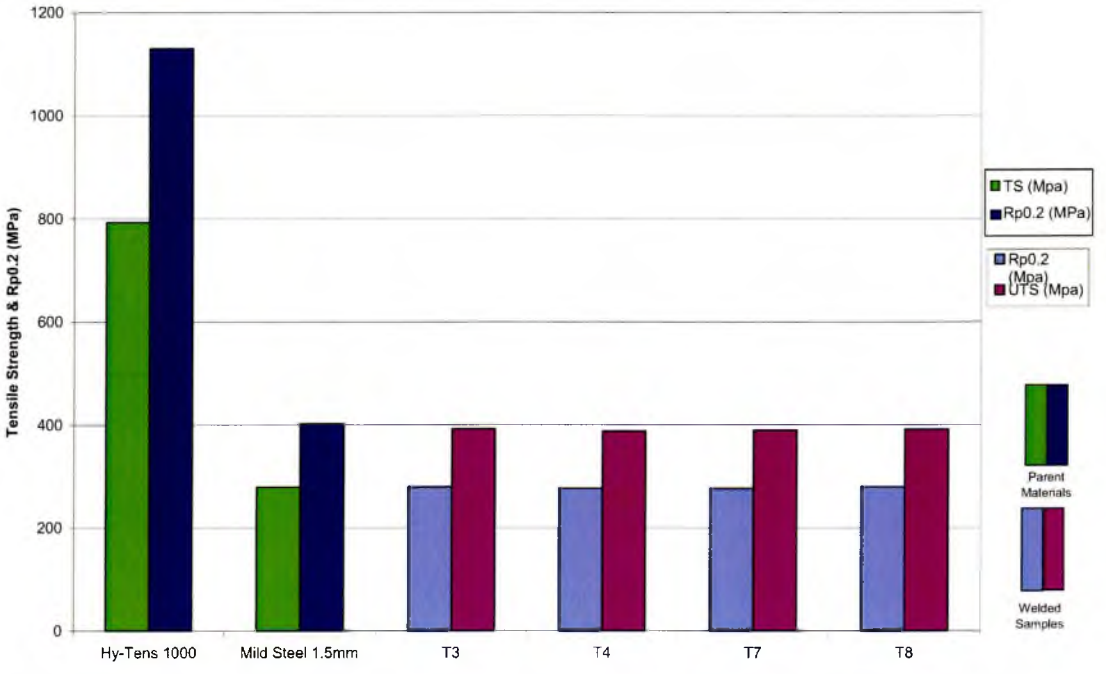

Figure 43. The results of tensile testing (UTS and $R_{p0.2}$) of LHW dissimilar metal butt joints using HyTens 1000 and zinc coated mild steel

See table 14 for details of weld joint configuration and filler wire used in figure 43. The UTS and $R_{p0.2}$ for both parent materials are also shown along with equivalent laser welds for reference.

Sample ID	Material 1	Material 2	Filler Wire	Max Load (KN)	CSA (mm^2)	Elongation (%)	UTS (MPa)	0.2% Proof Stress (MPa)
T1	LDX 2101 0.8mm	Mild Steel 1.5mm	308 1mm	7.0	15.0	19.5	385.7	276.5
T2	LDX 2101 1.5mm	Mild Steel 1.5mm	308 1mm	7.0	18.0	16.3	388.8	275.6
T3	Hy-Tens 1000 0.75mm	Mild Steel 1.5mm	308 1mm	7.0	18.1	16.8	389.5	276.2
T4	Hy-Tens 1000 1.5mm	Mild Steel 1.5mm	308 1mm	7.1	18.1	18.0	391.9	279.5
T5	LDX 2101 0.8mm	Mild Steel 1.5mm	309L 1mm	7.0	18.0	20.1	387.9	280.5
T6	LDX 2101 1.5mm	Mild Steel 1.5mm	309L 1mm	7.0	18.1	16.2	387.0	277.4
T7	Hy-Tens 1000 0.75mm	Mild Steel 1.5mm	309L 1mm	7.0	15.0	17.9	391.2	279.6
T8	Hy-Tens 1000 1.5mm	Mild Steel 1.5mm	309L 1mm	7.0	15.0	16.2	387.7	276.3

Table 14. Tensile test results for laser hybrid welded butt joints

4.2.2 Fatigue Results of Laser Hybrid Welded Butt Joints

Fatigue tests were carried out using the staircase method as described in chapter 3.6.2. A staircase was carried out for each of the 8 series of welds produced using the Laser Hybrid process. The results have been spilt into LHW using the LDX 2101 stainless steel, so series 1, 2, 5 and 6, and those produced using the HyTens 1000 material, series 3, 4, 7 and 8.

The fatigue tests were carried out on 4 fatigue machines, Table 15 below outlines the model of the testing machine, the location and the software operating system. Figures 44 to 47 below show each machine setup with a test running.

Machine	Software	Load Capacity	Load Range	Location	Series Tested
ESH Servo with Rubicon Controller	Rubicon	250kN	25kN	Sheffield Hallam University	F1,F6, F7 and C1
Instron 8516 and controller 8500+	Cyclic version 17.7	100kN	25kN	Outokumpu Avesta Research Centre	F4, F3
Instron 8502 and controller 8500+	Cyclic version 17.7	100kN	25kN	Outokumpu Avesta Research Centre	F2
Dartec M1000/RK with Inston controller 8500+	Cyclic version 17.7	100kN	25kN	Outokumpu Avesta Research Centre	F5, F8

Table 15. Outline of fatigue machines used during testing programme

Figure 44. *Instron 8516 and Instron console 8500+ with software Cyclic version 17.7 at Outokumpu Avesta Research Centre, Avesta, Sweden.*

Figure 45. *Instron 8502 and Instron console 8500+ with software Cyclic version 17.7 at Outokumpu Avesta Research Centre, Avesta, Sweden.*

Figure 46. *Dartec M1000/RK and Instron console 8500+ with software Cyclic version 17.7 at Outokumpu Avesta Research Centre, Avesta, Sweden*

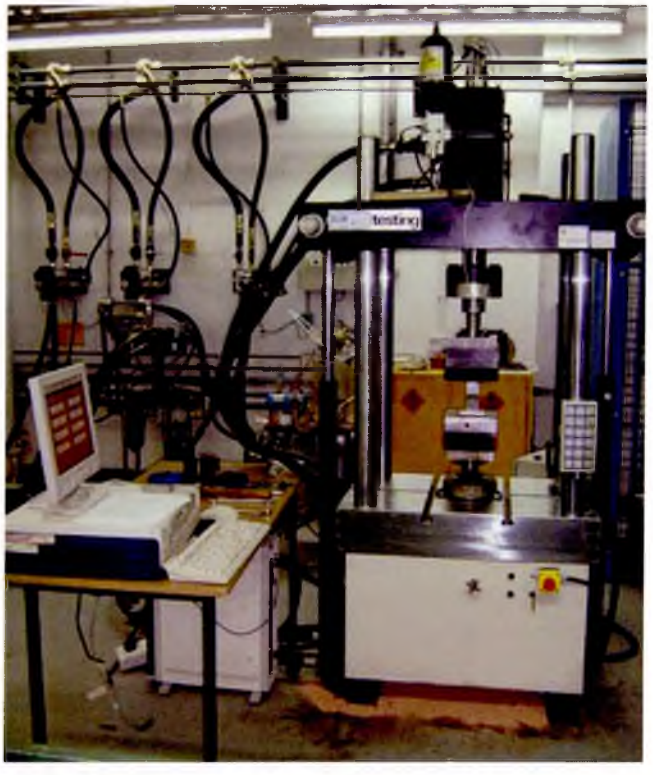

Figure 47. *ESH servo hydraulic mechanical testing machine with Rubicon digital controller, at Sheffield Hallam University*

4.2.2.1 Fatigue Results of LHW Butt Joints with LDX 2101

The results of the staircase fatigue tests for Laser Hybrid Welded butt joints with LDX 2101 and zinc coated mild steel using filler wires 308L-Si and 309L-Si are outlined below. The results are given in figures 48 to 55 which show the actual staircase fatigue results and values for mean fatigue strength (kN), standard deviation (kN), convergence factor and the standard error for mean fatigue strength in accordance with the procedure outlined in section 3. A graph of fatigue load (kN) verses cycles completed is also given, showing the results of the 25 individual tests carried out for each staircase fatigue test. Finally, the mean fatigue strength (kN) has been converted to a 'line load' which is a value of load per unit length measured in N/mm. This will allow these results to be compared to other joining processes of similar material and joint configuration.

Series F1

Load Range (kN)	Step No. (i)	Test Specimen Number																								Number of		Using LFE as N	
		1	2	3	4	5	6	7	8	9	10	11	12	13	14	15	16	17	18	19	20	21	22	23	24	25	Failures (f)	Runouts (r)	iN	i^2N
10.5	3													X		X								X		O	3	1	9	27
10.0	2								X				O		O		X				X		O		O		3	4	6	12
9.5	1	X						O		X		O						X		O		O					3	4	3	3
9.0	0		X		X		O				O								O								2	3	0	0
8.5				O		O																					0	2		
																											Σf	Σr	ΣiN	Σi^2N
																											11	14	18	42

Figure 48. Staircase fatigue results for F1 - LDX 2101 0.75mm to Dogal 260RP-X 1.5mm with 308L-Si filler wire

Step divide: 0.5kN

Least Frequent Event: Failures

Calculated Mean Fatigue Strength:

$$x = 9 + 0.5\left(\frac{18}{11} - \frac{1}{2}\right)$$

$$x = 9.568kN$$

Convergence Factor:

$$\left(\frac{(11*42) - 18^2}{11^2}\right) = 1.140$$

Standard Deviation:

$$s = 1.620 * 0.50\left(\frac{(11*42) - 18^2}{11^2} + 0.029\right)$$

$$s = 0.947kN$$

Standard Error for Mean Fatigue Strength:

$$S_x = \frac{0.947}{\sqrt{11}}.1.15$$

$$S_x = 0.328kN$$

Line Load: 213N/mm

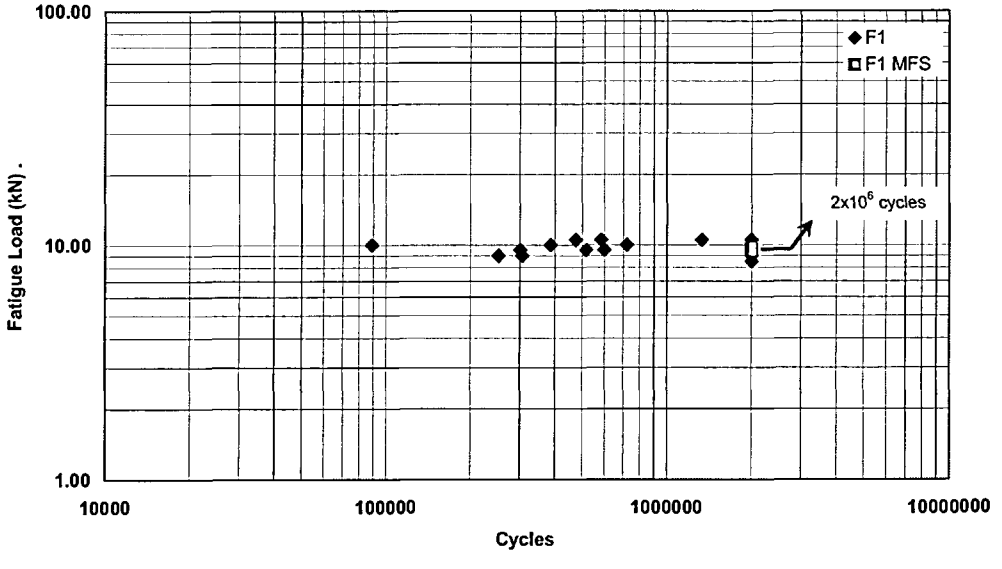

Figure 49. Graph to show fatigue load range for series F1 - LDX 2101 0.75mm to Dogal 260RP-X 1.5mm laser hybrid welded butt joint

Series F2

Load Range (kN)	Step No. (i)	Test Specimen Number																								Number of		Using LFE as N	
		1	2	3	4	5	6	7	8	9	10	11	12	13	14	15	16	17	18	19	20	21	22	23	24	25	Failures (f)	Runouts (r)	iN	i^2N
16.6	4															X											1	0	4	16
16.2	3						X				X				O		X						X				4	1	12	36
15.8	2					O		X		O		X		O				X				O		X		O	4	5	8	16
15.4	1				O				O				O						X		O				O		1	5	1	1
15.0	0	X		O																O							1	2	0	0
14.6			O																								0	1		
																											Σf	Σr	ΣiN	Σi^2N
																											11	14	25	69

Figure 50. Staircase fatigue results for F2 - LDX 2101 1.5mm to Dogal 260RP-X 1.5mm with 308L-Si filler wire

Step divide: 0.4kN

Least Frequent Event: Failures

Calculated Mean Fatigue Strength:

$$x = 15 + 0.4\left(\frac{25}{11} - \frac{1}{2}\right)$$

$$x = 15.709kN$$

Convergence Factor:

$$\left(\frac{(11*69) - 25^2}{11^2}\right) = 1.107$$

Standard Deviation:

$$s = 1.620 * 0.40\left(\frac{(11*69) - 25^2}{11^2} + 0.029\right)$$

$$s = 0.736kN$$

Standard Error for Mean Fatigue Strength:

$$S_x = \frac{0.736}{\sqrt{11}}.1.15$$

$$S_x = 0.255kN$$

Line Load: 349N/mm

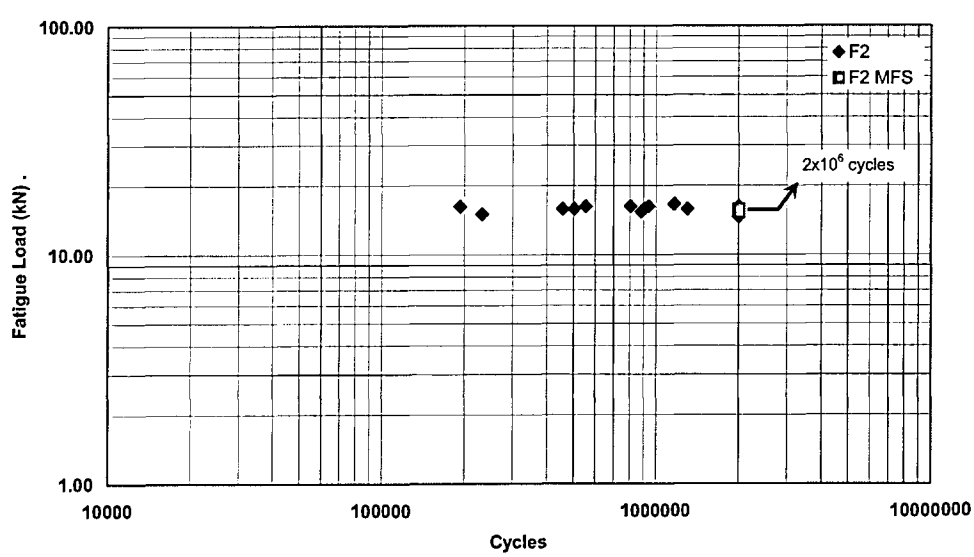

Figure 51. Graph to show fatigue load range for series F2 - LDX 2101 1.5mm to Dogal 260RP-X 1.5mm laser hybrid welded butt joint

Series F5

Load Range (kN)	Step No. (i)	Test Specimen Number																								Number of		Using LFE as N	
		1	2	3	4	5	6	7	8	9	10	11	12	13	14	15	16	17	18	19	20	21	22	23	24	25	Failures (f)	Runouts (r)	iN	i^2N
9.5	4			X						X																	2	0	0	0
9.0	3		O		X				O		X						X		X		X						5	2	6	18
8.5	2	O				X		O				X				O		O		O		X					3	5	10	20
8.0	1						O						X		O								X		X		3	2	2	2
7.5	0													O										O		O	0	3	0	0
																											Σf	Σr	ΣiN	Σi^2N
																											13	12	18	40

Figure 52. Staircase fatigue results for F5 - LDX 2101 0.75mm to Dogal 260RP-X 1.5mm with 309L-Si filler wire

Step divide: 0.5kN

Least Frequent Event: Survivals

Calculated Mean Fatigue Strength:

$$x = 7.5 + 0.5\left(\frac{18}{12} + \frac{1}{2}\right)$$

$$x = 8.5kN$$

Convergence Factor:

$$\left(\frac{(12 * 40) - 18^2}{12^2}\right) = 1.083$$

Standard Deviation:

$$s = 1.620 * 0.50\left(\frac{(12 * 40) - 18^2}{12^2} + 0.029\right)$$

$$s = 0.901kN$$

Standard Error for Mean Fatigue Strength:

$$S_x = \frac{0.901}{\sqrt{12}}.1.15$$

$$S_x = 0.299kN$$

Line Load: 189N/mm

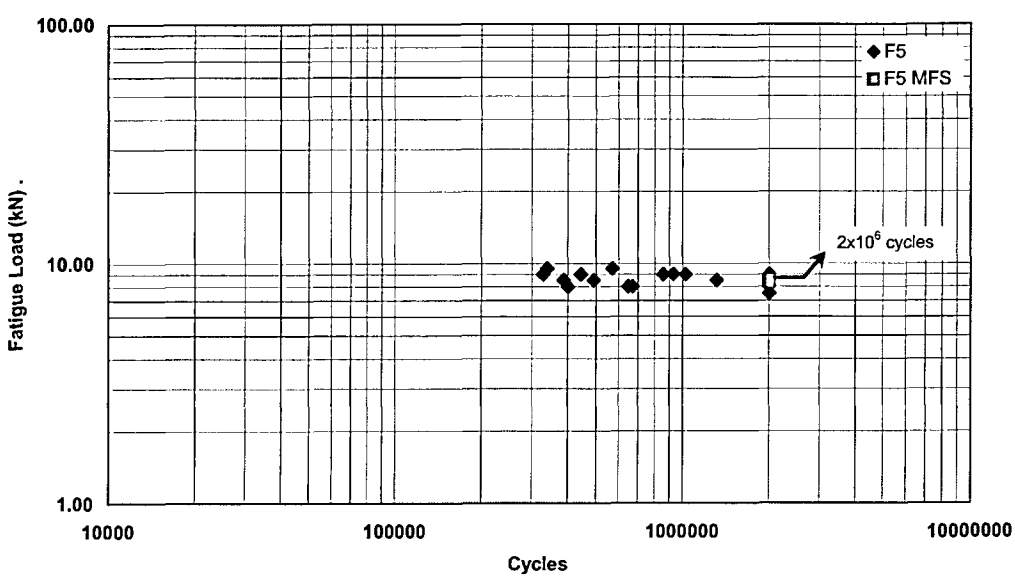

Figure 53. Graph to show fatigue load range for series F5 - LDX 2101 0.75mm to Dogal 260RP-X 1.5mm laser hybrid welded butt joint

Series F6

Load Range (kN)	Step No. (i)	Test Specimen Number																									Number of		Using LFE as N	
		1	2	3	4	5	6	7	8	9	10	11	12	13	14	15	16	17	18	19	20	21	22	23	24	25	Failures (f)	Runouts (r)	iN	i^2N
16.4	3																				X				X		2	0	6	18
15.7	2	X										X						X		O		X		O		O	4	3	8	16
15.0	1		X						X		O		X		X		O		O				O				4	4	4	4
14.3	0			X		X		O		O				O		O											2	4	0	0
13.6					O		O																				0	2		
																											Σf	Σr	ΣiN	Σi^2N
																											12	13	18	38

Figure 54. Staircase fatigue results for F6 - LDX 2101 1.5mm to Dogal 260RP-X 1.5mm with 309L-Si filler wire

Step divide: 0.7kN

Least Frequent Event: Failures

Calculated Mean Fatigue Strength:

$$x = 14.3 + 0.7\left(\frac{18}{12} - \frac{1}{2}\right)$$

$$x = 15.000kN$$

Convergence Factor:

$$\left(\frac{(12*38) - 18^2}{12^2}\right) = 0.917$$

Standard Deviation:

$$s = 1.620 * 0.70\left(\frac{(12*38) - 18^2}{12^2} + 0.029\right)$$

$$s = 1.072kN$$

Standard Error for Mean Fatigue Strength:

$$S_x = \frac{1.072}{\sqrt{12}}.1.15$$

$$S_x = 0.356kN$$

Line Load: 333N/mm

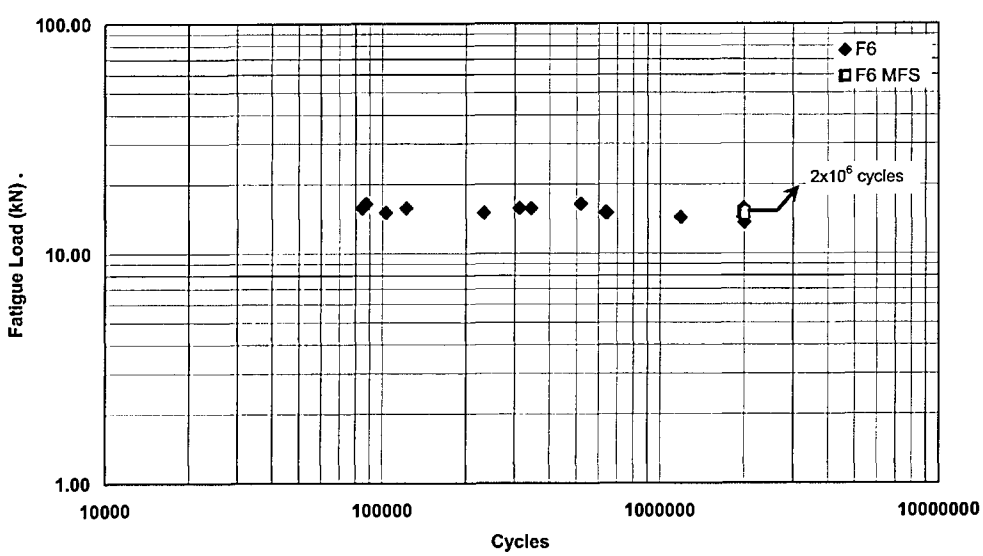

Figure 55. Graph to show fatigue load range for series F6 - LDX 2101 1.5mm to Dogal 260RP-X 1.5mm laser hybrid welded butt joint

4.2.2.2 Fatigue Results of LHW Butt Joints with HyTens 1000

The results of the staircase fatigue tests for Laser Hybrid Welded butt joints with HyTens 1000 and zinc coated mild steel using filler wires 308L-Si and 309L-Si are outlined below. The results are outlined in figures 56 to 63 which show the actual staircase fatigue results and values for mean fatigue strength (kN), standard deviation (kN), convergence factor and the standard error for the mean fatigue strength in accordance with the procedure outlined in section 3. In addition a graph of each staircase fatigue tests, 25 for each series, as fatigue load (kN) verses cycles completed. Finally the mean fatigue strength (kN) has been converted to a 'line load' which is a value of load per unit length measured in N/mm this will allow these results to be compared to other joining processes of similar material and joint configuration.

Series F3

Load Range (kN)	Step No. (i)	Test Specimen Number																									Number of		Using LFE as N	
		1	2	3	4	5	6	7	8	9	10	11	12	13	14	15	16	17	18	19	20	21	22	23	24	25	Failures (f)	Runouts (r)	iN	i^2N
10.5	3											X															1	0	3	9
10.0	2								X		O		X										X				3	1	6	12
9.5	1			X		X		O		O				X		X		X				O		X		X	7	3	7	7
9.0	0		O		O		O								O		O		X		O				O		1	7	0	0
8.5		O																		O							0	2		
																											Σf	Σr	ΣiN	Σi^2N
																											12	13	16	28

Figure 56. Staircase fatigue results for F3 - HyTens 1000 0.75mm to Dogal 260RP-X 1.5mm with 308L-Si filler wire

Step divide: 0.5kN

Least Frequent Event: Failures

Calculated Mean Fatigue Strength:

$$x = 9.0 + 0.5\left(\frac{16}{12} - \frac{1}{2}\right)$$

$$x = 9.417kN$$

Convergence Factor:

$$\left(\frac{(12 * 28) - 16^2}{12^2}\right) = 0.556$$

Standard Deviation:

$$s = 1.620 * 0.50\left(\frac{(12 * 28) - 16^2}{12^2} + 0.029\right)$$

$$s = 0.473kN$$

Standard Error for Mean Fatigue Strength:

$$S_x = \frac{0.473}{\sqrt{12}}.1.15$$

$$S_x = 0.157kN$$

Line Load: 209N/mm

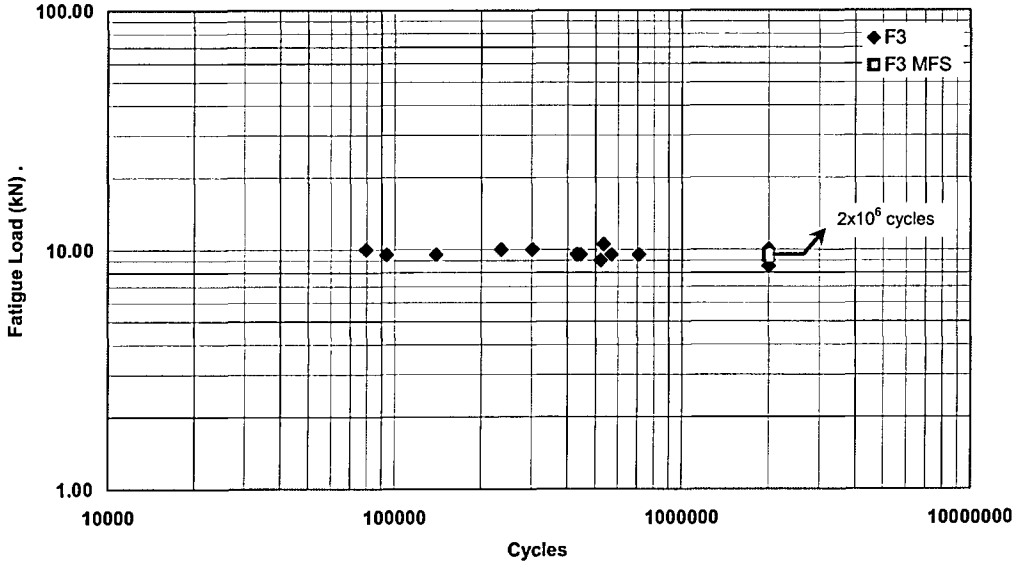

Figure 57. Graph to show fatigue load range for series F3 - HyTens 1000 0.75mm to Dogal 260RP-X 1.5mm laser hybrid welded butt joint

Series F4

Load Range (kN)	Step No. (i)	Test Specimen Number																									Number of		Using LFE as N	
		1	2	3	4	5	6	7	8	9	10	11	12	13	14	15	16	17	18	19	20	21	22	23	24	25	Failures (f)	Runouts (r)	iN	i^2N
16.5	11								X																		1	0	0	0
16.0	10							O		X																	1	1	10	100
15.5	9						O				X																1	1	9	81
15.0	8					O						X															1	1	8	64
14.5	7		X		O								X														2	1	7	49
14.0	6	O		O										X													1	2	12	72
13.5	5														X												1	0	0	0
13.0	4															X		X									2	0	0	0
12.5	3																O		X								1	1	3	9
12.0	2																			X				O			1	1	2	4
11.5	1																				X		O				1	1	1	1
11.0	0																					O					0	1	0	0
																											Σf	Σr	ΣiN	Σi^2N
																											13	10	52	380

Figure 58. Staircase fatigue results for F4 - HyTens 1000 1.5mm to Dogal 260RP-X 1.5mm with 308L-Si filler wire

Step divide: 0.5kN

Least Frequent Event: Survivals

Calculated Mean Fatigue Strength:

$$x = 11.0 + 0.5\left(\frac{52}{10} + \frac{1}{2}\right)$$

$$x = 13.850kN$$

Convergence Factor:

$$\left(\frac{(10 * 52) - 380^2}{10^2}\right) = -1438.8,$$

The value of the convergence factor is not larger than 0.3 therefore the standard deviation cannot be calculated.

$$s = -1165.4kN$$

Line Load: 308N/mm

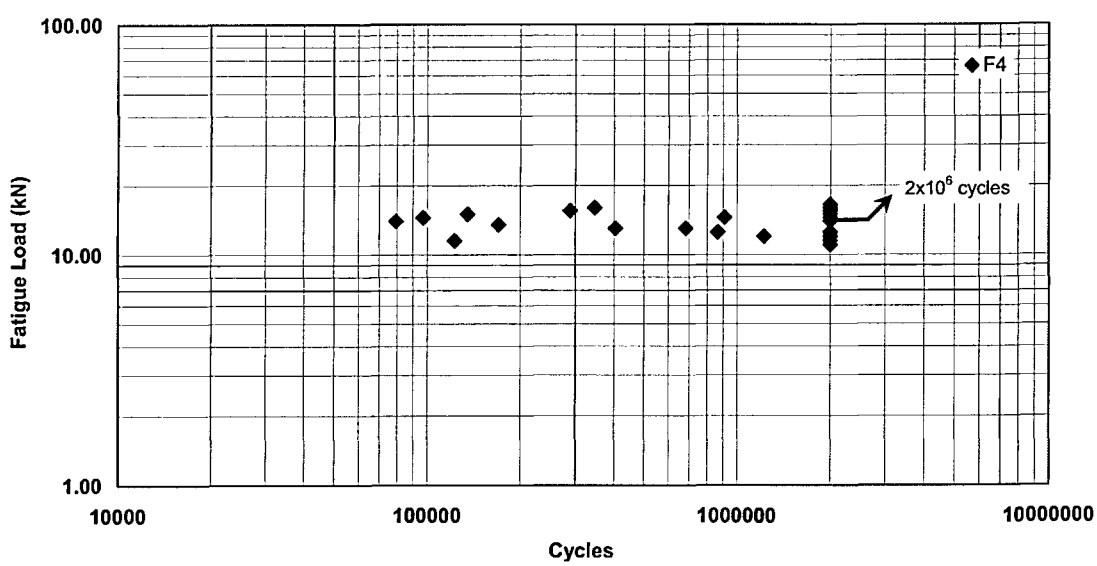

Figure 59. Graph to show fatigue load range for series F4 - HyTens 1000 1.5mm to Dogal 260RP-X 1.5mm laser hybrid welded butt joint

Series F7

Load Range (kN)	Step No. (i)	Test Specimen Number																								Number of		Using LFE as N	
		1	2	3	4	5	6	7	8	9	10	11	12	13	14	15	16	17	18	19	20	21	22	23	24	25	Failures (f)	Runouts (r)	iN	i^2N
9.0	4	X		X																							2	0	0	0
8.5	3		O		X				X								X		X								4	1	3	9
8.0	2					X		O		X				X		O		O		X				X		X	6	3	6	12
7.5	1						O				X		O		O						X		O		O		2	5	5	5
7.0	0											O										O					0	2	0	0
																											Σf	Σr	ΣiN	Σi^2N
																											14	11	14	26

Figure 60. Staircase fatigue results for F7 - HyTens 1000 0.75mm to Dogal 260RP-X 1.5mm with 309L-Si filler

Step divide: 0.5kN

Least Frequent Event: Survivals

Calculated Mean Fatigue Strength:

$$x = 7.0 + 0.5\left(\frac{14}{11} + \frac{1}{2}\right)$$

$$x = 7.750kN$$

Convergence Factor:

$$\left(\frac{(11*26) - 14^2}{11^2}\right) = 0.744$$

Standard Deviation:

$$s = 1.620 * 0.50\left(\frac{(11*26) - 14^2}{11^2} + 0.029\right)$$

$$s = 0.626kN$$

Standard Error for Mean Fatigue Strength:

$$S_x = \frac{0.626}{\sqrt{11}}.1.15$$

$$S_x = 0.217kN$$

Line Load: 172N/mm

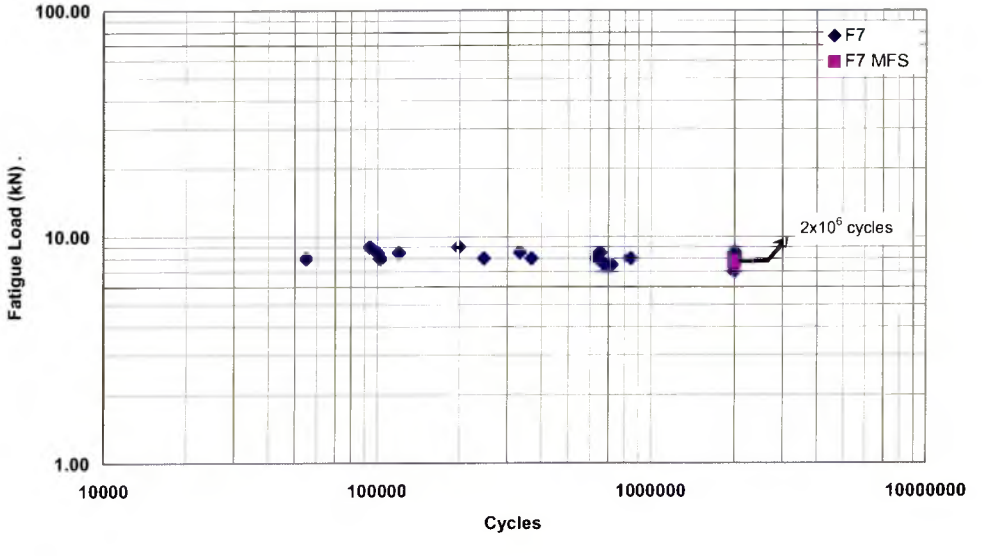

Figure 61. Graph to show fatigue load range for series F7 - HyTens 1000 0.75mm to Dogal 260RP-X 1.5mm laser hybrid welded butt joint

Series F8

Load Range (kN)	Step No. (i)	Test Specimen Number																									Number of		Using LFE as N	
		1	2	3	4	5	6	7	8	9	10	11	12	13	14	15	16	17	18	19	20	21	22	23	24	25	Failures (f)	Runouts (r)	iN	i^2N
15.4	4									X																	1	0	0	0
15.2	3								O		X																1	1	3	9
14.8	2					X		O				X		X													3	1	2	4
14.4	1		X		O		O						O		X												2	3	3	3
14.0	0	O		O												X											1	2	0	0
13.6																	X										1	0		
13.2																		X									1	0		
																											Σf	Σr	ΣiN	Σi^2N
																											10	7	8	16

Figure 62. Staircase fatigue results for F8 - HyTens 1000 1.5mm to Dogal 260RP-X 1.5mm with 309L-Si filler

Step divide: 0.4kN

Least Frequent Event: Survivals

Calculated Mean Fatigue Strength:

$$x = 14.0 + 0.4\left(\frac{8}{7} + \frac{1}{2}\right)$$

$$x = 14.520kN$$

Convergence Factor:

$$\left(\frac{(7*16) - 8^2}{7^2}\right) = 0.980$$

Standard Deviation:

$$s = 1.620 * 0.40\left(\frac{(7*16) - 8^2}{7^2} + 0.029\right)$$

$$s = 0.654kN$$

Standard Error for Mean Fatigue Strength:

$$S_x = \frac{0.654}{\sqrt{7}}.1.15$$

$$S_x = 0.284kN$$

Line Load: 322.67N/mm

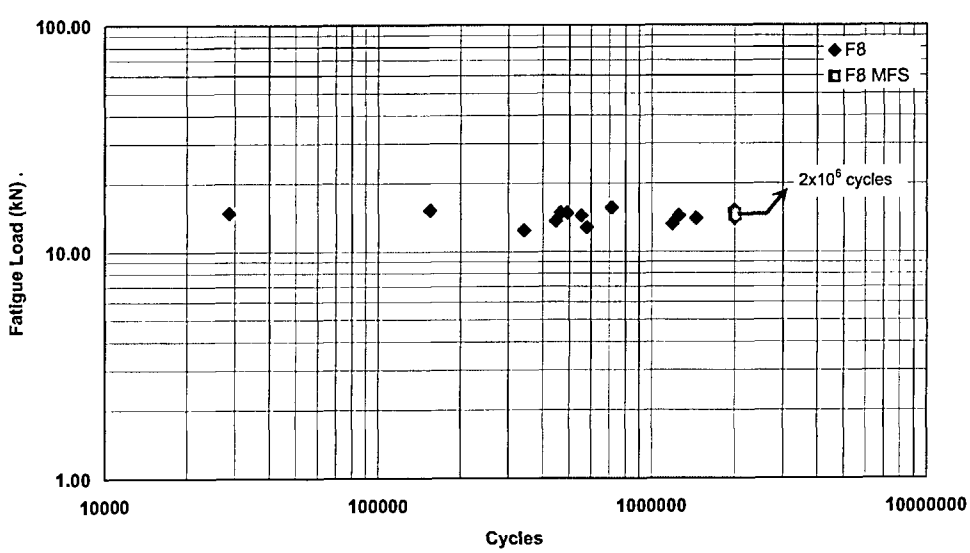

Figure 63. Graph to show fatigue load range for series F8 - HyTens 1000 1.5mm to Dogal 260RP-X 1.5mm laser hybrid welded butt joint

4.2.3 Fatigue Failure Analysis for Laser Hybrid Welded Butt Joints

The samples that failed during the fatigue tests were analysed to establish the origin of failure and to look for any factors that may have affected the fatigue life. Two types of joint geometry were considered in the fatigue testing, those of dissimilar thickness parent materials, series F1, F3, F5 and F7 and those which had parent materials of similar thickness, series F2, F4, F6 and F8.

4.2.3.1 Fatigue Failure Analysis of Dissimilar Thickness LHW Butt Joints

Fatigue failures are invariably controlled by the geometry of a sample and welds are no exception. The joints for series F1, F3, F5 and F7 used 0.75mm thick stainless steel (LDX 2101 or Hy-Tens 1000) to 1.5mm zinc coated mild steel (Dogal 260RP-X), allowing the mechanical properties of the two parent materials to be balanced out. Figure 64 shows the weld bead and a section through the weld, indicating joint fit up for the dissimilar thickness welds. For dissimilar thickness joint fatigue tests (series F1, F3, F5 and F7) a typical failure is illustrated in figure 66.

Fatigue tests for series F7 (HyTens 1000 0.75mm thick to Dogal 260RP-X 1.5mm) were filmed using a web camera and video capturing software. The footage was used to record how the failures of the fatigue tests were occurring. Figure 65 shows still photos taken from fatigue test F7.8.6 and the initiation of the crack and growth through the sample.

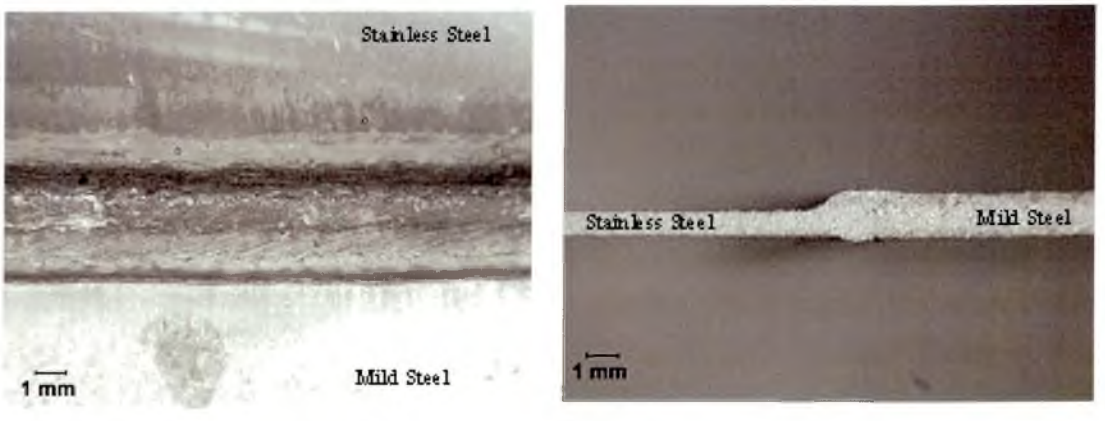

Figure 64. An example of a Laser Hybrid Welded Butt joints showing the weld bead and the joint fit up 1.5mm welded to 0.75mm plates

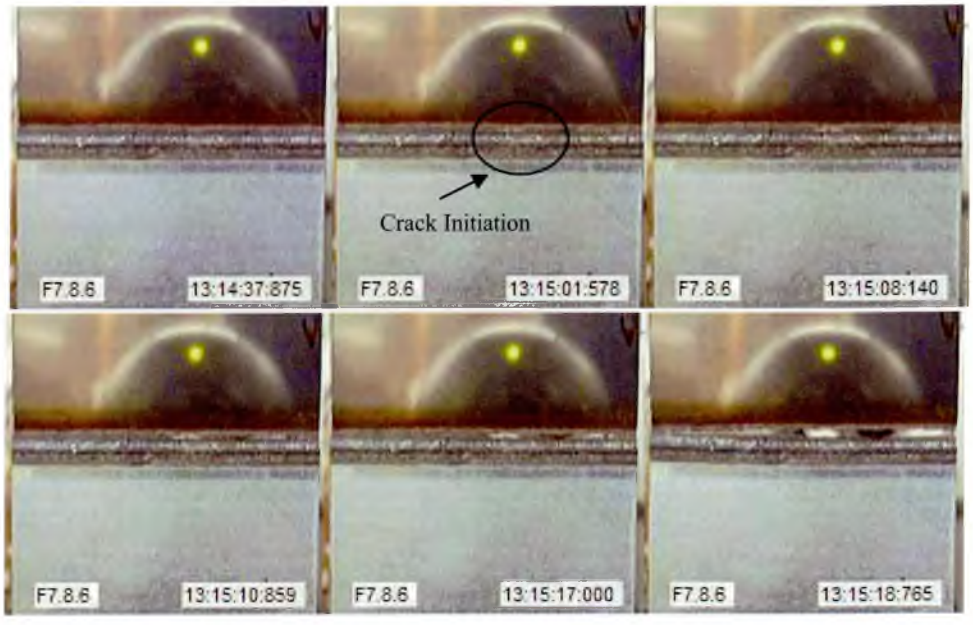

Figure 65. A series of still photos from the video capture of the fatigue test F7.8.6 showing the location, initiation and propagation of the fatigue crack.

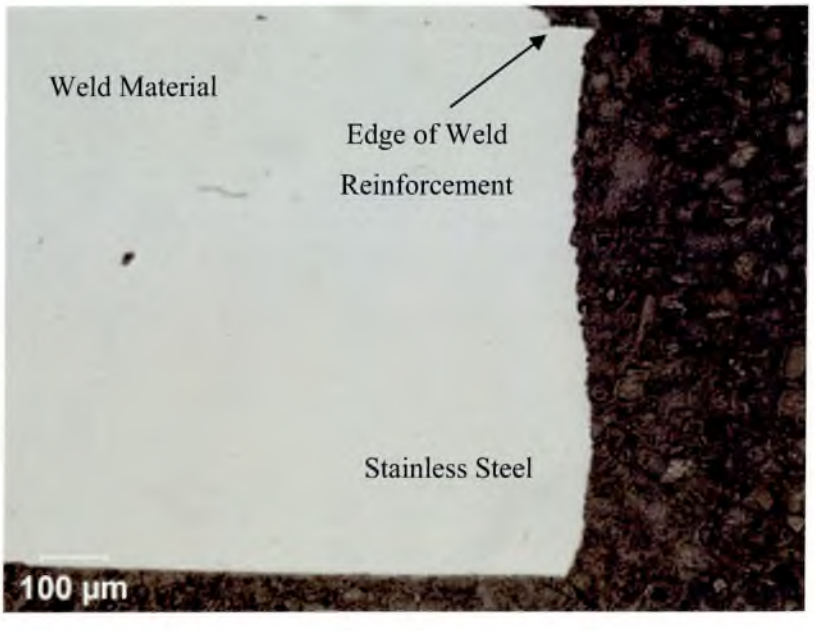

Figure 66. Photo showing fatigue failure for a LHW butt joint of dissimilar thickness, the failures occurs on the thinner stainless steel side of the joint.

4.2.3.2 Fatigue Failure Analysis of Similar Thickness LHW Butt Joints

The joints for series F2, F4, F6 and F8 used 1.5mm thick stainless steel (LDX 2101 or Hy-Tens 1000) to 1.5mm zinc coated mild steel (Dogal 260RP-X). Figure 67 shows the weld bead and a section through the weld, indicating joint fit up for the similar thickness welds.

Figure 68 below shows the common failure of the similar thickness butt joints, with the crack initiating at the root of weld and on the side of the mild steel.

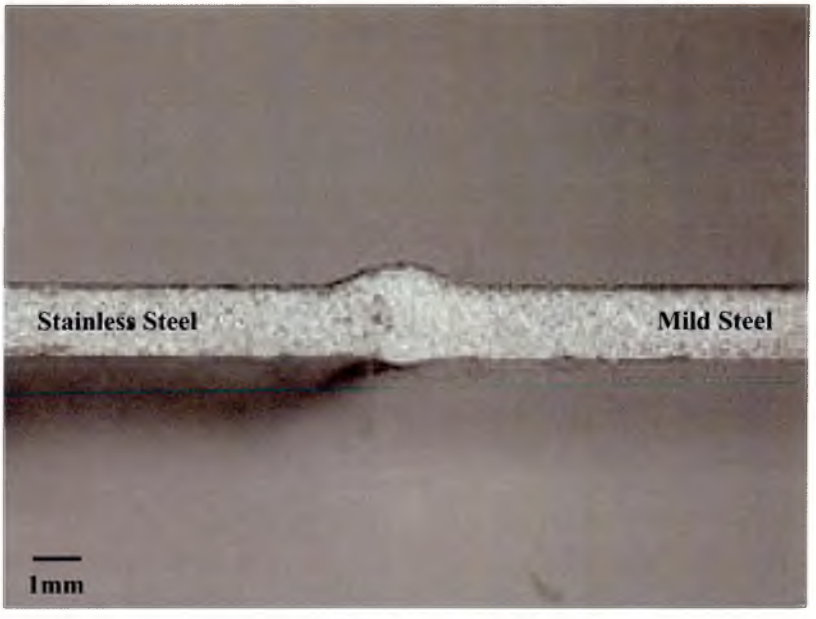

Figure 67. Example of the joint fit of similar thickness LHW butt joints.

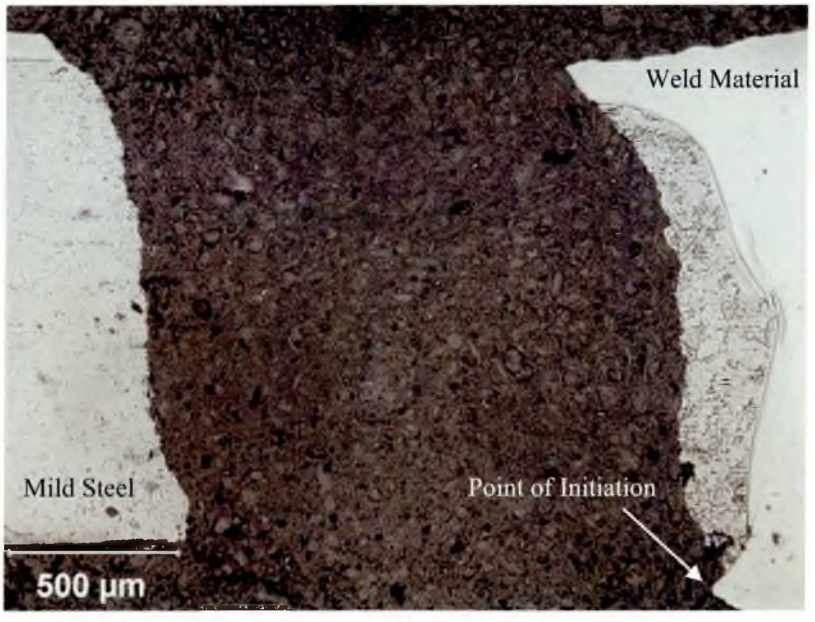

Figure 68. Photo showing fatigue failure for a LHW butt joint of similar thickness, the failure occurs on the weaker mild steel side of the joint.

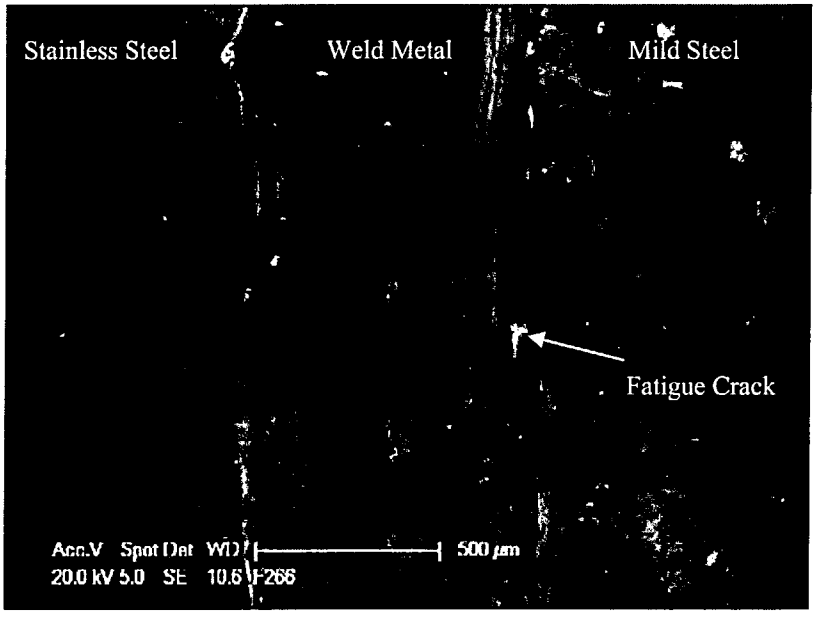

Figure 69. SEM image showing the underside of the weld bead of samples F2.6.6

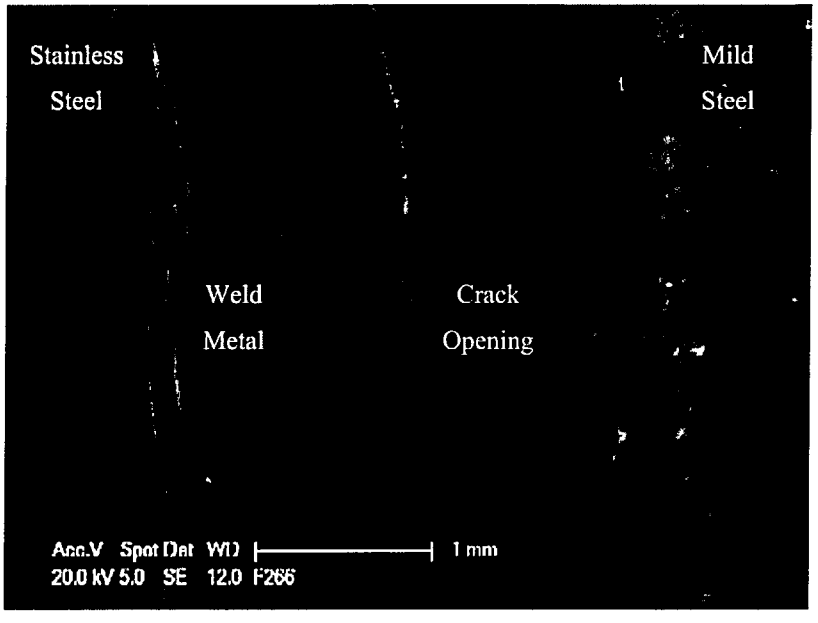

Figure 70. SEM image showing the underside of the weld bead illustrating the crack propagation on the edge of the weld on the mild steel side.

4.2.3.3 Root Angle Measurements for Similar Thickness LHW Butt Joints

Failure analysis of the fatigue samples led to an in depth look at the geometry of the joints. The root angle of the samples were measured and statistically analysed to determine whether there was a relationship between the root angle of a sample and fatigue life.

The procedure for measuring the angle is outlined in Section 3.7.4.3. An example of the image taken to measure the angle is shown in Figure 71. Figures 72 to 75 below outline the results of the measurements taken from each fatigue sample for series F2, F4, F6 and F8 and are represented as graphs of measured angle against fatigue life in cycles,

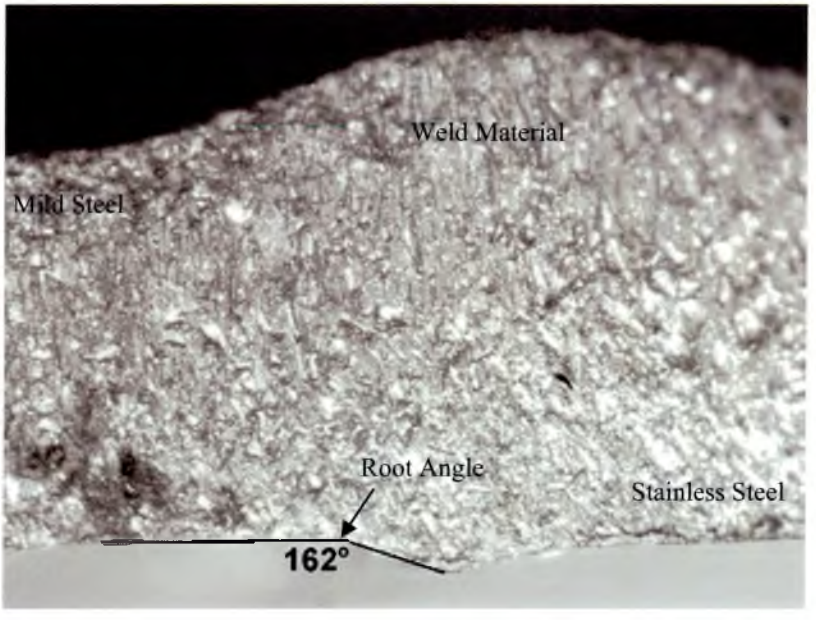

Figure 71. Image showing an example of how the root angle was measured for the fatigue tests in series F2, F4, F6 and F8. The sample in the image is F2.5.3 which completed 2 million cycles at a load of 15.4kN.

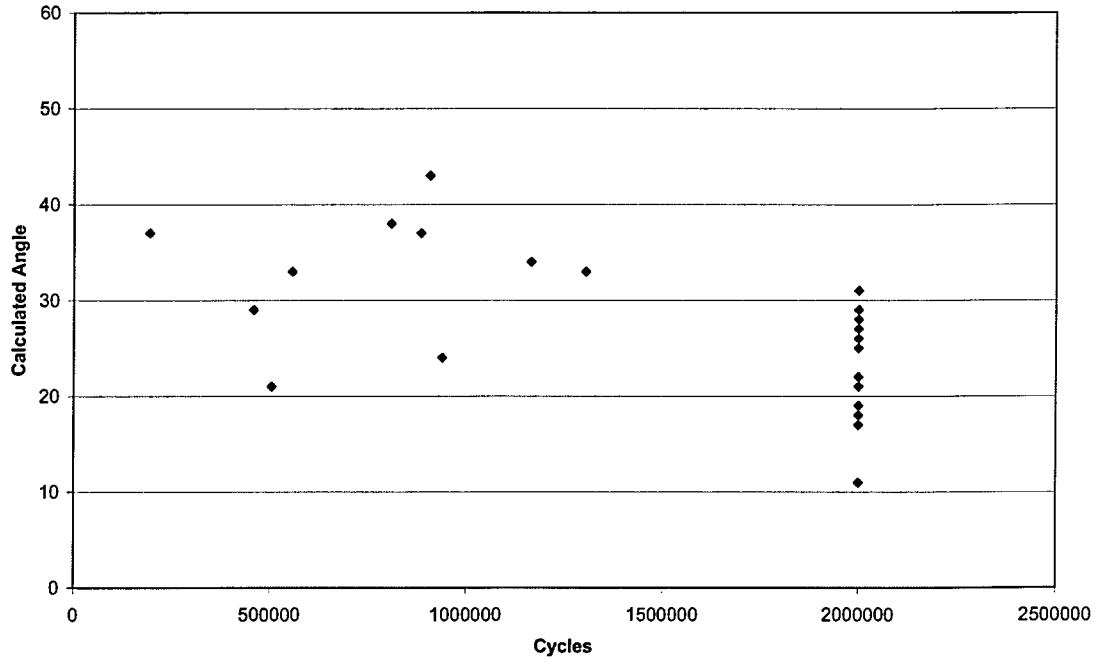

Figure 72. Graph showing the relationship of root angle and fatigue cycles completed (to fracture or runout) for series F2 - LDX 2101 1.5mm to Dogal 260RP-X 1.5mm with 308L-Si filler wire.

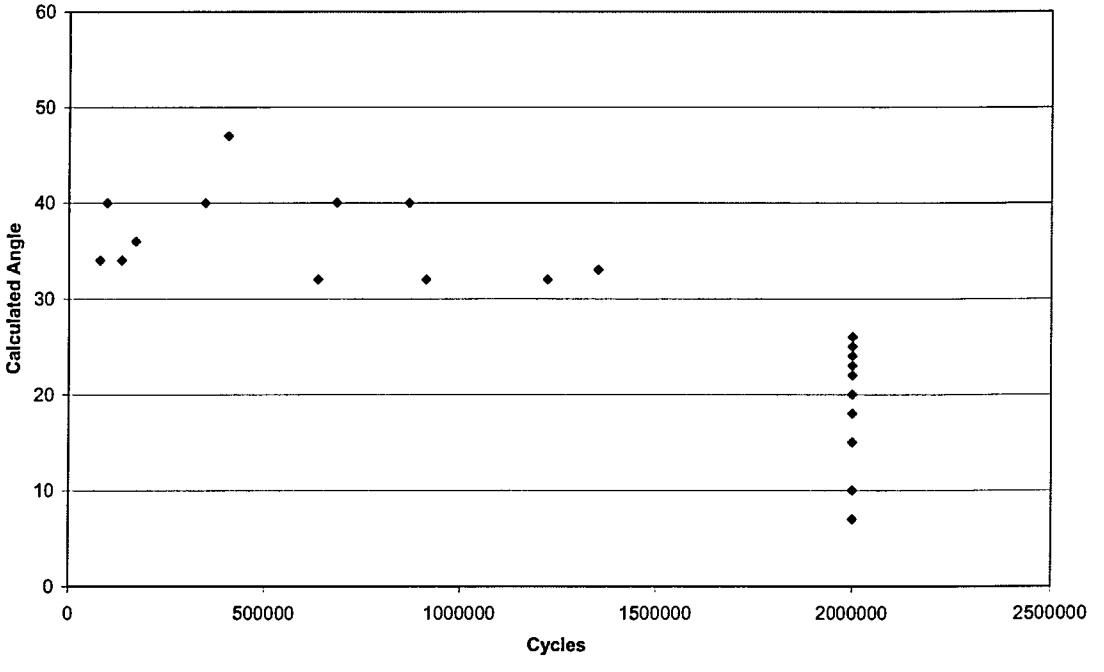

Figure 73. Graph showing the relationship of root angle at and fatigue cycles completed (to fracture or runout) for series F4 -HyTens 1000 1.5mm to Dogal 260RP-X 1.5mm with 308L-Si filler wire.

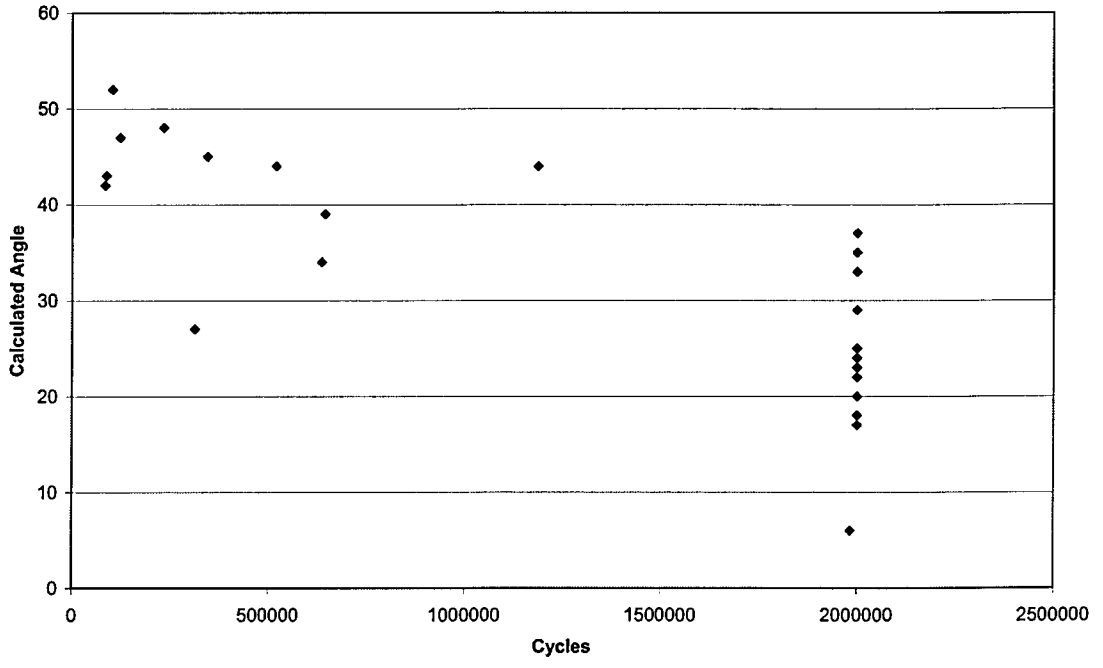

Figure 74. Graph showing the relationship of root angle and fatigue cycles completed for series F6 - LDX 2101 1.5mm to Dogal 260RP-X 1.5mm with 309L-Si filler wire.

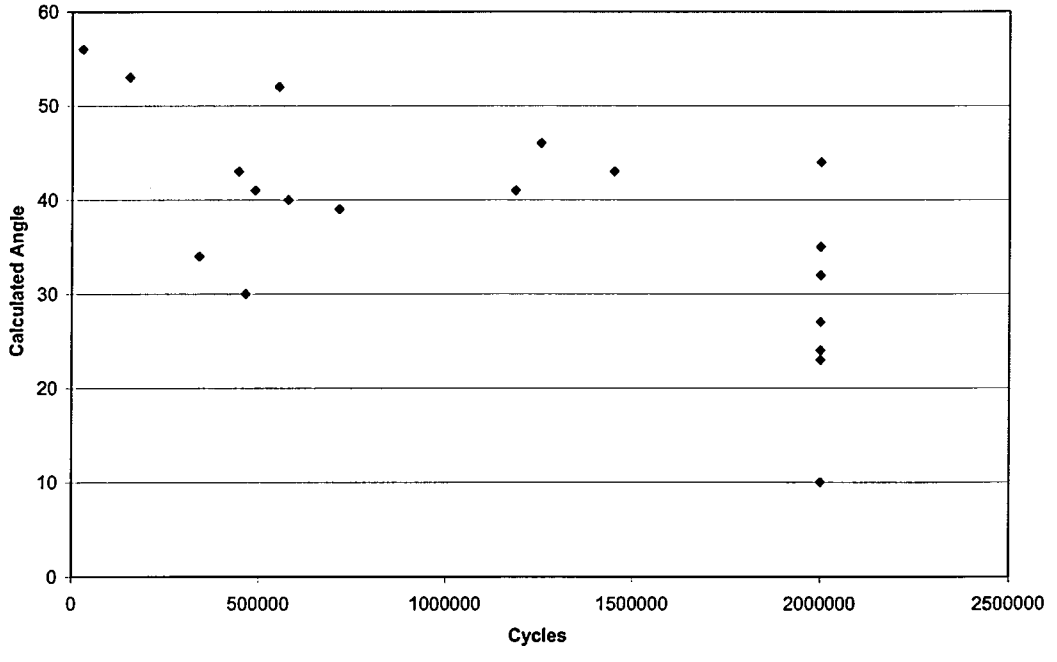

Figure 75. Graph showing the relationship of root angle and fatigue cycles completed for series F4 -HyTens 1000 1.5mm to Dogal 260RP-X 1.5mm with 309L-Si filler wire.

In order to confirm that there is a relationship between root angle and fatigue life a statistical T-Test was carried out. A T-Test assesses whether the means of two groups of data are statistically different from each other. The root angle data was split into two groups, those that failed under 500,000 cycles and those who survived to 2,000,000 cycles. The results of the test indicated that the two groups of data were significantly statistically different. The results of the T-Test are shown below in figure 76.

	Number of Samples	Mean	Standard Deviation
Group 1 <500,000 cycles	23	26.22	7.34
Group 2 Completed $2x10^6$ cycles	23	38.04	13.40

T-Test to determine whether they are statistically different groups.

T-Test of mean difference = 0 (vs not = 0):

95% CI for mean difference between: (-17.88, -5.77)

T-Value = -4.05

P-Value = 0.001

Figure 76. Results of T-Test carried out in Minitab to confirm relationship between root angle and fatigue life.

4.2.4 Results of Non-Destructive X-Ray Testing of Series F3 and F5

Prior to fatigue testing two series of samples were sent for non-destructive evaluation using X-Ray to determine whether the samples had any detectable defects that could potentially have a negative effect on the fatigue properties.

Table 16 below outlines the criteria for the test, only defects larger than 0.1mm were detected using this method of non destructive testing. A total of 70 samples were tested (35 for each series), out of these only 3 samples were detected as having defects and details can be found in table 17 below. The samples identified as having defects present were not included in the fatigue testing of the relevant series.

Test	Accept Limit	Image Quality	X-Ray Equipment	Rated Voltage	Focus Size
SS EN 1435 Class B	SS EN 12517 Level 1	0.1mm	Philips	300kV	1.2mm

Table 16. Outline of X-Ray testing criteria for series F3 and F5 fatigue samples.

Sample ID	Density Accepted	Defect Detected	Category of Defect	Degree of Defect
F5.3.2	Yes	Yes	D - Incomplete Penetration	
F5.3.3	Yes	Yes	D - Incomplete Penetration	
F3.6.1	Yes	Yes	D - Incomplete Penetration	2

Table 17. Samples with defects detected by X-Ray testing, samples were not fatigue tested as part of the staircase.

4.2.5 Microhardness Results for Laser Hybrid Welded Butt Joints

Microhardness tests were carried out on sections of the butt welded samples in order to create a profile of hardness through the centre of the weld and a hardness map across the whole area of weld. Each combination of material and joint configuration was examined for Laser Hybrid Welded butt joints and results are outlined in the following sections.

4.2.5.1 Microhardness Results for LHW Butt Joints of LDX 2101 Welded to Zinc Coated Mild Steel

Figure 77 below outlines the microhardness profiles for laser hybrid welded butt joints from series 1, 2, 5 and 6. These are the series with LDX 2101 welded to zinc coated mild steel using filler wires 308L-Si and 309L-Si.

Microhardness maps were carried out on 4 samples of each joint combination to show the variation in hardness, if any, across the weld pool, heat affected zones and parent materials of the joints. For each series samples were taken at around the mean fatigue load level from both failed and survived fatigue tests. Figures 78 to 85 show microhardness maps from a failed and survived fatigue test. The remainder of the maps can be found in Appendix A.

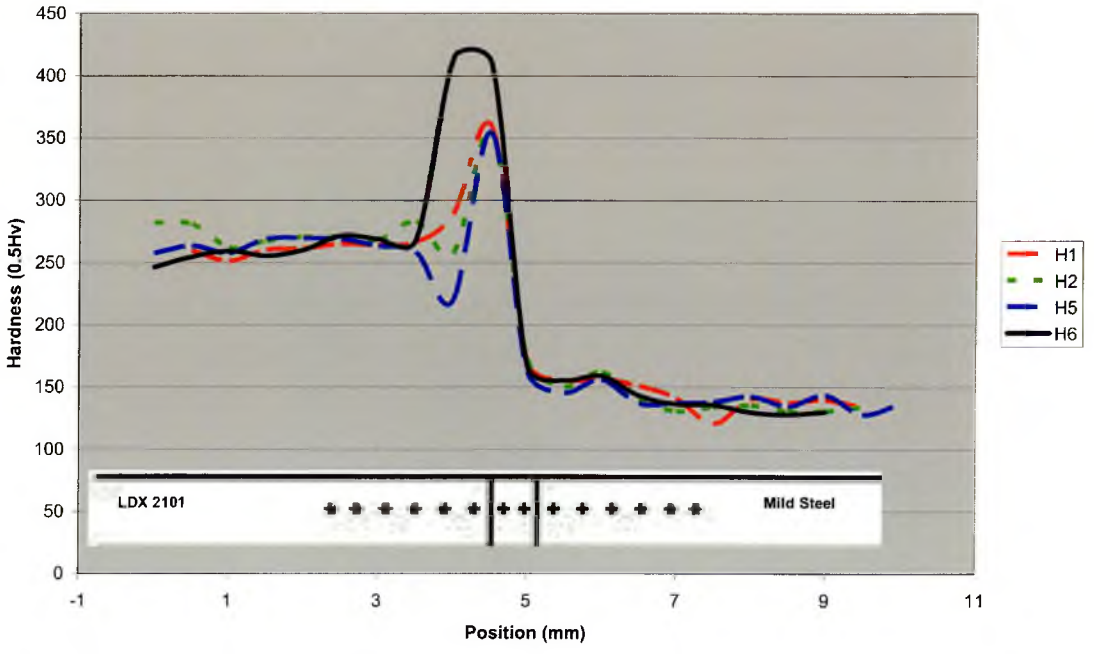

Figure 77. *Graph showing microhardness profile of laser hybrid butt joint of LDX 2101 to zinc coated mild steel using 308L-Si and 309L-Si filler wires*

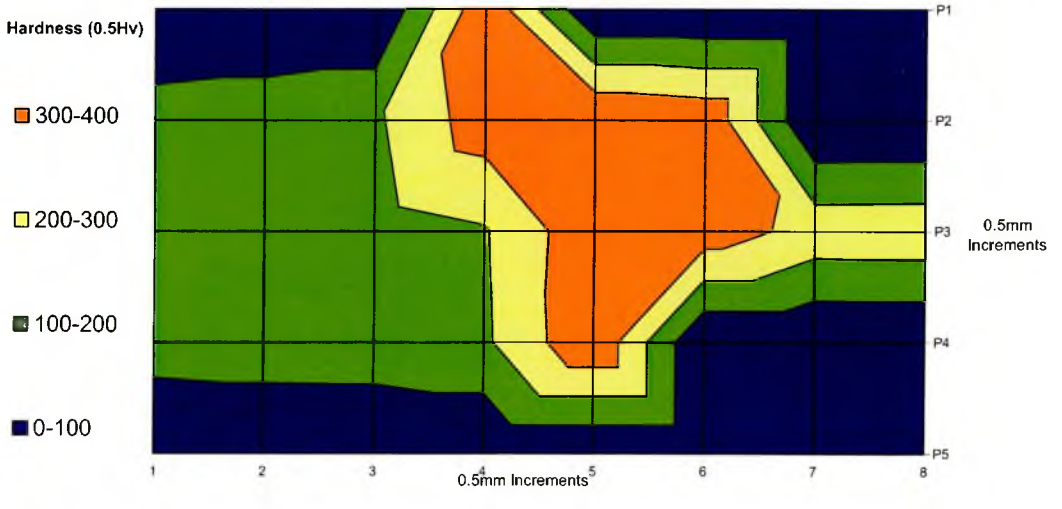

Figure 78. *Series 1 microhardness map of fatigue sample 1.3.1, the sample failed the fatigue test at 9.0kN after 252752 cycles.*

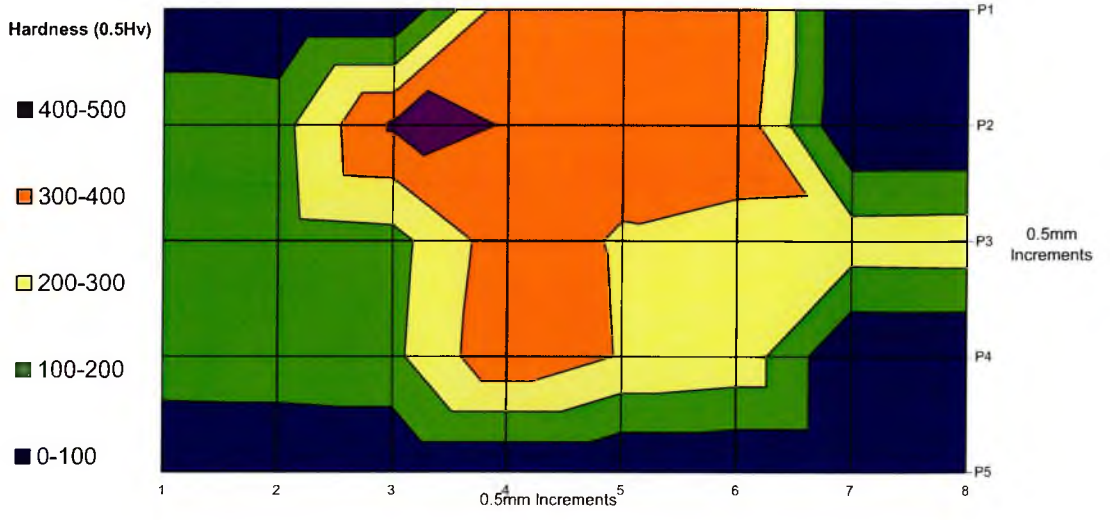

Figure 79. Series 1 microhardness map of fatigue sample 1.7.2, the sample survived the fatigue test at 9.5kN completing 2 million cycles.

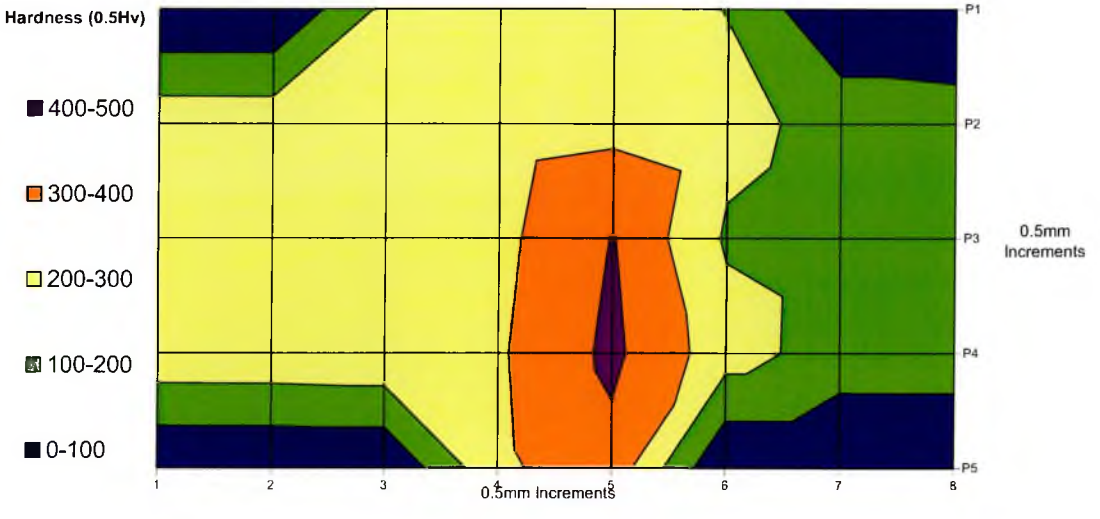

Figure 80. Series 2 microhardness map of fatigue sample 2.5.4, the sample survived the fatigue test at 15.8kN completing 2 million cycles.

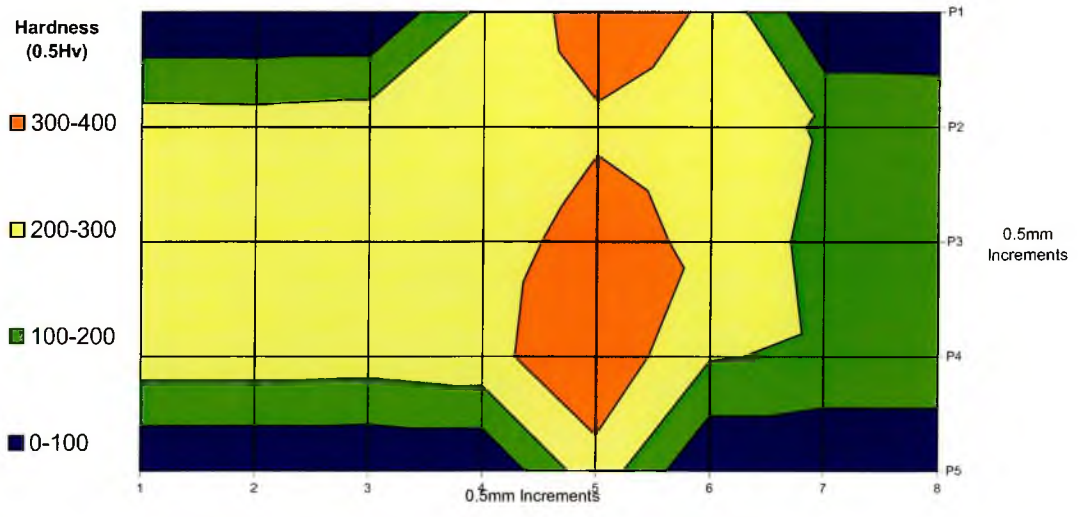

Figure 81. *Series 2 microhardness map of fatigue sample2.6.6, the sample failed the fatigue test at 15.8kN after 457113 cycles.*

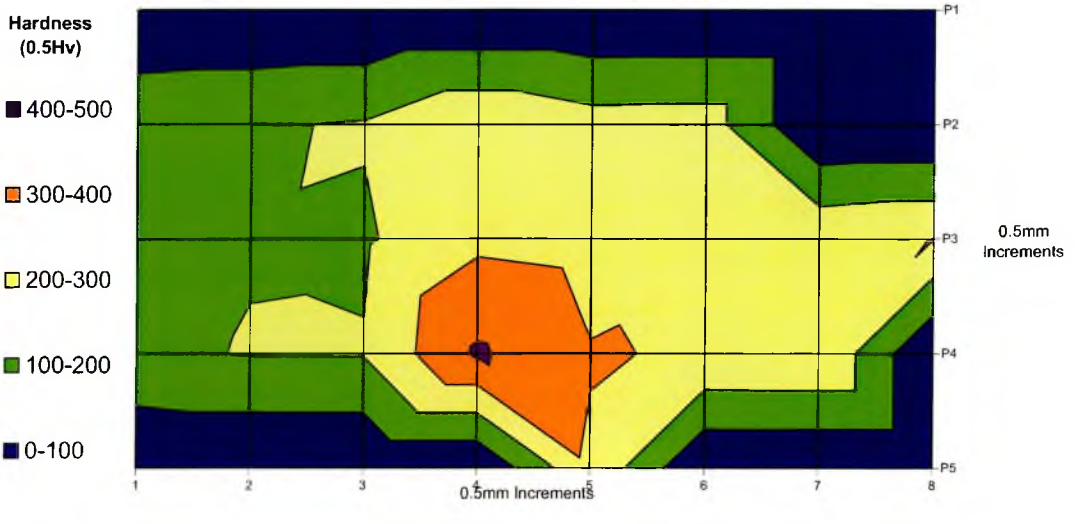

Figure 82. *Series 5 microhardness map of fatigue sample 5.1.6, the sample failed the fatigue test at 8.5kN after 1311423 cycles.*

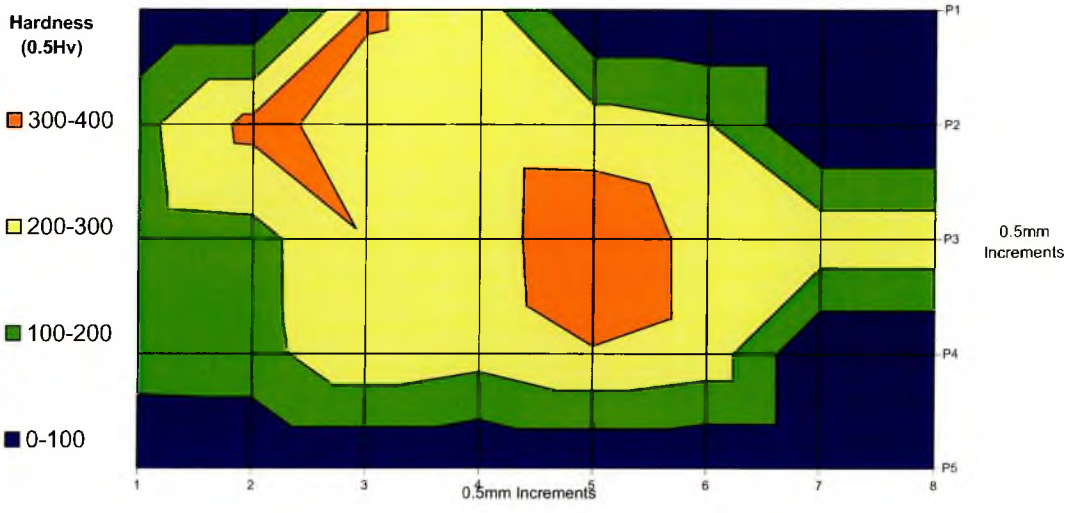

Figure 83. *Series 5 microhardness map of fatigue sample 5.4.2, the sample survived the fatigue test at 8.5kN completing 2 million cycles.*

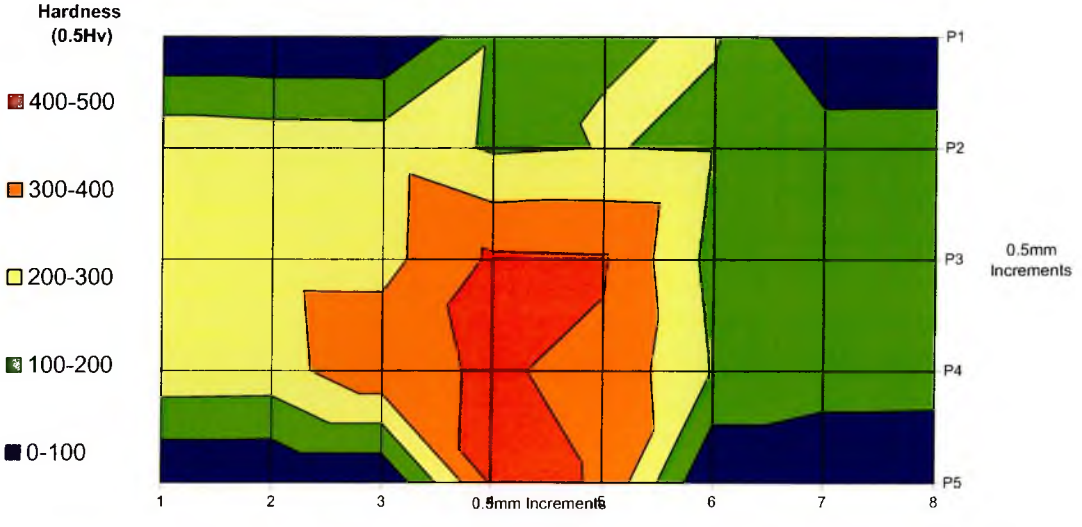

Figure 84. *Series 6 microhardness map of fatigue sample 6.1.2, the sample survived the fatigue test at 15.0kN completing 2 million cycles.*

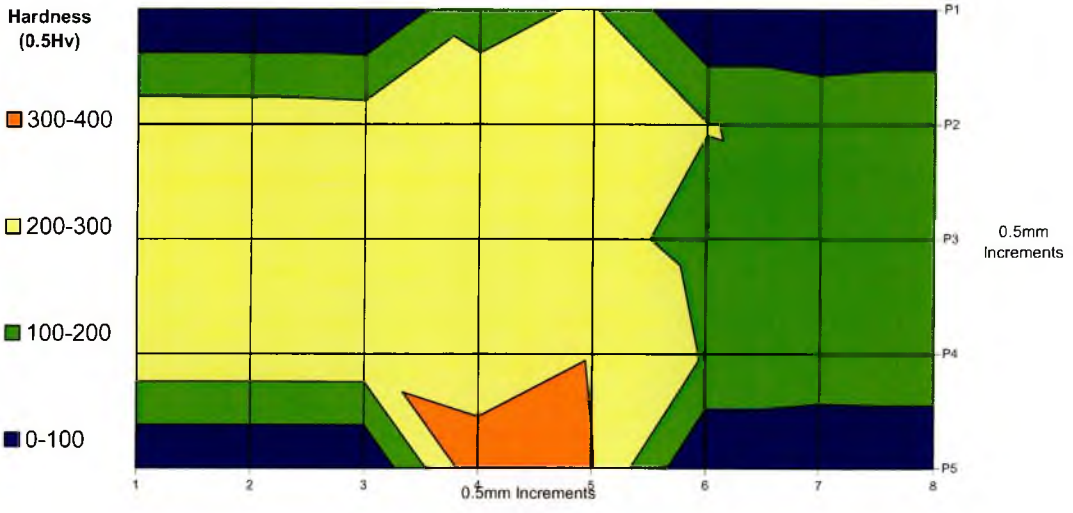

Figure 85. Series 6 microhardness map of fatigue sample 6.2.1, the sample failed the fatigue test at 15.0kN after 644544 cycles.

4.2.5.2 Microhardness Results for LHW Butt Joints of HyTens 1000 Welded to Zinc Coated Mild Steel

Figure 86 below outlines the microhardness profiles for laser hybrid welded butt joints series 3, 4, 7 and 8. These are the series with HyTens 1000 stainless steel welded to zinc coated mild steel using filler wires 308L-Si and 309L-Si.

Microhardness maps were carried out on 4 samples of each joint combination to show the variation in hardness, if any, across the weld pool, heat affected zones and parent materials of the joints. For each series, samples were taken at around the mean fatigue load level from both failed and survived fatigue tests. Figures 87 to 94 show microhardness maps from a failed and survived fatigue test. The remainder of the maps can be found in Appendix A.

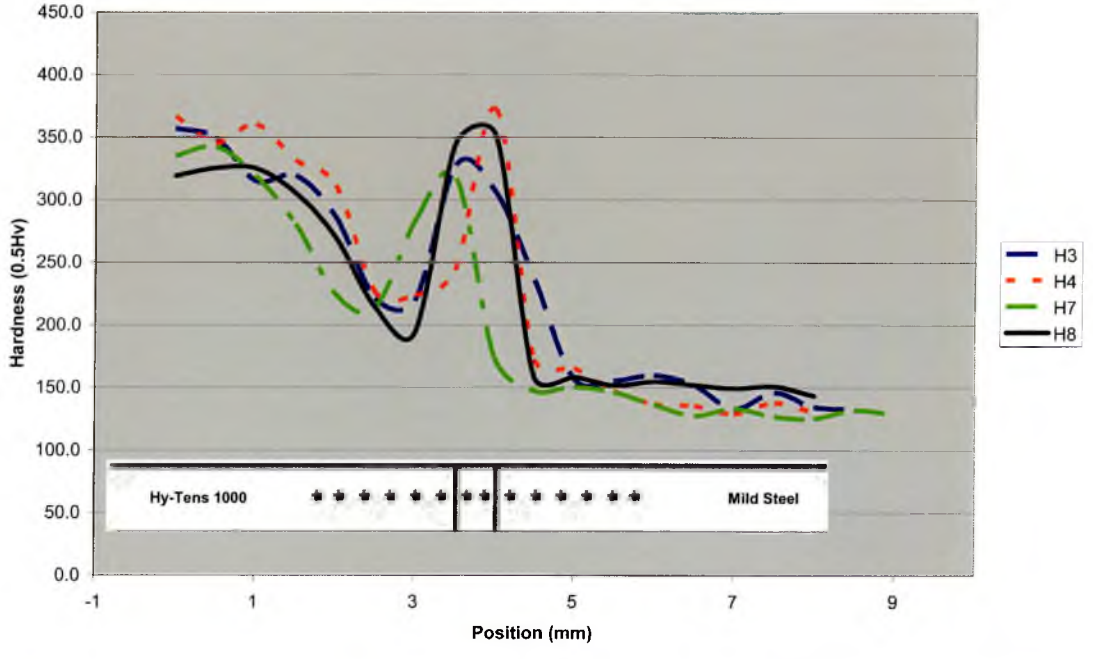

Figure 86. Graph showing microhardness profile of laser hybrid butt joint of HyTens 1000 to zinc coated mild steel using 308L-Si and 309L-Si filler wires

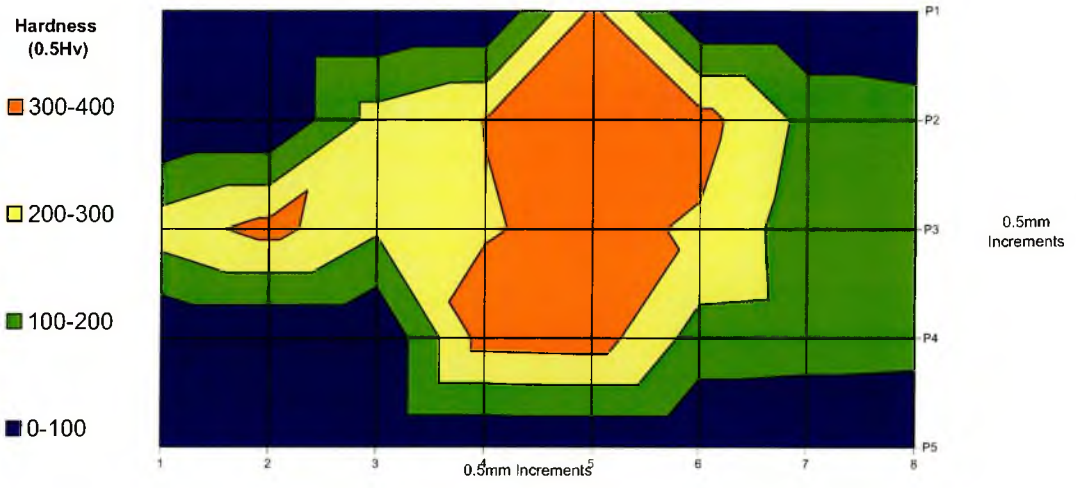

Figure 87. *Series 3 microhardness map of fatigue sample 3.4.6, the sample failed the fatigue test at 9.0kN after 521920 cycles.*

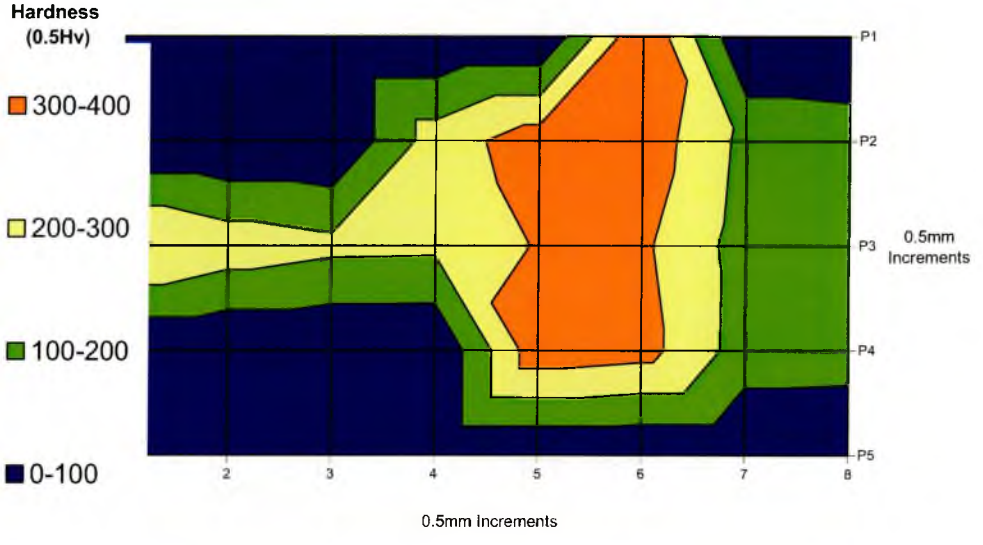

Figure 88. *Series 3 microhardness map of fatigue sample 3.5.2, the sample survived the fatigue test at 9.0kN completing 2 million cycles.*

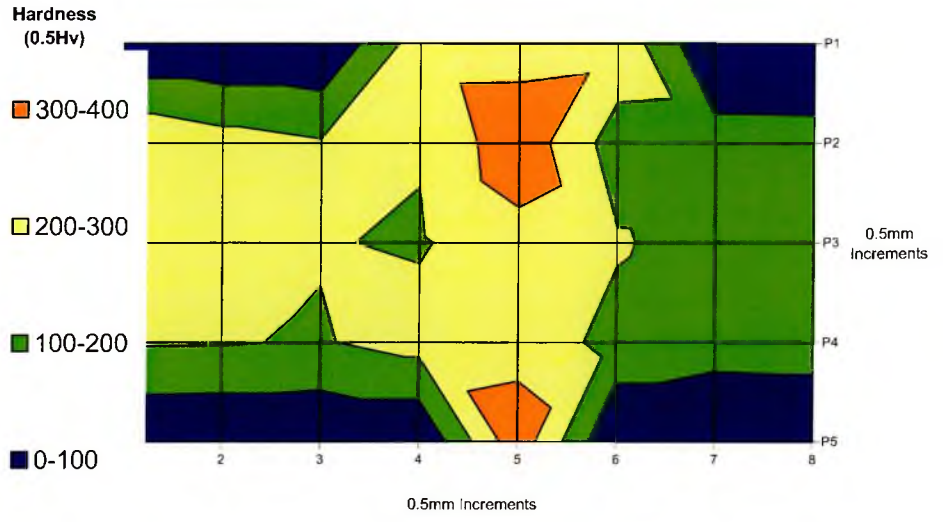

Figure 89. *Series 4 microhardness map of fatigue sample 4.6.6, the sample survived the fatigue test at 16.0kN completing 2 million cycles.*

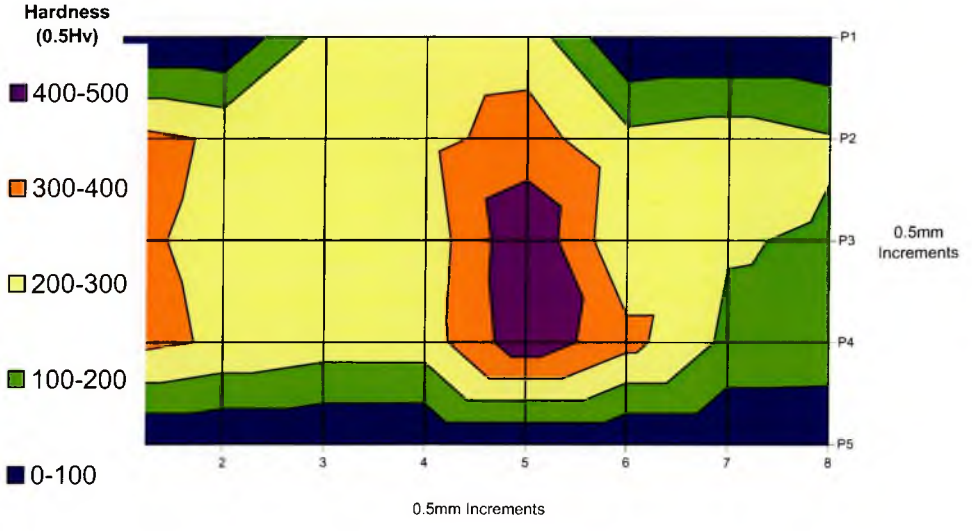

Figure 90. *Series 4 microhardness map of fatigue sample 4.7.5, the sample failed the fatigue test at 13.5kN after 170401 cycles.*

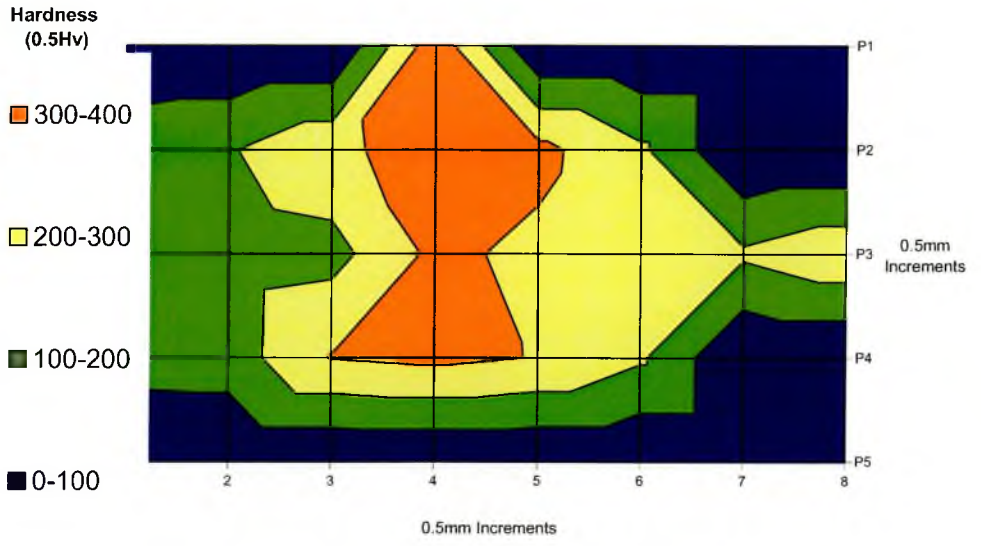

Figure 91. *Series 7 microhardness map of fatigue sample 7.3.3, the sample survived the fatigue test at 8.0kN completing 2 million cycles.*

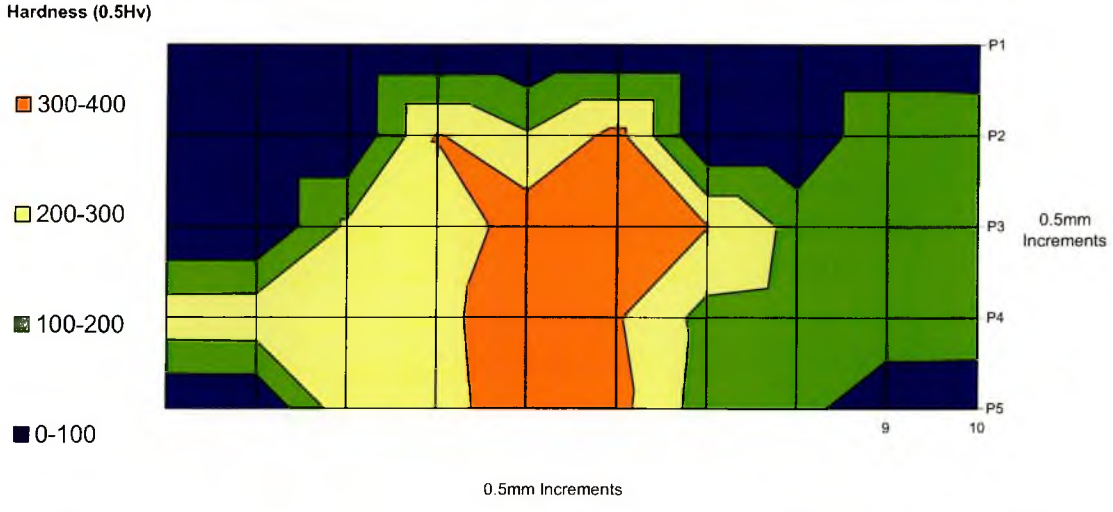

Figure 92. *Series 7 microhardness map of fatigue sample 7.8.6, the sample failed the fatigue test at 8.0kN after 843525 cycles.*

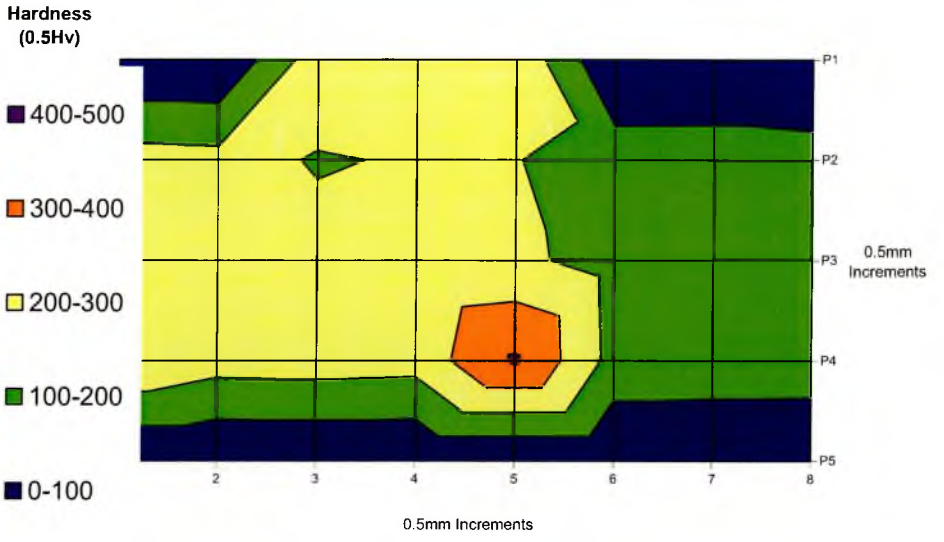

Figure 93. *Series 8 microhardness map of fatigue sample 8.6.1, the sample survived the fatigue test at 14.0kN completing 2 million cycles.*

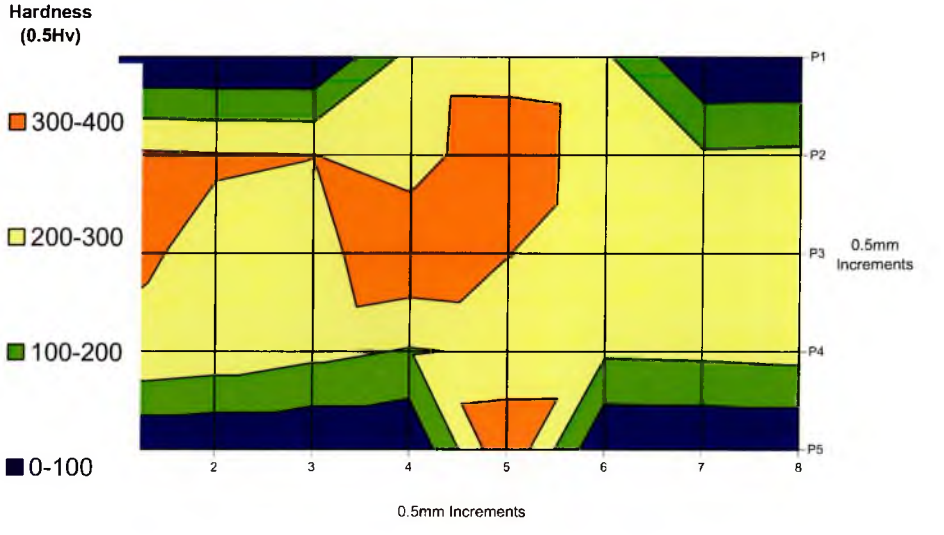

Figure 94. *Series 8 microhardness map of fatigue sample 8.6.4, the sample failed the fatigue test at 14.8kN after 465001 cycles.*

4.2.6 Elemental Mapping of the Weld Pool for the Laser Hybrid Butt Joints

Elemental mapping was carried out on samples from each series of Laser Hybrid butt welds. This was done using the SEM and semi-quantitative Energy Dispersive X-Ray (EDX) analysis. Elements scanned for were the main alloying elements of the predicated weld pool Fe, Cr and Ni.

Elemental distribution maps for each series for each element scanned for in addition to a secondary electron image of the samples can be found in figures 95 to 100 below. Additional maps for other samples can be found in Appendix B.

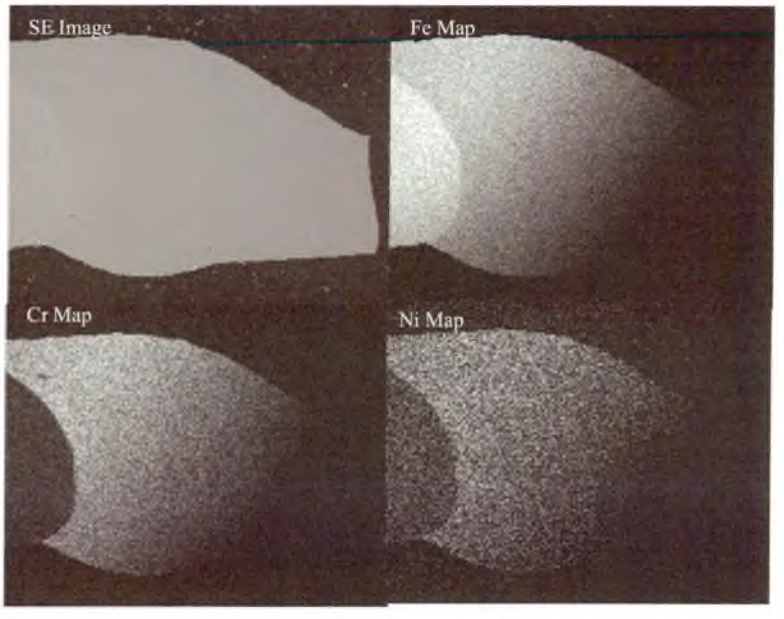

Figure 95. Elemental Mapping of Sample F1.3.1

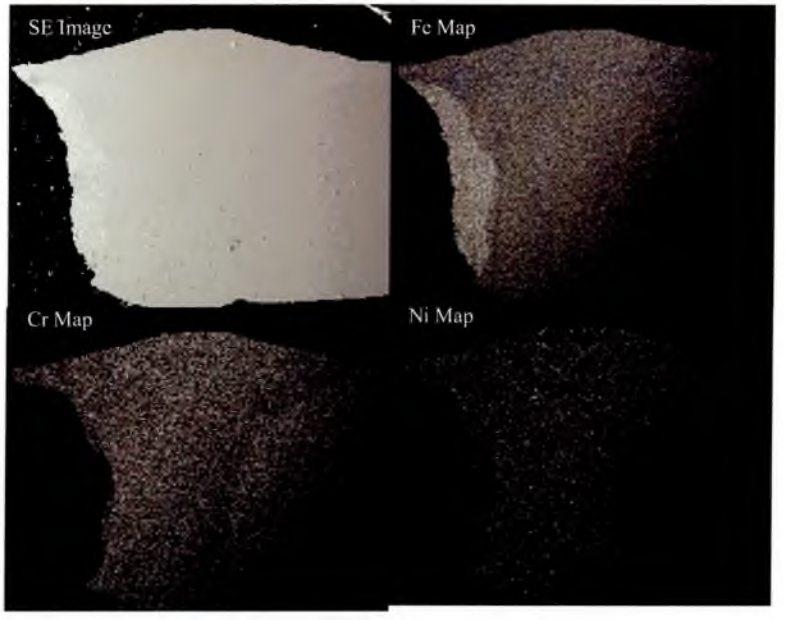

Figure 96. Elemental Mapping of Sample F2.5.2

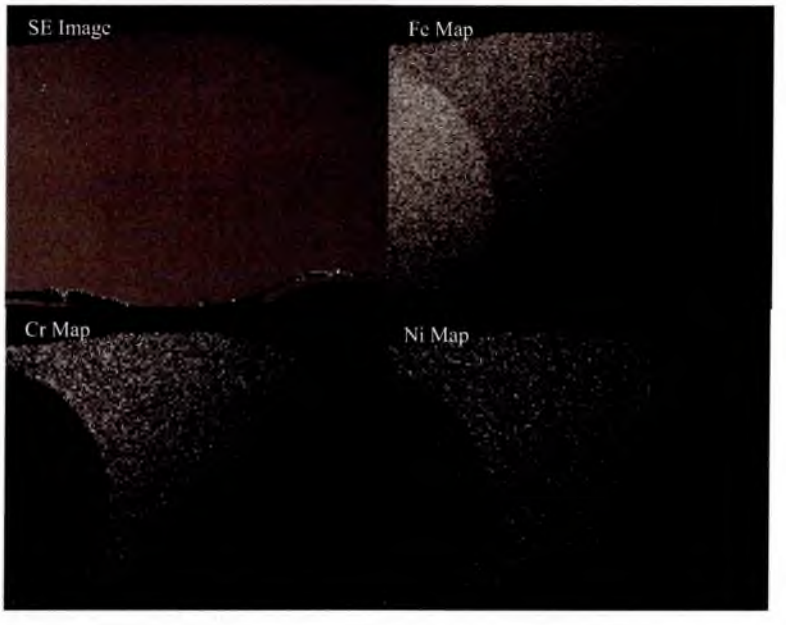

Figure 97. Elemental Mapping of Sample F3.2.6

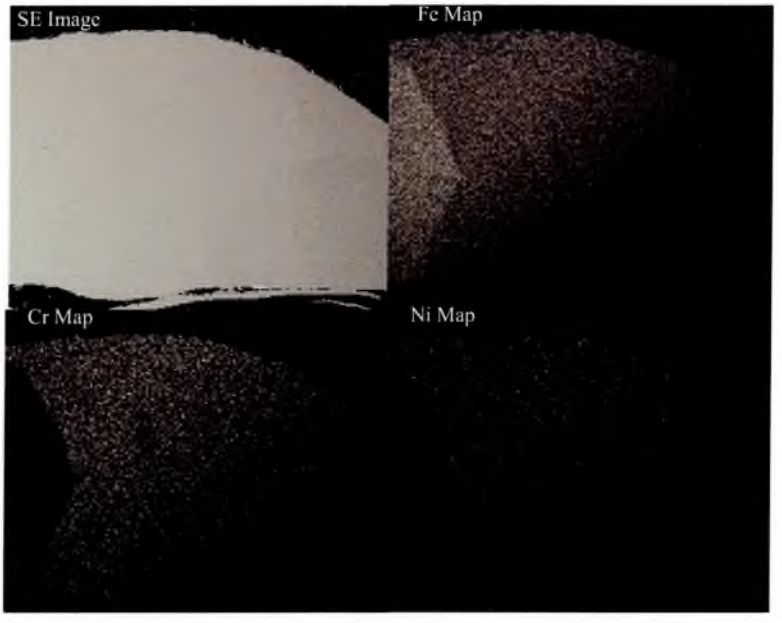

Figure 98. Elemental Mapping of Sample F5.4.2

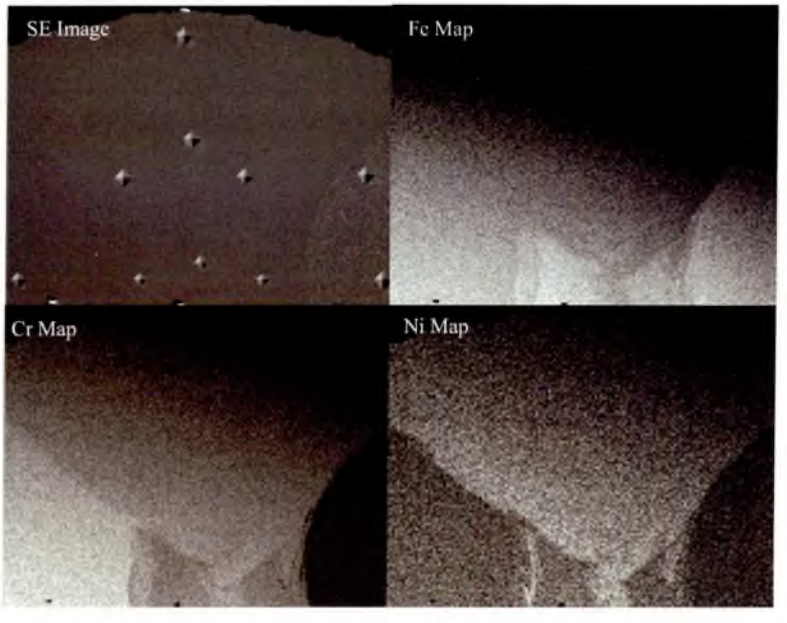

Figure 99. Elemental Mapping of Sample F6.1.2

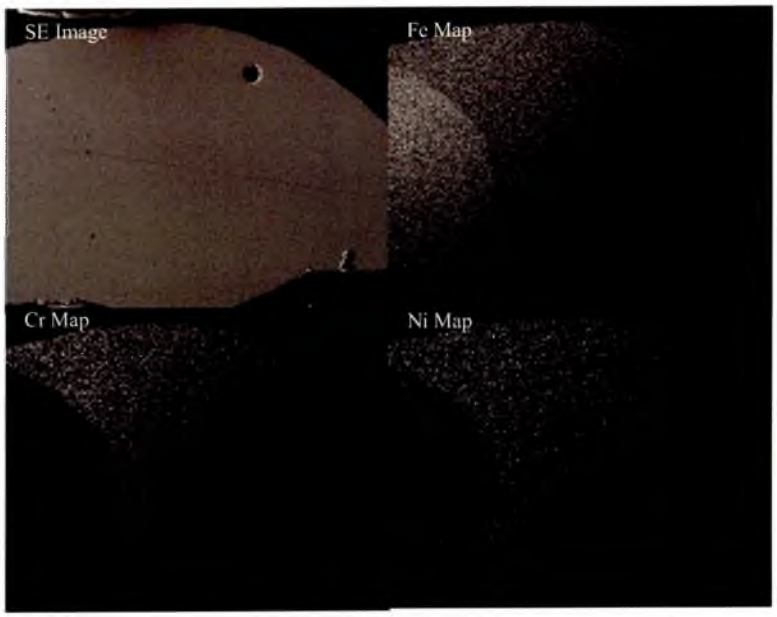

Figure 100. Elemental Mapping of Sample F7.3.3

4.2.7 Weld Pool Composition and Constitution Results for Laser Hybrid Welded Butt Joints

In order to assess the weld pool chemical composition and constitution, Semi-quantitative Energy Dispersive X-Ray (EDX) analysis with the Scanning Electron Microscope (SEM) and a Cobalt standard was carried out on the weld pool of each of the joint combinations. The samples used for this analysis were samples that completed 2 million cycles at the mean fatigue strength of the series. From the chemical composition profiles established, Schaeffler diagrams were plotted for each weld combination to determine the dilution in the welds. The Schaeffler diagrams for each series of joints are shown in figures 101 to 104

Table 19 outlines the dilution of the welded joints, where dilution is the percentage of parent metal melted. Dilution is based on the principal elements Fe, Cr, Ni, Mn, Mo and Si taken from the spot analysis. Table 19 also shows the predicted microstructure of the welds as a result of plotting a Schaeffler diagram for each series, the Schaeffler diagram relates the chemical composition of a weld pool to the phase constitution (or microstructure) (figures 101 to 104). These calculations assume that, in dissimilar metal joints, an equal proportion of each parent metal is melted.

Further analysis was carried out to determine the chemical composition in different areas of the weld pool, the top, the middle and the bottom weld area to establish any changes in chemical composition that may be present within a sample (figure 105) and between samples of the same series (figure 106).

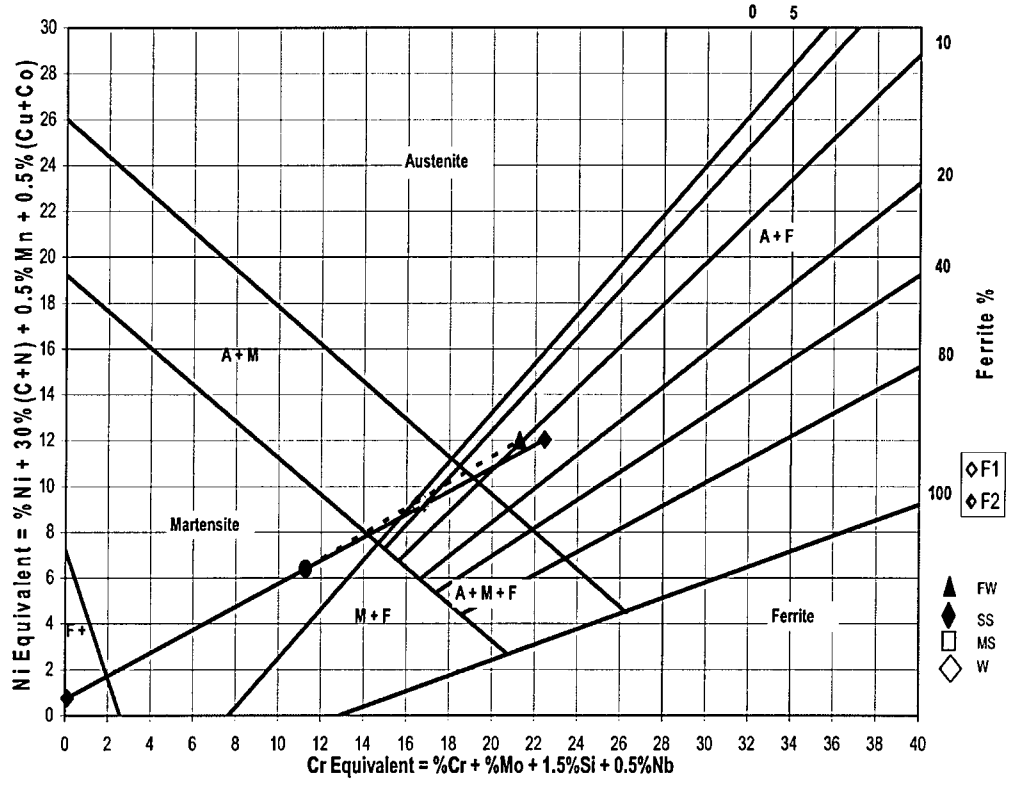

Figure 101. Schaeffler Diagram plotted from EDAX analysis for series F1 – LDX 2101 0.75mm to Dogal 260RP-X 1.5mm and series F2 – LDX 2101 1.5mm to Dogal 260RP-X 1.5mm with a 308L-Si Filler Wire.

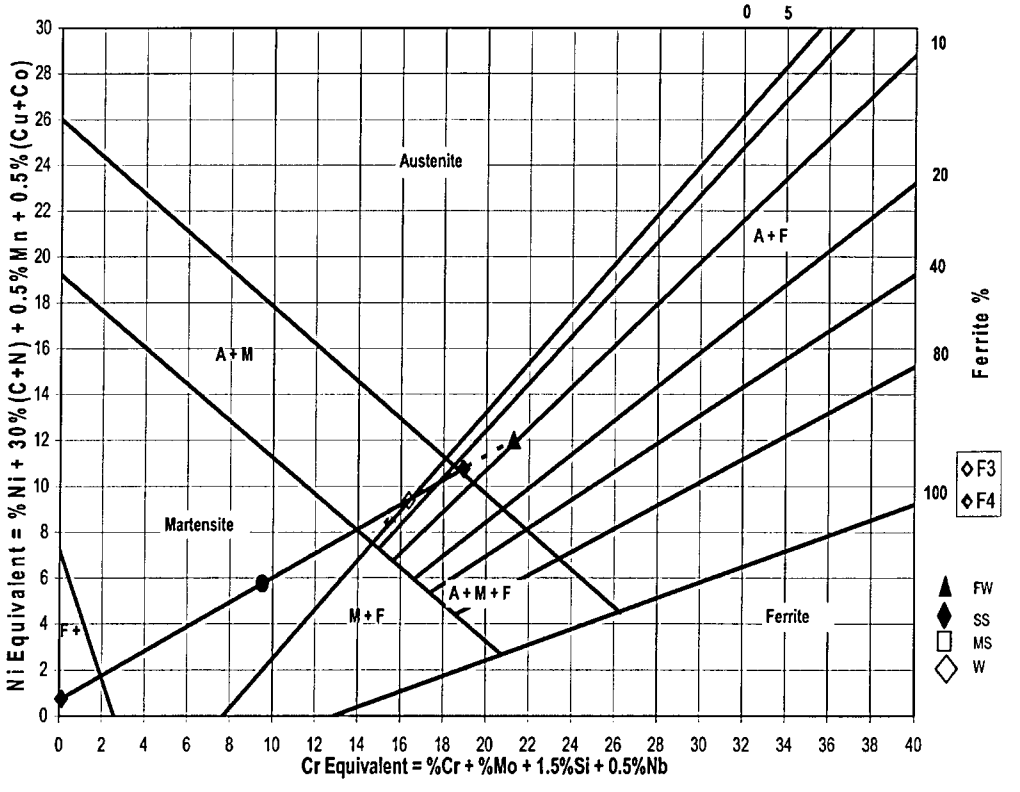

Figure 102. Schaeffler Diagram plotted from EDAX analysis for series F3 – HyTens 1000 0.75mm to HyTens 1000 1.5mm and series F4 – LDX 2101 1.5mm to Dogal 260RP-X 1.5mm with a 308L-Si Filler Wire.

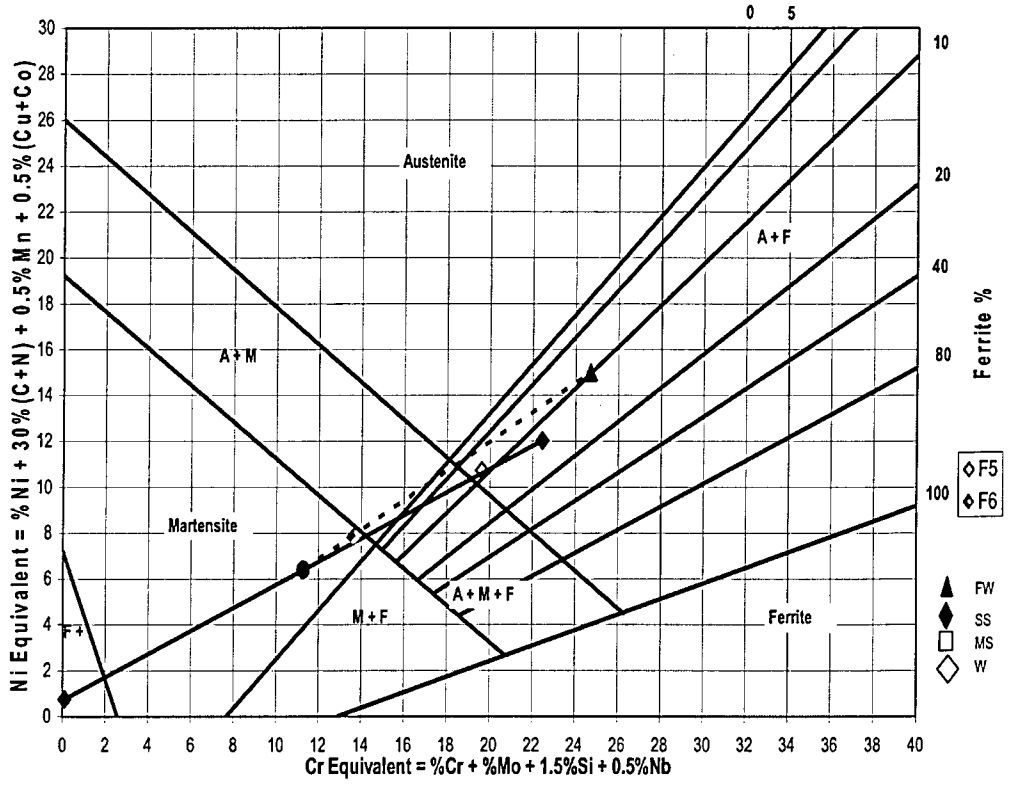

Figure 103. Schaeffler Diagram plotted from EDAX analysis for series F5 – LDX 2101 0.75mm to Dogal 260RP-X 1.5mm and series F6 – LDX 2101 1.5mm to Dogal 260RP-X 1.5mm with a 309L-Si Filler Wire

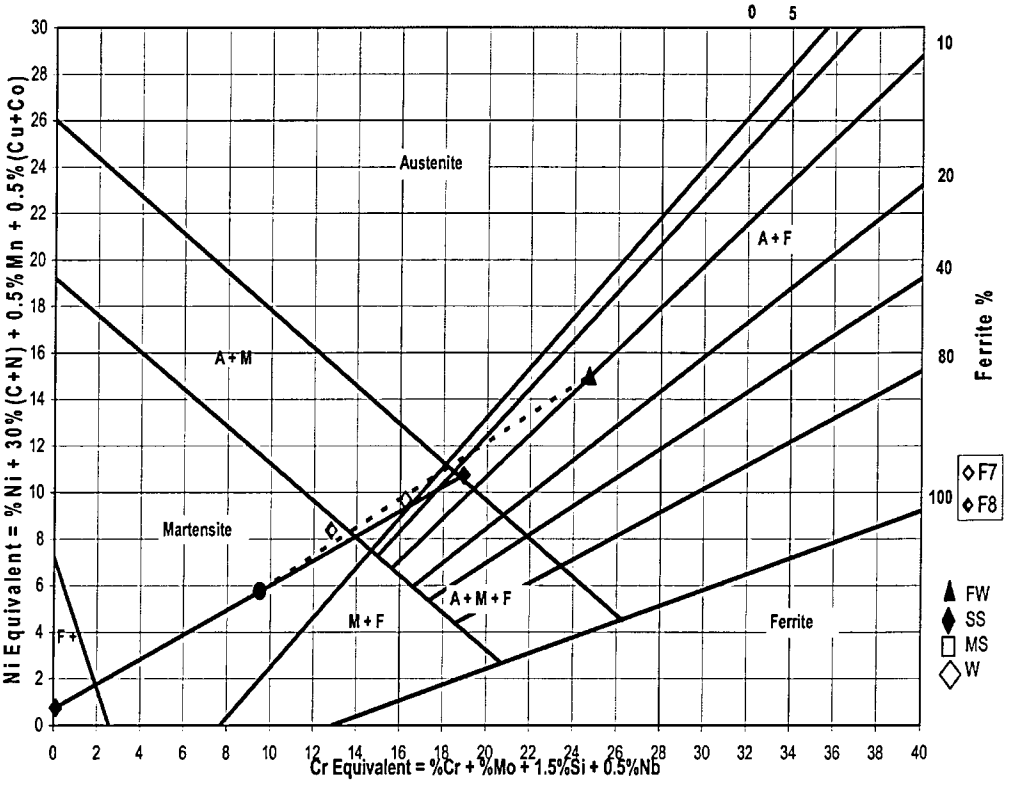

Figure 104. Schaeffler Diagram plotted from EDAX analysis for series F7 – HyTens 1000 0.75mm to HyTens 1000 1.5mm and series F8 – LDX 2101 1.5mm to Dogal 260RP-X 1.5mm with a 309L-Si Filler Wire.

Series ID	% Dilution	Predicted Weld bead Microstructure
1	55	Austenite, Martensite and Ferrite
2	51	Austenite, Martensite and Ferrite
3	54	Austenite, Martensite and Ferrite
4	58	Austenite, Martensite and Ferrite
5	46	Austenite, Martensite and Ferrite
6	89	Martensite
7	58	Austenite, Martensite and Ferrite
8	79	Martensite
Laser only welding[66]	79	Martensite

Table 18. Dilution (%) and predicted weld bead microstructure as determined using the chemical analysis results from the semi-quantitative Energy Dispersive X-Ray (EDX) analysis with the Scanning Electron Microscope (SEM) and a Cobalt standard with the Schaeffler Diagram for each series. Equivalent Laser welding results are shown for comparison.

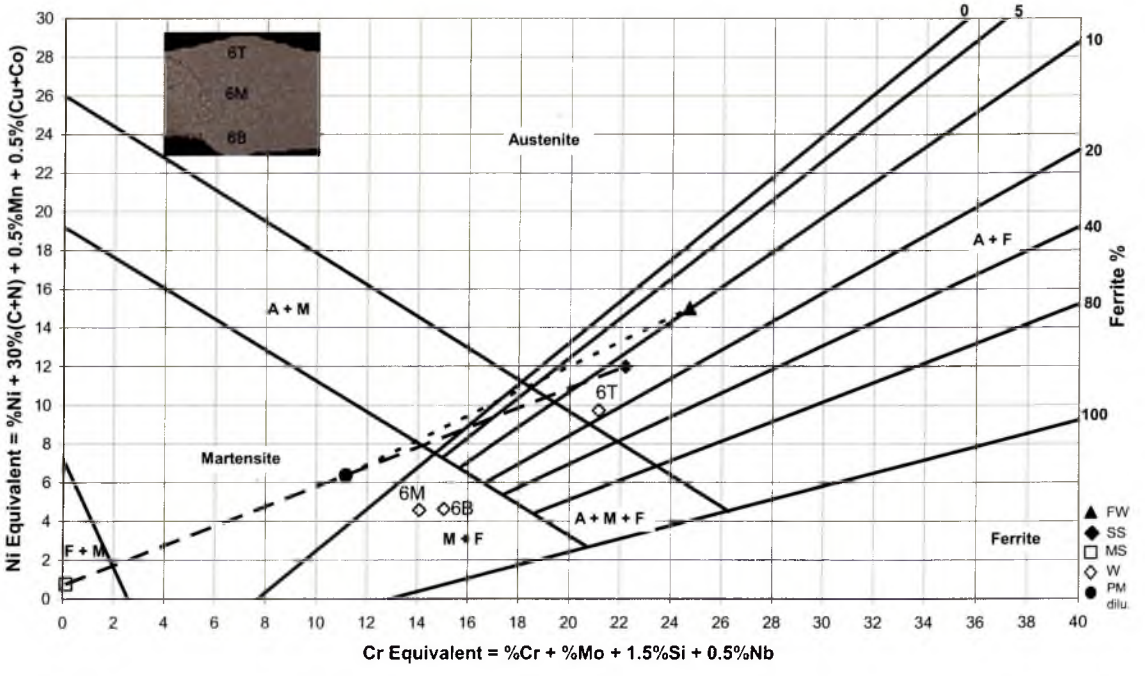

Figure 105. Schaeffler Diagram for series 6 of LDX 2101 1.5mm with Zinc coated mild 1.5mm steel with 309L-Si, spot analysis was taken at three different points, the top(T), the middle (M) and the bottom (B) of the weld pool as shown in the insert.

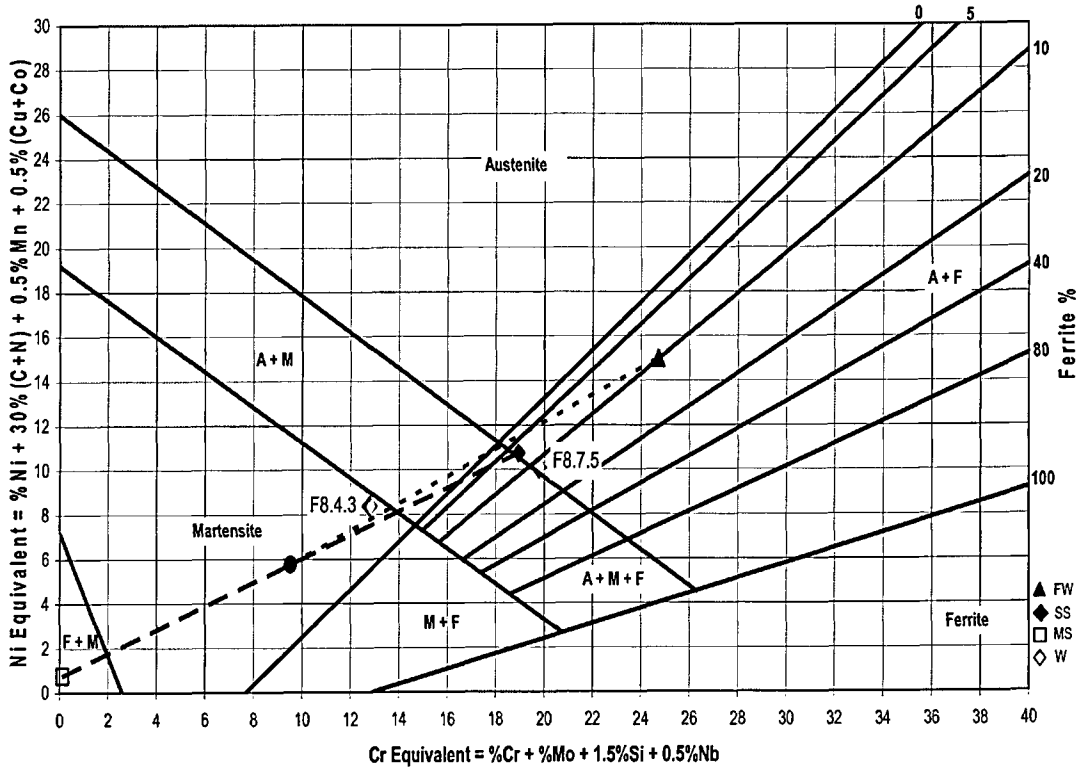

Figure 106. Schaeffler Diagram for series 8 of HyTens 1.5mm with Zinc coated mild 1.5mm steel with 308L-Si, spot analysis was taken from two different fatigue samples, F8.4.3 and F8.7.5 both samples yielded different results.

4.2.8 Grain Size Analysis Results for Laser Hybrid Welded Butt Joints

Grain size analysis was carried out using the mean linear intercept method, measurements were taken for the parent materials and the Heat Affected Zone (HAZ) in the dissimilar welded laser hybrid butt joints. The results can be seen in Figure 107 below.

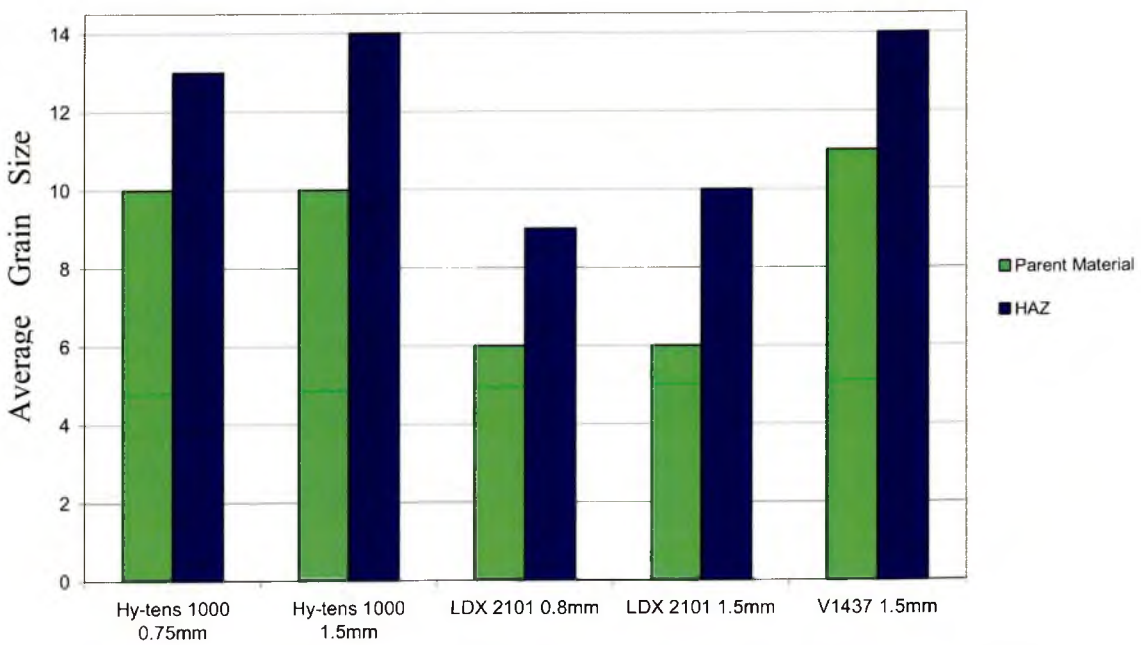

Figure 107. Graph showing average grain size (μm) in the parent materials and the Heat Affected Zone (HAZ)

4.2.9 Metallography for Laser Hybrid Welded Butt Joints

As previously outlined, due to the dissimilar metals in the joints a single cannot be used to reveal the surface structure of the whole welded joint, therefore several different etchants were used.

The mild steel was etched in 2% Nital to reveal the grain boundaries in order to analyse the grain size and any possible differences that may have occurred due to the heat input from the welding process. The general structure observed was equi-axed grains as seen in figure 108 and is typical of all the samples. The microstructure nearer to the weld metal, figure 109, has larger ferrite grains and inhomogeneous grain size indicating that grain growth has occurred during the heating /cooling weld cycle.

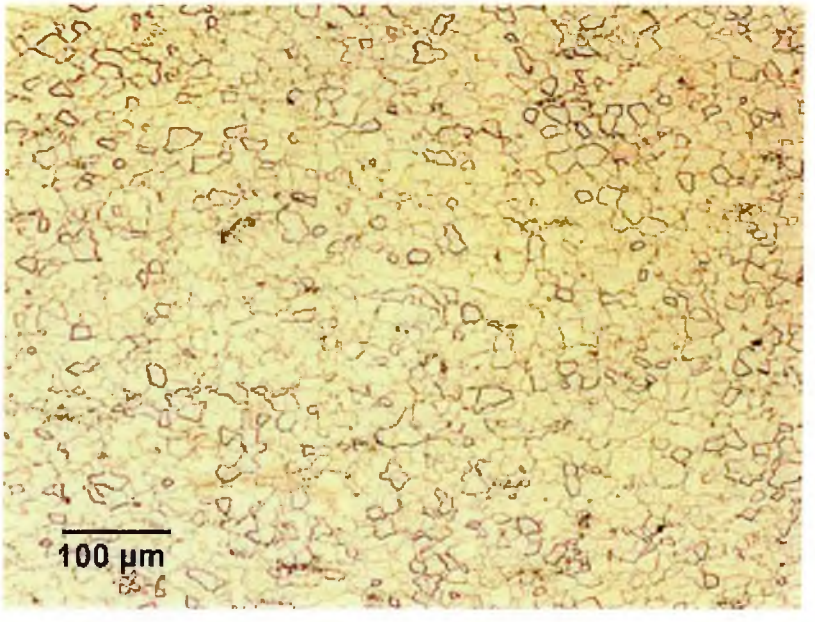

Figure 108. Mild steel microstructure etched in 2% nital

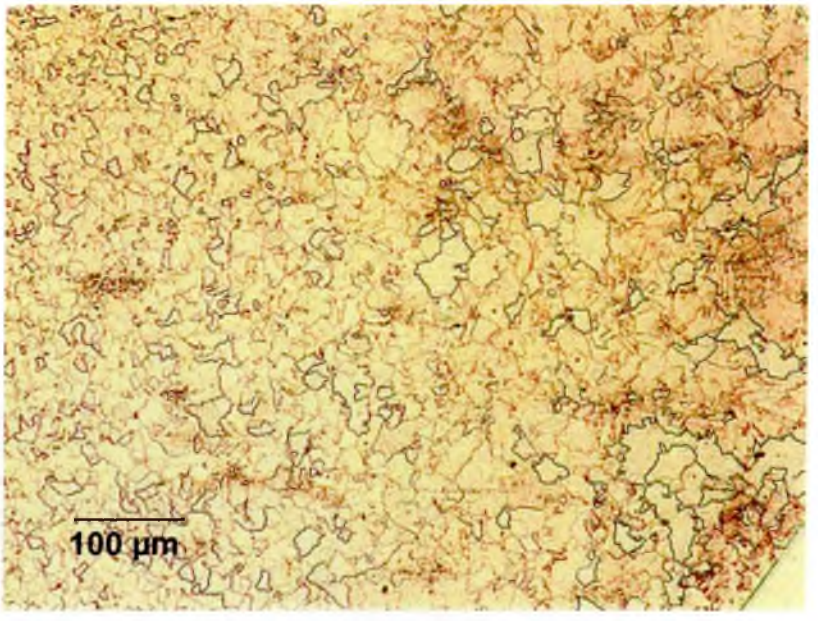

Figure 109. Mild steel HAZ microstructure etched in 2% nital

LDX 2101 samples were etched in 10% Oxalic acid to reveal the grain boundaries, the parent material microstructure can be seen in figure 110 and the microstructure nearer the weld can be seen in figure 111.

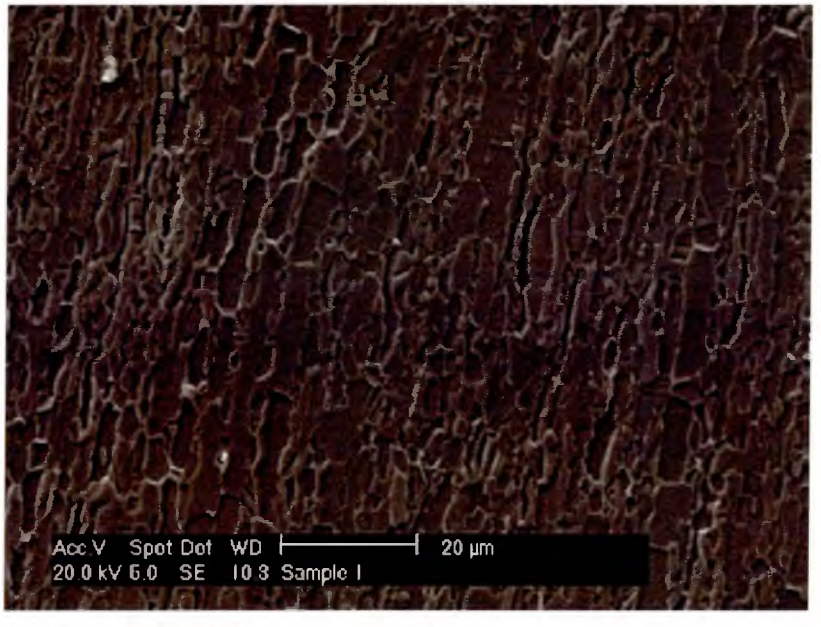

Figure 110. LDX 2101 microstructure etched in 10% oxalic acid, showing the typical as rolled microstructure of the austenite and ferrite phases present

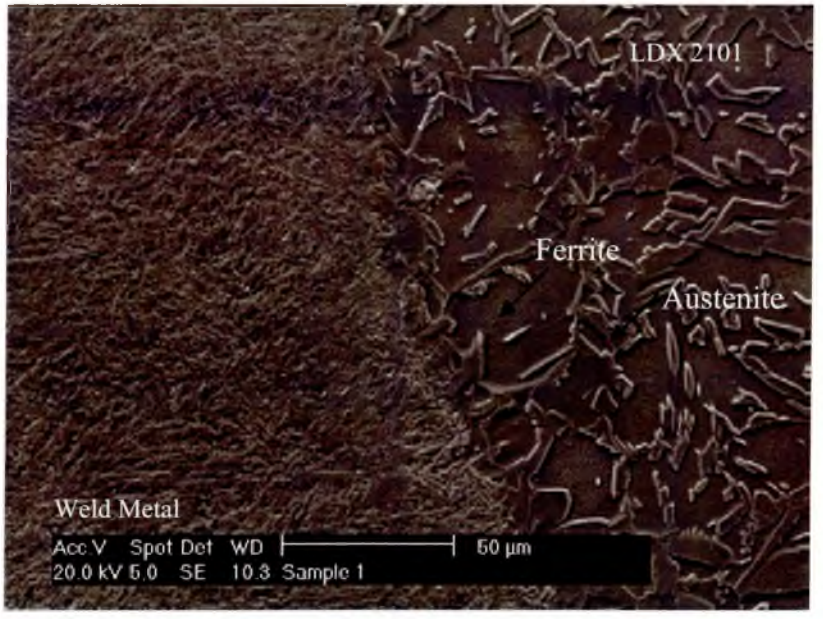

Figure 111. LDX 2101 Interface with weld etched in 10% oxalic acid showing the marked change in the austenite to ferrite ratio in the HAZ of the LDX 2101

Figure 112. Hy-tens 1000 and Weld Metal Interface etched in 10% oxalic acid martensite in the HAZ and the weld material.

Figure 111 shows the interface between the weld and LDX 2101 parent material. The Microstructure in the HAZ shows a marked change in the austenite ferrite ratio due to the transformation that has occurred.

Figure 112 shows the interface of a Hy-Tens 1000 butt weld. It illustrates that the HAZ consists of a fine grain structure of martensite due to the transformation from austenite to martensite during the heating and cooling cycle of the weld process. The weld metal also has a martensitic structure.

4.3 *Laser Hybrid Welded Lap Joints*

Lap joint configuration trials have been carried out on various occasions throughout this research at ESAB process and development centre for joining of Hy-Tens 1000 to zinc coated mild steel and LDX 2101 to the zinc coated mild steel using the laser hybrid process

Problems were encountered with laser hybrid welding of the lap joints, this included excessive spatter, surface breaking porosity and solidification cracking. Out of several initial samples that were welded in the first trials, samples 7 and 19 were the best welds produced in terms of aesthetic appearance, the details of the joints and the parameters used are outlined in table 20 below.

Initial samples were sectioned and examined, and solidification cracks were found in the samples of LDX 2101 and zinc coated mild steel, as shown in figure 113 below.

The depth of penetration of the initial laser hybrid lap joints was also measured as concerns were raised during trials that the penetration was coming through the underside of the bottom plate. Figures 114 and 115 show these results.

Optimisation of laser hybrid welded lap joints continued for the following combinations using the 309L-Si:

- Hy-Tens 1000 1.5mm to Dogal 260RP X 1.5mm
- LDX 2101 1.5mm to Dogal 260RP X 1.5mm

However, further problems arose due to the presence of the zinc coating, including porosity and cracking as demonstrated in figures 116 to 118. After initial trials were completed an effect of plate gap and torch angle on the frequency of underside cracking was observed and can be seen in figure 119.

Cracking observed in samples using the HyTens 1000 material was examined by using the SEM. The Results are shown in Figures 120 to 122.

Figure 120 shows the open crack and the blue/brown area indicates that the cracks occurred at high temperature. Figure 122 shows the SEM images of the crack and at the higher magnification cracking is observed in the samples following the grains of the material, as would be expected of liquid metal embrittlement.

Parameter		Lap Sample 7	Lap Sample 19
Base Material		LDZ 2101 1.5mm	Hy-Tens 1000 1.5mm
Top Material		Zinc coated mild steel 1.5mm	Zinc coated mild steel 1.5mm
Lap Length (mm)		10.0	10.0
Filler Wire		309L-Si	309L-Si
Diameter of Wire (mm)		1.0	1.0
MIG Shielding Gas		Ar + 30%He + 1%O_2	Ar + 30%He + 1%O_2
Welding Speed (m/min)		4.5	4.5
Wire Feed Speed (m/min)		12.0	12.0
Voltage (V)		30.5	30.5
Measured Values	**Current (A)**	203.9	203.0
	Voltage (V)	30.1	29.8
	MIG Power (kW)	6.23	6.18

Table 19. Welding parameters for initial lap samples using the Laser Hybrid Process

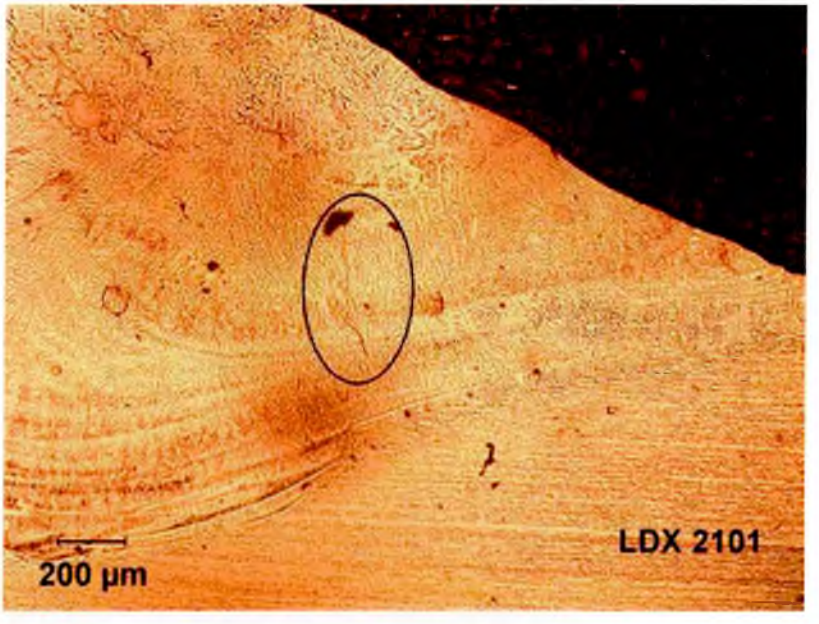

Figure 113. Solidification cracking observed in a lap joint of LDX 2101 laser hybrid welded to zinc coated mild steel

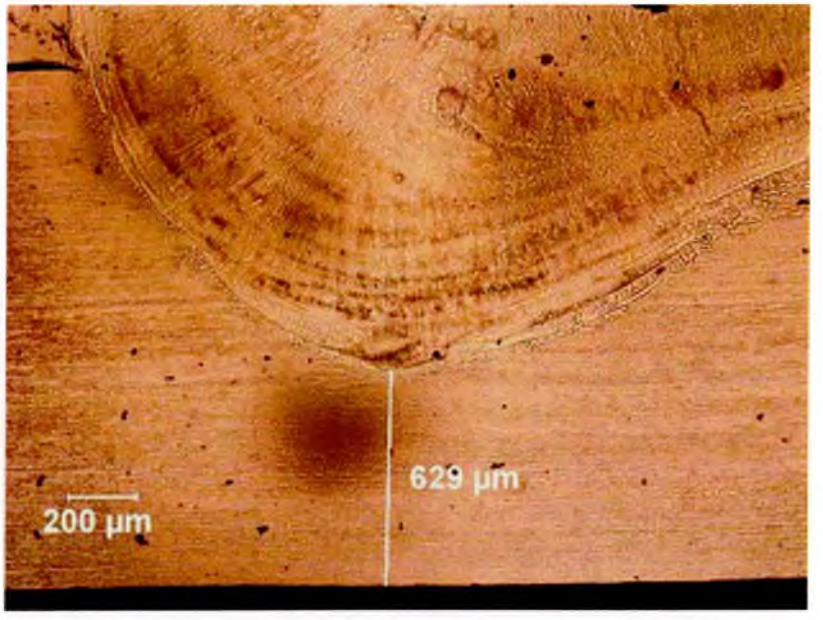

Figure 114. Depth of penetration for laser hybrid welded lap joint for LDX 2101 to zinc coated mild steel.

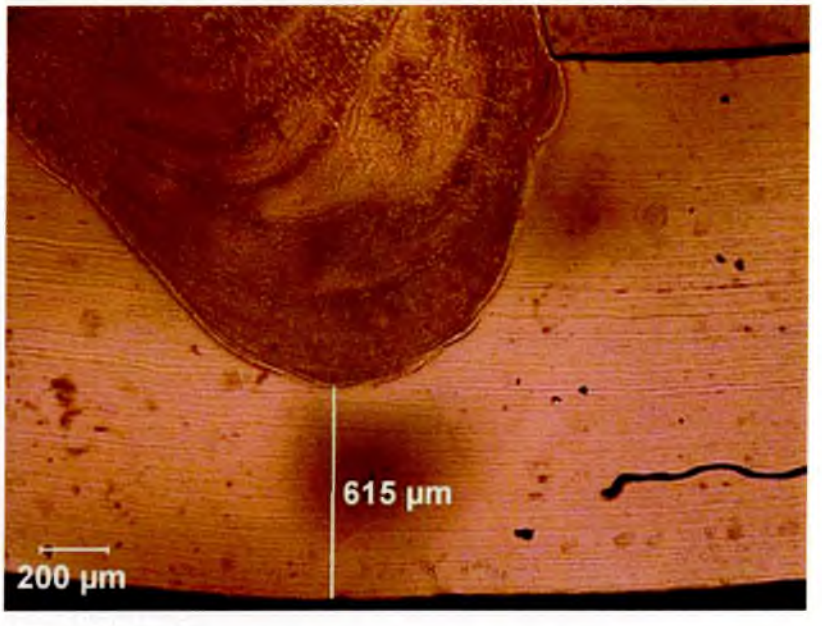

Figure 115. Depth of penetration for laser hybrid welded lap joint for Hy-Tens 1000 to zinc coated mild steel

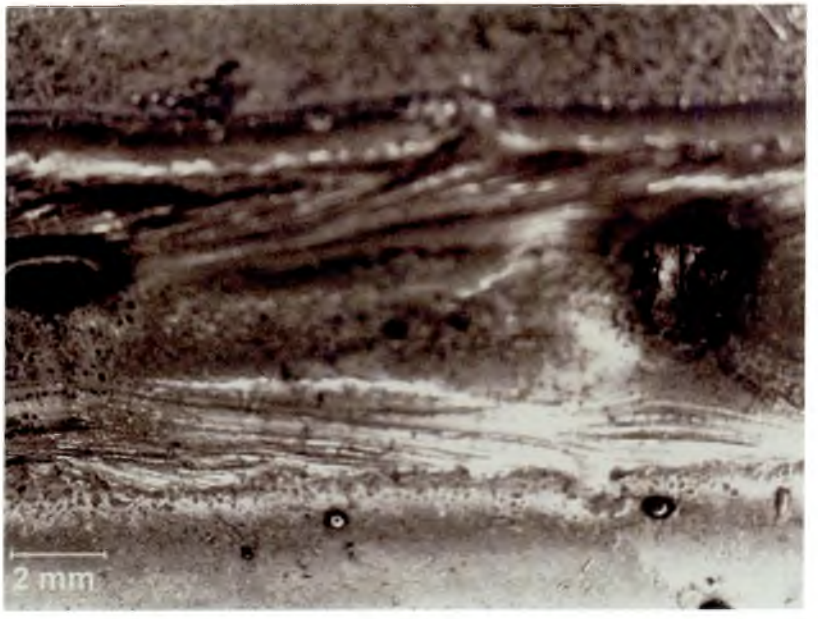

Figure 116. Photo showing surface breaking pores with cracking on a lap joint of Hy-Tens 1000 to Dogal 260RP-X with 309L-Si filler

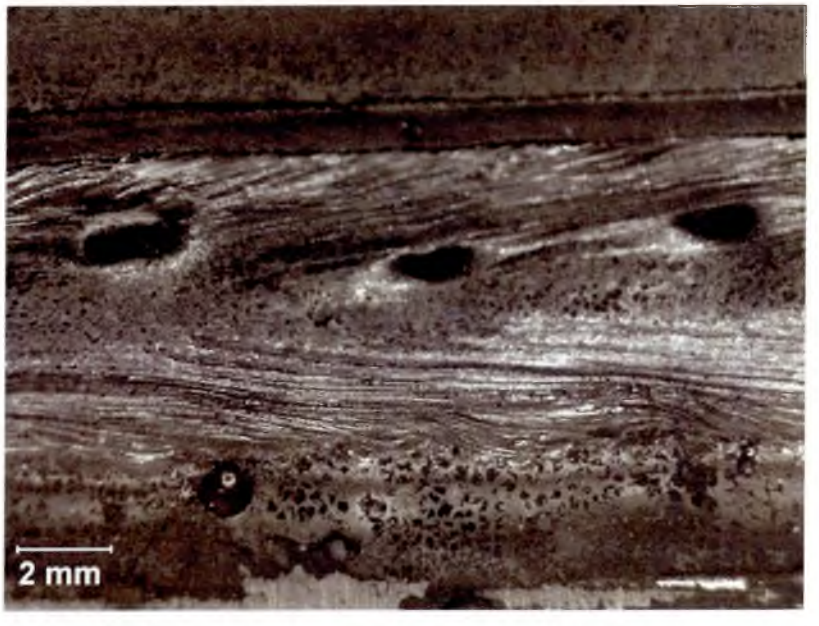

Figure 117. Photo showing surface breaking pores on a lap joint of LDX 2101 to Dogal 260RP-X with 309L-Si filler

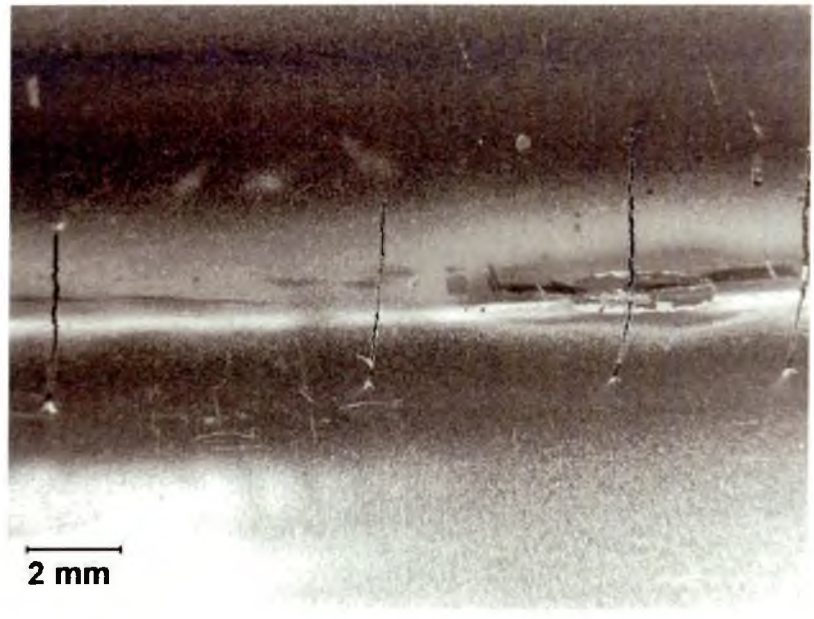

Figure 118. Photo showing transverse cracking on the underside of the Hy-Tens 1000 in a lap joint of Dogal 260RP-X with 309L-Si filler

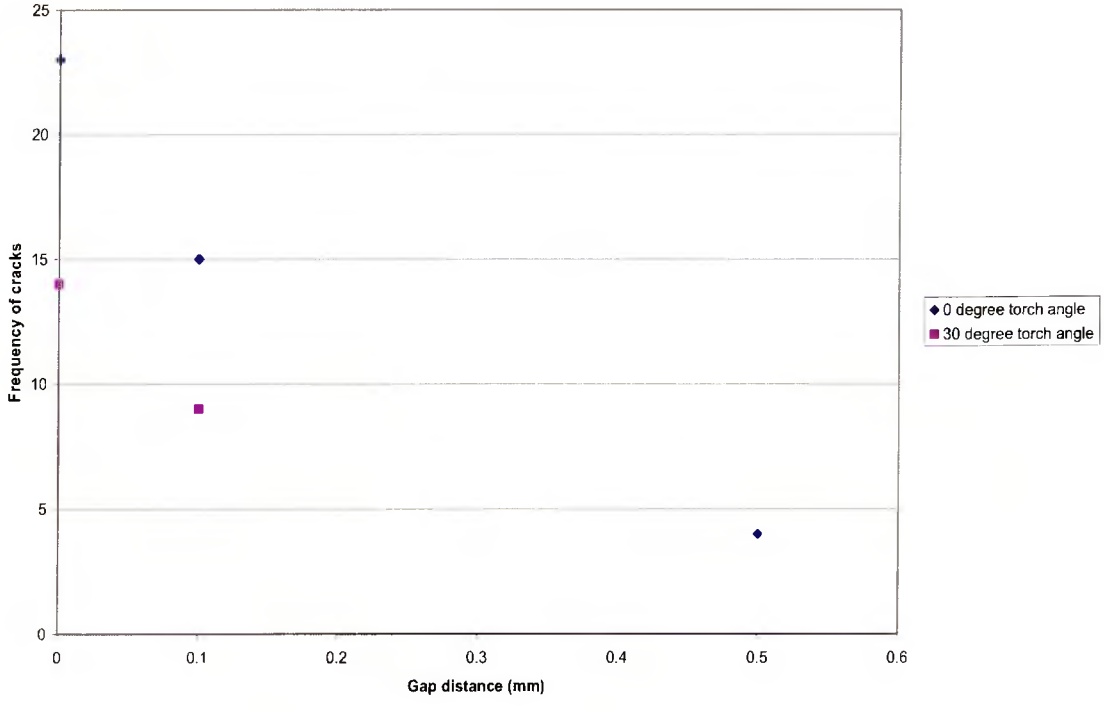

Figure 119. Graph showing that as the gap between the two plates and the welding angle increases the amount of observed cracking is greatly reduced

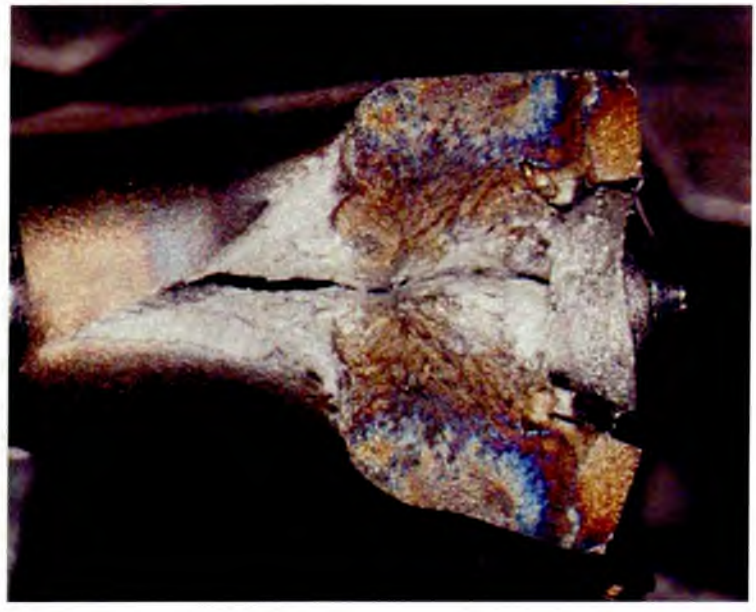

Figure 120. Macro Image of Underside Cracking Observed in Lap Joints using the HyTens 1000 Stainless (the crack has been opened top reveal the fracture surface).

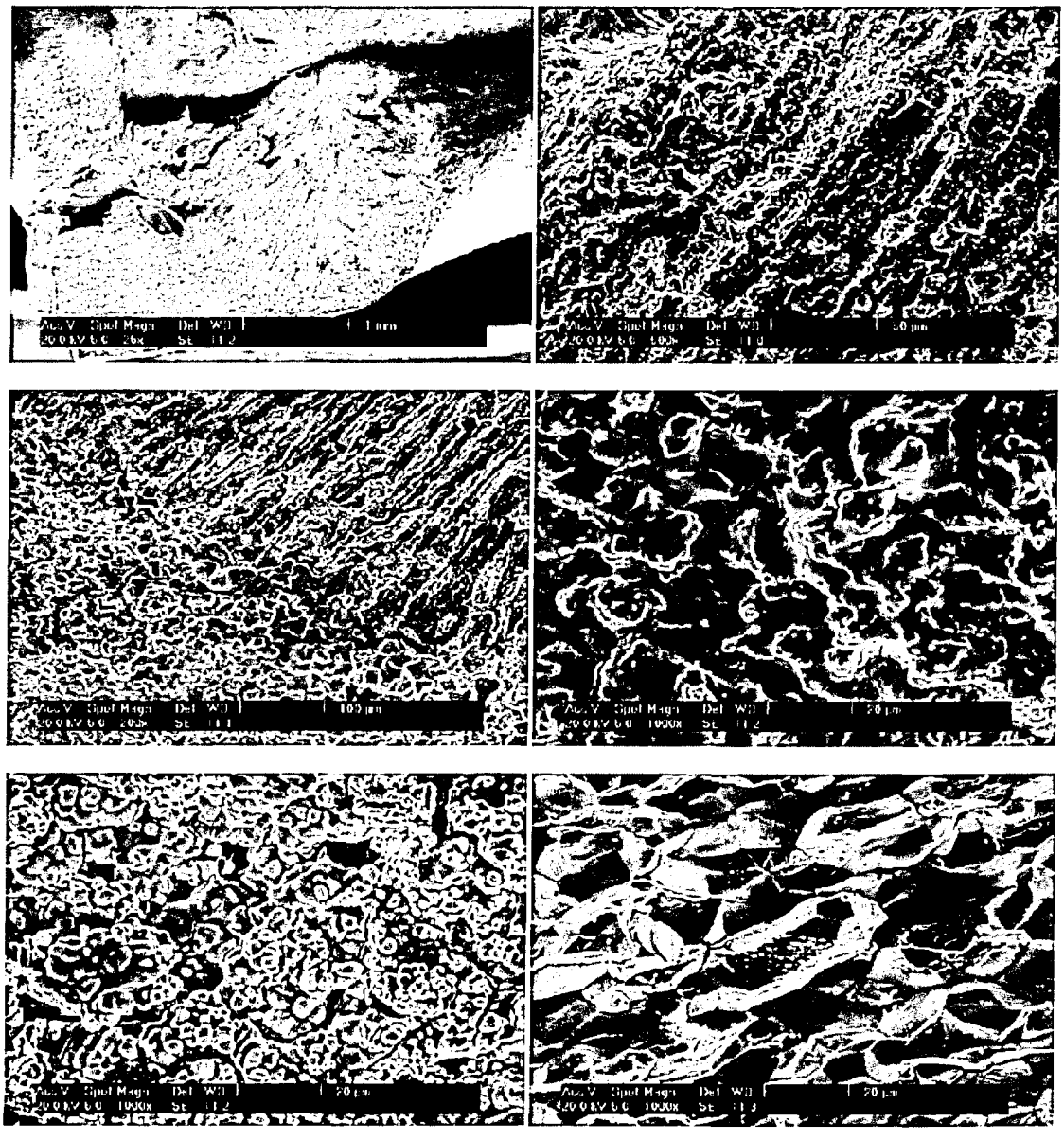

Figure 121. SEM Images of the fracture surface of an lap joint using HyTens 1000 Stainless Steel

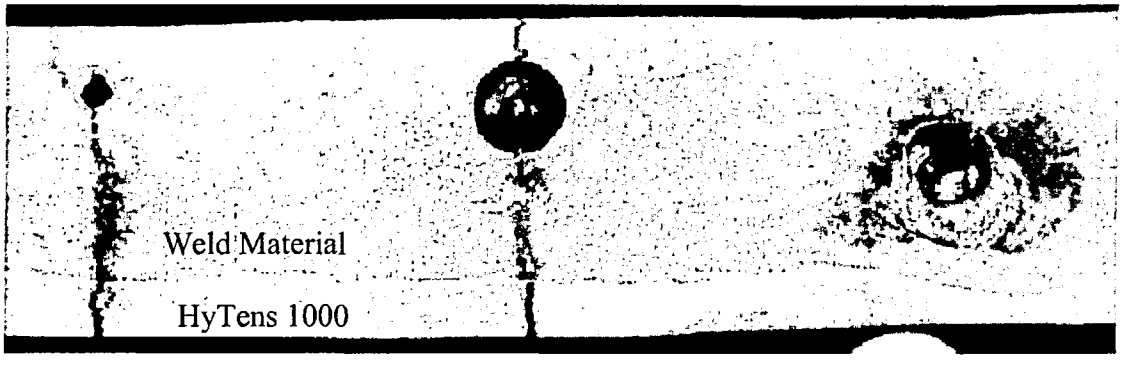

Figure 122. Macro Image of a Longitudinal Section Through an Lap Joint using HyTens 1000 Stainless, Cracks are Shown to go through the Full Thickness of the Weld and often Coincide with Porosity.

4.4 *Cold Metal Transfer Welded Butt Joints*

Butt joints were produced using the CMT process for LDX 2101 1.5mm thick to Dogal 260RP-X 1.5mm with the 308L-Si Filler wire, 1.0mm diameter. This series of joints is denoted as C1.

The following section outlines the results of the testing programme for Cold Metal Transfer Butt joints.

Optimisation took place to find the optimum process parameters for the material combination. Figure 123 below shows the effect that altering each parameter had on the quality of the joint produced. Optimum parameters for the material and joint combination can be found in table 21 below.

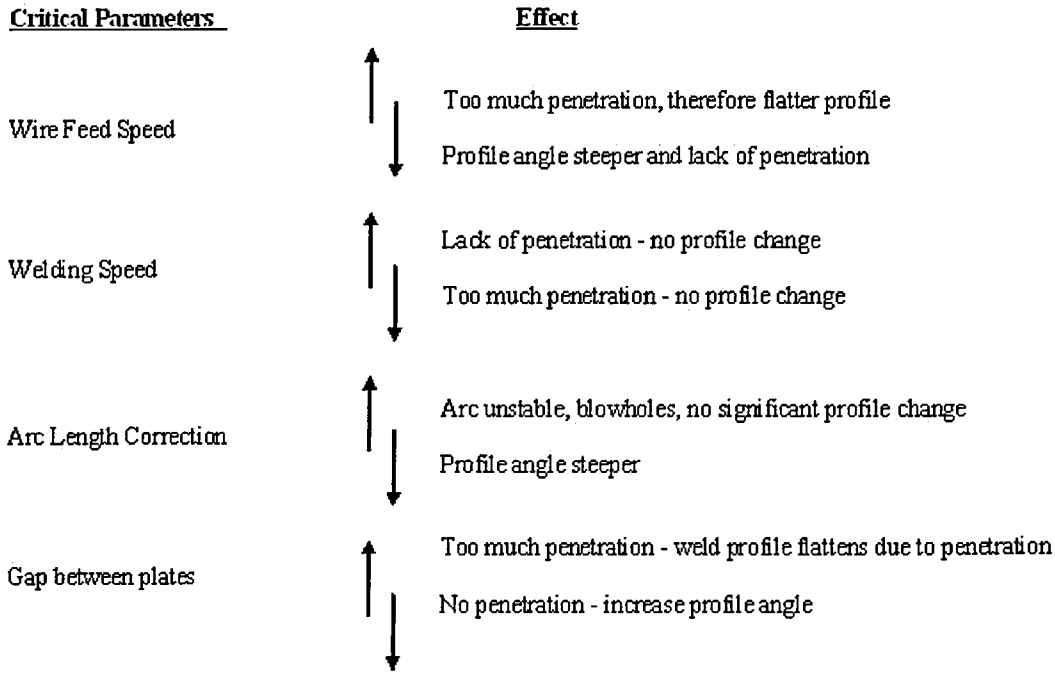

Figure 123. Diagram showing effect of critical parameters on resulting weld bead for Cold Metal Transfer joining

Sample ID	94
Material 1	LDX 2101, 1.5mm
Material 2	Dogal 260 RP-X, 1.5mm
Filler Wire	308L-Si
Filler Wire Diameter (mm)	1.00
Gap between plates (mm)	0.50
Mode	CMT
Welding Speed (m/min)	1.27
Wire Feed Speed (m/min)	8.00
Arc Length Correction (%)	20
Shielding Gas	2.5%CO_2 +Ar
Shielding Gas Flow Rate (L/min)	10

Table 20. Optimum parameters for CMT process for a butt joint configuration

4.4.1.1 Tensile Properties of Cold Metal Transfer Butt Joints

Figure 124 below shows the results for the tensile tests carried out on CMT welded Butt Joints of LDX 2101 (1.5mm thickness) to Dogal 260RP-X (1.5mm thickness) with 308L-Si filler wire (1mm diameter). The tests were carried out on each weld run produced for this series.

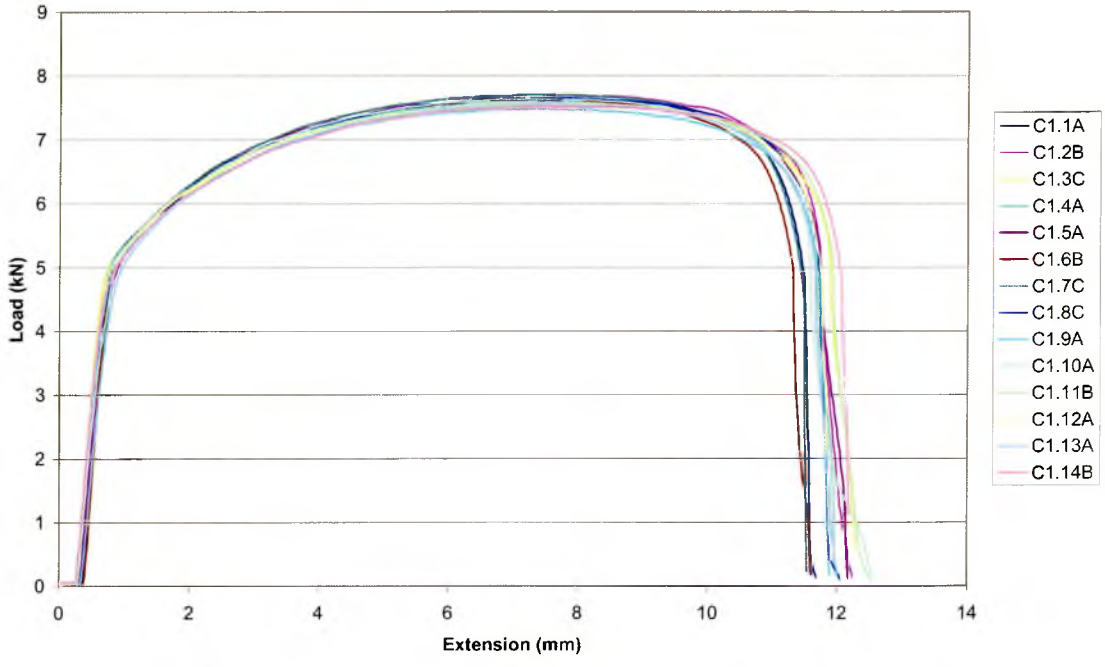

Figure 124. Graph showing Load vs Extension for the results of tensile tests carried out for Cold Metal Transfer Butt Joints, the average UTS was 422.6MPa

4.4.1.2 Fatigue Results of CMT Butt Joints with LDX 2101

The results of the staircase fatigue tests for Cold Metal Transfer butt joints with LDX 2101 and zinc coated mild steel using filler wire 308L-Si (series C1) are outlined below. The results are outlined in figures 125 and 126 which show the actual staircase fatigue results along with calculated values for mean fatigue strength (kN), standard deviation (kN) convergence factor and the standard error for the mean fatigue strength in accordance with the procedure outlined in section 3.

A graph of fatigue load (kN) verses cycles completed is also given, showing the results of the 25 individual tests carried out for each staircase fatigue test. Finally the mean fatigue strength (kN) has been converted to a 'line load' which is a value of load per unit length measured in N/mm and will allow these results to be compared to other joining processes of similar material and joint configuration.

Series C1

Load Range (kN)	Step No. (i)	Test Specimen Number																									Number of		Using LFE as N	
		1	2	3	4	5	6	7	8	9	10	11	12	13	14	15	16	17	18	19	20	21	22	23	24	25	Failures (f)	Runouts (r)	iN	i^2N
9.8	4									X																	1	0	0	0
9.4	3		X		X				O		X		X														4	1	3	9
9.0	2	O		O		X		O				O		X		X						X		X			5	4	8	16
8.6	1						O								O		X		X		O		O		X		3	4	4	4
8.2	0																	O		O						O	0	3	0	0
																											Σf	Σr	ΣiN	Σi^2N
																											13	12	15	29

Figure 125. Staircase fatigue results for C1 - LDX 2101 1.5mm to Dogal 260RP-X 1.5mm with 308L-Si filler wire

Step divide: 0.4kN

Least Frequent Event: Runouts

Calculated Mean Fatigue Strength:

$$x = 8.2 + 0.4\left(\frac{15}{12} - \frac{1}{2}\right)$$

$$x = 8.5kN$$

Convergence Factor:

$$\left(\frac{(12*29) - 15^2}{12^2}\right) = 0.854$$

Standard Deviation:

$$s = 1.620 * 0.40\left(\frac{(12*29) - 15^2}{12^2} + 0.029\right)$$

$$s = 0.572kN$$

Standard Error for Mean Fatigue Strength:

$$S_x = \frac{0.527}{\sqrt{12}}.1.15$$

$$S_x = 0.190kN$$

Line Load: 189N/mm

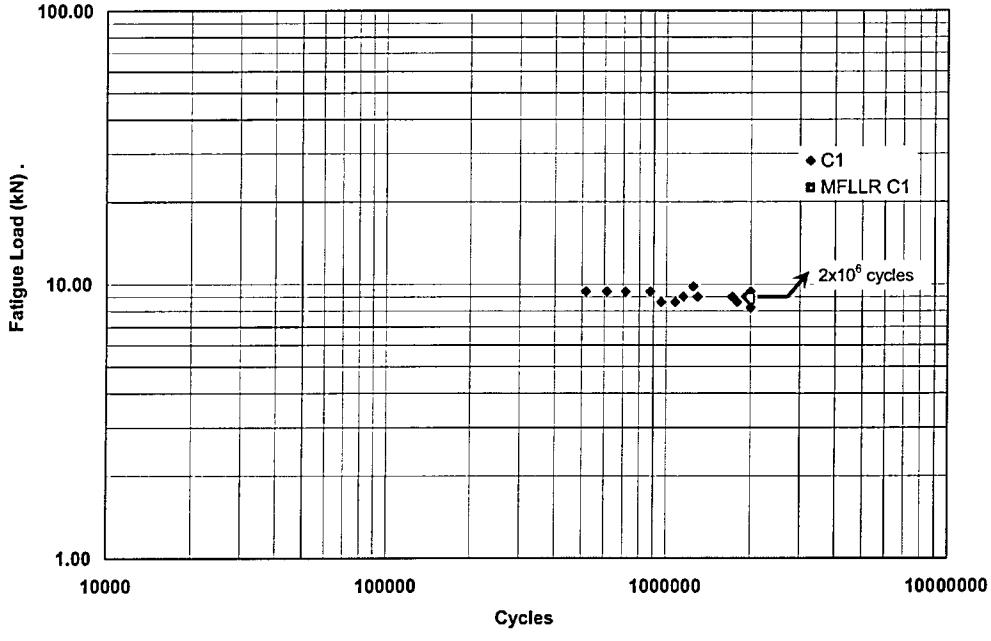

Figure 126. Graph to show fatigue load range for series C1 - LDX 2101 1.5mm to Dogal 260RP-X 1.5mm Cold Metal transfer welded butt joint

4.4.1.3 Fatigue Failure Analysis for Cold Metal Transfer Butt Joints

For the fatigue test specimens that failed before the 2000000 cycle runout criteria, failure analysis was carried out to determine the position of the fatigue failure and to assess whether the point of failure was consistent for all failed samples.

Figure 127 below shows an example of the common point of failure and figure 128 shows a typical fracture surface for the failed fatigue specimens for the C1 series.

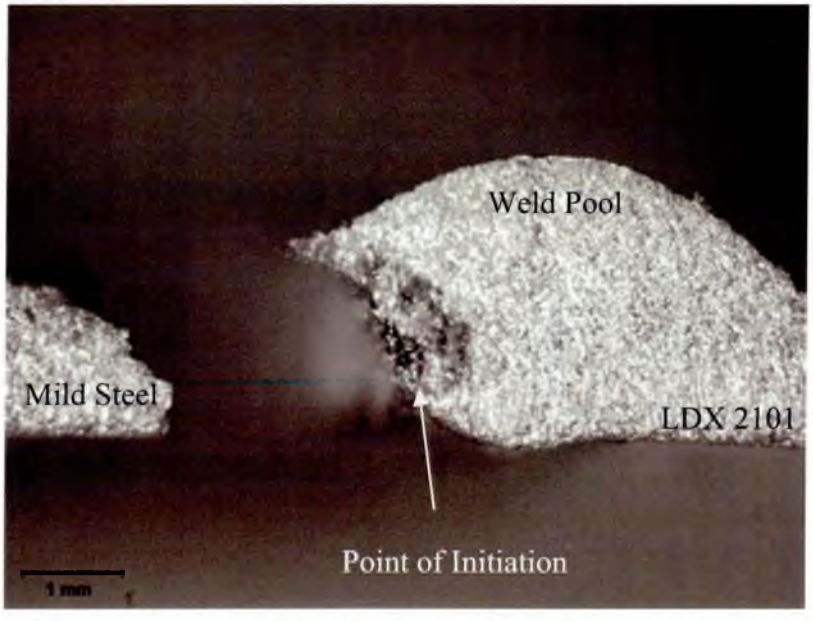

Figure 127. Showing point of failure for C MT similar thickness fatigue tests.

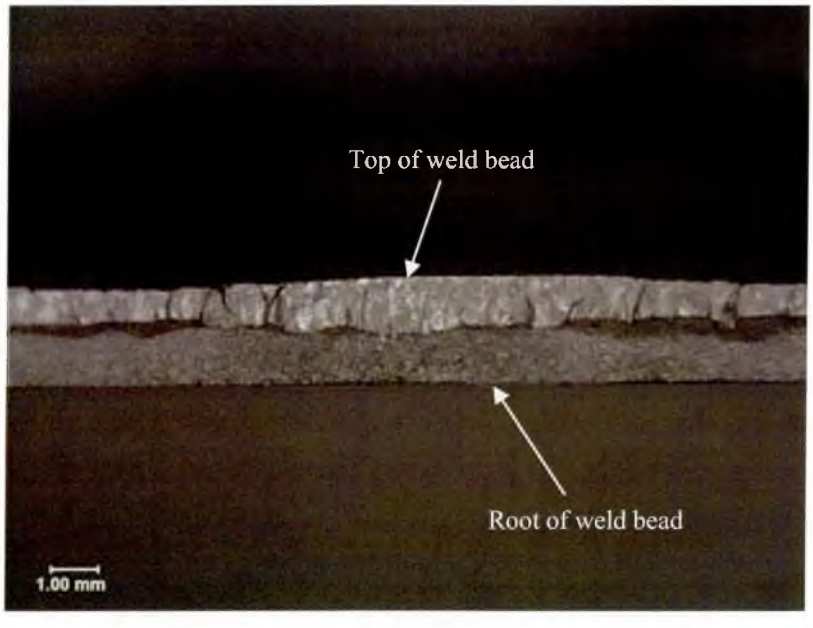

Figure 128. Typical fracture surface of CMT similar thickness fatigue specimen.

The point of failure for the fatigues tests was identified as the root of the weld on the mild steel side of the joint, this was this same mode of failure as the similar thickness LHW butt joints.

4.4.1.3.1 Root Angle Measurements for Similar Thickness CMT Butt Joints

Failure analysis of the fatigue samples led to an examination of the geometry of the joints. The Root angle of the samples were measured to determine whether there was a relationship between the root angle of a sample and fatigue life.

The procedure for measuring the angle is outlined in Section 3.7.4.3. The root angle was measured for each fatigue test for the C1 series, an example of the image taken to measure the angle is shown in figure 129. Figure 130 shows the results of the angle measurements represented as a graph of measured angle verses cycles to failure.

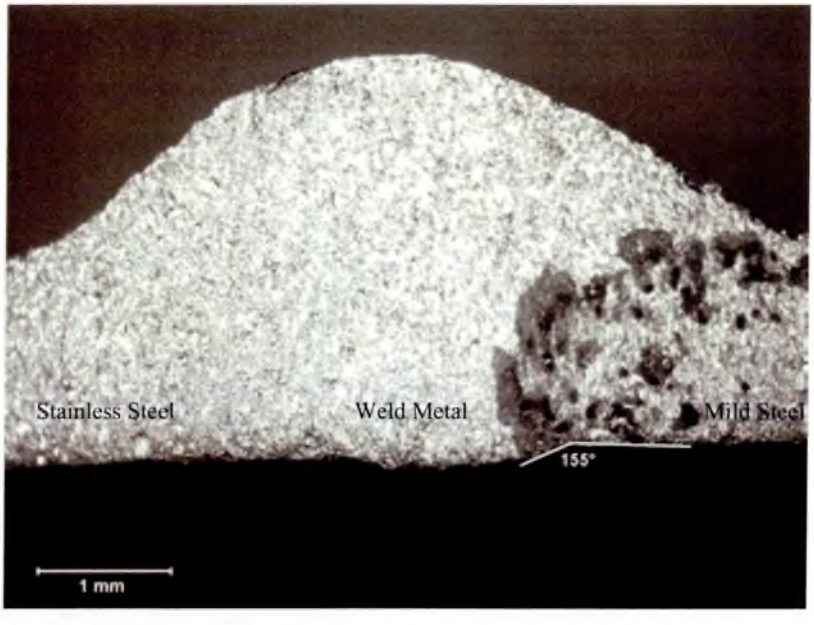

Figure 129. Example of root angle measurement on CMT similar thickness butt joint

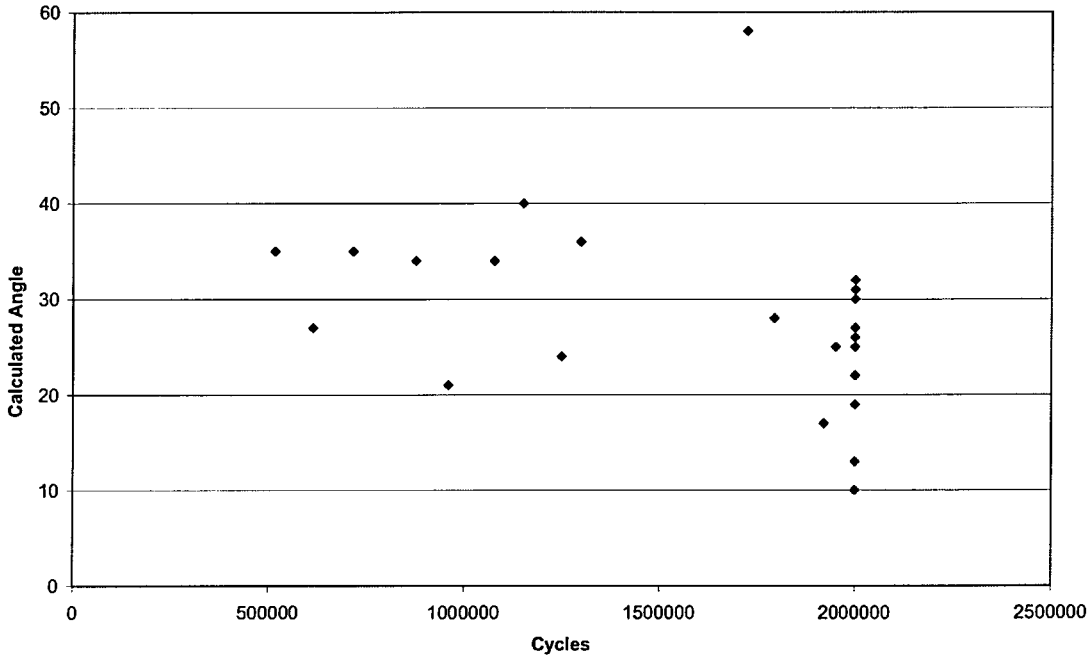

Figure 130. Graph showing relationship between root angle and fatigue life for CMT similar thickness butt joints (series C1)

4.4.1.4 Microhardness Results for Cold Metal Transfer Butt Joints

Microhardness measurements were taken for a selection of samples for cold metal transfer joints series C1 (LDX 2101 joined to Dogal 260RP-X using 308L-Si filler wire). The measurements were taken on a grid across the weld pool surface to allow microhardness maps to be plotted. The maps were carried out on 4 samples for the CMT joint combination to show the variation in hardness, if any, across the weld pool, heat affected zones and parent materials of the joints. For each series samples were taken at around the mean fatigue load level from both failed and survival fatigue tests. Figures 131 and 132 show microhardness maps from a failed and survived fatigue test with the remainder of the maps located in Appendix A.

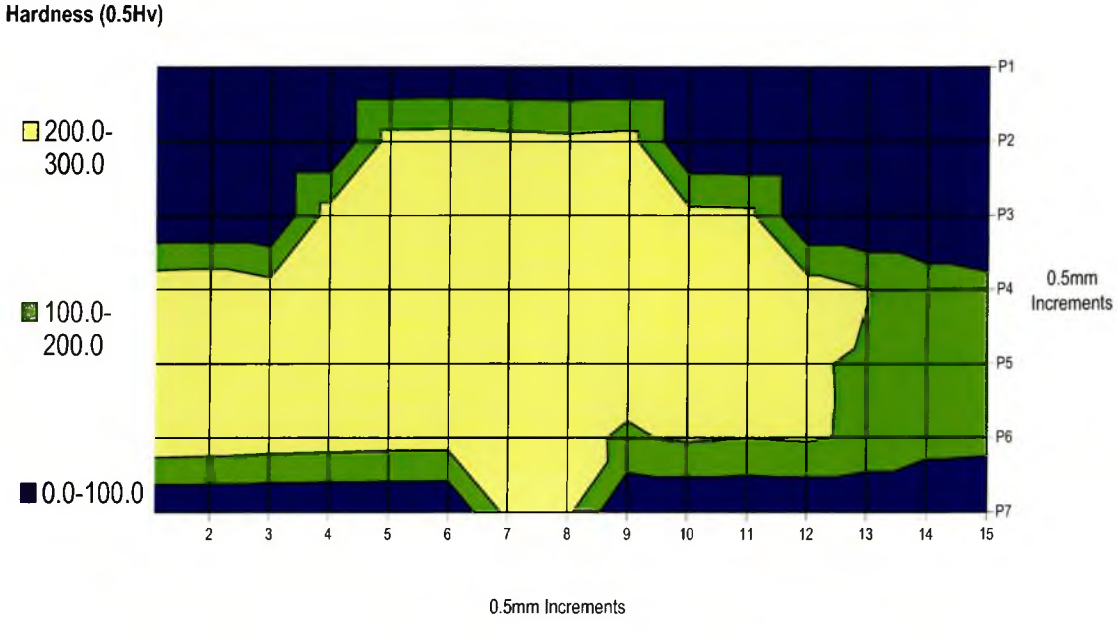

Figure 131. Series C1 microhardness map of fatigue sample C 1.14.4, the sample survived the fatigue test at 8.6kN completing 2 million cycles.

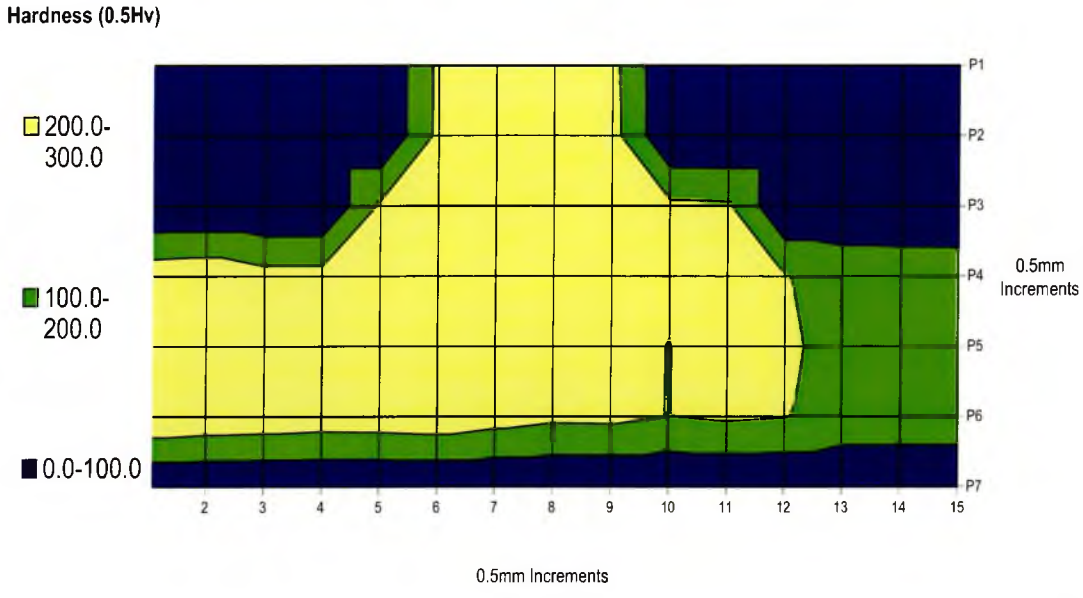

Figure 132. Series C1 microhardness map of fatigue sample C1.3.3, the sample failed the fatigue test at 9.0kN after 1150208 cycles

4.4.1.5 Metallography of Cold Metal Transfer Butt Joints

The optimum weld parameters were examined to reveal the microstructure of the parent materials and the weld pool. The sample was etched in 2% Nital to reveal the microstructure of the zinc coated mild steel (figure 133), the sample was subsequently etched in 25ml HCl, 75ml H_2O and 0.7g sodium metabisulphite to reveal the weld microstructure (figure 134) of austenite and martensite and LDX 2101 stainless steel (figure 135) exhibiting the duplex structure of austenite and ferrite.

Figure 133. Typical Microstructure of Dogal 260RP-X HAZ in a CMT Dissimilar weld

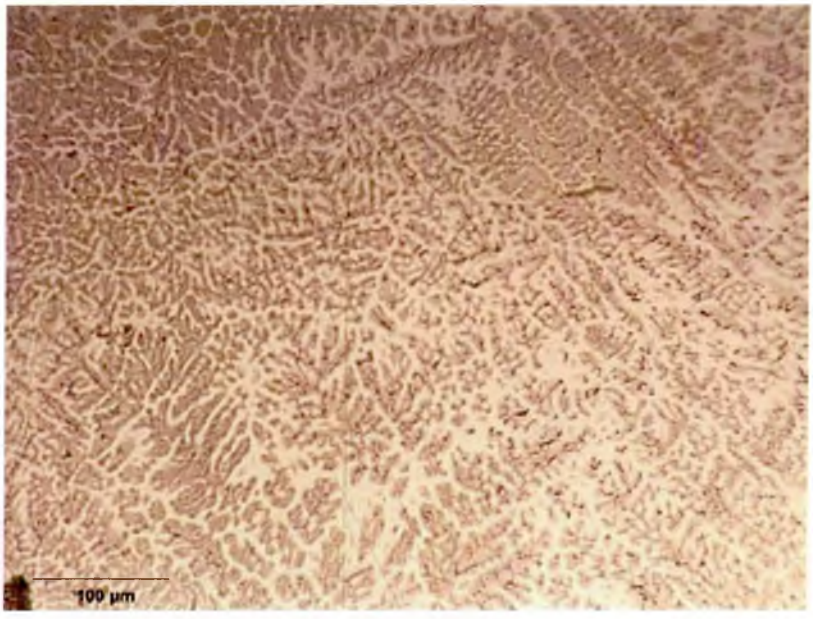

Figure 134. Typical Microstructure of Weld Material in a CMT Dissimilar Weld using 308L-Si Filler Wire, etched in 25ml HCl, 75ml H_2O and 0.7g sodium metabisulphite, showing austenite (light) and ferrite (dark) phases

Figure 134 above shows the fine grain dendritic structure in the weld material. Figure 135 below shows the typical cold rolled microstructure of duplex stainless steel, which leads into the HAZ where the austenite has transformed. In both figures the austenite is represented by the lighter phase and ferrite by the darker phase.

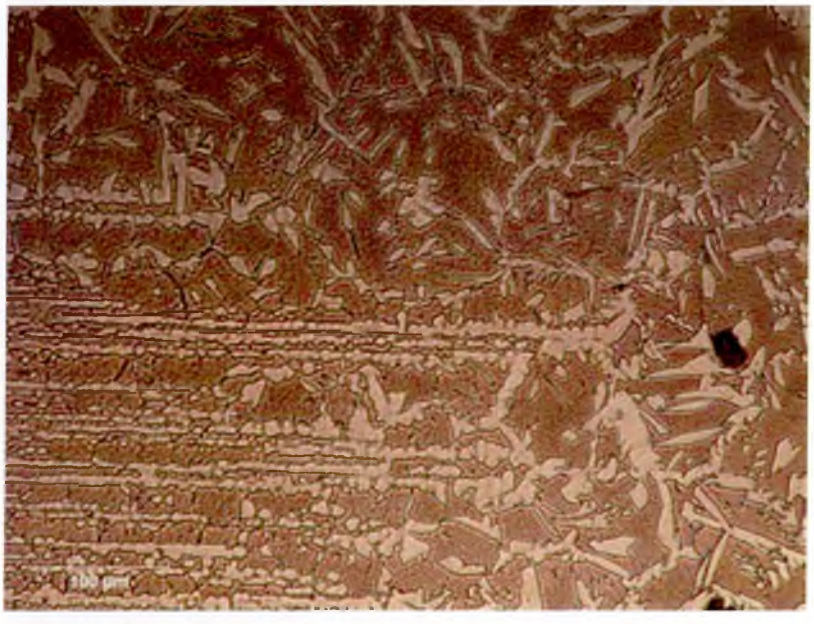

Figure 135. Typical Microstructure of LDX 2101 HAZ in a CMT Dissimilar Weld, etched in 25ml HCl, 75ml H_2O and 0.7g sodium metabisulphite, showing growth of the austenite (lighter) phase.

4.4.1.6 Elemental Mapping of the Weld Pool for the Laser Hybrid Butt Joints

Elemental mapping was carried out on samples from the series of Cold Metal Transfer butt welds. This was done using the SEM and semi-quantitative Energy Dispersive X-Ray (EDX) analysis. Elements scanned for were the main alloying elements of the predicated weld pool Fe, Cr and Ni.

Elemental distribution maps for each element in addition to a secondary electron image of the samples can be found in figures 136 to 139 below.

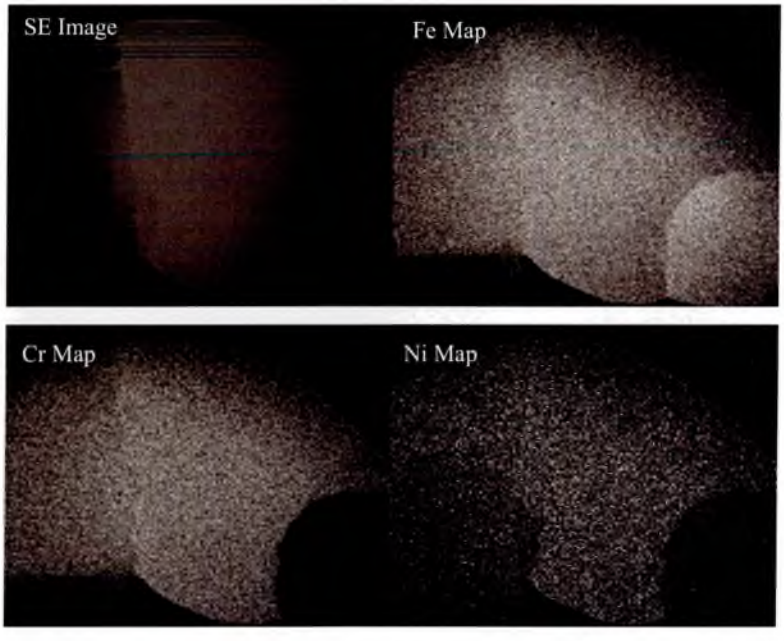

Figure 136. Elemental mapping of sample C1.3.3

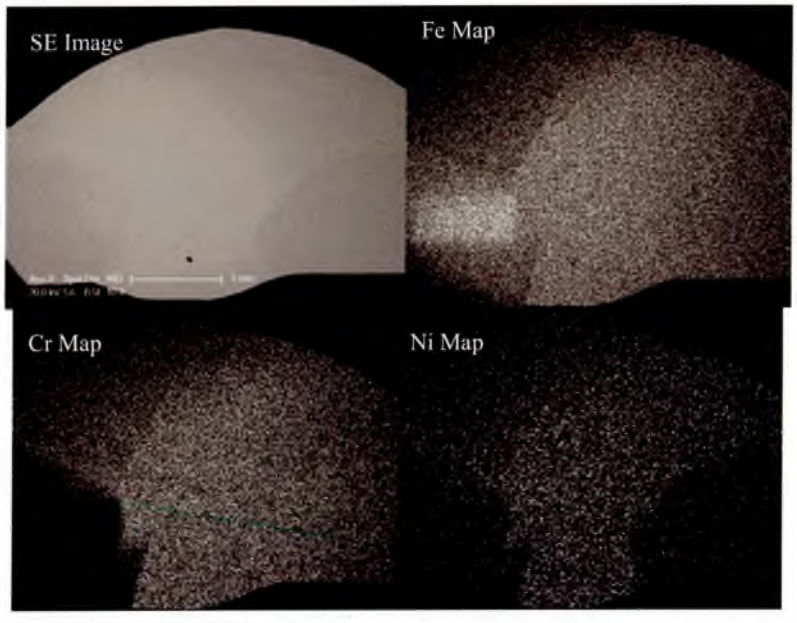

Figure 137. Elemental Mapping of sample C1.7.1

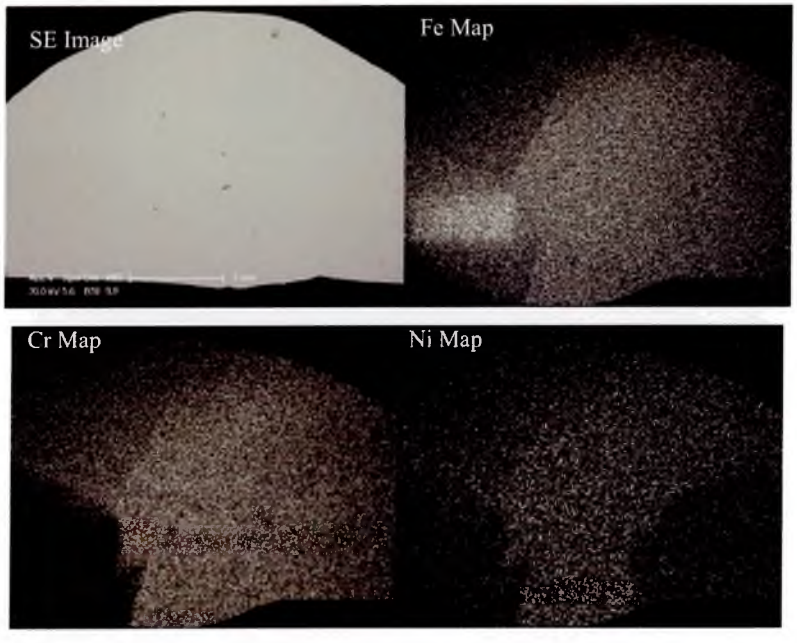

Figure 138. Elemental mapping of sample C1.9.3

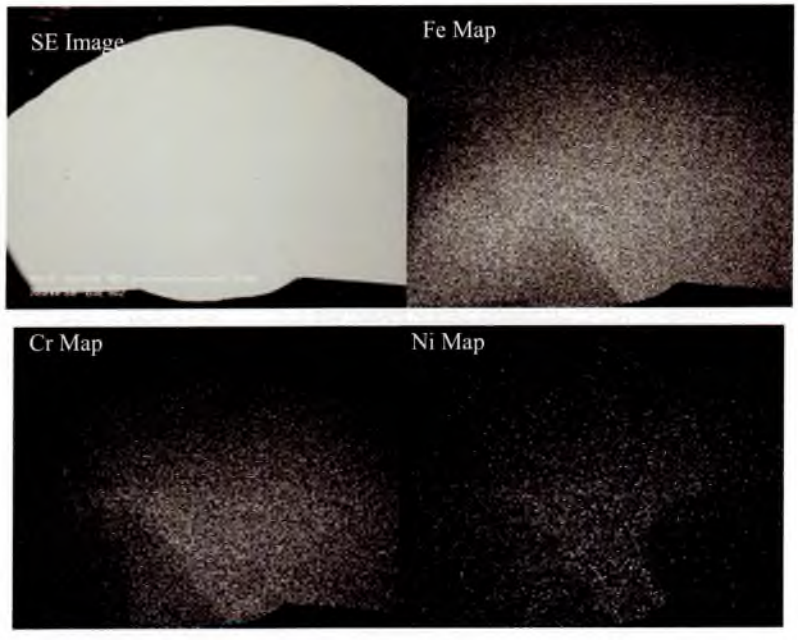

Figure 139. Elemental mapping of sample C1.14.4

4.5 *Infinite Focus Microscopy*

The Infinite Focus Microscope was used to analyse the surface profile of the welds produced using Laser Hybrid Welding and those produced by Cold Metal Transfer. Several samples from each series of similar thickness joints were analysed to assess the weld shape profile and the penetration root angle, this was to assess the consistency in the welding process and the effect of root angle on fatigue life.

3D images of the samples were attained along with profiles for 3 positions on the top and underside of the weld. One example for each of the series analysed (F2, F4, F6, F8 and C1) can be found in the figures 140 to 149 below. The remainder of the IFM analysis can be found in Appendix B.

Figures 150 and 151 shows the graphs representing the measured root angle against cycles to failure for the IFM measurements and figure 152 shows the HAZ hardness results for the mild steel side of both CMT and LHW similar thickness butt joints.

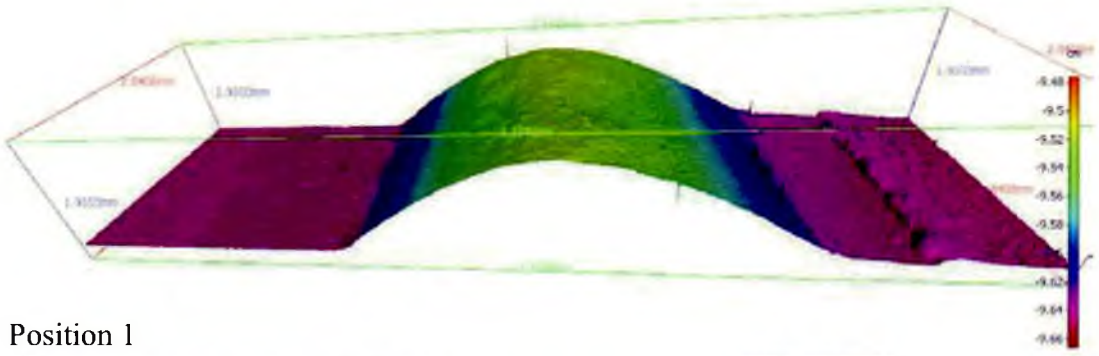

Position 1

Position 2

Position 3

Figure 140. IFM 3D surface image and surface profiles for the front of the weld bead of sample C1.5.2

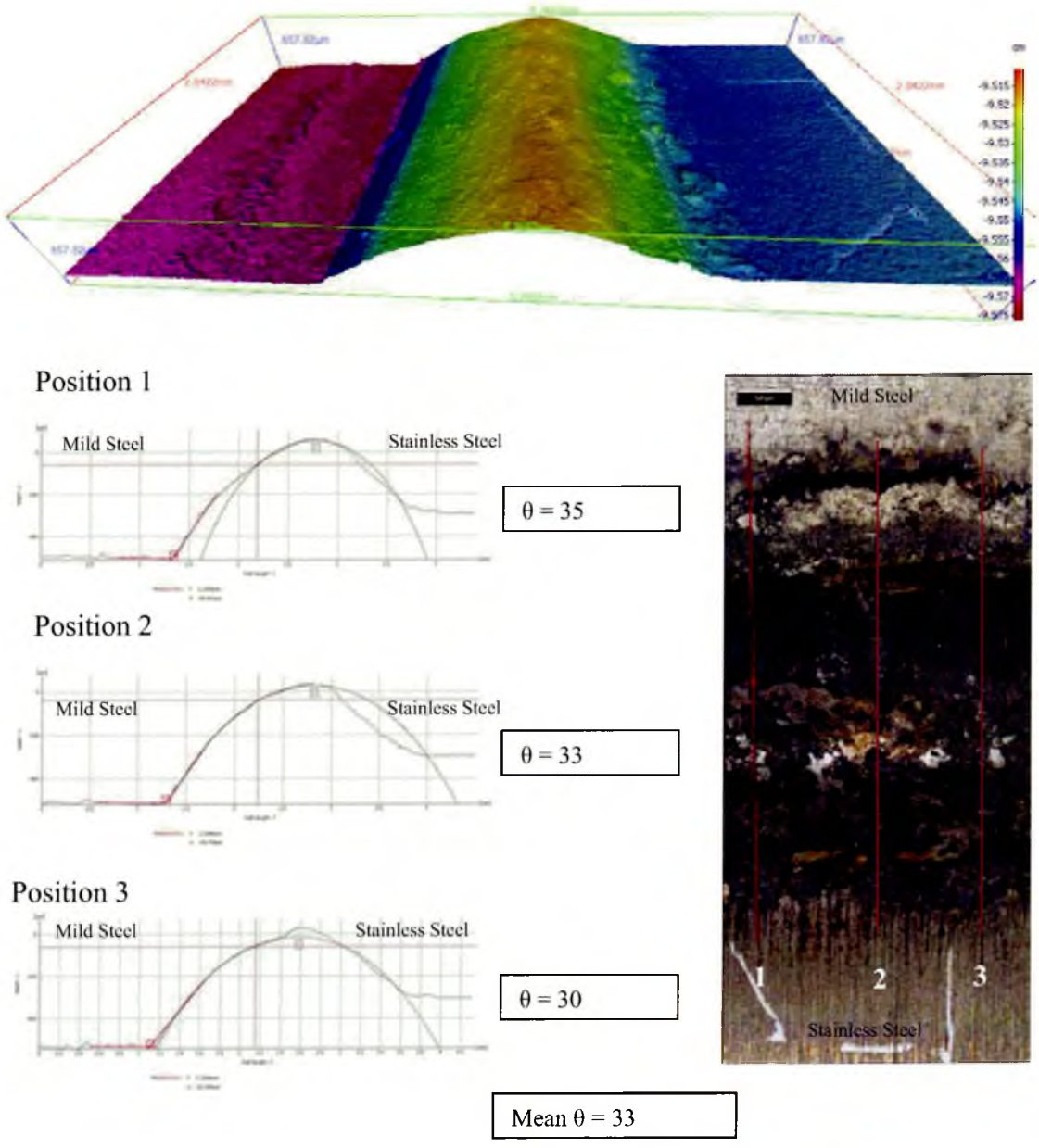

Figure 141. IFM 3D image and surface profiles for the underside of sample C1.5.2, including the penetration root angle measurements for the sample.

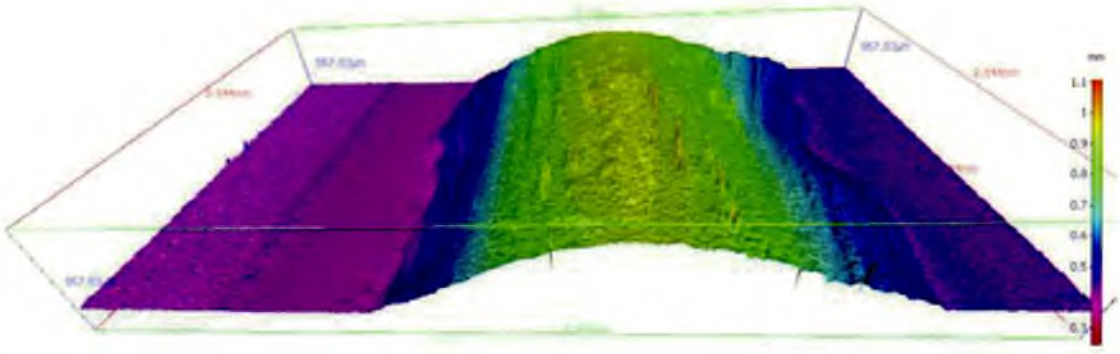

Position 1

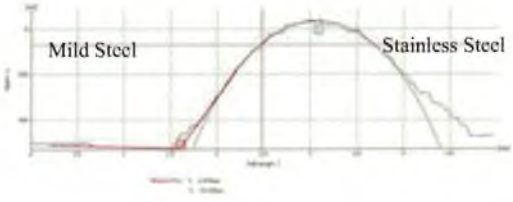

Position 2

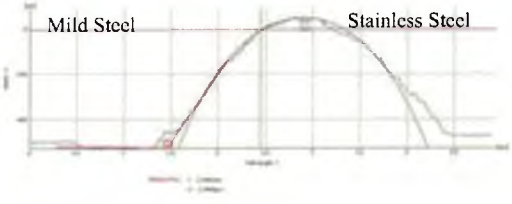

Position 3

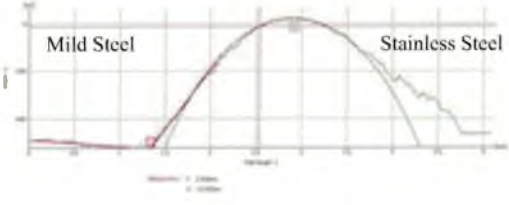

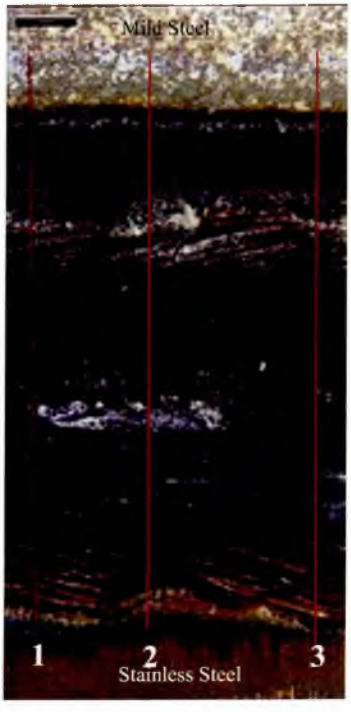

Figure 142. IFM 3D surface image and surface profiles for the front of the weld bead of sample F2.7.5

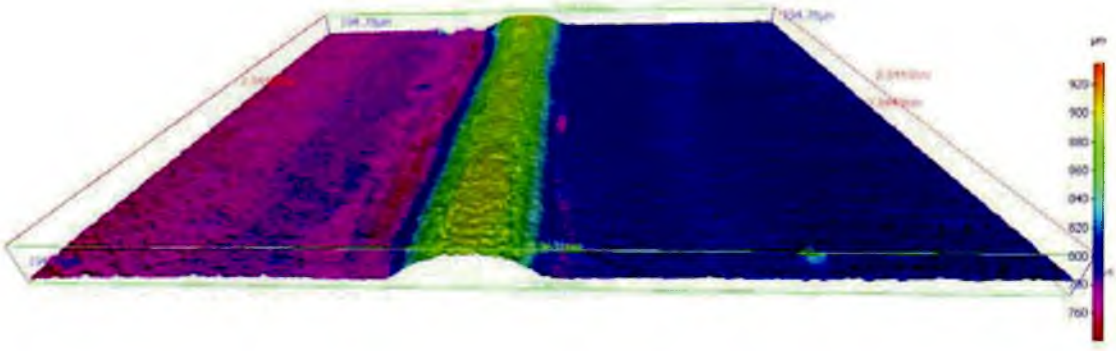

Position 1

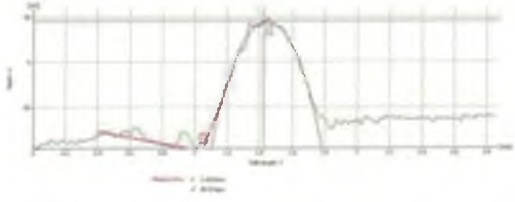

θ = 27

Position 2

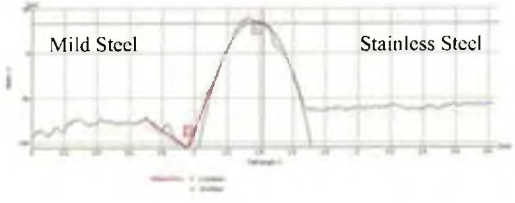

θ = 32

Position 3

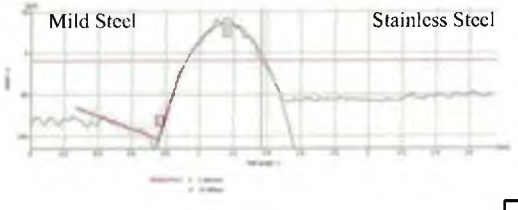

θ = 37

Mean θ = 32

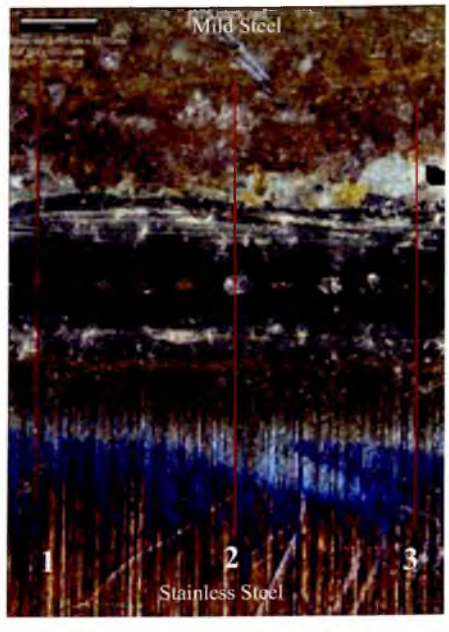

Figure 143. IFM 3D image and surface profiles for the underside of sample F2.7.5, including the penetration root angle measurements for the sample.

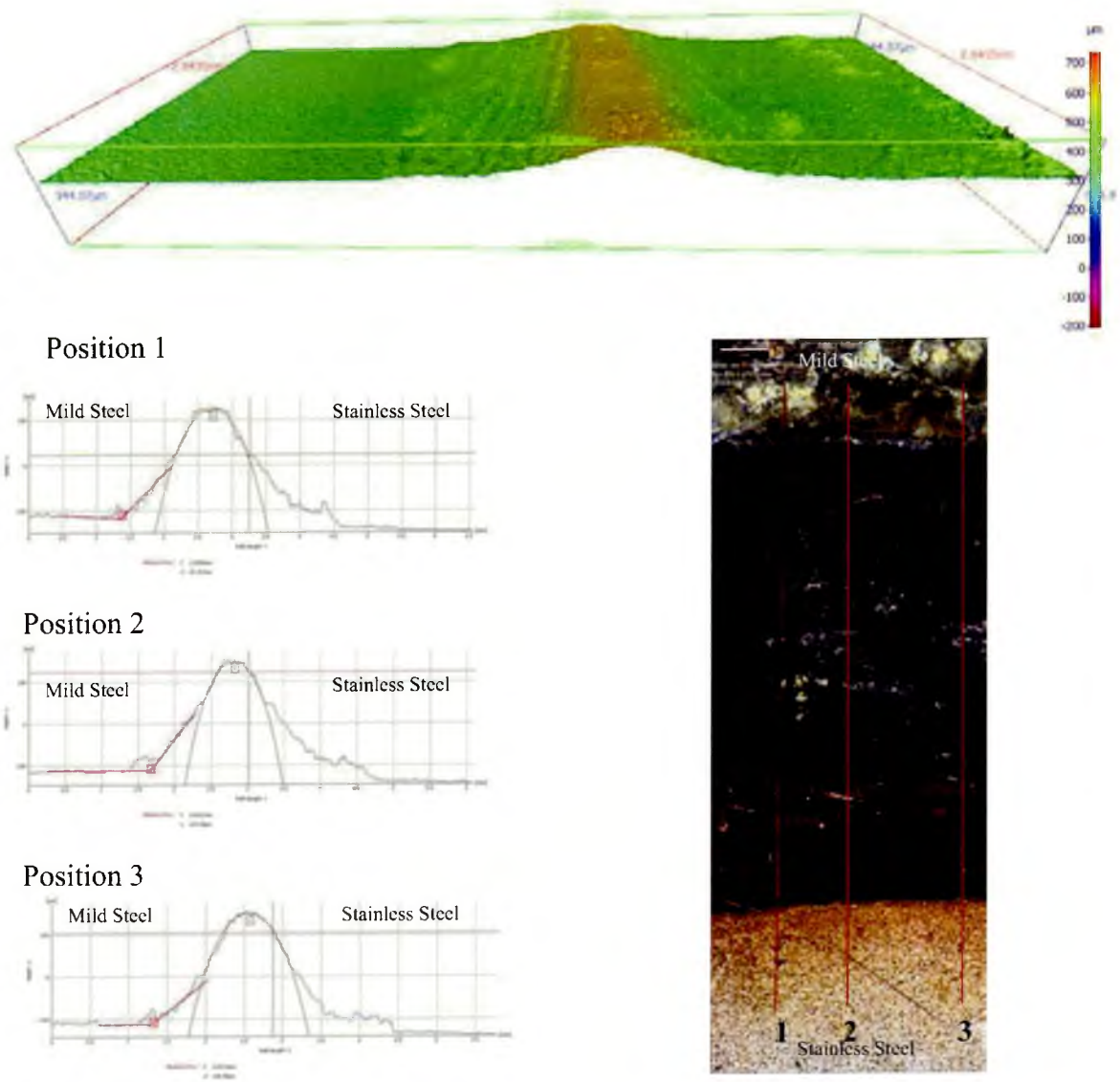

Figure 144. IFM 3D surface image and surface profiles for the front of the weld bead of sample F4.8.1

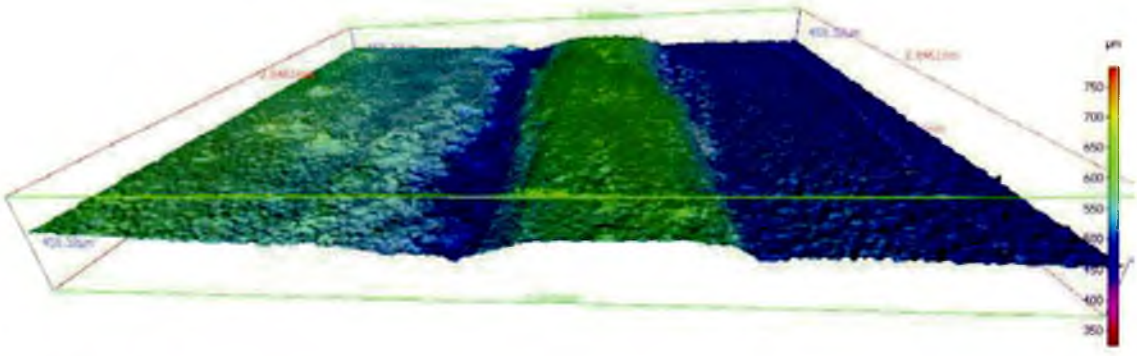

Position 1

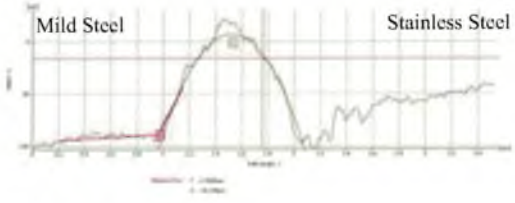

θ = 14

Position 2

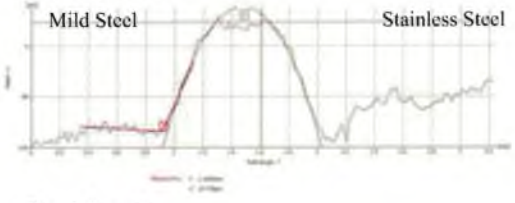

θ = 18

Position 3

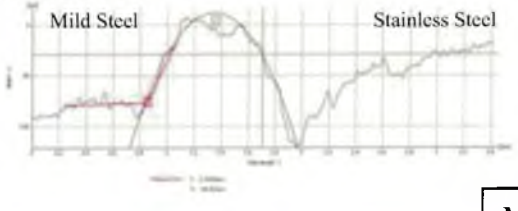

θ = 15

Mean θ = 16

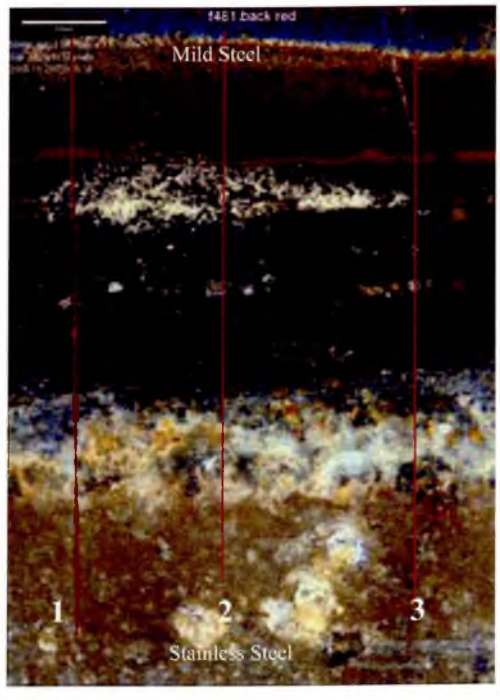

Figure 145. IFM 3D image and surface profiles for the underside of sample F4.8.1 including the penetration root angle measurements for the sample.

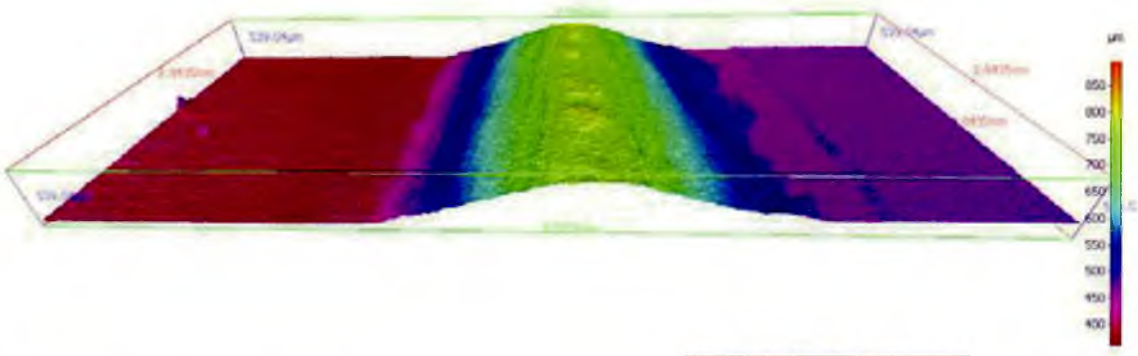

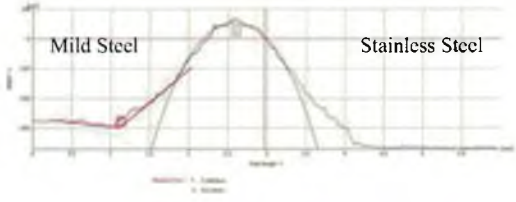

Position 2

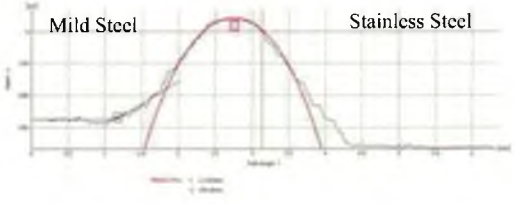

Position 3

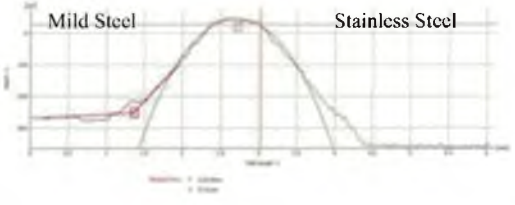

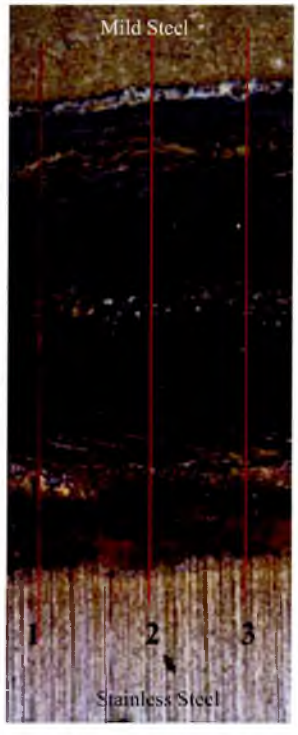

Figure 146. IFM 3D surface image and surface profiles for the front of the weld bead of sample F6.5.1

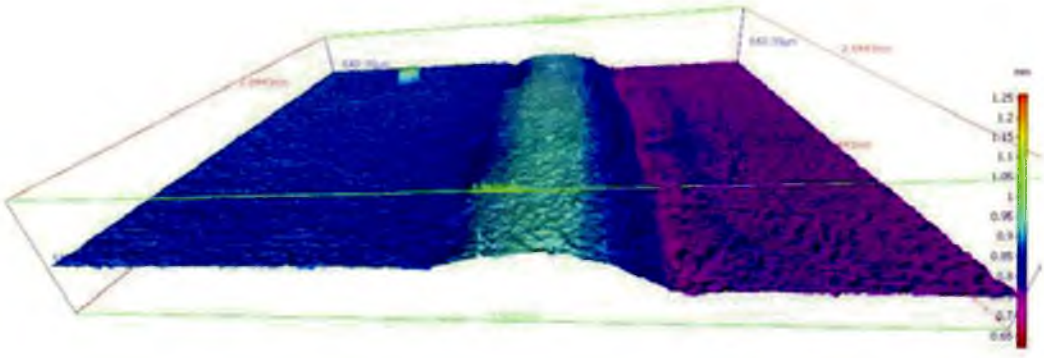

Position 1

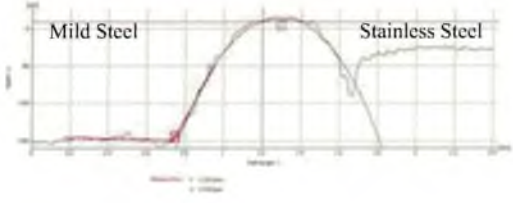

θ = 26

Position 2

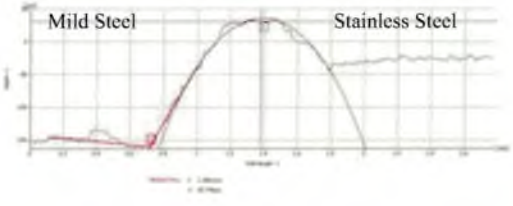

θ = 25

Position 3

θ = 36

Mean θ = 29

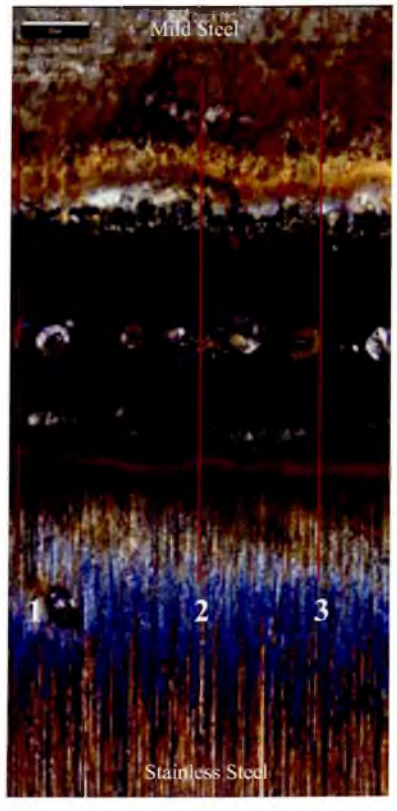

Figure 147. IFM 3D image and surface profiles for the underside of sample F4.8.1 including the penetration root angle measurements for the sample.

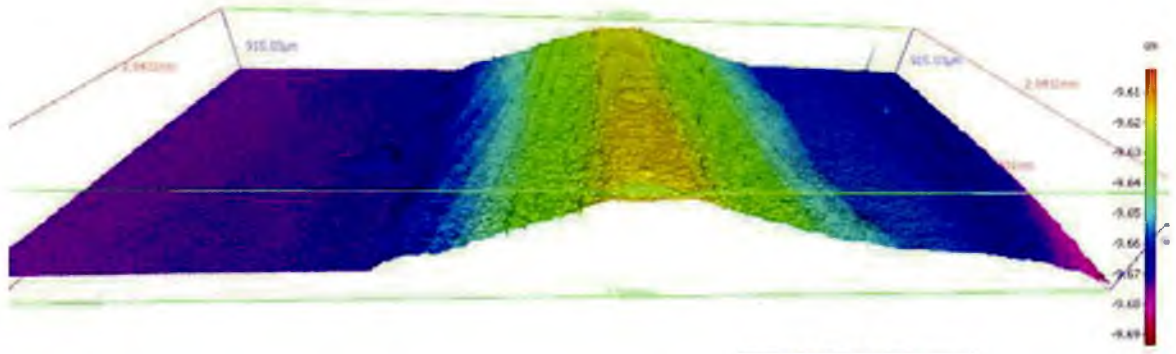

Position 1

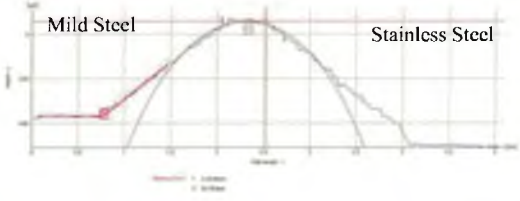

Position 2

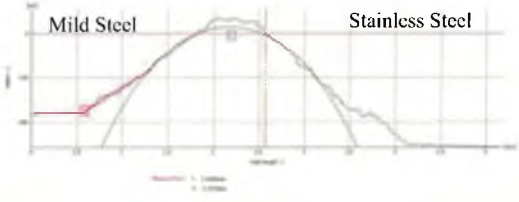

Position 3

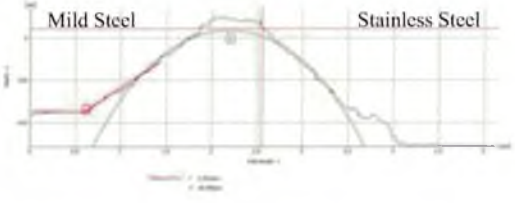

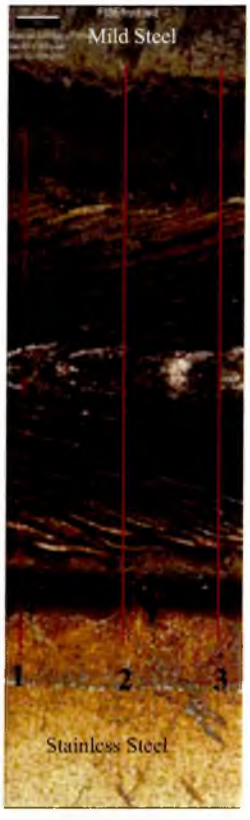

Figure 148. IFM 3D surface image and surface profiles for the front of the weld bead of sample F8.5.6

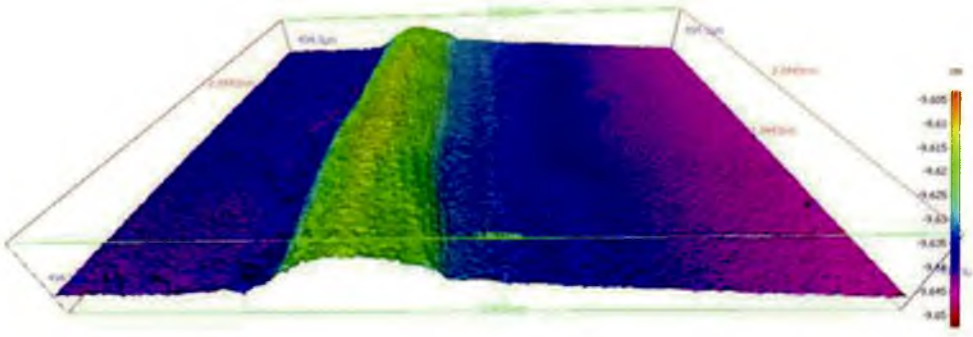

Position 1

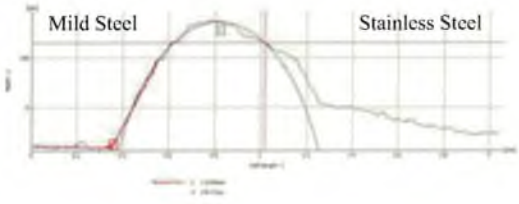

θ = 42

Position 2

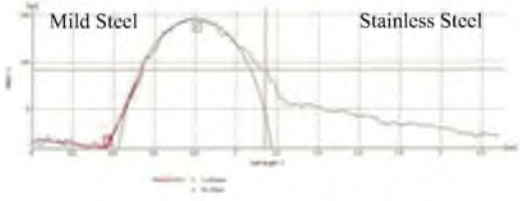

θ = 46

Position 3

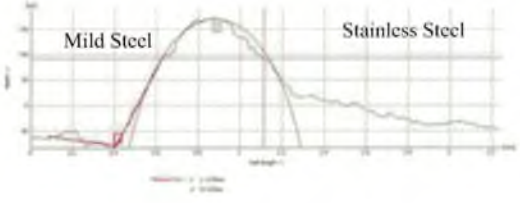

θ = 41

Mean θ = 43

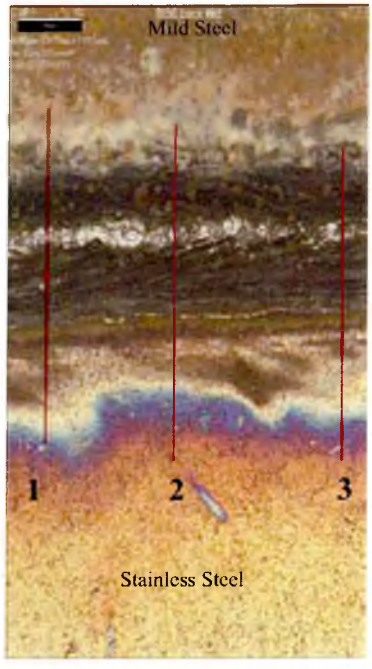

Figure 149. IFM 3D image and surface profiles for the underside of sample F8.5.6 including the penetration root angle measurements for the sample.

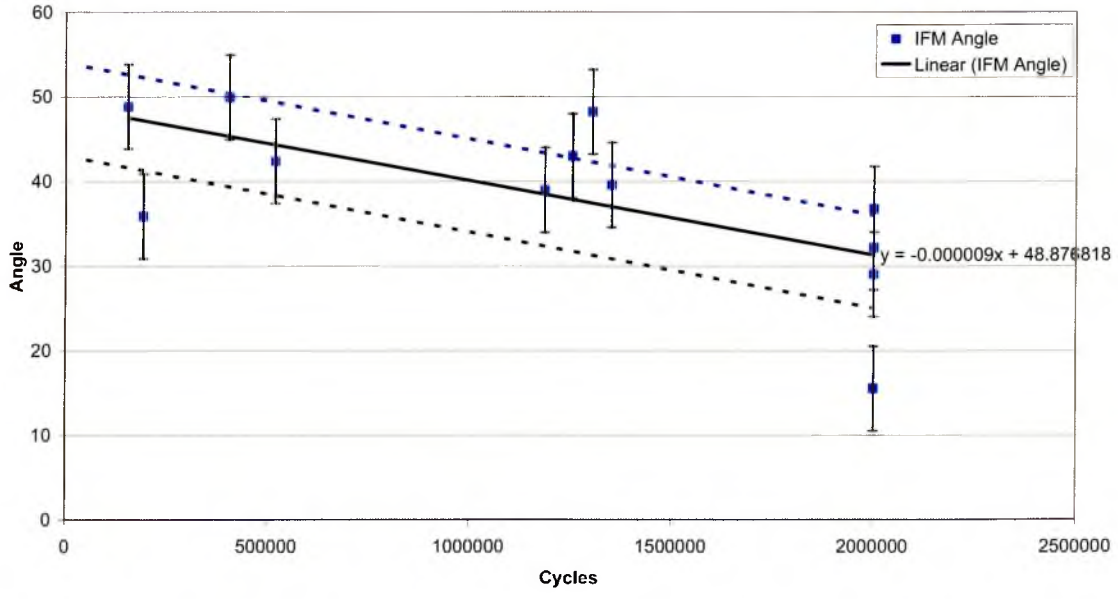

Figure 150. Graph showing the relationship between the penetration root angle and fatigue life, for similar thickness Laser Hybrid Welds

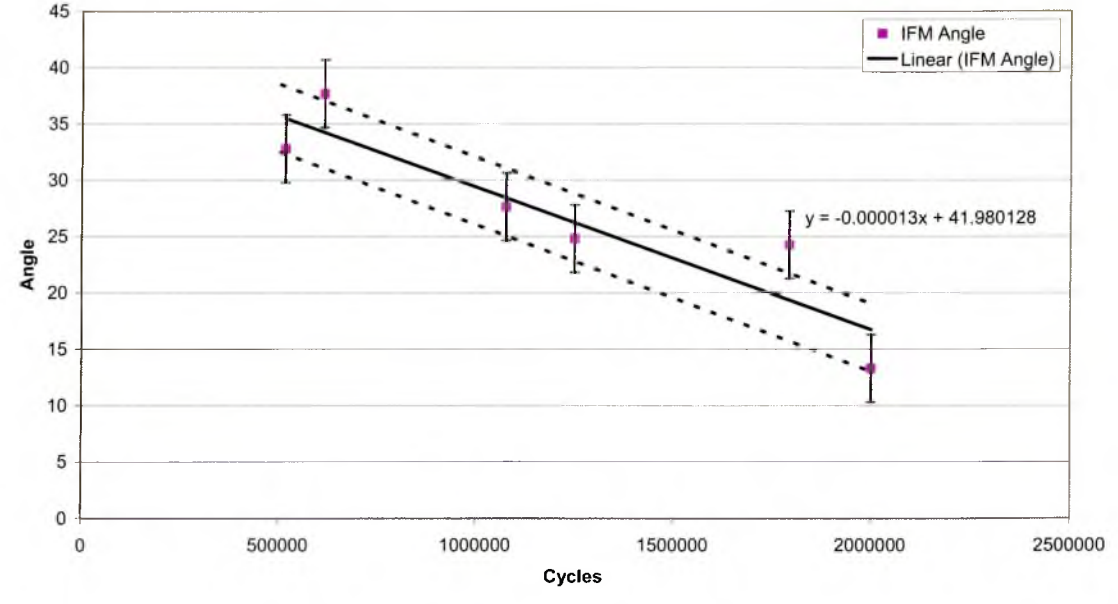

Figure 151. Graph showing the relationship between the penetration root angle and fatigue life, for similar thickness Cold Metal Transfer Welds

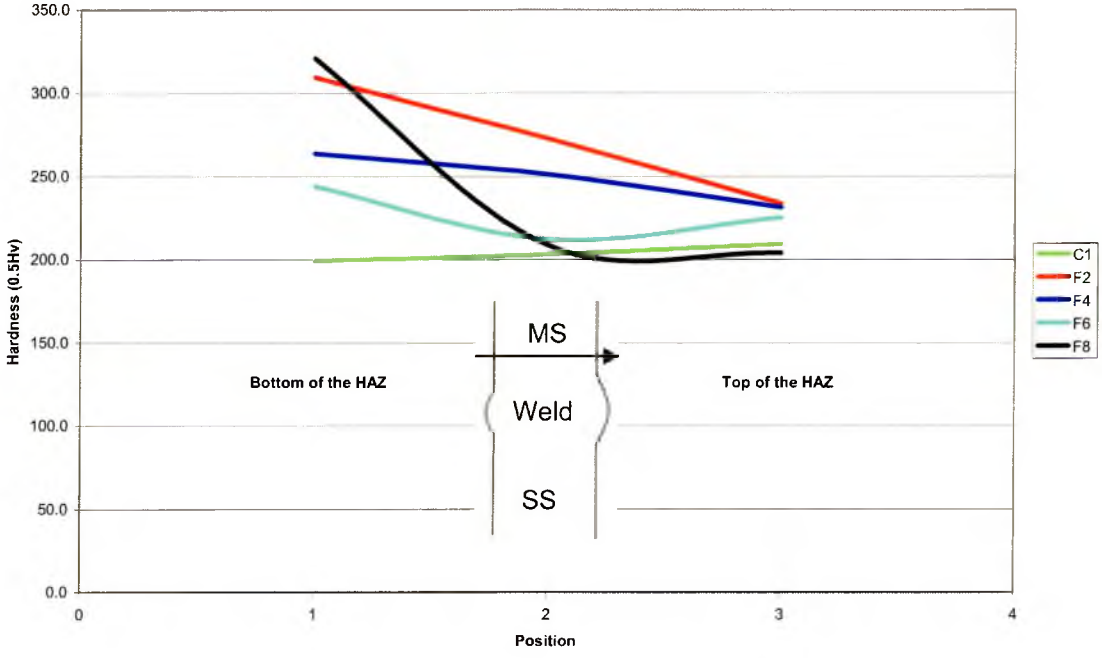

Figure 152. Graph showing hardness of Heat Affected Zone (HAZ) of the mild steel from bottom to the top of the fatigue specimens

4.6 *Comparison of Welding Techniques*

Many different welding techniques are used in a variety of industries for many different uses and applications, there is limited literature available reporting the mechanical properties of dissimilar joints, particular high strength stainless steel to zinc coated mild steel in thin sections. The following section shows comparisons of mechanical properties between the novel joining techniques and processes already established particularly in the automotive industry.

4.6.1 Comparison of Tensile Properties of Different Welding Techniques

Research was carried out at Sheffield Hallam University into fatigue properties of dissimilar metal laser welded joints[66]. This research included tensile properties of the laser welded joints and the tensile results of dissimilar metal butt joints for laser welding and laser hybrid welding are shown in figures 153 and 154.

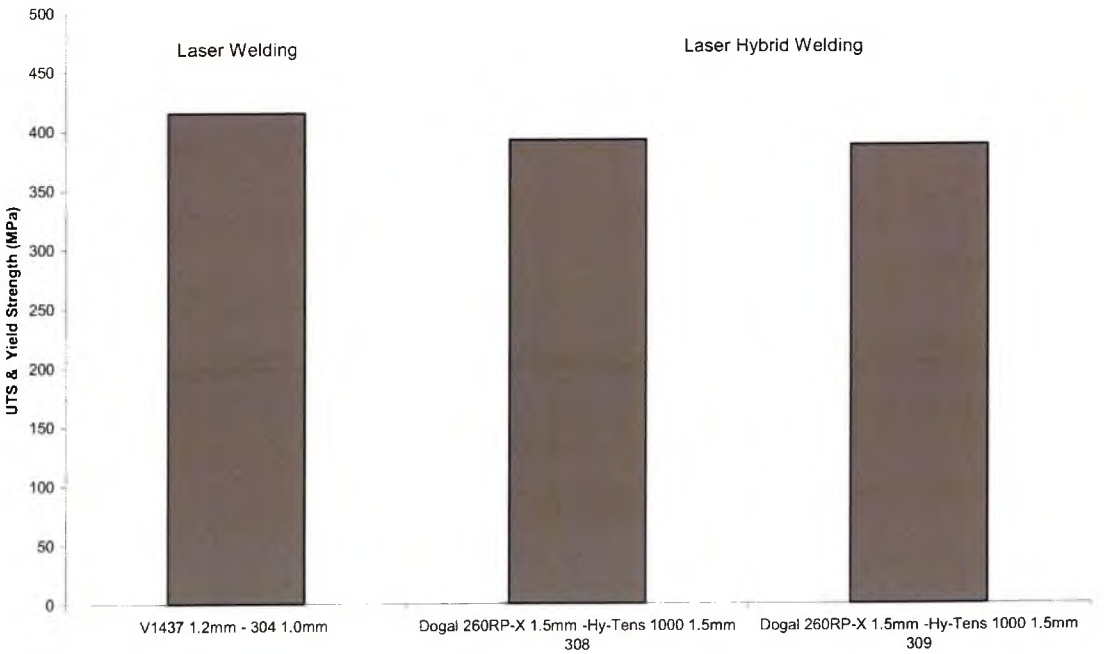

Figure 153. Comparison of UTS (MPa) Dissimilar Metal Welded Samples of Austenitic Stainless Steel and Zinc Coated Mild Steel Using Laser Welding and Laser Hybrid Welding

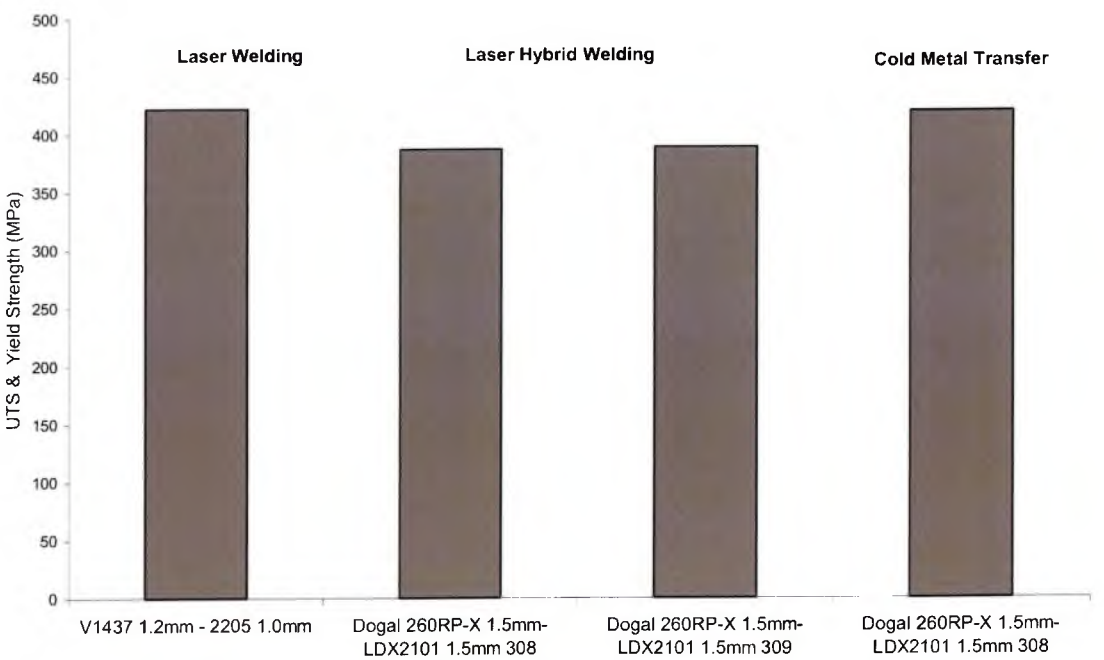

Figure 154. Comparison of UTS (MPa) Dissimilar Metal Welded Samples of Duplex Stainless Steel and Zinc Coated Mild Steel Using Laser Welding, Laser Hybrid Welding and Cold Metal Transfer

4.7 *Comparison of Fatigue Properties for Various Welding Methods*

Figure 155 below shows a graph of the Mean Fatigue Line Load (measured in N/mm) for each series of LHW joints as a result of staircase fatigue testing, and the results for a joint of the same material combination using Laser Welding. The exact joint configuration used in the Laser Welding is given in Table 21 along with all the calculated results for the fatigue test.

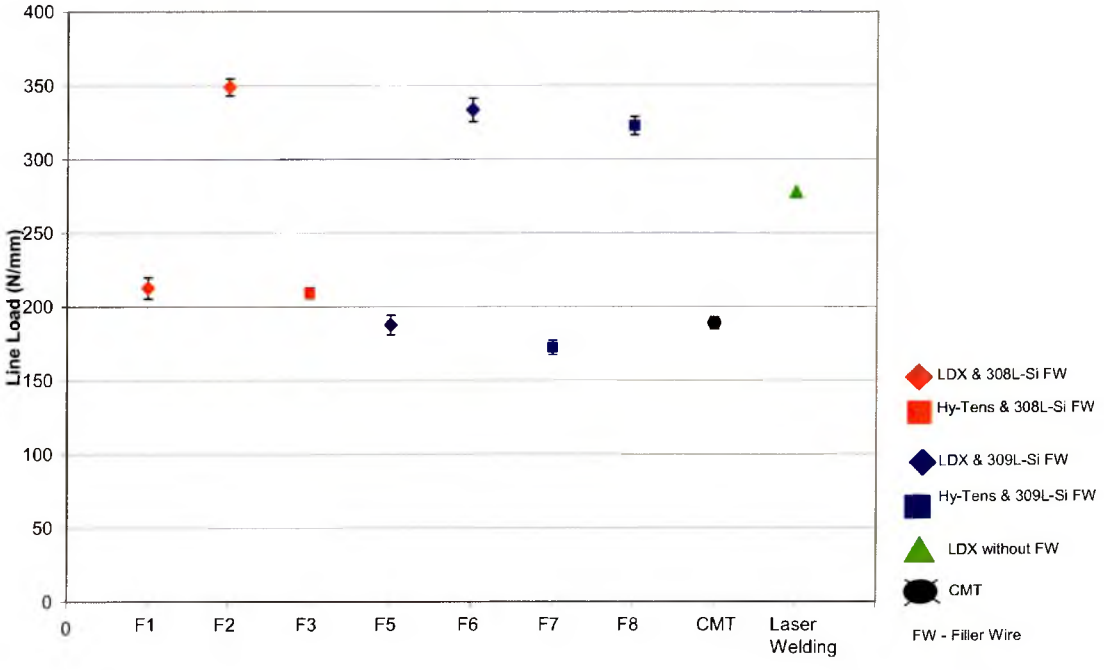

Figure 155. The staircase results represented as Mean Fatigue Line Load Range (MFLLR), at 2million cycles for LHW dissimilar metal butt joints using LDX 2101, Hy-Tens 1000 and zinc coated mild steel with two filler wires. The comparative laser welded results are included for reference.

Series ID	Calculated Mean Fatigue Strength (kN)	Standard Deviation (kN)	Convergence Factor (>0.3 or <1.2 for test validity)	Standard Error for the Mean Fatigue Strength (kN)	Mean Fatigue Line Load (N/mm)
F1	9.57	0.95	1.14	0.33	213
F2	15.70	0.74	1.11	0.26	349
F3	9.42	0.47	0.56	0.16	209
F5	8.44	0.90	1.08	0.30	188
F6	15.00	1.07	0.92	0.36	333
F7	7.75	0.63	0.74	0.22	172
F8	14.52	0.65	0.98	0.28	323
C1*	8.5	0.57	0.85	0.28	189
Laser only welding**	12.5	0.32	0.96	0.19	278
*LDX 2101 1.5mm joined to Dogal 260RP-X 1.5mm thick using Cold Metal Transfer					
** LDX 2101 1.0mm thick joined to Dogal 260RP-X 1.2mm thick using laser welding					

Table 21. The results of staircase fatigue tests of LHW dissimilar metal butt joints using LDX 2101, Hy-Tens 1000 and zinc coated mild steel with two filler wires, see Table 13 for details of weld joint configuration and filler wire used.

5 Discussion

5.1 *Material Characterisation*

Results of the material characterisation of the parent materials confirmed mechanical and metallurgical properties of the supplied material to relevant specifications.

The results of the characterisation showed that the Hy-Tens 1000 stainless material is the superior parent material in terms of tensile strength and hardness, 1150MPa and 381Hv respectively, compared to 800MPa and 260 Hv for LDX 2101 with the zinc coated mild having the lowest tensile strength of 400MPa and lowest hardness of 144Hv.

5.2 *Laser Hybrid Welded Butt Joints*

Initial trials in Gothenburg for the production of laser hybrid butt welds were successful and it was found that the critical parameters for producing consistent, uniform and aesthetically pleasing welds were, laser power, GMAW power, welding speed, wire feed speed and voltage.

Manipulation of these parameters led to 16 welds being produced which were satisfactory in appearance, and the parameters for each combination of materials are given in tables 13 and 14. The Schaeffler diagrams (table 19 and figures 38 and 41) indicates that the weld pools should have a microstructure consisting of austenite, martensite and up to 10% ferrite for both the LDX 2101 and Hy-Tens 1000 joint combinations with the 308L-Si filler wire. For autogenous laser welding of the same parent materials and joint configuration, the predicted weld bead microstructure was martensite[66].

These welds were then tested and analysed to assess the quality and suitability of the joints. The tensile test results (figures 42 and 43) show that for all the materials and filler wire combinations failure occurred in the parent material of the mild steel and away from the Heat Affected Zone (HAZ). The results meet the criteria set out for the dissimilar metal welds in that the joints should be as strong as the weakest parent material, indicating that the LHW joints under test exhibit a joint efficiency of 100%. These results are also comparable to laser only welded joints of similar material[66] using the same material combinations.

Two different filler wires were used in this work, 308L-Si and 309L-Si; the main difference between the two wires is that 309L-Si has increased Cr and Ni contents 24% and 13% respectively compared with 20% Cr and 10% Ni for the 308L-Si filler wire. 309L-Si offers increased corrosion protection and was designed for use when joining stainless to mild steel. Both filler wires were included in the testing matrix in order to determine the effect, if any, that the filler wire compositions has on overall weld integrity and whether a cost saving could be made by using the lower alloyed filler wire 308L-Si.

For this reason the results will be considered in terms of comparing identical material and joint configurations but with a change in filler wire. For example Series 1 (LDX 2101 0.75mm welded to 1.5mm mild steel with 308L-Si filler wire) will be compared with Series 5 (LDX 2101 0.75mm welded to 1.5mm mild steel with 309L-Si filler wire).

The microhardness traverse of the joints (figures 77 and 86) reveal an increase in hardness of the weld fusion zone for all of the material/filler combinations. All the hardness profiles start with a nominal value for the stainless steel then undergo a decrease in hardness in the Heat Affected Zone (HAZ) with a sharp increase in hardness in the weld material. The hardness then decreases through the Heat Affected Zone (HAZ) of the mild steel until reaching a nominal value for the mild steel. The increase in hardness in the weld metal will be due to the change in chemical composition and resulting microstructure caused by the alloying, fusion and dilution effect of the three constituents of the joints i.e. the stainless steel, the filler wire (308L-Si or 309L-Si) and the zinc coated mild steel.

As shown in figure 86 two samples of Hy-tens 1000 had a substantial increase in hardness in the weld material, they were samples H4 and H8 both of these samples were welded using the 308L-Si filler wire.

The samples of LDX 2101 stainless steel had a less varied microhardness profile with one exception, sample H6. This sample had a greater hardness in the weld material when compared to other samples and also been welded using 309L-Si filler wire.

Initial analysis of the results suggest that the choice of filler wire has little affect on the mechanical properties of the joints, e.g. H1 and H5, H3 and H7, H4 and H8 all exhibit similar hardness profiles, however, H2 and H6 have markedly different hardness profiles. There is clearly a significant difference between the joint mid point and hardness of the filler wires. The results (figure 77) show that for H6, (a weld of similar thickness LDX 2101 to zinc coated mild steel welded with a 309L-Si filler wire), there is a greater increase in hardness in the weld pool when compared with H2, an identical joint but welded with a 308L-Si filler wire.

To examine the difference in hardness between H2 and H6 the chemical compositions from the as received parent materials and the weld pools as determined using the EDX spot analysis on the Scanning Electron Microscope (SEM) were plotted on a Schaeffler diagram (see table 19 and figures 101 and 108) to determine the constituents of the weld pool and estimate the % dilution.

The results indicate that for series 2 (figure 101) the weld pool will be a mixture of austenite, martensite and ferrite with a calculated dilution of 51%. The initial result for series 6 indicates a resulting microstructure of martensite and 89% dilution (figure 103). These results showed that there was a change in weld chemical constitution between series 2 and series 6.

It is interesting to note that the weld composition of sample H6 is similar to that of grade EN 1.4313 martensitic stainless steel. This particular grade has an as received tensile strength of 850Mpa and 0.2% yield strength of 700Mpa[79]. The hardness ranges from 230-335Hv[79]. This exceeds the strength of the strongest parent material LDX 2101; therefore, it would expect the joints to provide 100% joint efficiency with the failure occurring in the mild steel as the weakest constituent which was true for the tensile results T6.

In order to explore the increased hardness in the weld fusion zone of series 6 additional EDX spot analysis was carried out at three different positions of the weld (top, middle and bottom as shown in figure 105). The results were then plotted onto the Schaeffler diagram (figure 105), which indicated a variation in chemical composition in different areas of the weld pool. The top of the weld indicated an austenitic structure with approximately 20% ferrite and an approximate dilution of 40%, while the middle and bottom of the weld pool indicated martensitic structure and 85% and 89% dilution respectively.

Finally, a hardness map of series 6 was carried out (figure 84) clearly indicating a change in microhardness across the weld pool. This correlated to the change in local chemistry from the spot analysis. The results have highlighted that the weld pool produced by LHW is inhomogeneous as a result of the effect of the laser and the GMAW process.

The bottom of the pool is predominately controlled by the highly penetrating laser giving a martensitic structure mainly consisting of the two parent materials and giving a similar dilution as laser welded joints[66]. The top part of the weld is influenced more by the addition of the filler wire, exhibiting a chemical composition closer to that of the GMAW filler wire.

There was also a difference in dilution for series 4, 58% (Hy-Tens 1000 1.5mm to mild steel 1.5mm with 308L-Si filler wire) and series 8, 79% identical joint configurations but with 309L-Si filler wire. This is also as a result of the chemical inhomogeniety of the weld pool.

Further microhardness measurements were taken from a selection of fatigue samples for each series in order to assess the change in hardness through the weld bead. The tests were also carried out to determine whether the change in microhardness observed in series 6 (figure 84) was representative of joints of this type. Four fatigue samples from each series were assessed, two that had survived the fatigue tests and two that failed before the 2 million cycle runout. These are outlined in figures 78 to 85 for joints with LDX 2101 and figures 87 to 94, the remainder of the maps can be seen in Appendix A.

There was a variation in hardness observed across the samples with some samples showing very high hardness in particular areas, towards the lower part of the weld, confirming that in some samples an inhomogeneous weld pool was being produced.

The results for the fatigue tests are given for each series in figures 48-63, the results are represented in terms of the actual staircase results, the calculations and working for each series and a graph of load against number of cycles completed. Table 21 and figure 155 give an overall summary of the fatigue results and show that joints produced using the 309L-Si filler wire gives slightly lower mean fatigue strength than identical joint and material configurations but welded with the 308L-Si filler wire.

Series F1 (LDX 2101 0.75mm welded to mild steel 1.5mm with a 308L-Si filler wire) has a mean fatigue strength of 9.57kN compared with series F5 with a mean fatigue strength of 8.44kN. Series F2 (LDX 2101 1.5mm welded to mild steel 1.5mm with a 308L-Si filler wire) has a mean fatigue strength of 15.70kN compared with 15.00kN for series F6 which has the same joint configuration but welded with 309L-Si filler.

The Hy-Tens 1000 samples, F3 (Hy-Tens 1000 to zinc coated mild steel welded with a 308L-Si filler wire) has a mean fatigue strength of 9.42kN compared with F7 which exhibits a lower mean fatigue strength of 7.75kN. Fatigue tests for series F4 (similar thickness Hy-Tens 1000 to zinc coated mild steel with 308L-Si filler) and series F8 identical joint and material configuration but with the 309L-Si filler wire were carried out, the results showed a high spread of load levels. For series F4 this resulted in the calculated value for the convergence factor being outside the boundaries necessary for producing a set of valid values for mean fatigue strength and standard deviation. Series F8 did, however, fall within the calculation boundaries for the convergence factor and standard deviation; only 17 samples were tested compared to 25 samples for the other fatigue series. This was due to a lack of suitable samples available for test due to a large variance in weld quality and difficulties faced within the setup tests. It is thought that had more samples been available the test would have become invalid due to the variation in weld quality. Therefore the results of series F8 are to be treated with caution and ideally in the future the tests would be repeated to confirm the results.

There is a significant difference in mean fatigue strength between the 1.5mm stainless (F2 and F6) samples and the 0.75mm stainless (F1, F3, F5 and F7). It would be expected that the mean fatigue strength should be similar for both thicknesses, however, the significant change in geometry from the weld bead to the 0.75mm stainless (as illustrated in figure 64) is causing a stress concentration at the weld toe resulting in the lower fatigue strength. All the samples in the F1, F3, F5 and F7 series failed through the Heat Affected Zone on the stainless steel side of the weld at this stress concentration, as shown in figure 66.

The results obtained from the staircase fatigue tests indicate that the standard deviation, which represents the variation in fatigue strength between joints made to the same configuration, for each joint configuration is notably higher than that seen in similar joining processes, such as laser only welding. There is an additional process and a filler wire involved in LHW when compared to Laser only welding increasing the process variability and therefore a higher than anticipated standard deviation was obtained.

The results of the fatigue testing are represented by line loads in figure 155, the mean fatigue strengths have been converted into a 'line load' value, measured in Newton's per

unit length, this allows for the results to be compared to discontinuous welding processes, such as resistance spot welding. Figure 155 shows that for LDX 2101 a laser hybrid welded joint can withstand a greater load over a unit length than a laser only welded joint of similar parent material. The results are indicating that laser hybrid welding can produce joints with increased fatigue strength when compared to laser only welding. The standard error for mean fatigue strength was also calculated, this allowed an error for the tests to be given on the overall fatigue graph (figure 155). For all the series the error was consistent with the value for the error calculated between 0.16kN and 0.36kN for the welding techniques evaluated and compared in this study.

For the similar thickness LHW joints (series F2, F4, F6 and F8) figure 68 shows the typical position of failure for the fatigue specimens. The failures appear to begin at the root of the weld bead on the mild steel side of the joint. Established fatigue literature suggests that the fatigue properties of welded joints are dependant on the geometry of the joint. The root of the weld bead potentially will act as a stress raiser, therefore the angle was measured using optical microscopy and an image analysis package. The greater the root angle the greater the potential stress concentration therefore limiting the fatigue life of the sample. Figures 72 to 75 show the root angle measurements for series F2, F4, F6 and F8 against the fatigue life of the samples.

The general trend observed is that the greater the root angle the shorter the fatigue life. In order to confirm that there is a relationship between angle and fatigue life a statistical T-Test was carried out.

A T-Test assesses whether the means of two groups of data are statistically different from each other. The root angle data was split into two groups, those that failed under 500,000 cycles and those who survived to 2,000,000 cycles.

The 95% confidence interval for the mean difference of the test was -17.88 and -5.77, the T-Value was calculated to -4.05 which were outside the confidence limits of the data and a P-Value was calculated to 0.001, therefore the test indicated that the two groups of data were significantly statistically different. This means that the two groups of data are not from the same data set thus confirming that the angle at the root of the weld could determine whether or not it would survive a fatigue test. The results of this test gave an initial indication as to whether or not a relationship between the fatigue

property and geometry of a weld existed within the scope of this project. Further analysis was carried out and is explained in section 5.5.

5.3 *Laser Hybrid Welded Lap Joints*

Problems were encountered when welding trials for the lap joint configurations were carried out. In order to assess the process for lap joints several initial samples were welded. Two samples which appeared the best were selected, Sample 7 (LDX 2101 1.5mm to zinc coated mild steel with a 10mm overlap) and Sample 19 (Hy-Tens 1000 1.5mm to zinc coated mild steel with a 10mm overlap). These samples were mounted polished, etched and subjected to a microstructural examination.

There were concerns that the level of penetration was too great therefore the depth was measured and figures 114 and 115 show that both samples had a penetration of approximately 0.9mm through the 1.5mm thick bottom plate. From an aesthetic viewpoint penetration through the bottom plate is undesirable, however, microscopic examination illustrated that there is no through penetration of the samples examined and the depth of penetration was no longer a concern.

Solidification cracks were also observed in sample 7 (figure 113), ESAB process and development centre carried out a metallurgical investigation[80] and concluded that the cracking was likely to be from stress developed during cooling i.e. solidification cracking, which was caused by the differences in thermal expansion between the regions present in the joint. The recommendation from the report to eliminate such cracking was to speed up the solidification rate of the weld and this could be done by increasing the overall welding speed.

During further optimisation of lap joints it was found that the process was very unstable, producing large amounts of spatter, and surface breaking porosity in both material combinations (figures 116 and 117). In addition to these defects transverse cracking was observed on the underside of the Hy-Tens 1000 weld samples (figure 118). Different welding speeds, torch angles and inter plate gaps using shims were tested however, optimum process parameters could not be found, which eliminated further work into lap joints within the scope of this project.

Surface breaking porosity probably caused by the zinc vapour with up to 20 visible pores in a 300mm length of weld was observed. In order to attempt to eliminate this problem welding speeds from 1.3m/min to 8.5m/min were attempted, with no success. One option to eliminate this problem would be to decrease the welding speed further

below 1.3m/min. If the welding speed was reduced then the laser hybrid would no longer exhibit the advantage of higher processing speeds when compared with the normal GMAW process.

The relationship between the torch angle, interplate gap and the number of cracks appearing on a sample with the Hy-Tens 1000 (figure 119) showed that as the gap between the two plates and the welding angle increases the amount of observed cracking is greatly reduced.

However, introducing a gap between the plates in an industrial and manufacturing setting will have a negative effect on productivity. In addition the introduction of a gap between two sheets of material will have a detrimental effect on the fatigue, the larger the gap the more detrimental the effect will be on the fatigue life properties of the joints[66]. This will not appeal to the manufacturers and this may affect their decision to use the Laser Hybrid process for lap welding.

The cracking on the underside of the welds produced (figure 120) only appeared on samples using the HyTens 1000 material. The blue and brown areas present on the surface of the crack suggest that the crack took place at high temperature. The surface of the crack was examined and imaged (figure 121) using EDX analysis and a high concentration of Zn was present in some areas of the fracture surface. Figure 122 shows a longitudinal cross section through the weld and shows that the pores and cracks appear simultaneously. This suggests that the cracking had been caused by Liquid Metal Embrittlement (LME) due to the zinc coating from the mild steel and the volatile nature of the zinc during laser hybrid welding. HyTens 1000 stainless steel is an austenitic grade and highly susceptible to LME.

LME was not observed in samples containing LDX 2101 stainless steel, this is a duplex stainless steel containing phases of ferrite and austenite. Research and literature suggests that LDX 2101 is not at risk from LME attack[81,82].

Occasionally throughout the trials a section of a weld would exhibit the desirable weld appearance. However, when the parameters were kept constant and the weld repeated it was found that the consistency and reliability of the welding process for a lap joint was poor.

5.4 *Cold Metal Transfer Similar Thickness Butt Joints*

The cold metal transfer process was optimised for the joining of LDX 2101 1.5mm thick to Dogal 260RP-X 1.5mm thick using a 308L-Si filler wire.

308L-Si filler wire was chosen because Laser Hybrid Welded samples of similar material combination the joints using 308L-Si filler wire gave the higher fatigue life and more consistent results. The results for series C1 will be directly comparable to series F2 (LDX 2101 1.5mm thick to Dogal 260RP-X 1.5mm thick with 308L-Si filler wire) of the LHW joints.

The critical parameters during the optimisation were found to be wire feed speed, welding speed, arc length correction and the plate gap. The effects of varying these parameters on the resulting weld bead can be found in figure 123. It was found that the penetration of the welding process could be controlled by finding the correct wire feed speed in balance with the optimum welding speed. As the wire feed speed increases too much penetration occurred whereas as the welding speed increases the penetration decreased.

The Arc Length Correction (ALC) value controlled the stability of the arc and the spread of the weld reinforcement during deposition as the ALC was increased the arc became unstable producing spatter, however, if it was reduced too much the weld bead profile became a lot steeper. Variation in plate gap caused the penetration to become too much or too little so the correct balance needed to be found in conjunction with the correct welding and wire feed speed.

An observation made during the optimisation process, was that the weld bead deposited (reinforcement) was substantially more prominent than the weld bead produced using the laser hybrid process.

Table 21 outlines the optimum parameters for the material combination used in this research for the Cold Metal Transfer process, a number of identical welds (14 in total) were produced with these parameters and denoted as series C1. The welds were then tested and analysed to assess the quality and suitability of the joints as outline in section 4.4.

For each of the 14 identical welds produce for series C1, 1 tensile test was carried out, the results are shown in figure 124. The results show that for all the tests carried out failure occurred in the parent material of the mild steel and away from the Heat Affected Zone (HAZ). Theses results meet the criteria set out for the dissimilar metal welds in that the joints should be as strong as the weakest parent material, indicating that the CMT joints under test also exhibit a joint efficiency of 100%. These results are also comparable to laser only welded joints[66] and laser hybrid welded joints produced with similar material combinations (figure 134).

Microhardness measurements were taken from a selection of fatigue samples in order to assess the change in hardness through the weld bead and determine an effect if any the microhardness had on the fatigue properties. Four fatigue samples were assessed two that had survived the fatigue tests (figure 132 and Appendix A figure 18) and two that failed before the 2 million cycle runout (figure 131 and Appendix A figure 17). The microhardness maps show that there are no significant changes in microhardness from the stainless steel to the weld pool. The change observed between the weld pool and the mild steel is one to be expected. The microhardness is consistent across all four samples and exhibits no high hard spots or changes in microhardness through the weld as previously seen on the laser hybrid welded joints of comparable material combination.

Elemental mapping was carried out on the joints produced using the Cold Metal Transfer process. Elements mapped for were the main alloying elements of the materials, iron, chrome and nickel. The results of the mapping can be seen in figures 103 to 106, the results show that the elements within the weld pool are distributed evenly suggesting that the weld pool is mixing equally and producing a homogenous weld pool, as is desirable in welding. The hardness results also confirm that a homogenous weld pool is being consistently produced using the CMT process unlike similar welds produced using the laser hybrid process.

The results for the staircase fatigue tests carried out for series C1 are outlined in figures 125 and 126. The calculated mean fatigue strength is 8.5kN with a standard deviation value of 0.57kN. The convergence factor was calculated to be 0.85 meaning that the results of the fatigue tests are statistically valid. When compared to the laser hybrid weld series F2 which had a mean fatigue strength of 15.70kN almost double that of the CMT joints.

Fatigue failure analysis of the fatigue specimens indicated that the fatigue failure occurred through the HAZ of the mild steel with the point of origin at the root of the weld, figures 127 and 128 demonstrate this. The origin and cause of the fatigue failure is similar to that of the Laser Hybrid fatigue specimens.

As with any form of welding there is an immediate effect of change in geometry from the parent materials, the change in geometry will always affect the fatigue properties as outlined in section 2.7. At the root of the weld bead there is a stress concentration as there is a change in geometry, this then causes localised stresses to increase and cause failure through the weaker of the two parent materials. The crack has initiated at the stress concentration then propagated through the HAZ of the mild steel.

In order to evaluate the effect, if any, the stress concentration at the root of the weld was having on the fatigue properties of the joint, the angle between the mild steel and the penetration of the weld was measured. The angle for each fatigue samples was measured as shown in figure 129 and then plotted in figure 130 as angle against fatigue life. The graph shows a trend between the angle at the root of the weld and the fatigue life, as the angle get smaller the fatigue life increases. Thus in reality the smaller angle the less dramatic the change in geometry is between the weld pool and therefore a reduction in local stress. The effect of root angle on the fatigue properties of the welded joints will be discussed in further in the next section (section 5.5).

5.5 *Infinite Focus Microscopy*

A relationship between the penetration root angle and fatigue life appeared to exist for both Cold Metal Transfer joints and Laser Hybrid Welded joints. In order to assess and determine this relationship the Infinite Focus Microscope (IFM) was employed. 3D images were produced using the Infinite Focus Microscope for the similar thickness fatigue series for LHW and CMT, F2, F4, F6, F8 and C1. The fatigue samples were categorised into three groups, samples which failed below 500,000 cycles, samples which failed between 1000,000 to 1500,000 cycles and ones which survived to 2,000,000 cycles. For each series one sample was randomly selected from each group. Each sample was imaged on both the top of the weld and the underside of the welds creating 3D images.

The 3D images for the tops of the welds show the consistency of the welding profile, samples from the C1 series (figure 140) , those produced using CMT, show a much more consistent weld bead profile than LHW welds (figure 142,144,146 and 148). The weld bead on the C1 series samples are almost perfect circles when compared to those of LHW, however, the weld bead on the CMT samples is much more prominent with much more reinforcement than the LHW samples. This excess reinforcement may also explain the reduced fatigue life when compared to similar LHW fatigue results as the weld is much bigger and would therefore produce a bigger stress concentration at the weld/parent material interface.

The top side surface profiles for series F2 (figure 142) and F6 (figure 144) are consistent along the length of the weld. However, they do vary in shape slightly, F6 is has a more acute weld profile than F2 and the only difference between these two sets of samples are the filler wires. Both samples are LDX 2101 1.5mm thick joined to Dogal 260RP-X 1.5mm thick, F2 with 308L-Si filler wire and F6 with 309L-Si filler wire. F4 and F8 are joints produced using Hy-Tens 1000 stainless steel where as the other 3 series are joints produced using LDX 2101.

The top side profiles for series F4 (figure 146) and series F8 (figure 148) don't appear to be as consistent as the other series along the area of weld examined, with a variation in profile occurring. This isn't such a surprise because F4 and F8 had inconclusive fatigue results due to the spread of load levels being too wide. This suggests that the

process of LHW for joints produced using Hy-Tens 1000 stainless steel was not wholly optimised and the joints produced were not consistent.

The profiles measured on the underside of the welds for all four series show that the penetration does vary between processes (figures 141, 143, 145, 147 and 149). CMT tends to have a wider bead of penetration than those samples produced using LHW. The consistency across the weld sample for series C1, F2 and F6 is very good, however, there is some variation observed in the profiles for the penetration on series F4 and F8, and this is probably because of the less than optimised process for these samples.

The angle between the mild steel and the weld bead penetration was measured for all five series of fatigue testing using the IFM. For each of the 3 surface profiles analysed the angle was measured for each sample. The results were then averaged for each sample and plotted against the fatigue life of the sample, the results are shown in figures 150 and 151.

Figure 150 shows the results of the analysis carried out on LHW samples, the graph indicates a relationship between root angle at the point of failure and fatigue life. As the angle at the root of the weld decreases the fatigue life increases. A best fit line was plotted and the relationship between angle and fatigue life for LHW joints can be defined as:

$$\theta = -0.9 * 10^{-5} x + 48.88$$

Where,

θ = angle at root penetration (°)

x = fatigue life in cycles

Equation 13. Relationship between angle at weld root and fatigue life for LHW

Therefore if the angle at the root of the weld was measured prior to testing, equation 13 above could be used to estimate the fatigue life, or if the sample had previously been tested the root angle could be predicted from the result of the fatigue life. For example for a laser hybrid welded sample to survive to 2 million cycles the maximum angle of the root penetration is 30.88° and can be calculated as shown below:

$$\theta = -0.9 * 10^{-5} * 2000000 + 48.88$$
$$\theta = -18 + 48.88$$
$$\theta = 30.88°$$

Fatigue samples produced using the CMT process also showed a similar relationship, as the angle at the root decreases the fatigue life increases (figure 151), with the relationship defined as:

$$\theta = -1.3 * 10^{-5} x + 41.98$$

Where,

θ = angle at root penetration (°)

x = fatigue life in cycles

Equation 14. Relationship between angle at weld root and fatigue life for LHW

Therefore to predict the root angle required for a sample to complete 2 million cycles of a fatigue test the maximum angle would be 15.98° and can be calculated as shown below.

$$\theta = -1.3 * 10^{-5} * 2000000 + 41.98$$
$$\theta = -26 + 41.98$$
$$\theta = 15.98$$

The relationship between the angle at the root and the fatigue life suggests that the fatigue properties of welded joints are heavily dependent on the geometry of the joint. Any change in geometry will in turn effect the stress concentration at the point of fatigue crack initiation.

The model presented for the fatigue life and the angle at the root of the weld shows a linear relationship with a negative gradient. The validity of this model is only relevant within the bounds of the testing carried out in this research. If the relationship was extrapolated beyond the bounds there would be a value of angle when the number of cycles to failure is 0. In theory this is un true as a fatigue test is carried out below the materials value of UTS, therefore the test would always produce x number of cycles before failure even if the stress of the root angle was high. It is expected that if the tests carried out in this study were expanded beyond the linear model, then the model would in fact become a non-linear model, when the angle becomes small enough to produce infinite fatigue life.

However, results of the two processes show different values of angle for the same cycles to failure yet the fatigue properties are dependant on the geometry. Overall the

joints produced with the CMT process require a smaller angle to initiate and cause fatigue failure than the LHW joints. A number of factors could contribute to this, the stress concentration in the CMT joints is higher than that of the LHW joints. This is because CMT joints have a larger weld bead, the reinforcement. Secondly when a stress concentration is evident crack initiation and propagation occurs at a faster rate in the CMT joints than the LHW. This is probably due to the difference in hardness observed at the fatigue initiation site.

Figure 152 shows the hardness of the 5 series of fatigue samples in the HAZ on the mild steel side of the joints adjacent to the bottom of the weld, this is the point of failure for the failed samples, up to the HAZ adjacent to the upper part of the weld. The hardness in the HAZ closest to the bottom of the weld is consistently higher in the LHW joints than the CMT joints.

As described previously in section 5.2 the LHW process produces an inhomogeneous weld pool with a predominately martensitic structure in the lower half of the weld pool, which also means the HAZ of the LHW is predominately martensitic. The UTS properties of martensite are greater than those of the mild steel, therefore for the LHW welds, the angle for a surviving fatigue sample is greater than that of joints produced using the CMT process because the material properties in the HAZ differ. Hardness is proportional to ultimate tensile stress which is proportional to fatigue life, therefore if the hardness is greater in the HAZ for LHW joints then the fatigue life is going to be increased when compared to CMT joints.

The angle at the root of the weld bead represents the stress concentration, as the angle decreases the relative stress concentration would also decrease and the fatigue life of the specimen would increase. Therefore the relationship between root angle and fatigue life is a linear relationship with a negative gradient.

CMT joints overall produced poorer fatigue results than similar joints using the LHW process. However, the consistency of the CMT joints is much improved and more predictable than the consistency of joints produced using the laser hybrid process. In reality if the geometry of the welds produced can be controlled with either processes then the fatigue properties can be controlled and possibly improved.

5.6 *Comparison of Welding Techniques*

The overall aim of this research was to assess these novel joining techniques in terms of their ability to produce joints similar in tensile, fatigue properties and appearance to techniques already widely used within the automotive industry. One widely used application in industry is laser welding and to date the results for the tensile tests of the butt joints can be compared favourably to laser welded butt joints as shown in figures 153 and 154.

Figure 153 shows current results for austenitic stainless steels and zinc coated mild steel. As seen on figure 153 the results are very similar and the joints failed within the mild steel away from the HAZ. The results for the LDX 2101 to mild steel materials are also similar as shown in figure 154 with UTS of around 400MPa. This is representative of the tensile strength of zinc coated mild steel with values expected of 380-400MPa.

The results of the fatigue testing (figure 155) indicate that Laser Hybrid Welding compares favourably to the results of Laser Welding in terms of mean fatigue strength. Currently both processes are used in the automotive industry, however, laser welding is more widely used than Laser Hybrid Welding. With comparable fatigue properties there is potential for LHW to be used for more application in particular dissimilar metal joining. Cold Metal Transfer joints were also tested and showed much lower mean fatigue strength when compared to similar joints with the laser hybrid process and the laser only welding, as explained in section 5 this is most likely due to the geometrical factors involved in this process.

The results obtained from the staircase fatigue tests indicate that the standard deviation, which represents the variation in fatigue strength between joints made to the same configuration, for each joint configuration is notably higher for Laser Hybrid Welding than that seen in similar joining processes, such as laser only welding and Cold Metal Transfer. There is an additional process and a filler wire involved in LHW when compared to Laser only welding increasing the process variability and therefore a higher than anticipated standard deviation was obtained. CMT has an additional filler wire but showed that the reproducibility in weld quality and consistency in joint geometry was much better than LHW.

5.7 *Summary of Discussion*

Table 22 below shows a summary of the results of this research, this can be used to assess whether the objectives at the beginning of the research were met.

Series ID	Stainless Grade and Thickness (mm)	Filler Wire	Calculated Mean Fatigue Strength (kN)	Ultimate Tensile Strength (MPa)	Average Hardness of Weld (Hv)
1	LDX 2101 0.75	308L-Si	9.57	385.7	305.0
2	LDX 2101 1.5	308L-Si	15.70	388.8	284.1
3	Hy-Tens 1000 0.75	308L-Si	9.42	389.5	312.0
4	Hy-Tens 1000 1.5	308L-Si	Not valid	391.9	288.6
5	LDX 2101 0.75	309L-Si	8.44	387.9	267.6
6	LDX 2101 1.5	309L-Si	15.00	387.0	268.6
7	Hy-Tens 1000 0.75	309L-Si	7.75	391.2	284.3
8	Hy-Tens 1000 1.5	309L-Si	14.52	387.7	249.9
C1	LDX 2101 1.5	308L-Si	8.5	422.6	225.1

Table 22. Comparison of Fatigue, tensile and hardness properties of weld combinations tested in the research

Acceptable process windows were found for Laser Hybrid Welding of LDX2101 to zinc coated mild steel for the combinations tested in the work (F1, F2, F5 and F6). After initial visual assessment of Laser hybrid welded samples using Hy-Tens 1000 stainless steel it was decided that the parameters were acceptable, unfortunately the consistency of the weld quality was poor and series F4 and F8 had unacceptable fatigue results. For welds produced using CMT with LDX 2101, an acceptable process window was achieved, however in the future controlling of the weld reinforcement could improve the fatigue properties.

Mechanical properties for all joint combinations were assessed in terms of tensile and fatigue properties. All nine joint combinations passed the acceptance criteria that the joint was to exhibit similar properties as the weakest parent material, e.g. the mild steel. The fatigue properties varied throughout the series and it was found that the geometry of the joint controlled the fatigue properties. The point of failure for all series was the

underside at the root of the weld. For similar thickness joints this occurred on the mild steel side of the joints and a relationship between root angle and fatigue life has been proposed.

It was found that series F2 and F6 produced overall the best fatigue results, it is thought that with further optimisation series F4 and F8 could produced similar fatigue results. Series C1 was identical in material combination to series F2, however the fatigue properties were almost half the value of F2. It is thought that this is due to the excess reinforcement of welds produced using the CMT process, work in to the effect of the reinforcement needs to be assessed.

In terms of hardness properties, series produced using LHW could have areas of hard spots and produce a inhomogeneous weld pool, within the research this was found not to have a negative effect on the fatigue properties as this was controlled predominately by the geometry of the welds produced. Joints produced using CMT had a more consistent hardness across the weld pool and exhibited a lower average weld pool hardness when compared to laser hybrid joints.

6 Conclusions

The research detailed in this report has investigated the properties of dissimilar metal joints produced by two novel joining techniques. After assessment of the current literature surrounding this subject, the experimental results and analysis the following conclusions can be made. The conclusions have been sub divided into, mechanical properties, metallurgical properties and novel joining techniques.

- For similar and dissimilar thickness fatigue samples the fatigue results indicate that they are influenced more by geometry than the metallurgy of the welded samples.

- Fatigue properties of similar thickness laser hybrid welded joints and cold metal transfer welded joints are linearly related with a negative gradient to the value of the root angle on the mild steel side of the joints, as the angle at the root decreases the fatigue life increases.

- The fatigue properties of the series of welded joints with dissimilar thickness parent materials are affected by the joint geometry, displaying lower mean fatigue line load range than the similar thickness joints. This is due to the increase in stress concentration on the stainless steel side of the joint.

- The uni-axial tensile strength of the laser hybrid welded and the Cold Metal Transfer joints tested in this study meet the established criteria indicating that they exhibit 100% joint efficiency.

- Fatigue properties of similar thickness laser hybrid welded joints can be described by the equation $\theta = -0.9 * 10^{-5} x + 48.88$, under the conditions of test described in this research.

- When joining the material combinations outlined in this research with Laser Hybrid Welding the resulting solidified weld pool will be chemically inhomogeneous. The chemical inhomogeneity leads to a change in constitution with a commensurate change in hardness through the thickness of the weld pool.

- It was difficult to optimise the laser hybrid welding process for joints containing Hy-Tens 1000 due to the presence of zinc and the high strength of the material.

- LHW lap joints of all material combinations are greatly affected by the presence of zinc vapour during the welding process, causing porosity and cracking.

- The position of the laser and GMAW torch during welding is critical and greatly affects the LHW process for joints of all material and joint combinations.

- The poor consistency observed with the fatigue samples welded with Hy-tens 1000 material is caused by the less than optimum welding process.

- Fatigue properties of similar thickness cold metal transfer welded joints can be described by the equation $\theta = -1.3 * 10^{-5} x + 41.98$, under the conditions of test outlined in this research.

- Welds produced using CMT resulted in a chemically homogenous weld pool and consistent microhardness and constitution

- Samples produced using Cold Metal Transfer were considerably more consistent in terms of process stability and weld geometry than those produced with LHW. LHW welds outperformed CMT in terms of fatigue performance, this was due to the large reinforcement the CMT welds possessed.

- Overall, joints produced with the LDX 2101 stainless material produced more consistent and reproducible joints than identical joints using the Hy-Tens 1000 stainless grade. The results of the research suggest that under identical conditions of testing LDX 2101 possesses greater weldability than Hy-Tens 1000.

- Laser hybrid welding and cold metal transfer can produce joints with mechanical properties comparable with laser only welding currently being used in the automotive industry.

7 Further Work

After assessment of the work carried out during this research project the following suggestions for further work can be made:

- It was found under the scope of this project that Hy-Tens 1000 and LDX 2101 behave differently during welding with respect to the presence of zinc. Therefore an investigation into the metallurgical differences between LDX 2101 and Hy-Tens 1000 should be carried out, with particular attention on the effect of the zinc vapour which is present during laser hybrid welding.

- Using initial parameters (samples 7 and 19) described in this research, design and carry out a Design of Experiments (DOE) to determine optimum parameters for lap welding using LHW. Assess and evaluate the DOE in terms of surface cracking and porosity.

- Investigate potential ways of removing the zinc coating prior to welding. Assess the implications of cost this would have on the manufacturer looking at implementing LHW or CMT into production.

- Assessment of the suitability of CMT for other material combinations including Hy-Tens 1000 for both butt and lap joint configurations. This would allow a full comparison of both LHW and CMT for the materials focussed on in the current research.

- In order to further the work using the CMT equipment at Sheffield Hallam University it is recommended that consideration is giving to purchasing a robot. The current trolley system relies a great deal on human reaction to line up the specimen and to begin the process. A 5 axis robot would allow a greater accuracy in production and reproducibility of samples. It would also mirror what is more likely to be used in an industrial setting.

- Work including Finite Element Analysis in order to quantify the effect the root angle has on the fatigue life by determining the stress concentration as the angle changes. This would enable further development of the model between the two factors to take place.

- Carry out a feasibility study to determine the practicality of controlling the weld geometry to ensure suitable fatigue properties are achieved.

- Carry out a cost analysis of both CMT and LHW for an industrial application to assess if there are economical benefits of using one process over the other.

8 References

[1] Richards, K.G. Weldability of Steel. The Welding Institute. Fourth Reprint, 1980.

[2] Schubert, E. et al. Light-weight structures produced by laser beam joining for future applications in automobile and aerospace industry. Journal of Materials Processing Technology, 115, pp 2-8, 2001.

[3] Gourd, L.M. Principles of Welding Technology. Third Edition, 1995, ISBN 0 340 61399 8.

[4] Mazumder, J. Laser-Beam Welding, ASM Handbook 1, pages 262-269.

[5] Davies, A.C. The science and practice of welding volume: The practice of welding. Tenth Edition, 1993. ISBN 0 521 43566 8

[6] Larsson, J.K. Laser welding a mature process technology with various application fields. Svetsaren, Volume 54, No 1-2, pp 43-50, 1999.

[7] Moore, P.L. Wallach, E.R & Howse, D.S. Development of Laser and Laser/Arc Hybrid Welding for Land Pipeline Applications. Welding and Cutting, No3, pp 186-191. 2004.

[8] Yang, Y.S, Lee, S.H. A study on the joining strength of laser spot welding for automotive applications. Journal of Materials Processing Technology, 94 pages 151-156, 1999.

[9] Lozach, G. The Future of Galvanised Steel Sheets as a Material for the Automotive Body-In-White. Galvanised Steel Sheet Forum - Automotive, IOM3, 15-16 May 2000.

[10] Holliday, D.B. Gas-Metal Arc Welding. ASM Handbook 1, pages 180-185.

[11] Cary,H.B. Helzer, S.C. Modern Welding Technology. Sixth Edition 2005. ISBN 0 13 113029 3.

[12] American Welding Society. Welding Handbook - Welding Processes. Volume 2, Chapter 4, pages 110-155.Eighth Edition.1991 ISBN 0 87171 354 3.

[13] http://www.belasnet.be/nl/Nieuws/Hylas.jpg

[14] Eboo, M., Steen, W.M.& Clarke, J. May 1978, Arc Augmented Laser Welding, paper 17, Advances in Welding Processes 4th International Conference, Harrogate, UK.

[15] Alexander, J. & Steen, W.M. April 1981, Arc Augmented Laser Welding - Process Variables, Structure and Properties, The Joining of Metals: Practice and Performance, Coventry, UK.

[16] Walduck, R.P. Biffin, J. Plasma Arc Augmented Laser Welding, Welding and Metal Fabrication, Volume 62, No 4, April 1994.

[17] Bagger, C. Flemming, O. Review of Laser Hybrid Welding, Journal of Laser Applications, Vol 17, No 1, February 2005.

[18] Campana, G et al. The influence of arc transfer mode in hybrid laser-mig welding, Journal of Materials Processing Technology, Vol 191, pp 111-113, 2007.

[19] Tani, G et al. The influence of Shielding Gas in Hybrid Laser-Mig Welding.

[20] Vitek, J.M. et al. Weld Pool Shape Prediction in Plasma Augmented Laser Welded Steel. Science and Technology of Welding and Joining, Volume 6, No 5, pp 305 – 314, 2001.

[21] Wouters, M. Hybrid Laser-MIG welding – An investigation of geometrical considerations. Licentiate Thesis, Lulea University of Technology, 2005.

[22] Graf, T. Staufer, H. Laser Hybrid process at Volkswagen, www.fronius.com , 2005.

[23] Staufer, H et al. Laser Hybrid Welding and Laser Brazing: State of the Art in Technology and Practice by the Examples of Audi A8 and VW Phaeton, *www.fronius.com*, 2005.

[24] The Welding Institute Information.

[25] www.tps-fronius.co.uk

[26] Glover, M. Griffiths, J. Problem Partners, Automotive Engineer, pp 34-35, November, 2005.

[27] The new revolution in digital GMA welding, Fronius International GmbH, 2005.

[26] Himmelbauer, K. The CMT Process - A Revolution in Welding Technology, Fronius International GmbH, 2005.

[29] Pinto, H. et al. A comparative study of microstructure and residual stresses of CMT –MIG and Laser-Hybrid Welds. Materials Science Forum, Volume 534-525, pp 627-632, 2006.

[30] Society of Manufacturing Engineers News Archive January 2006 www.sme.org/cgi-bin/get-press.pl?&&20061021&&'A1000'&SME& .

[31] Kull, JE. Welding of galvanized carbon steel to HyTens with the new MIG/MAG CMT technique. Master of Science Thesis, KTH Industrial Engineering and Management, Stockholm 2006.

[32] Leffler, B. Stainless - Stainless steels and their properties, 2nd revised edition, Avesta Sheffield AB, 1998.

[33] Lula, R.A. Stainless Steel, American Society for Metals, 3rd Printing,1989.

[34] Castner, H.R. What you should know about austenitic stainless steels, 8th .Annual North American Welding Research Conference, Columbus, Ohio, October 1992.

[35] Honeycombe, R.W.K. Bhadeshia, H.K.D.H, Steels - Microstructure and Properties, Metallurgy and Materials Science, 2nd Edition, Butterworth-Heinemann. 2000.

[36] Westin, E.M. et al. Laser Welding of a Lean Duplex Stainless Steel. Paper 609. Avesta Research Centre, Outokumpu, 2007.

[37] Material Data Sheet for Dogal 260 RP-X from www.ssabdirect.com

[38] www.aztecgalvanizing.com/Process.htm.

[39] BS EN 10142:2000 - Continuously hot-dip zinc coated low carbon steels strip and sheet for cold forming. Technical delivery conditions.

[40] HSE. Zinc Embrittlement of austenitic stainless steel. Guidance notes PM13 from the Health and Safety Executive, December 1997.

[41] Nakata, K et al. Hybrid Laser-MAG Welding of Galvanized Steel Sheets. IIW Doc. XII-1820-04.

[42] Moriaki, O et al. Development of Laser-arc Hybrid Welding, NKK technical Review, No 8, 2002.

[43] Pan, Y. Richardson, I.M. Study of Laser Welding of Zinc Coated Steel Sheets in Overlap Configuration. Netherlands Institute for Metal Research, Delft, Netherlands.

[44] Wiklund, G. Nilsson,T. Kaplan, A.F.H. Laser Hybrid Welding of Zinc Coated Ultra High Strength Steel. Lulea University of Technology and SSA Tunnplat, Bolange, Sweden. 2007.

[45] Barnhouse, E.J. Lippold, J.C. Microstructure/Property Relationships in Dissimilar Welds between Duplex Stainless Steels and Carbon Steels. Welding Journal, Volume 77, Issue 12, pp 477-487, December 1998.

[46] Matsunawa, A. El-Batahgy, A-M. Zaghloul. Laser Beam Welding of Lap Joints of Dissimilar Materials. Joining and Welding Research Institute. Osaka University, Volume 27, Issue 2, 1998.

[47] Andersson, J. Nd:YAG Laser- MIG/MAG hybrid welding. A process optimisation for coated C-Mn high strength steel, and a parameter investigation of C-Mn high strength steel, stainless steel and aluminum alloys. KiMAB. April 2005.

[48] Mann, J.Y. Fatigue of Materials - An introductory text. Melbourne University Press, 1967.

[49] International Organization for Standardization, General Principles for Fatigue Testing of Metals, I.S.O, R373 (Geneva 1964).

[50] Clifton, A.J. A Statistical Analysis of the Fatigue Behaviour of Single and Multi-Spot Welded Joints. PhD Thesis, Sheffield Hallam University, 2007.

[51] Suresh, S. Fatigue of Materials. Cambridge University Press, 2nd Edition. 2004.

[52] Committee E-9 on Fatigue. A guide for fatigue testing and the statistical analysis of fatigue data. American Society for Testing and Materials Special Publication No 91-A. 2nd Edition, 1963.

[53] Maddox, S.J. Fatigue Strength of Welded Structures. Abington Publishing. 2nd Edition. 1991.

[54] Dixon, W.J. Mood, A.M. A Method for Obtaining and Analyzing Sensitivity Data. American Statistical Association.

[55] Song, J., Mourelatos, Z.P., Gu, R.J., 2005. Sensitivity Study of Staircase Fatigue Tests
Using Monte Carlo Simulation. SAE 2005-01-0803.

[56] Weibull. W. Fatigue testing and the Analysis of Results. Pergamon Press, Oxford. 1961

[57]Hans Nordeberg. Om Utvarderingsmetoder Vid Utmattning. (On Evaluation Methods for Fatigue). Institute of metals Research. Stockholm.1973.

[58] NDT Resource Centre. Available from:
www.ndted.org/EducationResources/CommunityCollege/Materials/Structure/fatigue.htm
(Accessed March 2008)

[59] Smith, W.F. Principles of Materials Science and Engineering. McGraw-Hill, Inc. 3rd Edition. 1996. Page 311-315.

[60] Smallman, R.E. Modern Physical Mettalurg. Butterworths. 4th Edition.1985. Pages 470-473.

[61] Higgins, R.A. Properties of Engineering Materials. Hodder and Stoughton. 1985. Pages 348-349.

[62] Gough, H.J. Sopwith, D.G. Atmospheric action as a factor in fatigue of metals. Journal of the Institute of Metals, 49 pg 92-122. 1932

[63] Steen, B: Eboo, M. Arc augmented laser welding - A low power arc and a laser in synergy offer high quality welds at high speed with reduced undercut, Metal Construction, V11 No7 July 1979.

[60] Ono,M et al. Welding Properties of Thin Steel Sheets by Laser-Arc Hybrid Welding - Laser focused arc welding, 1st International Symposium on High Power Laser Macro processing V4831 May 2002.

[65] Nordberg, H. McCann, S. Rotation of Overlap Joints Under Load, AvestaPolarit Research Foundation, 2004.

[66] Dinsley, C. Fatigue Properties of Dissimilar Metal Laser Welded Lap Joints, Ph.D Thesis, Sheffield Hallam University, 2004.

[67] Marples, M. Incomplete Ph.D work at Sheffield Hallam University.

[68] Wray, T. Resistance Spot Welding of Duplex Stainless Steel, Ph.D Thesis, Sheffield Hallam University, 2004.

[69] Nordberg, H. Fatigue Properties of Stainless Steel Lap Joints. Outokumpu Research Foundation and Sheffield Hallam University, 2005.

[70] Taylor, D. Barret, N. Lucano,G. Some new methods for predicting fatigue in welded joint. International Journal of Fatigue, Volume 24, pp509-518, 2002.

[71] Li, X.Y. et al. Finite element analysis of the effect of weld geometry and load condition on fatigue strength of lap joint. International Journal of Pressure Vessels and Piping, Volume 78, pp 591-597, 2001.

[72] Teng,T-L. Fung, C-P. Chang, P-H. Effect of weld geometry and residual stresses on fatigue in butt-welded joints. International Journal of Pressure Vessels and Piping, Volume 79, pp 467-482, 2002.

[73] Nguyen, T.N. Wahab, M.A. Theoretical study of the effect of weld geometry parameters on fatigue crack propagation life. Engineering Fracture Mechanics, Volume 5. No1. pp 1-18, 1995.

[74] CASPER FINAL YEAR PROJECT, Sheffield Hallam University, 2007-2008

[75] BS EN 10002-1:2001 - Metallic Material - Tensile Testing - Part 1: Method of test at ambient temperature.

[76] BS EN 895:1995 -Destructive tests on welds in metallic materials - Transverse tensile test.

[77] A Guide for Fatigue Testing and the Statistical Analysis of Fatigue Data. ASTM STP 91-A, 1963

[78] Alicona Infinite Focus®.Operating manual and website, www.infinitefocus.info/technique.

[79] Outokumpu Stainless. *Steel Grades, Properties and Global Standards.* Avesta Research Centre, Outokumpu website 2007.

[80] Arcini, H. *Investigation of a Laser Hybrid Dissimilar Base Metals Joint - Mild Steel/LDX 210,*ESAB AB Metallographic Laboratory, Report No- TECM-06021, February 2006.

[81] Private communication between Emma Ashcroft and Research staff at Avesta Research Centre

[82] Burgin, F. *Liquid Metal Embrittlement In The Arc Brazing of Stainless Steel.* Ongoing PhD research at Sheffield Hallam University, 2002 onwards

9 Appendix A -

Additional Microhardness Maps for Laser Hybrid Welded (LHW) Joints and Cold Metal Transfer (CMT) Joints

Additional Microhardness Maps for LHW Butt Joints with LDX 2101

Series 1

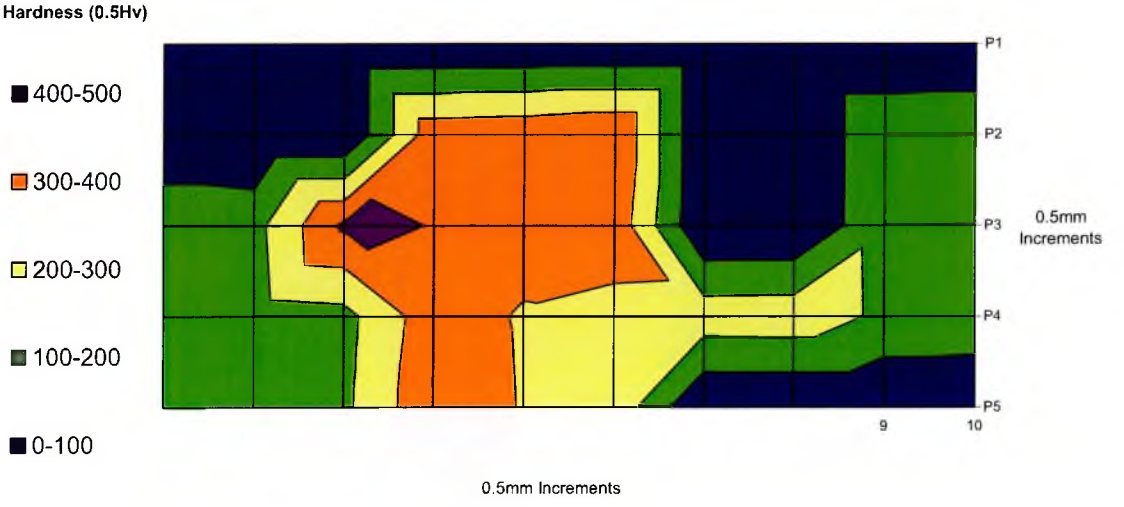

Figure 1. *Series 1 microhardness map of fatigue sample 1.5.3, the sample failed the fatigue test at 10.5kN after 1330564 cycles.*

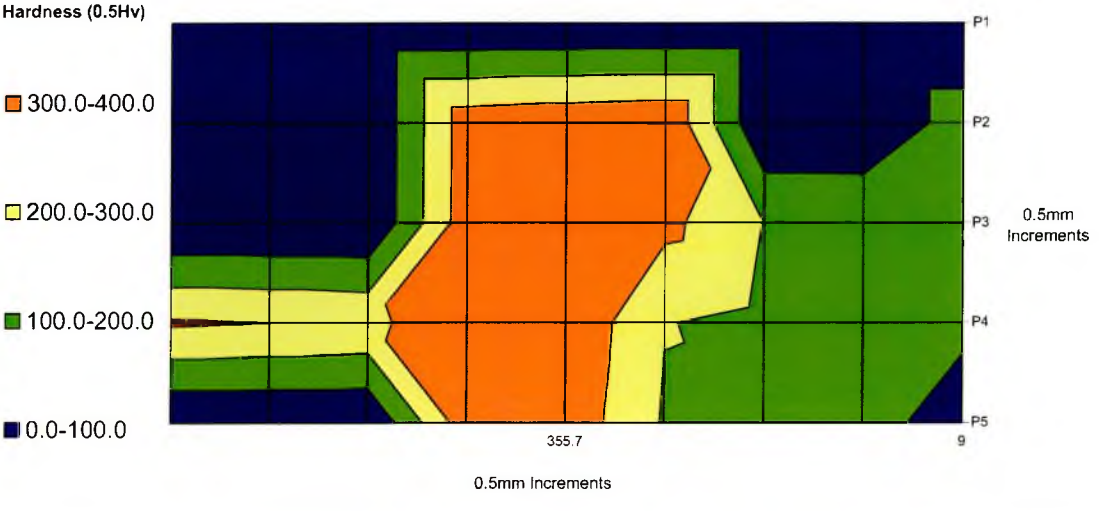

Figure 2. *Series 1 microhardness map of fatigue sample 1.8.5, the sample survived the fatigue test at 10.0kN completing 2 million cycles.*

Series 2

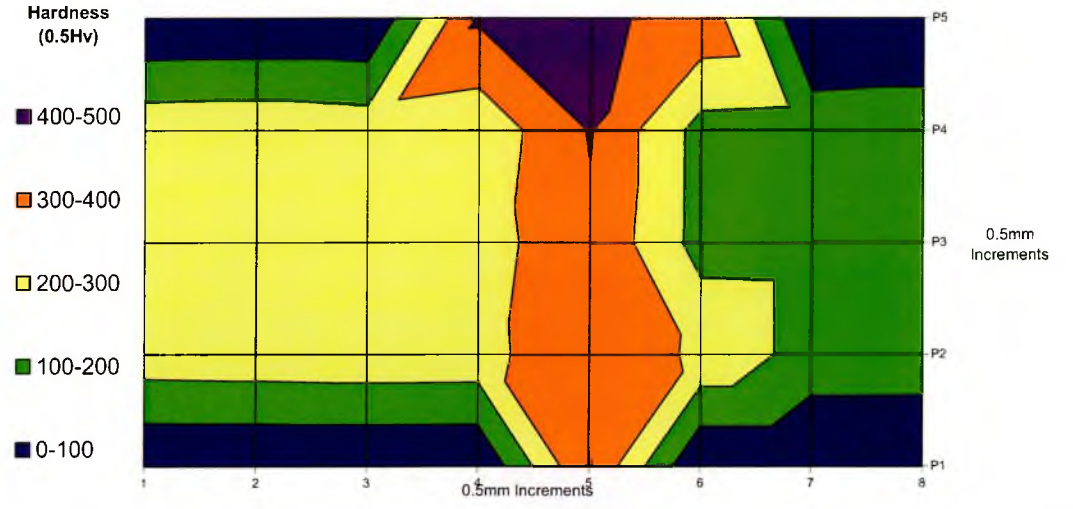

Figure 3. *Series 2 microhardness map of fatigue sample 2.4.6 the sample survived the fatigue test at 15.8kN completing 2 million cycles.*

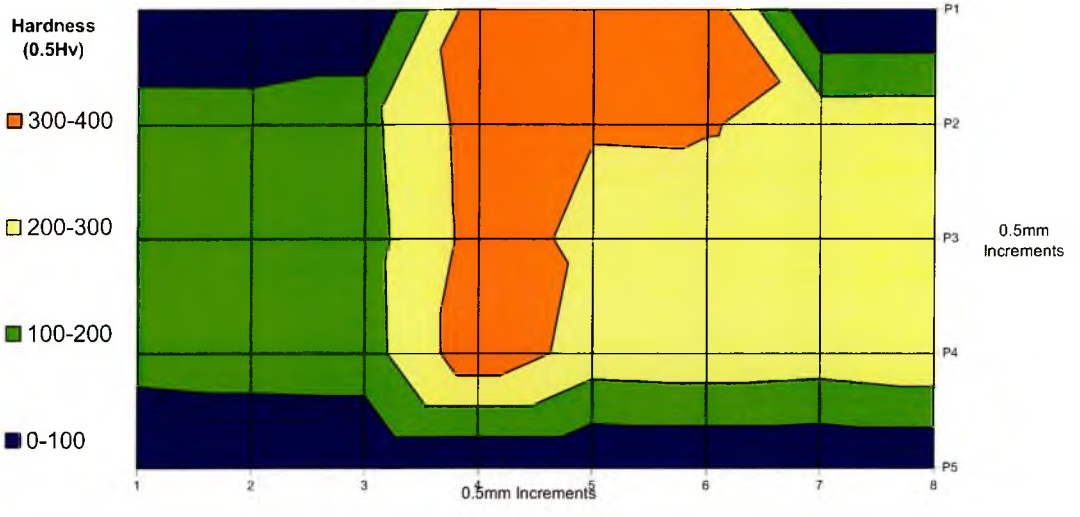

Figure 4. *Series 2 microhardness map of fatigue sample 2.5.2, the sample failed the fatigue test at 15.8kN after 503410 cycles.*

Series 5

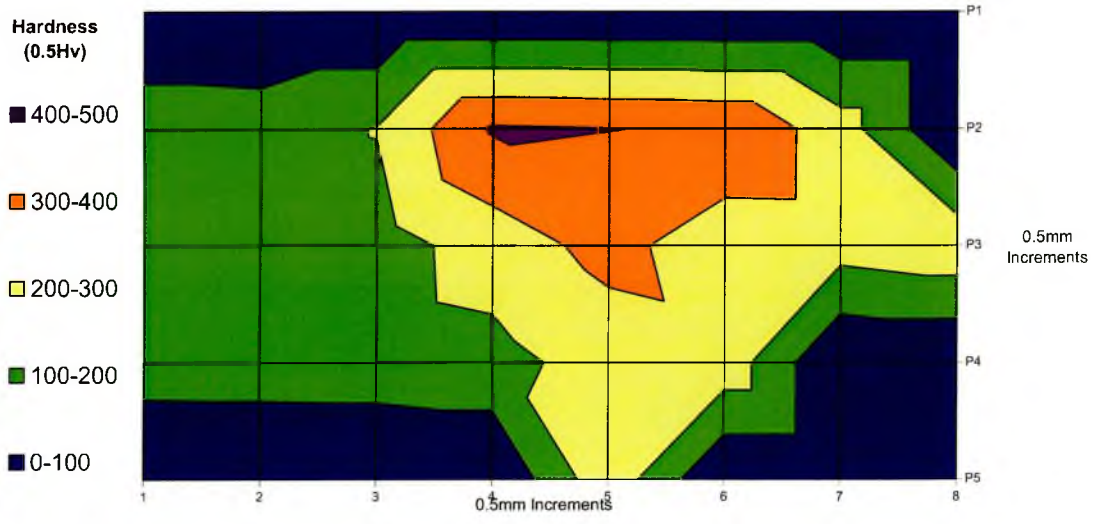

Figure 5. *Series 5 microhardness map of fatigue sample 5.2.1 the sample survived the fatigue test at 8.0kN completing 2 million cycles.*

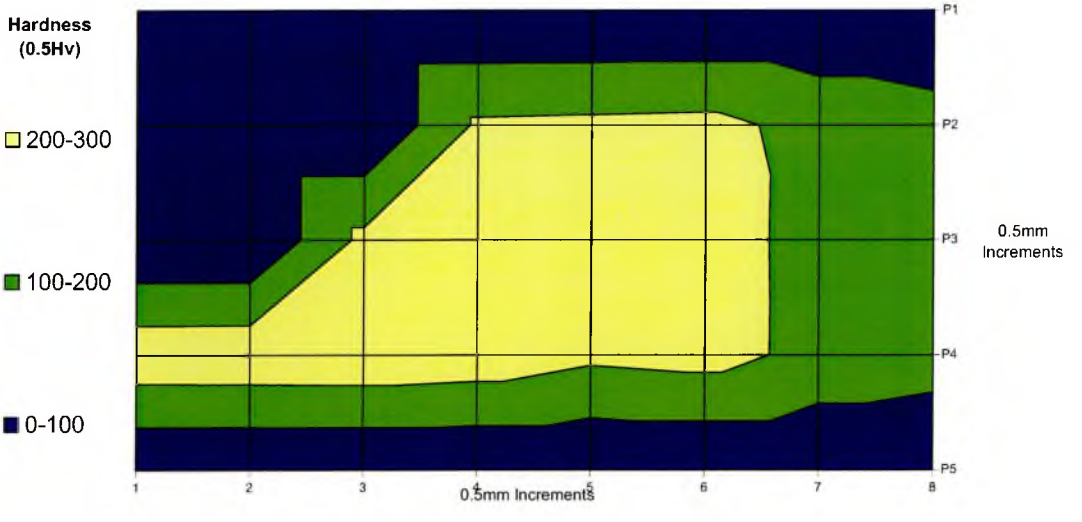

Figure 6. *Series 5 microhardness map of fatigue sample 5.3.5, the sample failed the fatigue test at 8.0kN after 645880 cycles.*

Series 6

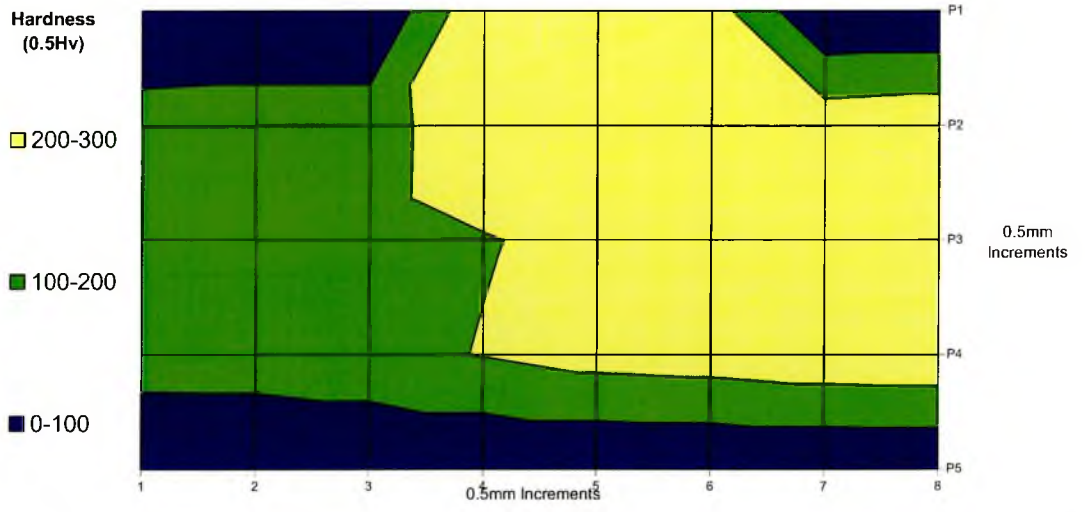

Figure 7. *Series 6 microhardness map of fatigue sample 6.0.2, the sample failed the fatigue test at 15.0kN after232584 cycles.*

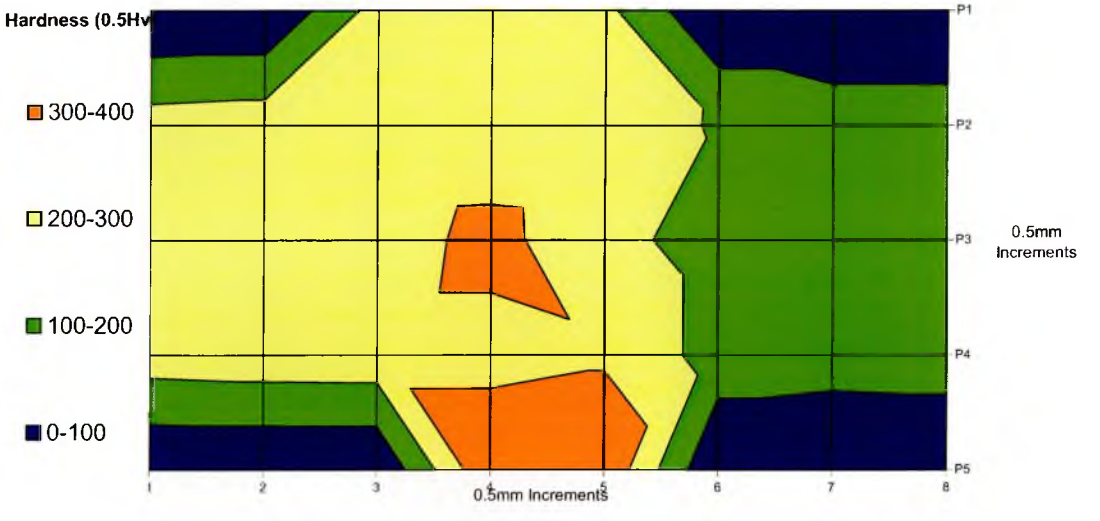

Figure 8. *Series 6 microhardness map of fatigue sample 6.4.3 the sample survived the fatigue test at 15.0kN completing 2 million cycles*

Additional Microhardness Maps for LHW Butt Joints with HyTens 1000

Series 3

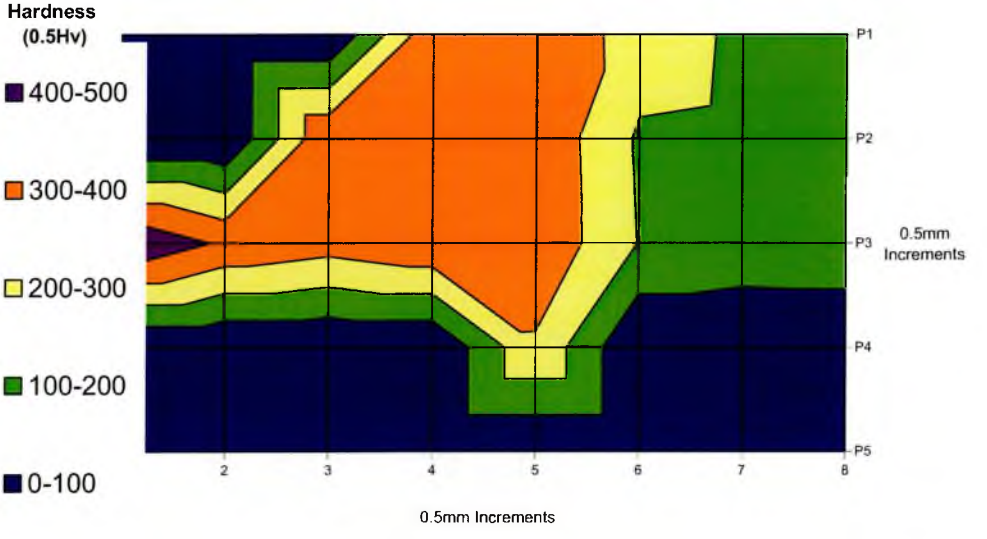

Figure 9. *Series 3 microhardness map of fatigue sample3.1.4, the sample failed the fatigue test at 9.5kN after567546 cycles.*

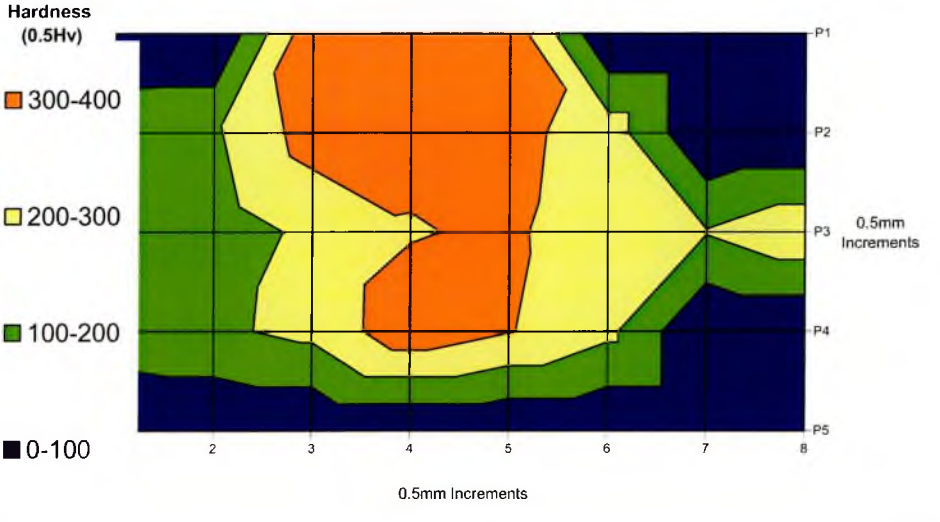

Figure 10. *Series 3 microhardness map of fatigue sample 3.2.6 the sample survived the fatigue test at 15.0kN completing 2 million cycles.*

Series 4

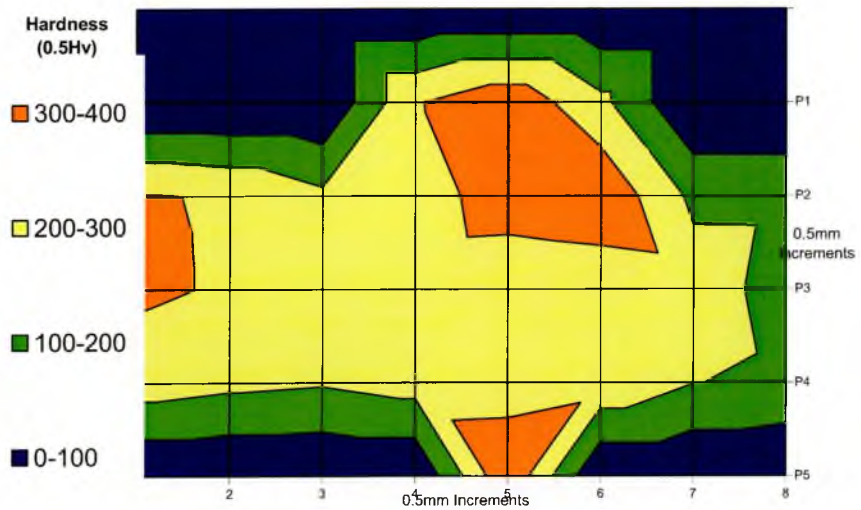

Figure 11. *Series 4 microhardness map of fatigue sample 4.7.6, the sample failed the fatigue test at 13.0kN after 683158 cycles.*

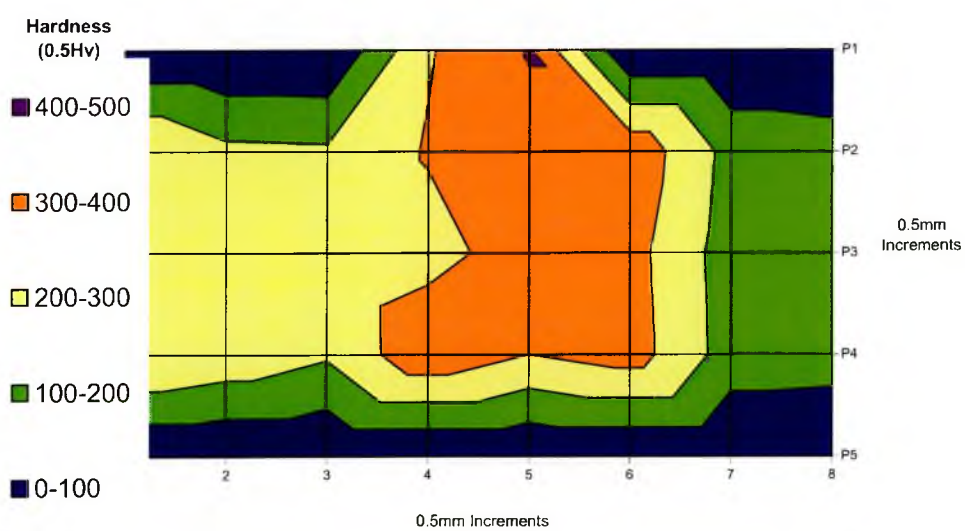

Figure 12. *Series 4 microhardness map of fatigue sample 4.8.1 the sample survived the fatigue test at 12.5kN completing 2 million cycles.*

Series 7

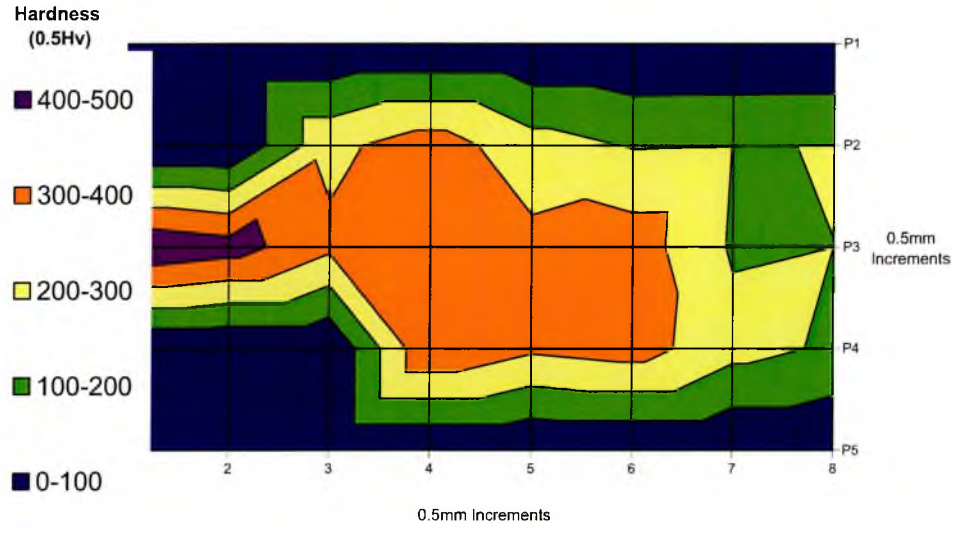

Figure 13. Series 7 microhardness map of fatigue sample 7.4.1, the sample failed the fatigue test at 7.5kN after 675616 cycles.

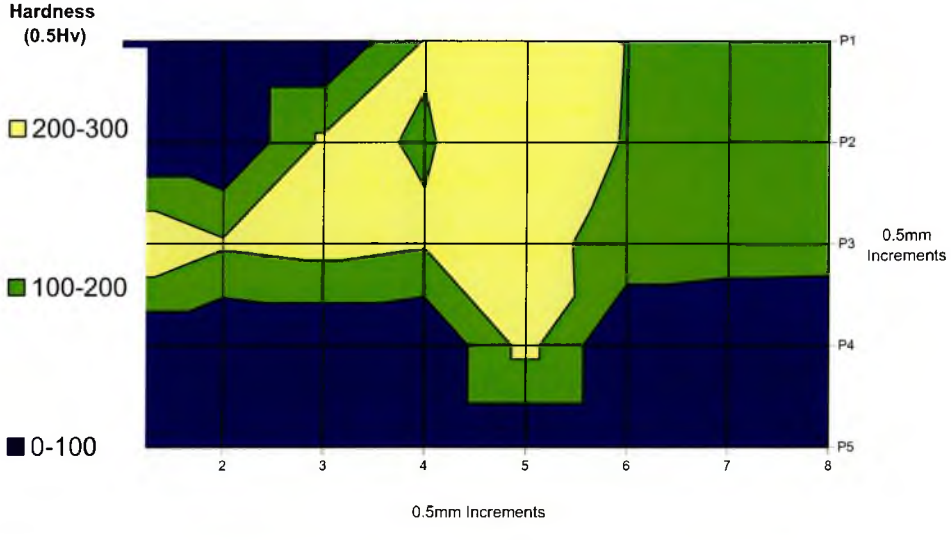

Figure 14. Series 7 microhardness map of fatigue sample 7.7.4 the sample survived the fatigue test at 7.5kN completing 2 million cycles.

Series 8

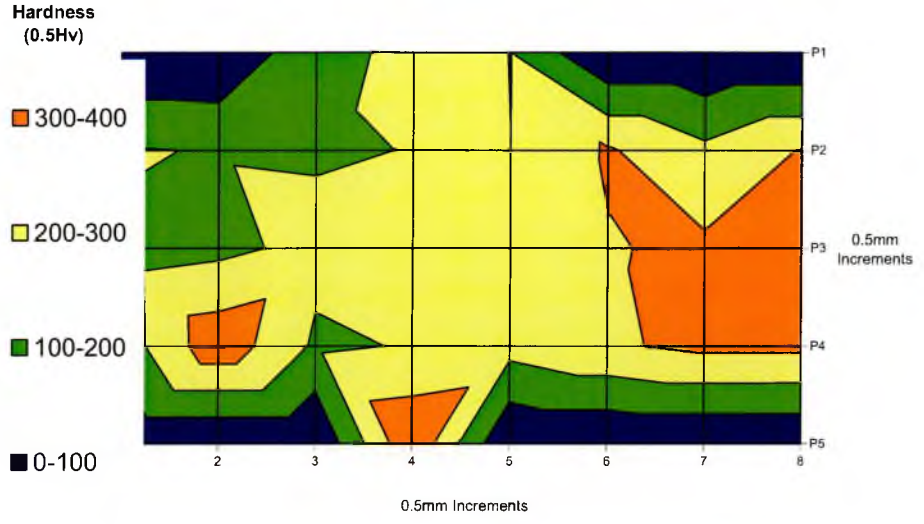

Figure 15. Series 8 microhardness map of fatigue sample 8.7.4, the sample survived the fatigue test at 15.2kN completing 2 million cycles.

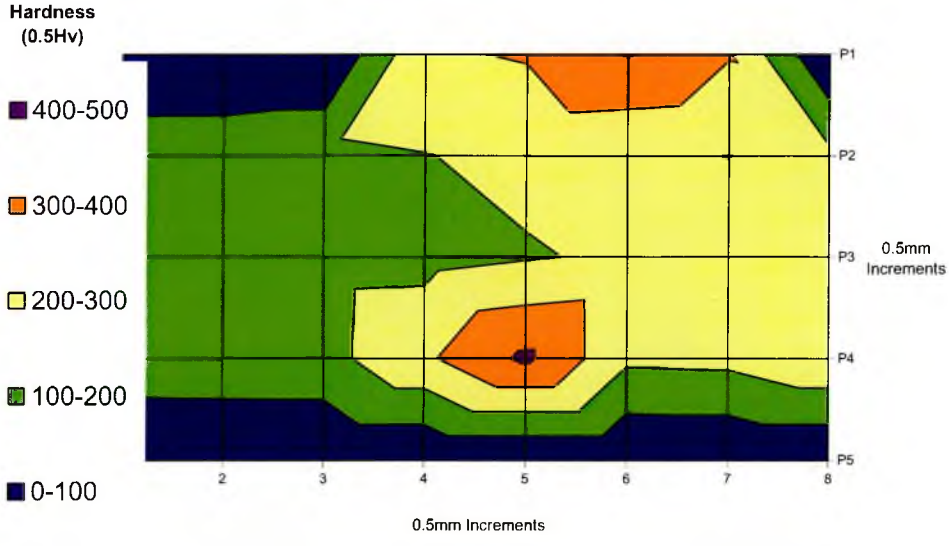

Figure 16. Series 8 microhardness map of fatigue sample 8.7.5 the sample failed the fatigue test at 15.6kN after 714085cycles.

Additional Microhardness Maps for CMT Butt Joints with LDX 2101

Series C1

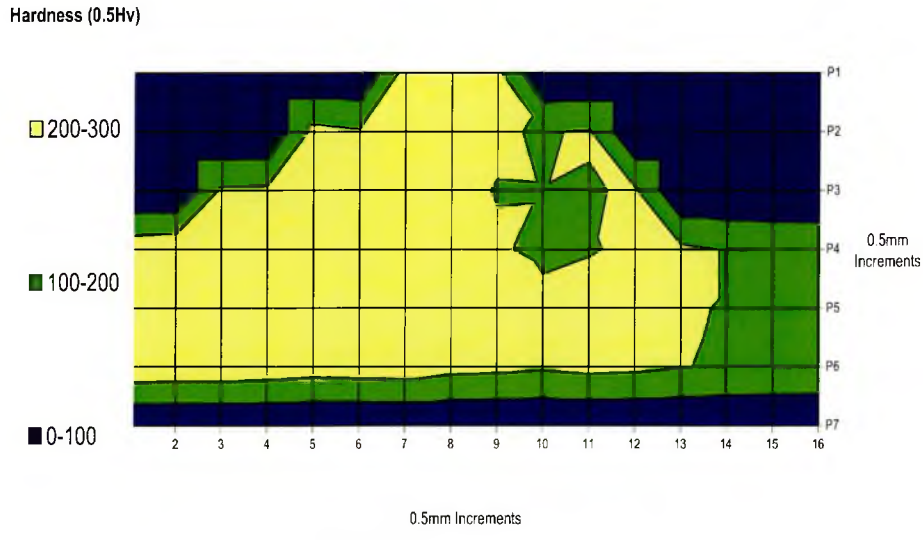

Figure 17. Series C 1 microhardness map of fatigue sample 1.9.3, the sample failed the fatigue test at 8.6kN after 959104 cycles.

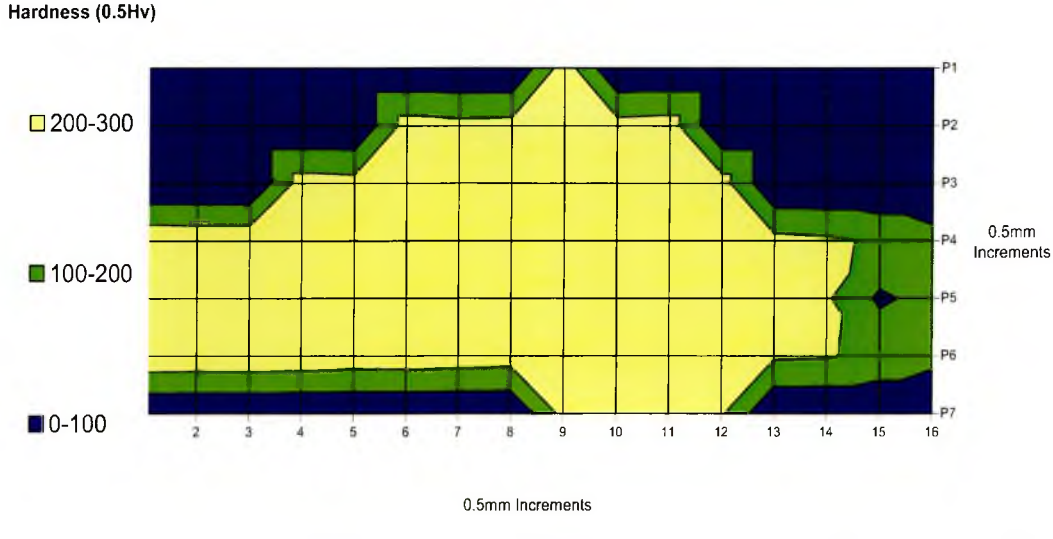

Figure 18. Series C1 microhardness map of fatigue sample 1.7.1, the sample survived the fatigue test at 9.0kN completing 2 million cycles.

10 Appendix B -

Additional IFM 3D Images and Surface Profiles for Laser Hybrid Welded (LHW) Joints and Cold Metal Transfer (CMT) Joints

Additional IFM 3D Images and Surface Profiles for LHW Butt Joints with LDX 2101

Series 2

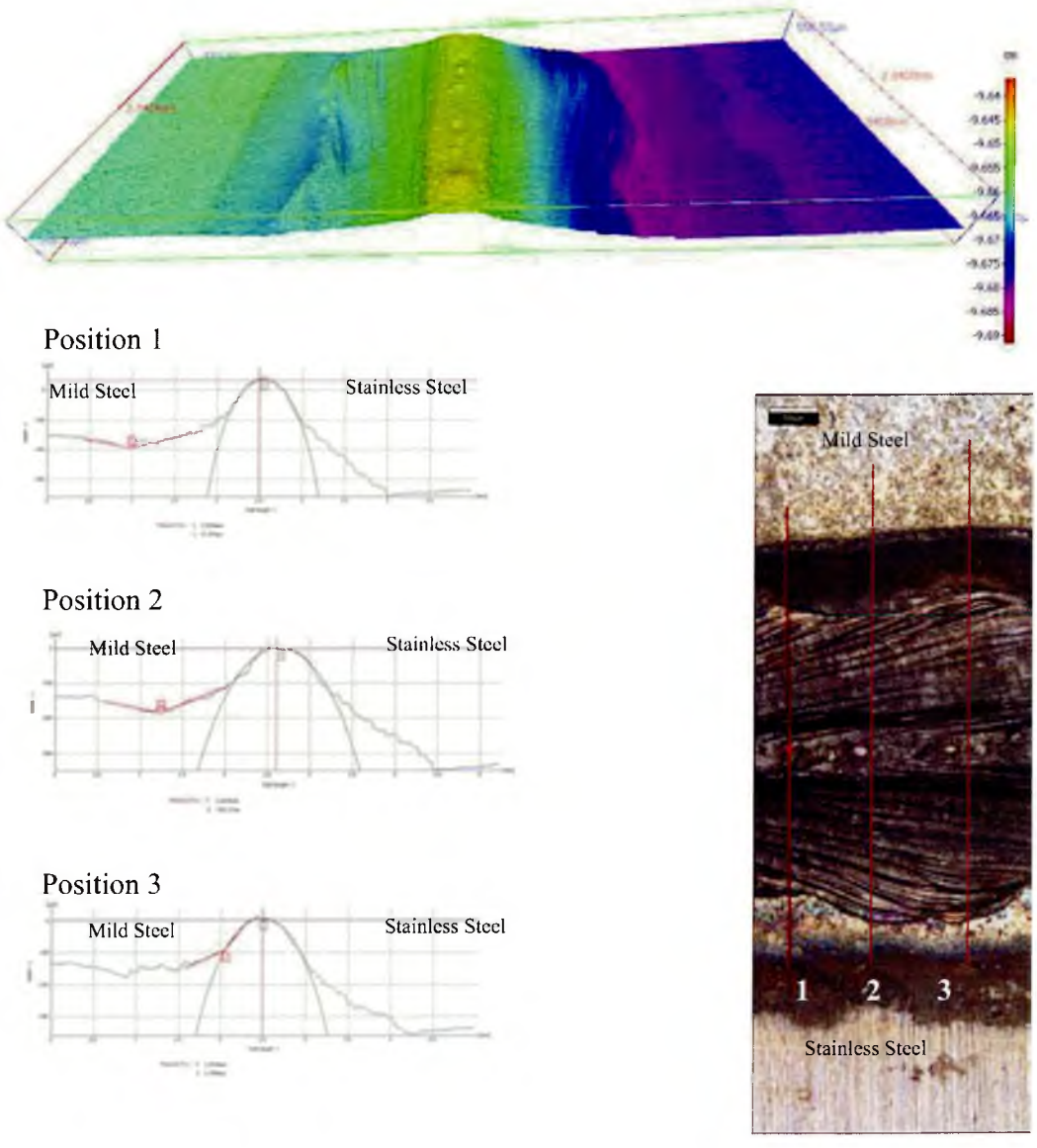

Figure 1. *IFM 3D surface image and surface profiles for the front of the weld bead of sample F2.5.1*

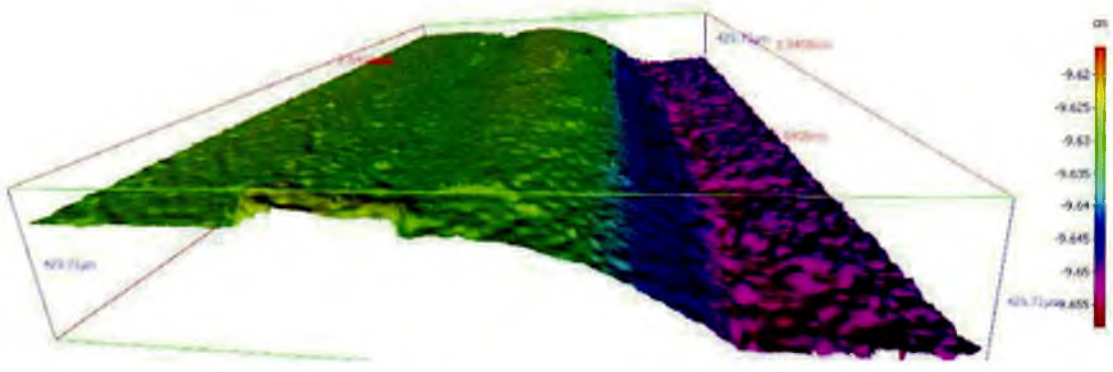

Position 1

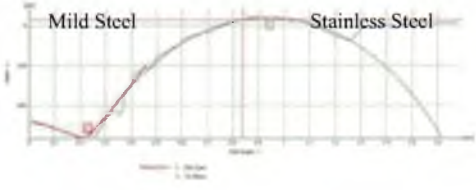

θ = 51

Position 2

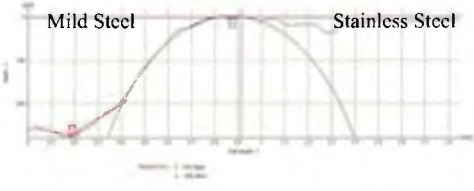

θ = 28

Position 3

θ = 29

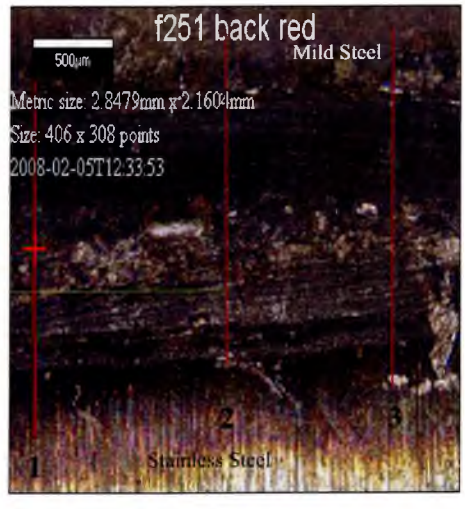

Mean θ = 36

Figure 2. *IFM 3D image and surface profiles for the underside of sample F2.5.1 including the penetration root angle measurements for the sample.*

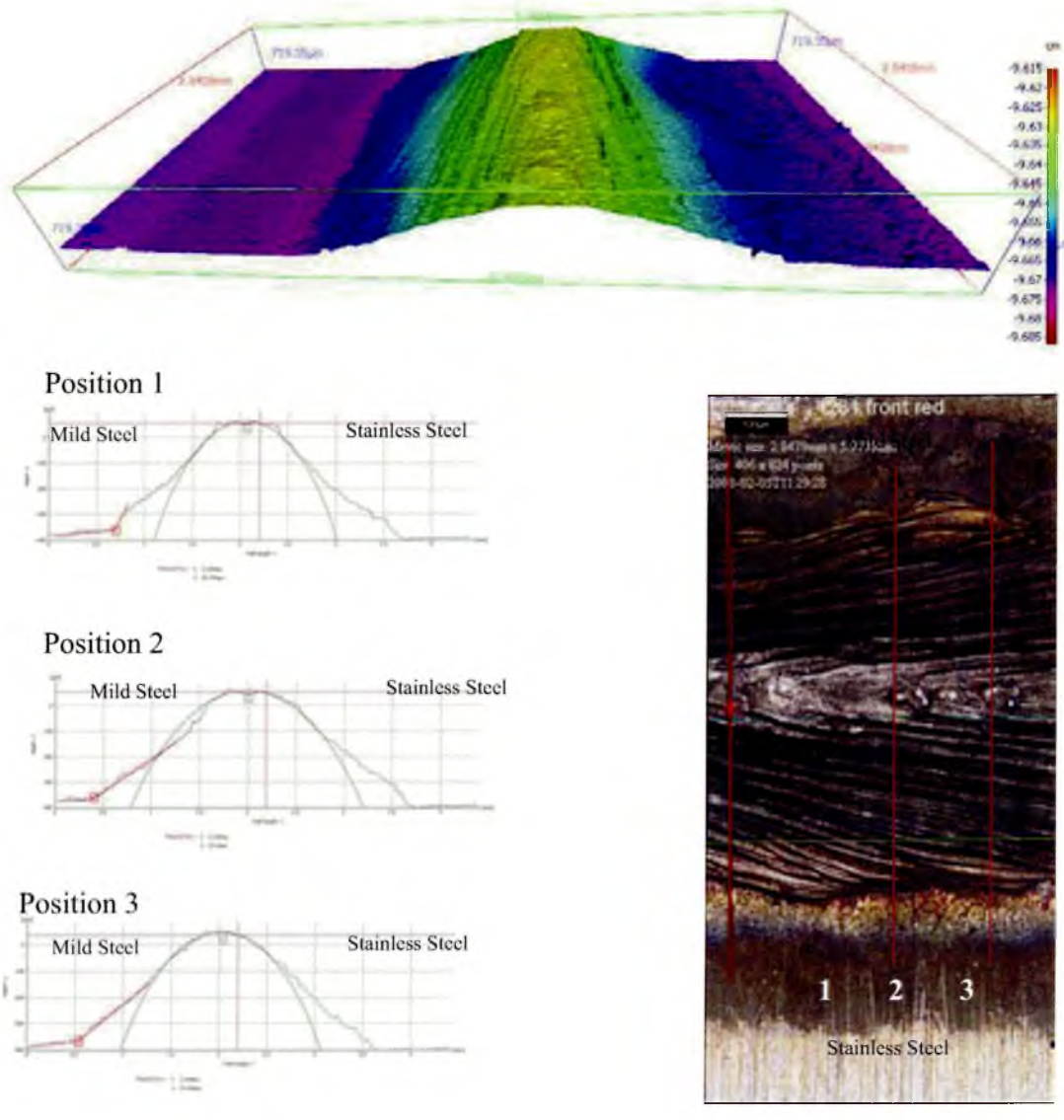

Figure 3. *IFM 3D surface image and surface profiles for the front of the weld bead of sample F2.8.1*

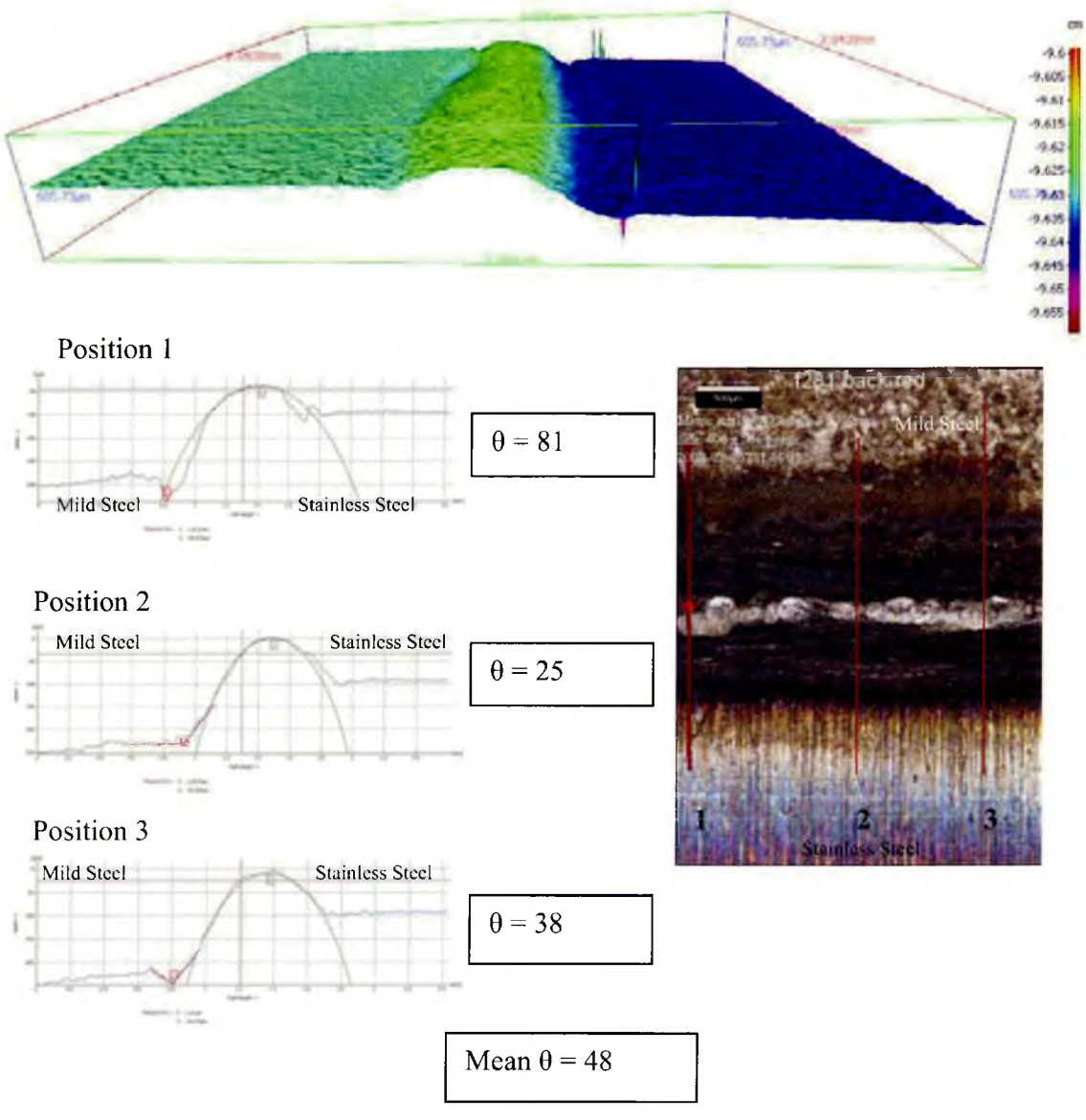

Figure 4. *IFM 3D image and surface profiles for the underside of sample F2.8.1 including the penetration root angle measurements for the sample.*

Series 6

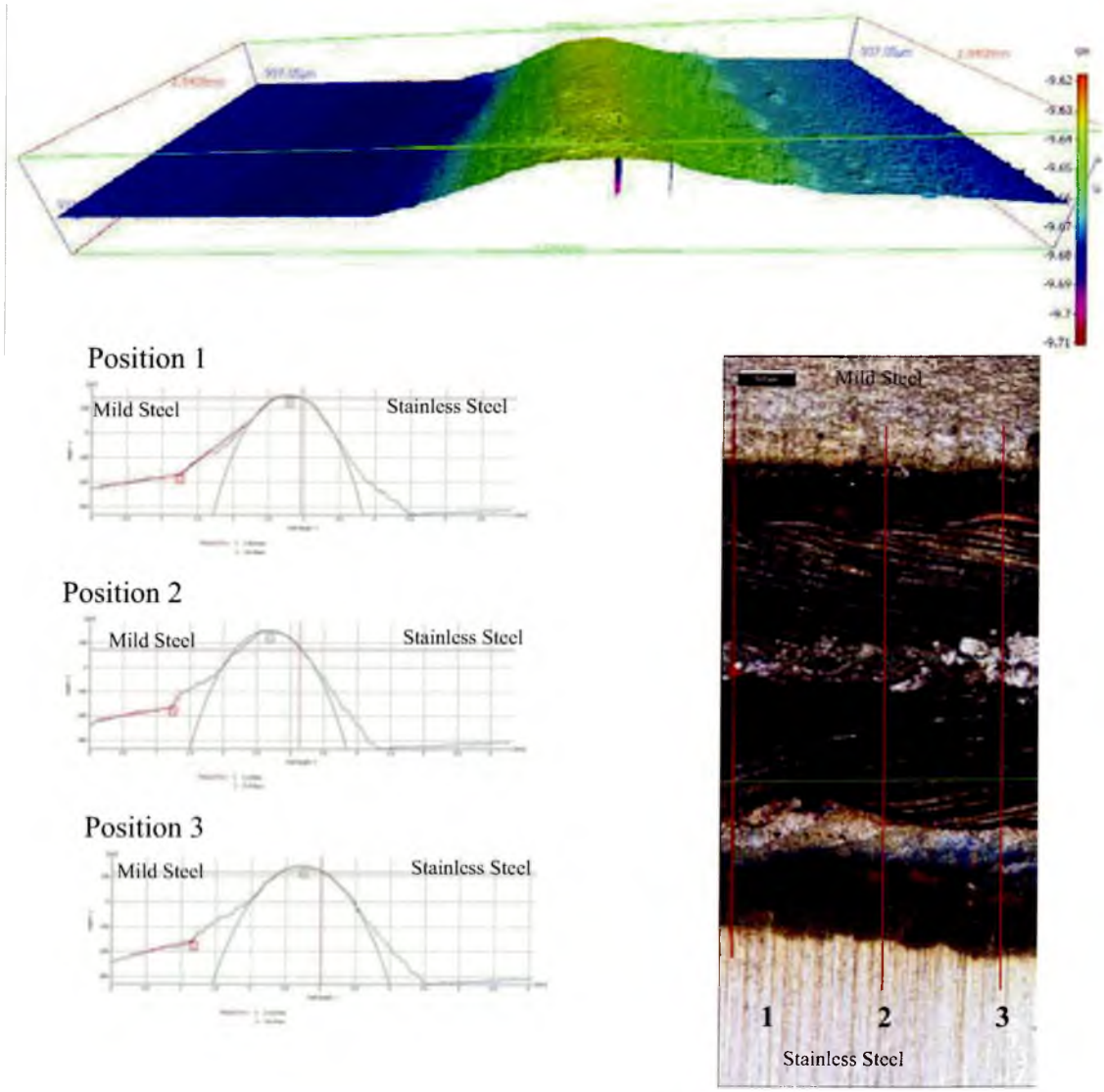

Figure 5. *IFM 3D surface image and surface profiles for the front of the weld bead of sample F6.0.3*

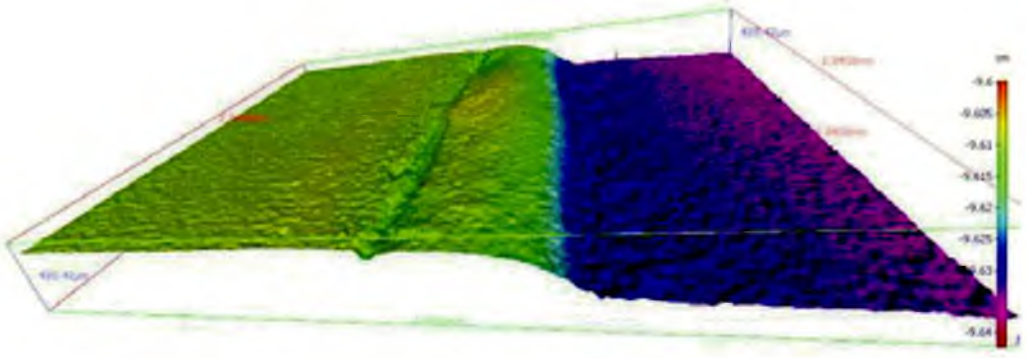

Position 1

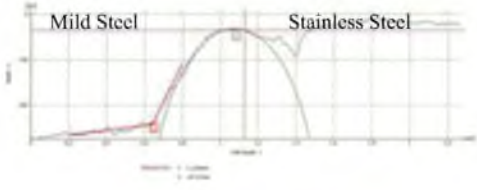

θ = 37

Position 2

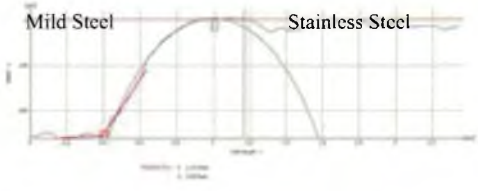

θ = 30

Position 3

θ = 49

Mean θ = 39

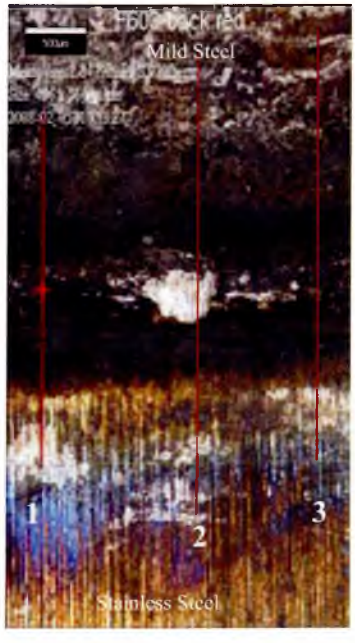

Figure 6. *IFM 3D image and surface profiles for the underside of sample F6.0.3 including the penetration root angle measurements for the sample.*

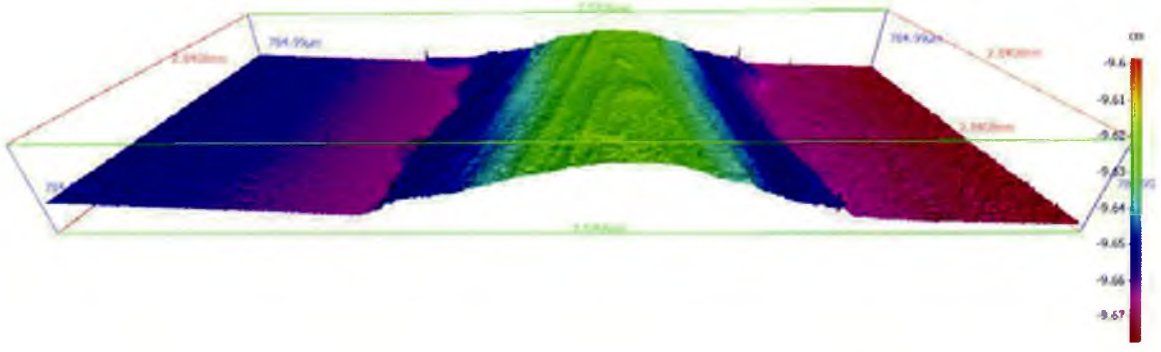

Position 1

Position 2

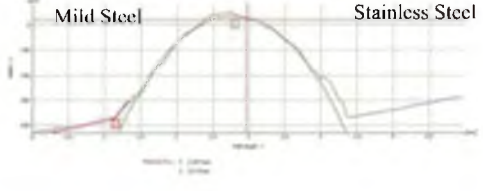

Position 3

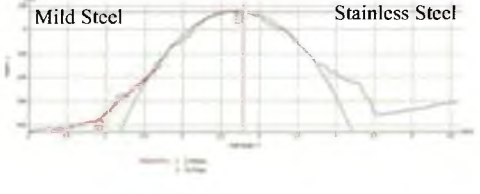

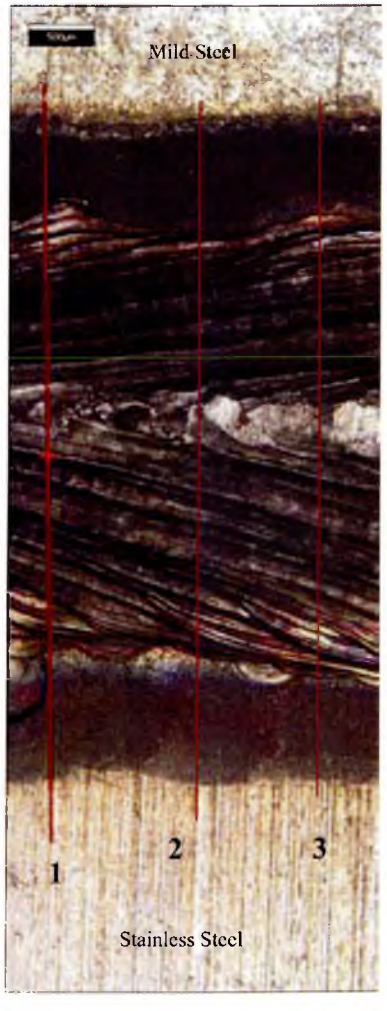

Figure 7. *IFM 3D surface image and surface profiles for the front of the weld bead of sample F6.4.6*

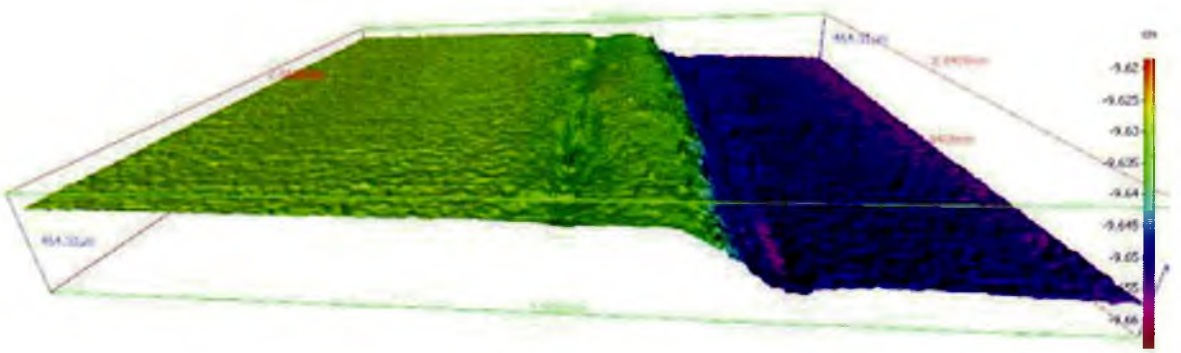

Position 1

θ = 41

Position 2

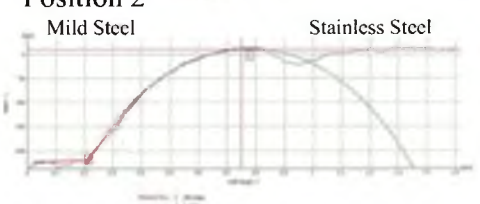

θ = 34

Position 3

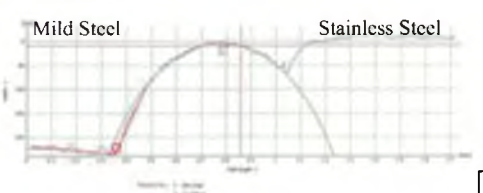

θ = 52

Mean θ = 42

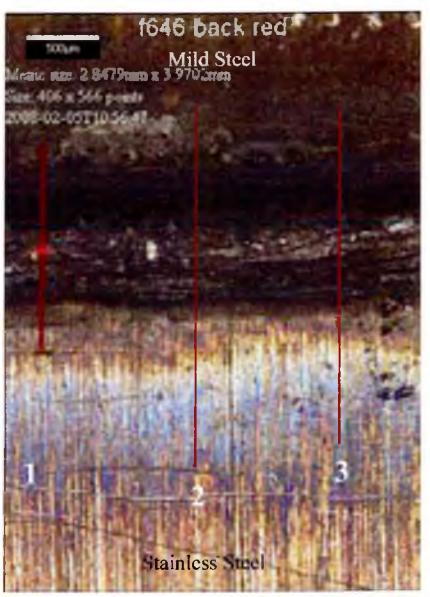

Figure 8. *IFM 3D image and surface profiles for the underside of sample F6.4.6 including the penetration root angle measurements for the sample.*

Additional 3D Images and Surface Profiles for LHW Butt Joints with HyTens 1000

Series 4

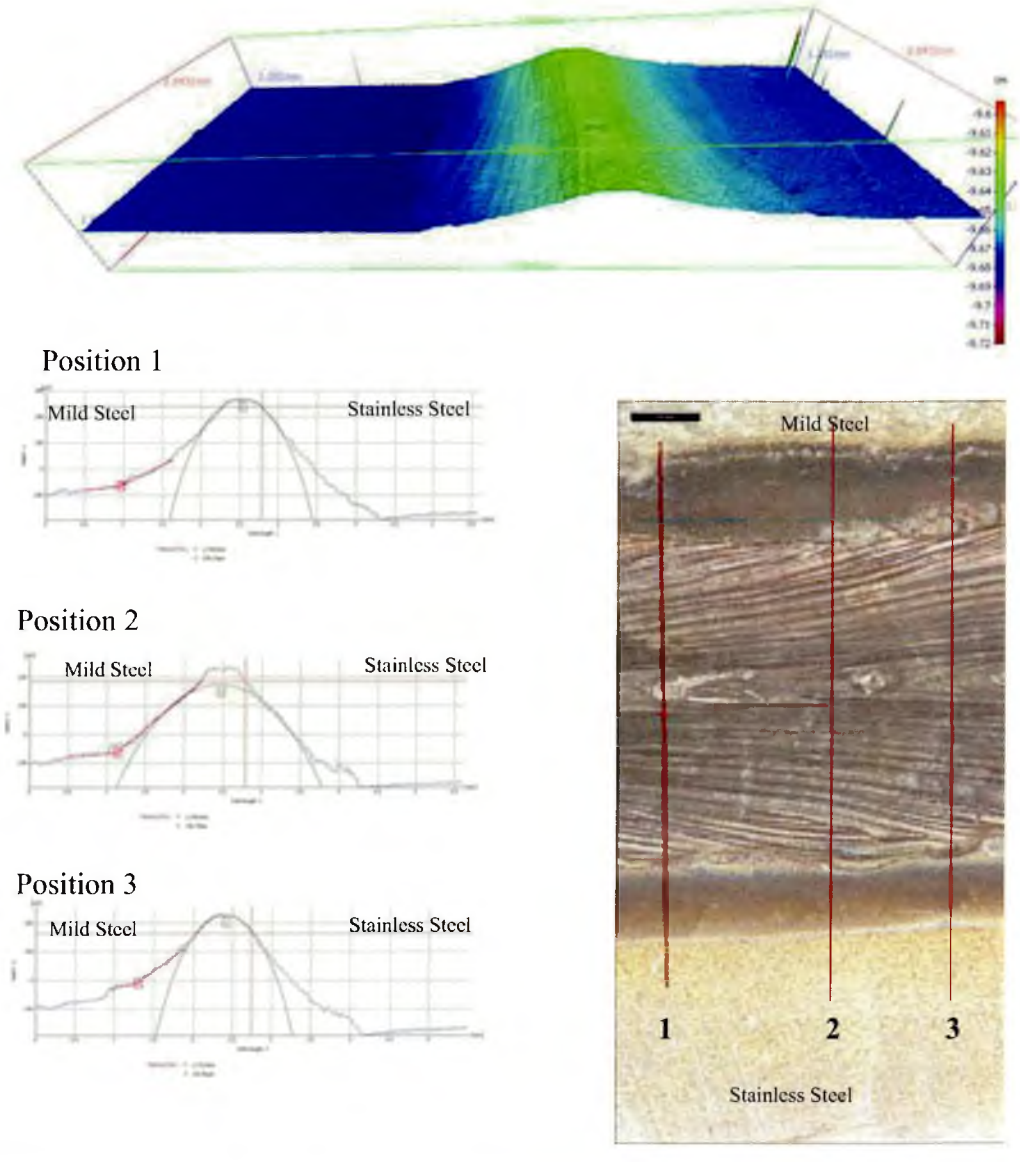

Figure 9. *IFM 3D surface image and surface profiles for the front of the weld bead of sample F4.4.3*

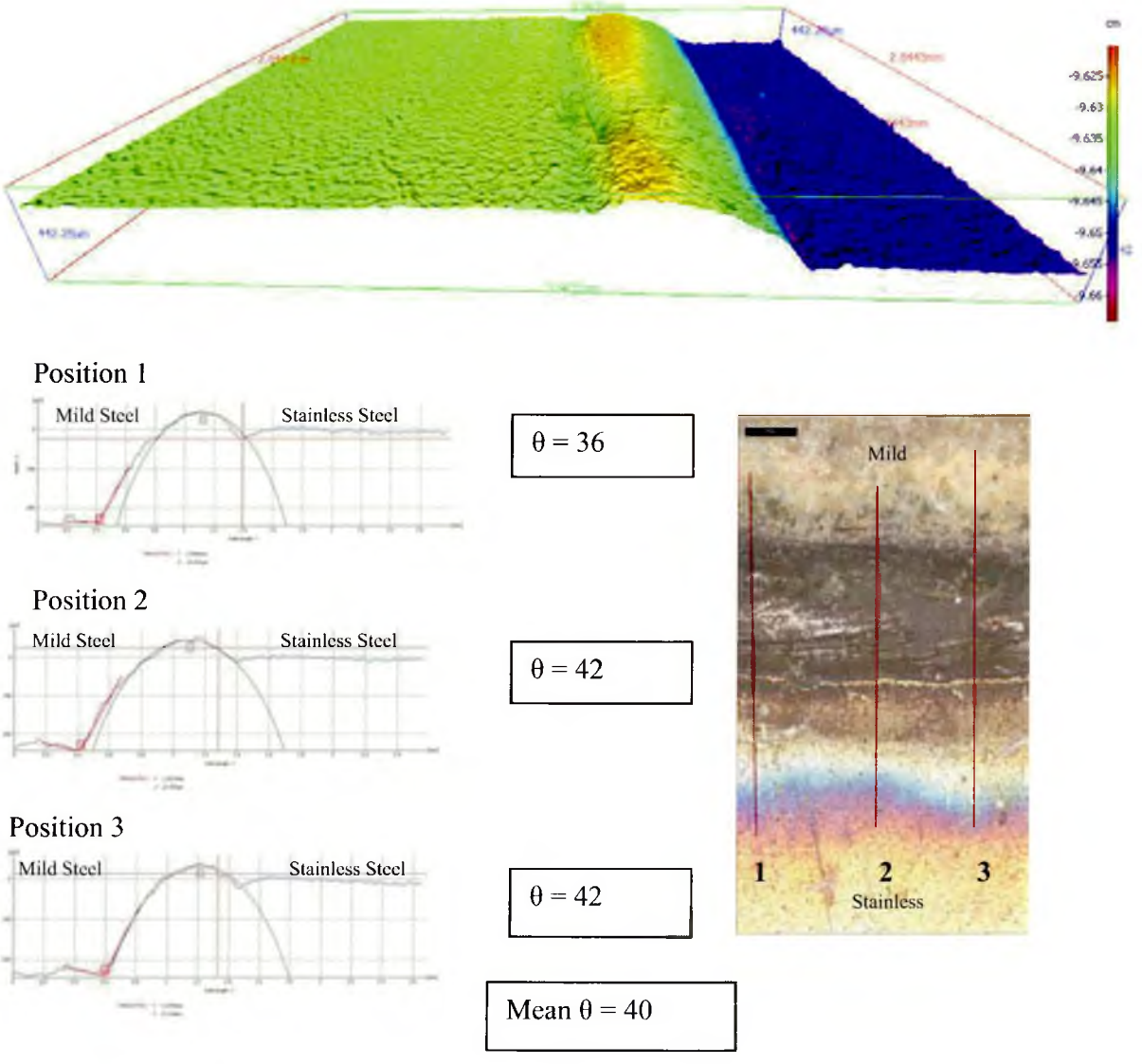

Figure 10. *IFM 3D image and surface profiles for the underside of sample F4.4.3 including the penetration root angle measurements for the sample.*

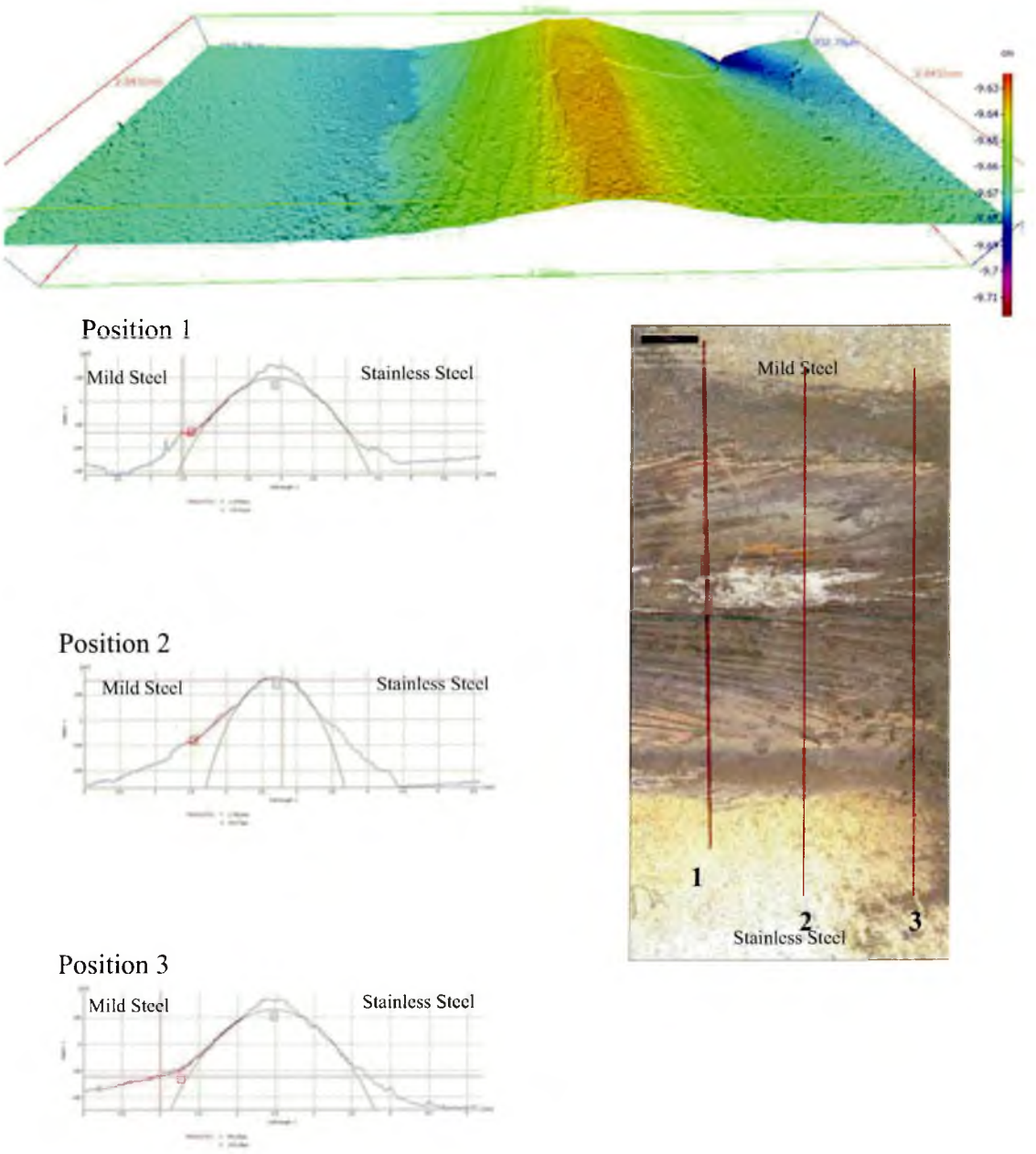

Figure 11. *IFM 3D surface image and surface profiles for the front of the weld bead of sample F4.8.3*

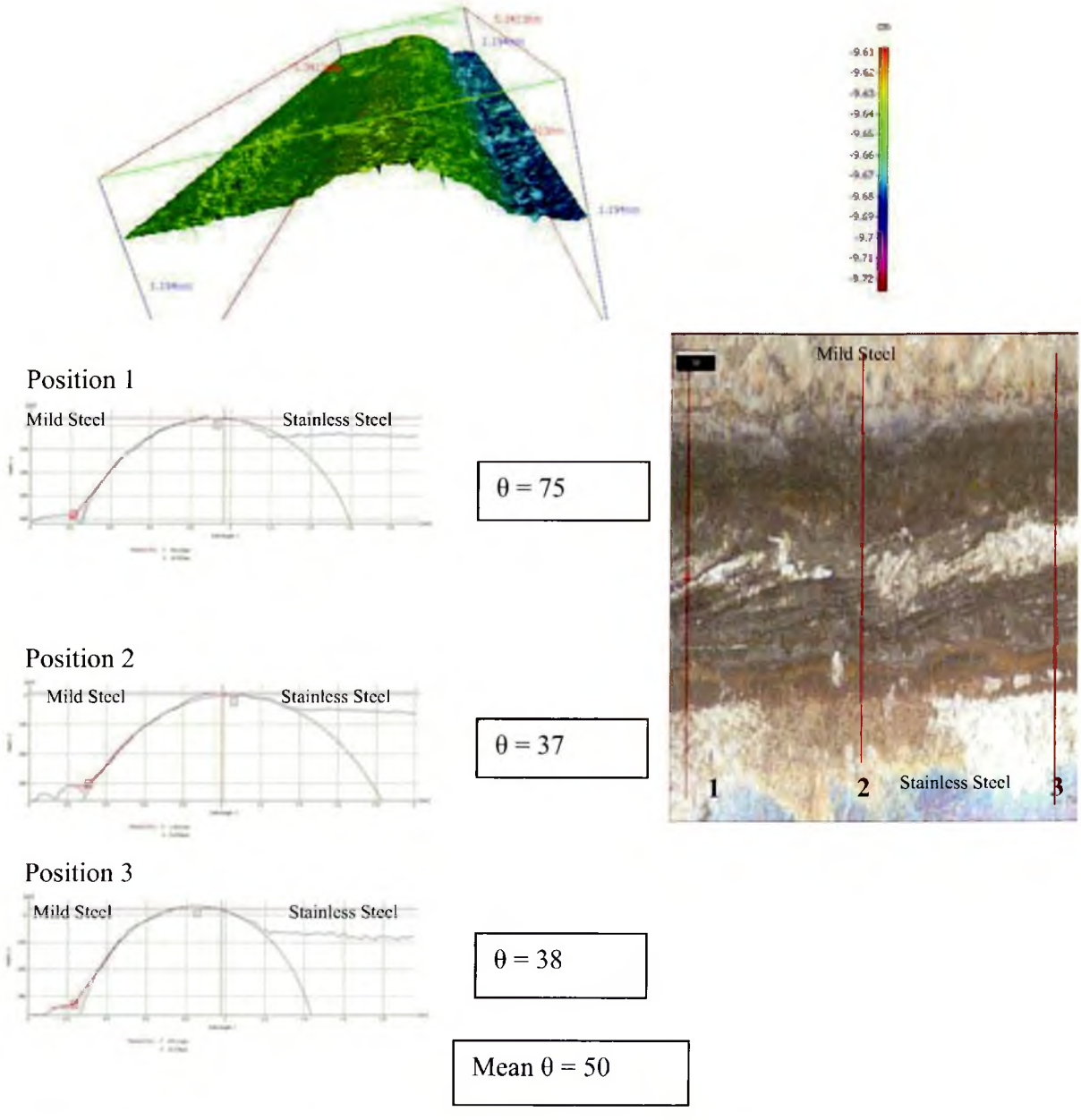

Figure 12. *IFM 3D image and surface profiles for the underside of sample F4.8.3 including the penetration root angle measurements for the sample.*

Series 8

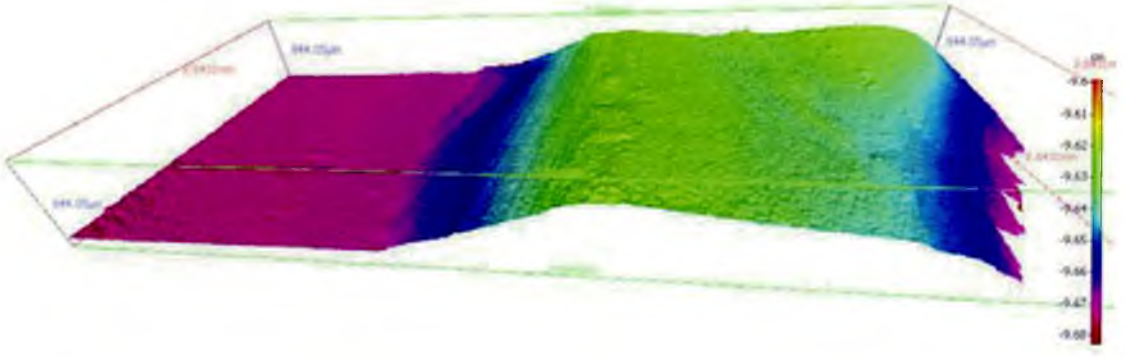

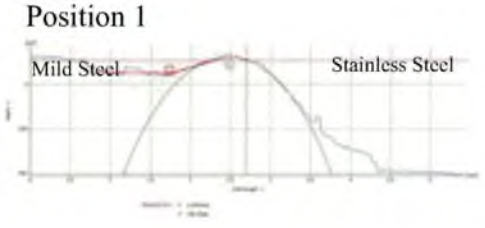

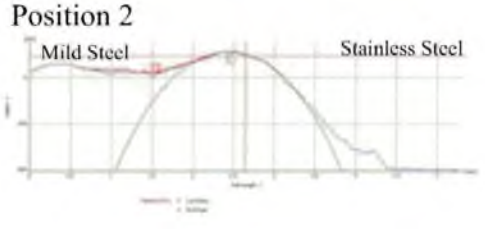

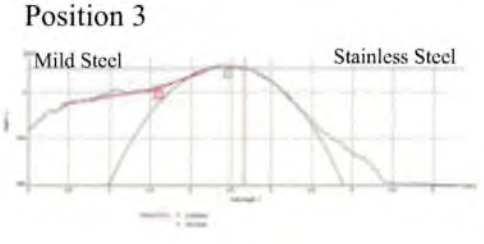

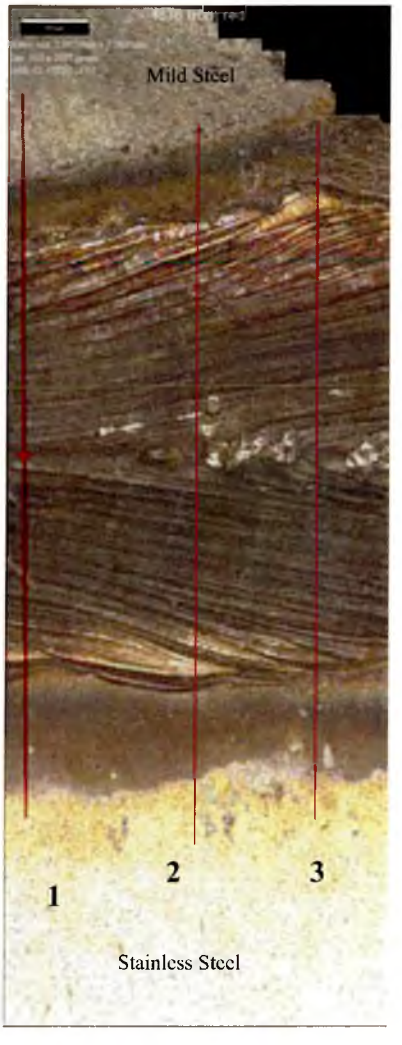

Figure 13. *IFM 3D surface image and surface profiles for the front of the weld bead of sample F8.7.6*

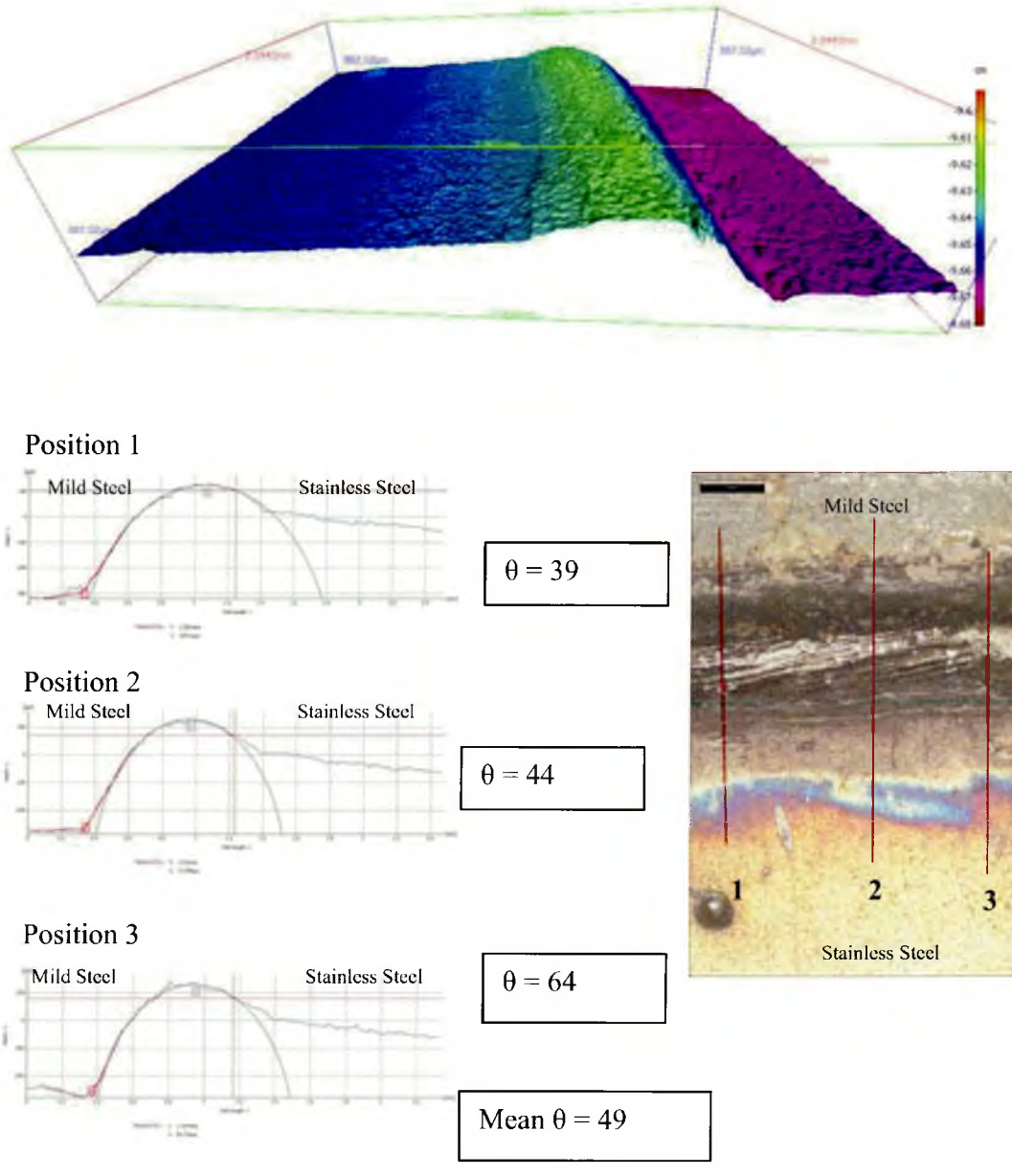

Figure 14. *IFM 3D image and surface profiles for the underside of sample F8.7.6 including the penetration root angle measurements for the sample.*

Additional IFM 3D Images and Surface Profiles for CMT Butt Joints with LDX 2101

Series C1

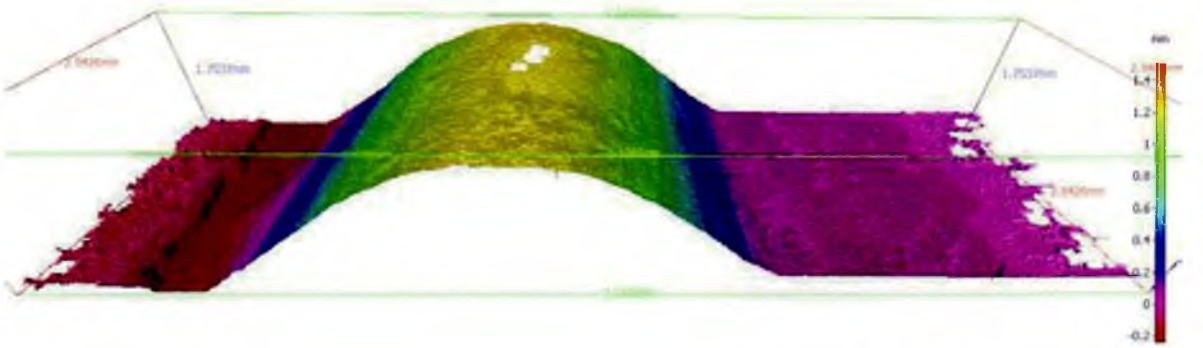

Position 1

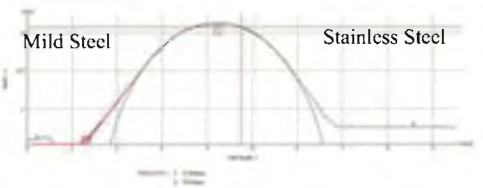

Position 2

Position 3

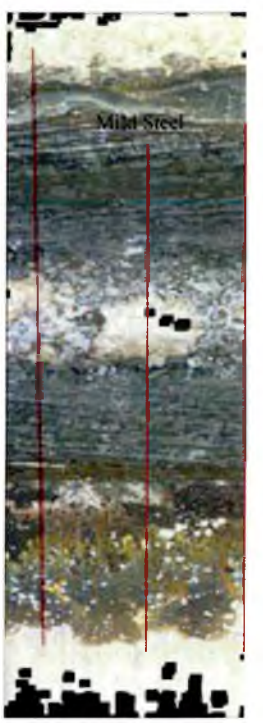

Figure 15. *IFM 3D surface image and surface profiles for the front of the weld bead of sample C1.2.4*

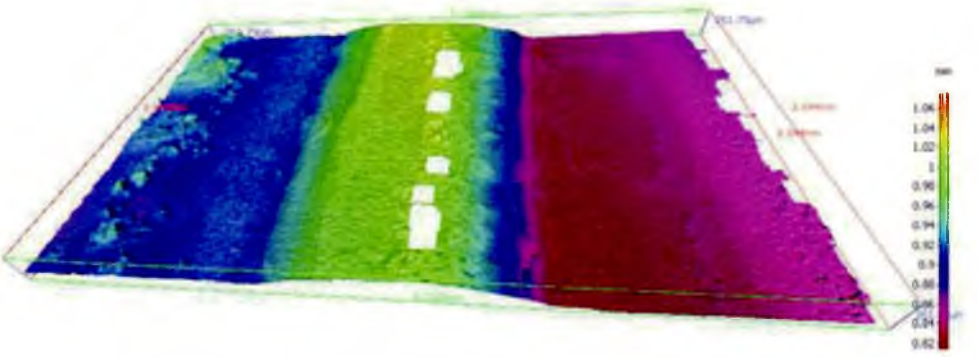

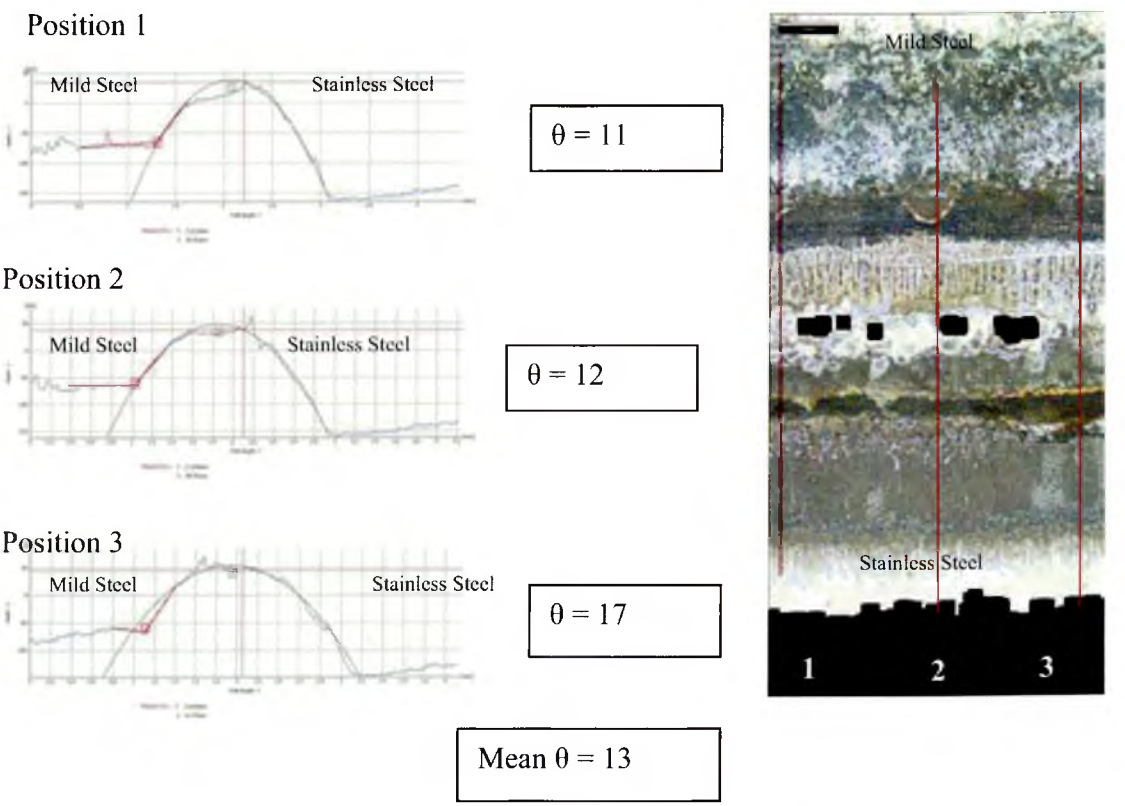

Figure 16. *IFM 3D image and surface profiles for the underside of sample C1.2.4 including the penetration root angle measurements for the sample.*

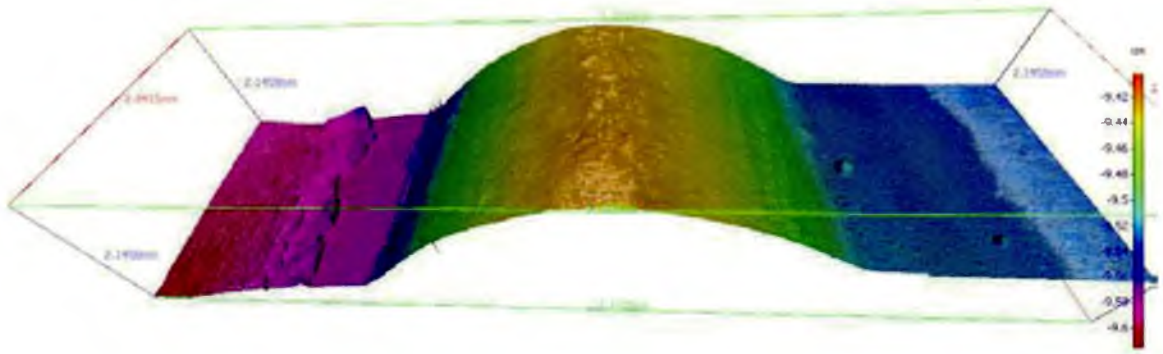

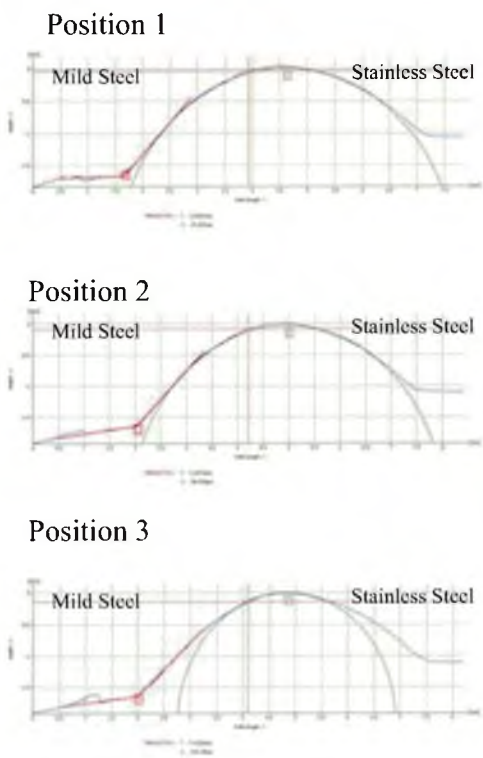

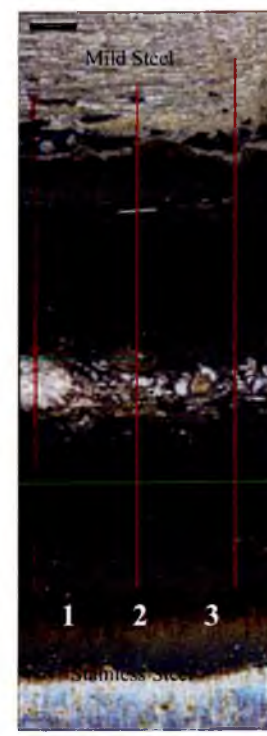

Figure 17. *IFM 3D surface image and surface profiles for the front of the weld bead of sample C1.6.1*

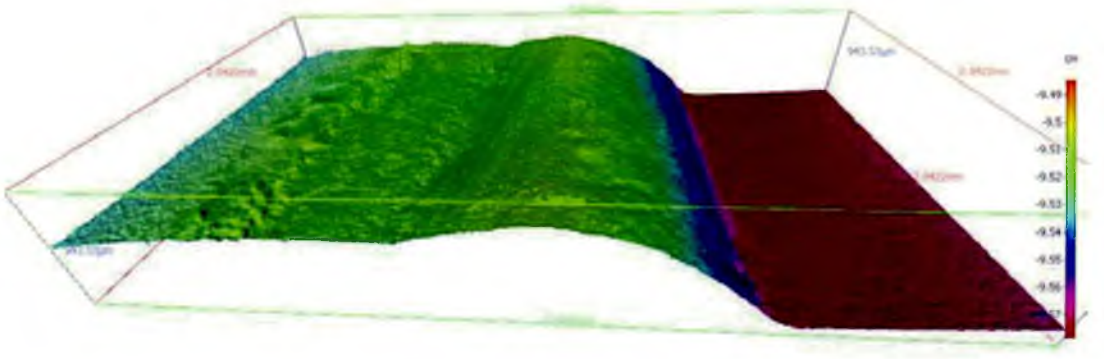

Position 1

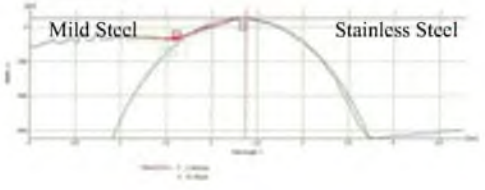

θ = 30

Position 2

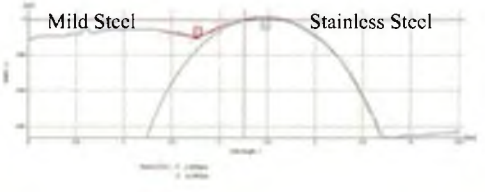

θ = 30

Position 3

θ = 23

Mean θ = 28

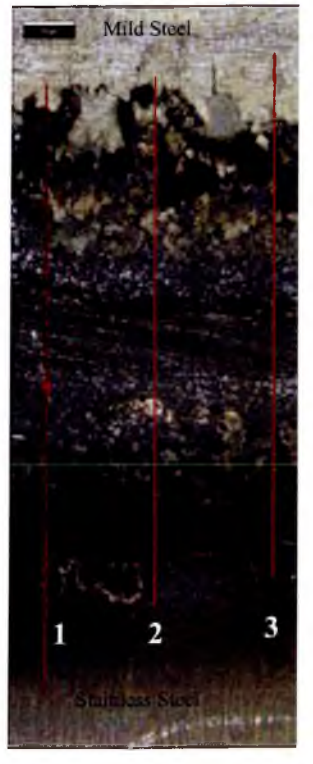

Figure 18. *IFM 3D image and surface profiles for the underside of sample C1.6.1 including the penetration root angle measurements for the sample.*

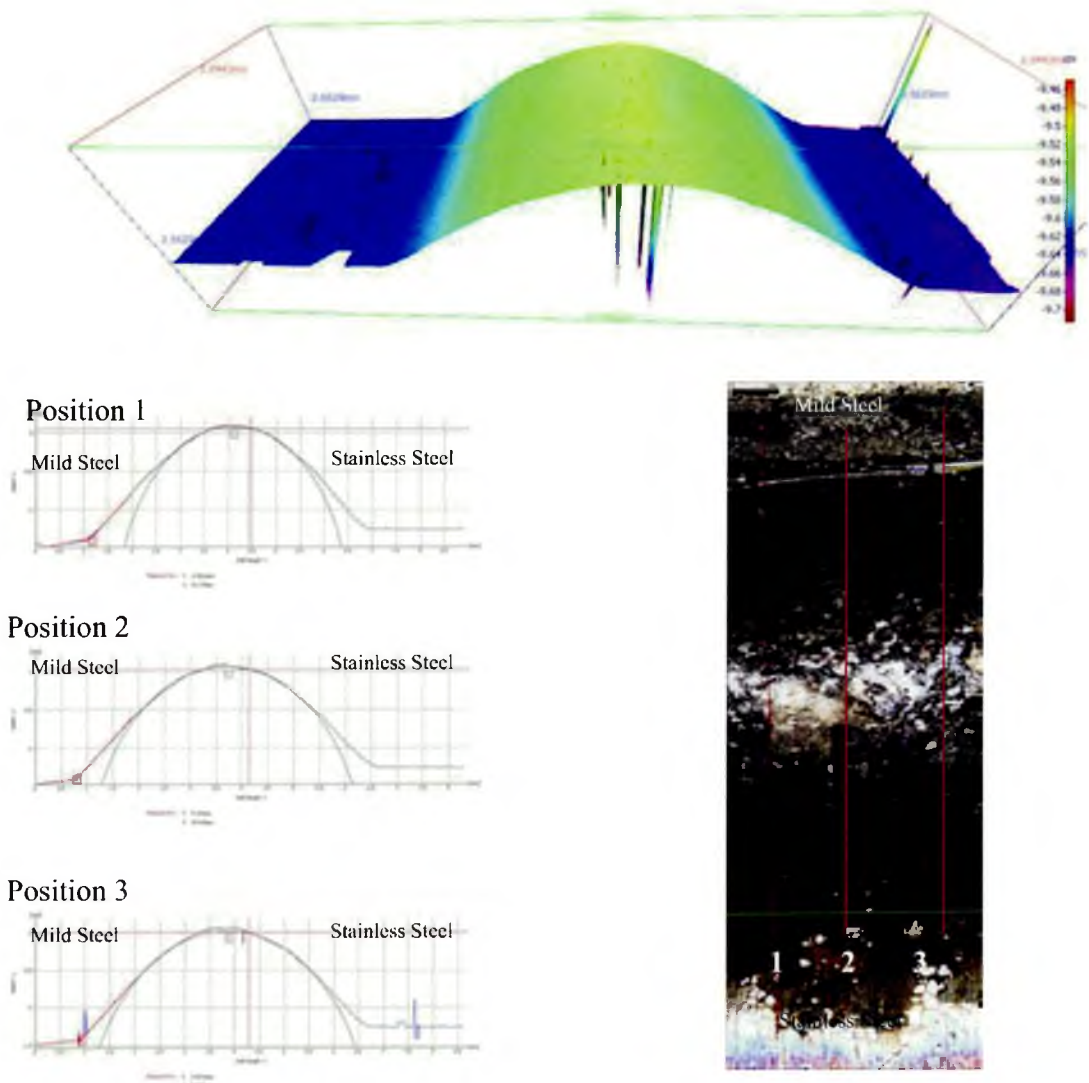

Figure 19. *IFM 3D surface image and surface profiles for the front of the weld bead of sample C1.6.3*

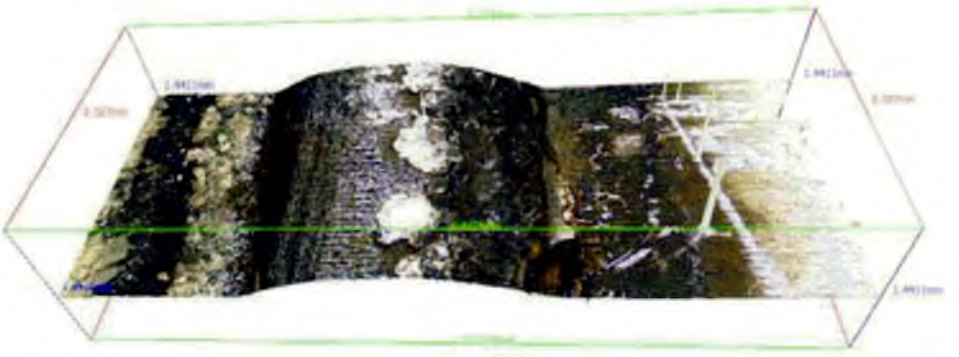

Position 1

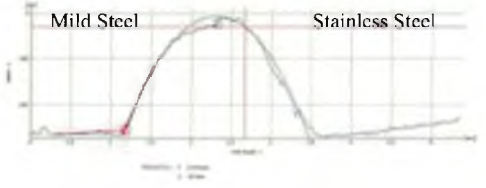

θ = 20

Position 2

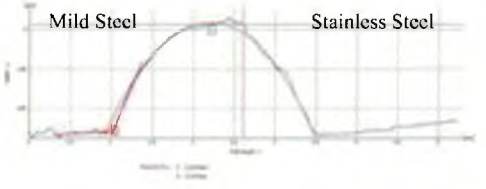

θ = 25

Position 3

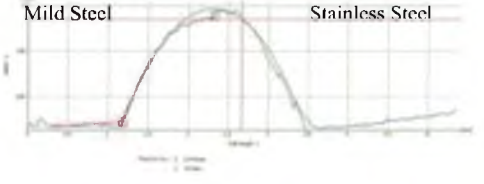

θ = 29

Mean θ = 25

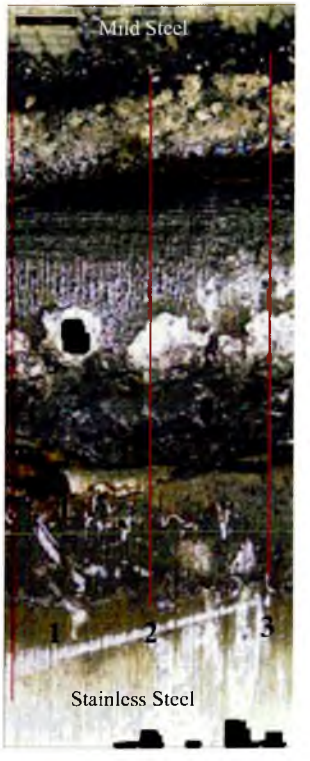

Figure 20. *IFM 3D image and surface profiles for the underside of sample C1.6.1 including the penetration root angle measurements for the sample.*

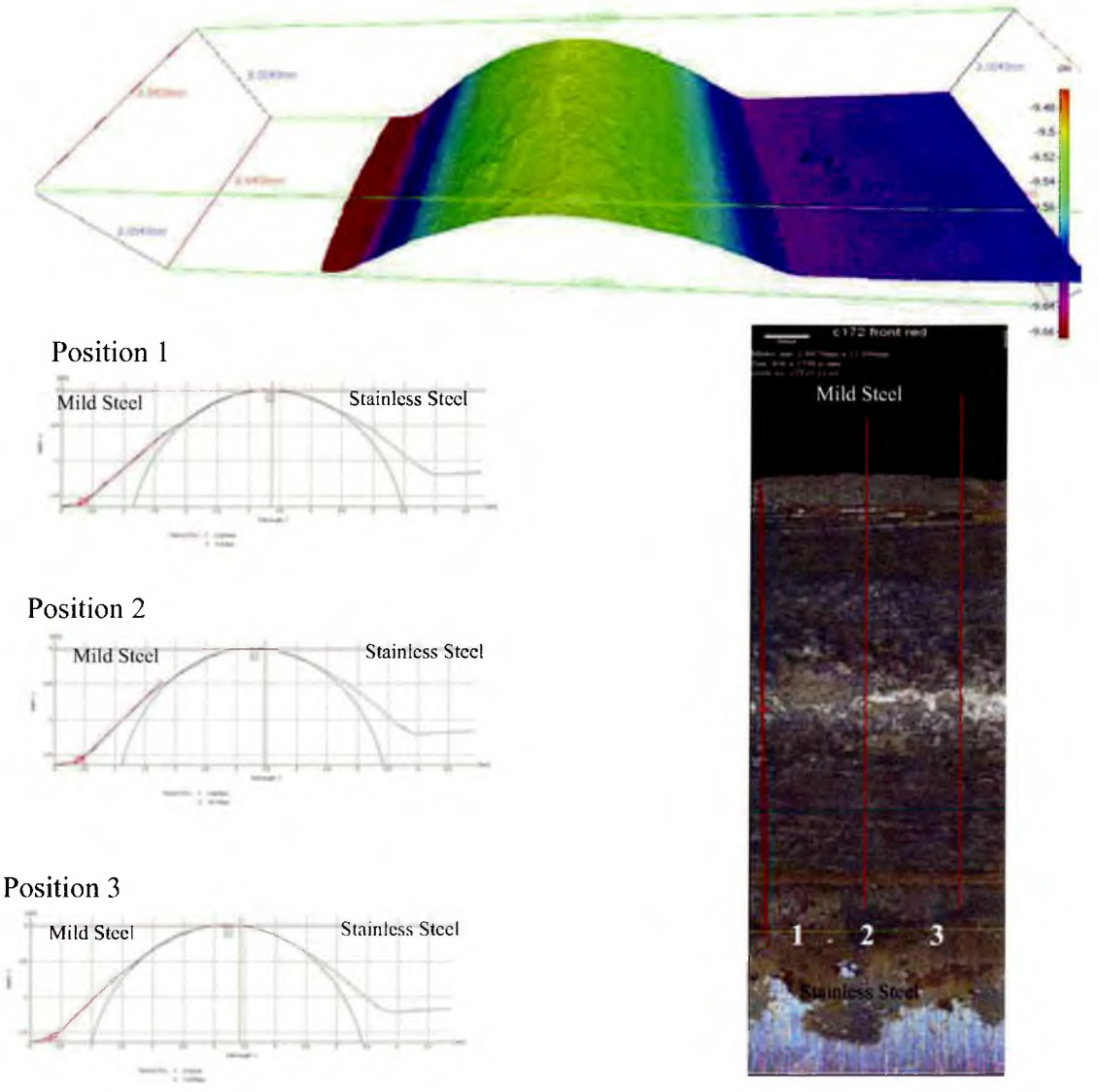

Figure 21. *IFM 3D surface image and surface profiles for the front of the weld bead of sample C1.7.2*

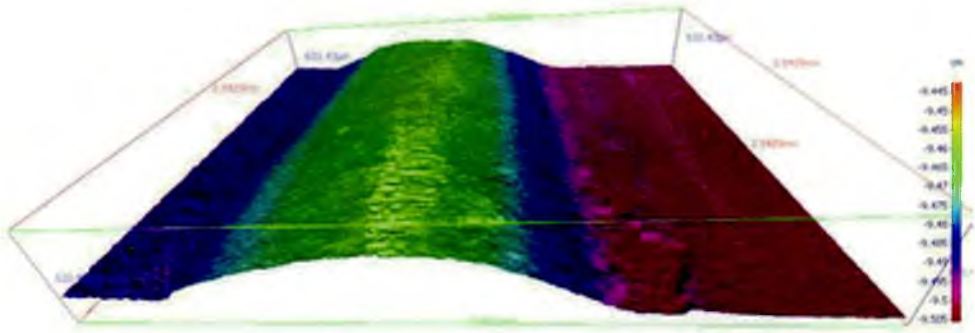

Position 1

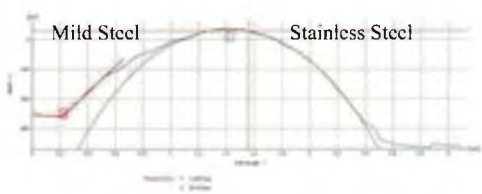

θ = 25

Position 2

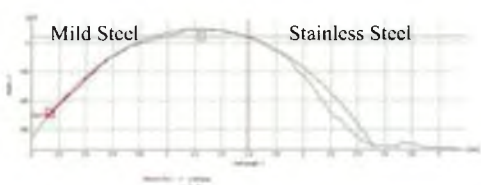

θ = 21

Position 3

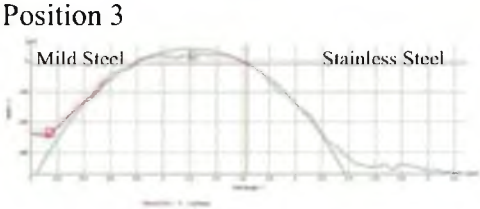

θ = 27

Mean θ = 24

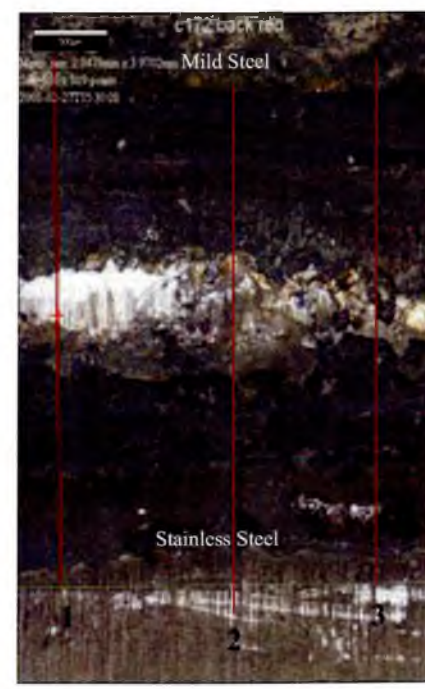

Figure 22. *IFM 3D image and surface profiles for the underside of sample C1.7.2 including the penetration root angle measurements for the sample.*

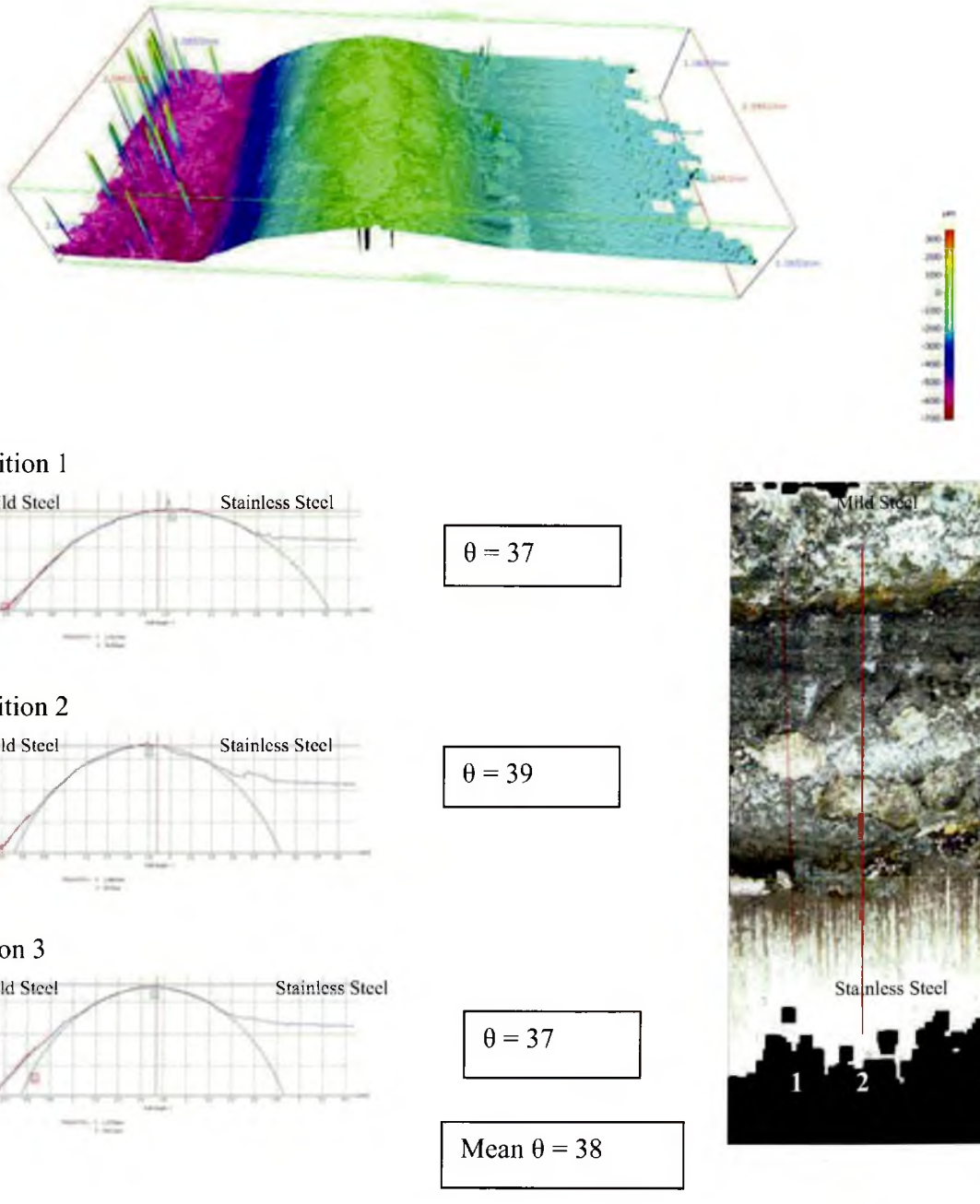

Figure 23. *IFM 3D image and surface profiles for the underside of sample C1.5.3 including the penetration root angle measurements for the sample.*